GEOLOGICA ULTRAIECTINA

Mededelingen van de
Faculteit Aardwetenschappen der
Rijksuniversiteit te Utrecht

No. 85

AQUEOUS GEOCHEMISTRY OF THE RARE EARTH ELEMENTS IN MARINE ANOXIC BASINS

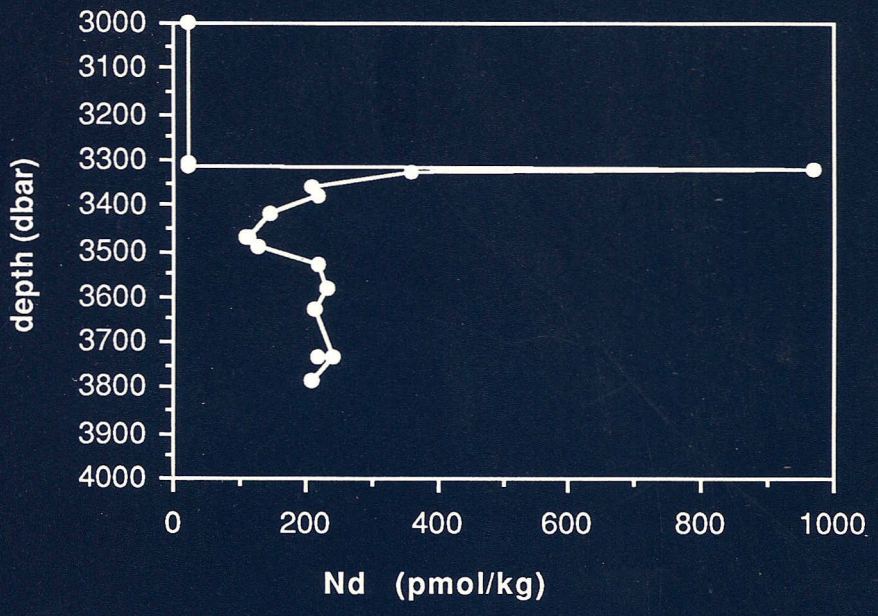

JOHAN SCHIJF

GEOLOGICA ULTRAIECTINA

Mededelingen van de
Faculteit Aardwetenschappen der
Rijksuniversiteit te Utrecht

No. 85

AQUEOUS GEOCHEMISTRY OF THE RARE EARTH ELEMENTS IN MARINE ANOXIC BASINS

CIP-GEGEVENS KONINKLIJKE BIBLIOTHEEK, DEN HAAG

Schijf, Johan
Aqueous geochemistry of the rare earth elements in marine anoxic basins / Johan Schijf.- [Utrecht: Faculteit Aardwetenschappen der Rijksuniversiteit Utrecht].-
(Geologica Ultraiectina, ISSN 0072-1026; no. 85)
Proefschrift Rijksuniversiteit Utrecht.- Met lit. opg.-
Met samenvatting in het Nederlands.
ISBN 90-71577-40-6
Trefw: geochemie.

AQUEOUS GEOCHEMISTRY OF THE RARE EARTH ELEMENTS IN MARINE ANOXIC BASINS

GEOCHEMIE VAN DE ZELDZAME AARDEN IN HET WATER VAN MARIENE ANOXISCHE BEKKENS

(MET EEN SAMENVATTING IN HET NEDERLANDS)

PROEFSCHRIFT

TER VERKRIJGING VAN DE GRAAD VAN DOCTOR AAN DE RIJKSUNIVERSITEIT TE UTRECHT OP GEZAG VAN DE RECTOR MAGNIFICUS, PROF. DR. J.A. VAN GINKEL, INGEVOLGE HET BESLUIT VAN HET COLLEGE VAN DEKANEN IN HET OPENBAAR TE VERDEDIGEN OP WOENSDAG 27 MEI 1992 DES VOORMIDDAGS TE 10.30 UUR

DOOR

JOHAN SCHIJF

GEBOREN OP 9 SEPTEMBER 1965 TE NOORDWIJKERHOUT

PROMOTOREN: PROF. DR. C.H. VAN DER WEIJDEN
PROF. DR. H.N.A. PRIEM
PROF. DR. W.G. MOOK

CO-PROMOTOR: DR. IR. H.J.W. DE BAAR

How inappropriate to call this planet Earth, when clearly it is Ocean.

Arthur C. Clarke

Dankwoord

Gerard Klaver zei eens tijdens een telefoongesprek, nadat ik had zitten klagen over hoe zwaar het promoveren is en hoe zielig ik wel niet was: "promoveren is een asociale bezigheid." Daar heeft hij gelijk in. Mijn familie kan dat van harte onderschrijven: zij hebben mij de afgelopen anderhalf jaar nauwelijks gezien. Ik dank daarom in de eerste plaats mijn vriendin Martina, mijn moeder, mijn zus en de familie van Martina voor het geduld dat zij tijdens mijn promotie-onderzoek met mij hebben gehad. In ruil voor mijn voortdurende afwezigheid en als antwoord op de vraag: "waarom kom je toch nooit meer langs?" kon ik ze vaak niet meer bieden dan de volledig onbevredigende verklaring: "ik ben aan het promoveren."

Voor een andere groep mensen heeft "promoveren is een asociale bezigheid" een heel andere betekenis. Dit zijn alle mensen die op één of andere manier direct aan het totstandkomen van dit proefschrift hebben meegewerkt of het van dichtbij hebben zien groeien. Zij hebben mij de afgelopen anderhalf jaar juist veel meer gezien dan hun lief zal zijn geweest. Een aantal van hen wil ik hier graag met name noemen.

Mijn collega-a.i.o.'s en -o.i.o.'s in Amsterdam, Paul, Peter, Kay, José, Marian, Geert-Jan, Pieter en sinds kort ook Max, Rick en Jurian bedank ik voor hun voortdurende steun en belangstelling, ondanks dat ik, als lid van de 'watermaffia', me bezig hield met zaken waarvoor een echte geoloog maar moeilijk enthousiasme kan opbrengen. Ik dank Paul in het bijzonder voor de talloze vruchtbare discussies, voor het kritisch lezen van de vele manuscripten en voor zijn begrip voor het feit dat promoveren bij mij niet altijd het 'Zwitserleven-gevoel' teweeg bracht, waarbij ik soms mijn slechte humeur op hem afreageerde. Ik beschouw het als een voorrecht dat Paul en Kay bereid zijn om als mijn paranimfen op te treden. Angélique Souren betoonde zich een gezellige en zeer ijverige bijvakstudente. Door haar inzet zijn monsters van de Southern Ocean geanalyseerd die anders zeker waren blijven liggen. Haar volkorenkoekjes hebben mij gedurende lange meetnachten en -weekenden op de been gehouden. Ik hoop dat zij het onderzoek als o.i.o. zal kunnen voortzetten. Mijn collega-a.i.o.'s en -o.i.o.'s in Utrecht, Jack, Else, Bertil en Peter heb ik helaas te weinig gezien, maar ondanks dat hadden ze belangstelling voor mijn werk en werd ik tijdens mijn sporadische bezoeken door hen altijd als een echte collega ontvangen. Else bedank ik speciaal voor het feit dat ze mij leerde de Shimadzu DOC-analyzer te bedienen. Deze kennis heb ik tijdens de JGOFS vaartocht in praktijk kunnen brengen, wat onlangs heeft geleid tot een publicatie.

De medewerkers van het IGO bedank ik voor hun gastvrijheid en voor hun bijdragen, van uiteenlopende aard, aan het onderzoek. Frans Benavente leerde mij het puntlassen van bandjes voor de Finnigan en het opbrengen van monsters. Koos van Belle stond de eerste paar jaar belangeloos een gedeelte van zijn budget af, waarmee heel wat schone reagentia en dure Teflon flessen en potjes zijn bekostigd. Samen met Richard en Piet toonde hij altijd grote interesse voor mijn werk en zorgde hij voor een prettige sfeer in het cleanlab. Lodewijk IJlst schafte een wagentje aan waarmee honderden liters zeewater tussen het magazijn en het cleanlab heen en weer zijn gesleept. Erhard Hebeda bedacht het geniale 'freon-experiment' (Section 3.2.6.), wat na een intensieve maar helaas kortstondige samenwerking in minder dan geen tijd tot een veelgevraagde publicatie leidde. Rob Scheveers hielp bij de bouw van het gasinlaatsysteem, zonder welk het meten van La-concentraties vrijwel onmogelijk zou zijn geweest. Nico Dijkstra en Wim van der Plas hebben regelmatig de Finnigan opgelapt als er weer eens iets doorgebrand was. Rossana Jong Loy was altijd te vinden voor een ontspannend kletspraatje of een kopje thee. Paul Andriessen gaf goede raad bij het gebruik van het tekstverwerkingsprogramma Microsoft Word. Peter Ploeger van de werkplaats maakte met veel geduld en vakmanschap en vooral ook altijd zeer snel een groot aantal opstellingen en technische hulpmiddelen, zoals kolommenrekken, verdamperpotten, een installatie voor het schoonmaken van monsterflessen, onderdelen voor het gasinlaatsysteem en een houder voor het laden van losse bandjes.

Ook een aantal werknemers van de Vrije Universiteit heeft mij bijzonder goed geholpen. Joop Meijer van de tekenkamer bedank ik voor het gebruik van de lichtbak die

uitstekend dienst deed bij het inplakken van de figuren. Wim Bergenhenegouwen maakte de prachtige foto's op pagina 78. Mieke de Vries van de bibliotheek slaagde er steeds weer in om zelfs de meest obscure referenties te vinden. De uitgebreide referentielijst achterin dit proefschrift is grotendeels dankzij haar hulp tot stand gekomen. Saskia Kars voorzag mij van koffie, thee, sigaren, sterke drank en conversatie, allemaal van een kwaliteit die voor een eenvoudige a.i.o. over het algemeen niet zijn weggelegd. John Kist stond Paul en mij het gebruik van de GFAAS toe voor het bepalen van spoormetaal-concentraties in Bannock Basin (Chapter 4).

Fred Quint van de tekenkamer in Utrecht bedank ik voor adviezen en hulp bij het totstandkomen van de figuren. Izaak Santoe maakte met veel geduld en vakmanschap en op basis van mijn vaak nogal onbeholpen schetsen een aantal prachtige figuren, die verspreid in dit proefschrift te bewonderen zijn. Zelfs als ik een figuur voor de zoveelste maal weer wilde veranderen bleef hij vriendelijk en behulpzaam. Gert de Lange stond mij het gebruik van zijn nog niet gepubliceerde Bannock Basin data toe, waarvoor ik hem zeer erkentelijk ben. Pauline van Gaans gaf mij een kopie van het speciatie-programma WATEQX, alsmede uitleg over het gebruik ervan en over metaalspeciatie in het algemeen.

Ook een aantal mensen op het NIOZ wil ik hier graag bedanken. Allereerst natuurlijk Hein de Baar, die de geestelijke vader van het onderzoek is en die mij de afgelopen vier en een half jaar met raad en daad terzijde heeft gestaan. Ik heb bewondering voor zijn grote doorzettingsvermogen, ondanks het onbegrip en de tegenslagen die hij te verduren heeft gehad, en voor het enthousiasme waarmee hij iedere nieuwe wetenschappelijke uitdaging te lijf gaat. Dit alles is een bron van inspiratie voor mij geweest en ik hoop dat door zijn inzet de chemische oceanografie in Nederland een blijvende impuls heeft gekregen. Rob Nolting bepaalde met de vlam absorptie spectrofotometer Mn-concentraties in het zwevend materiaal uit de Zwarte Zee (Chapter 6) en stond Paul en mij vaak het gebruik van de GFAAS toe. Jeroen de Jong bepaalde met de GFAAS Mn-concentraties in de Bannock brine (Chapter 4). Anita Buma bedank ik voor haar gezelschap tijdens het AGU/ASLO congres in New Orleans, waar wij onze gemeenschappelijke voorliefde voor goed eten en jazz-muziek ten volle hebben kunnen uitleven. Alle mensen die aan boord van de Tyro waren tijdens de WINDOW en JGOFS vaartochten bedank ik voor hun morele en technische steun.

Ik bedank mijn promotors Prof. van der Weijden, Prof. Priem en Prof. Mook en de leden van de leescommissie voor de belangstelling die ze hadden voor het uiteindelijke resultaat van mijn onderzoek.

Finally I want to thank a number of people whom I must address in English. Pauline Smedley taught me how to operate the Finnigan as well as the basic principles of isotope dilution mass spectrometry. She herself is now working on REE geochemistry in natural waters using an ICP-MS and I sincerely hope that we will meet again soon to talk about old (and new) times. I thank Henry Elderfield for his interest in my work, in particular for reading the manuscript and for supporting my WHOI application and I thank him and his wife for their hospitality during my short stay at the University of Cambridge. Bill Landing kindly provided me with a copy of the speciation program EASEQL and showed me how to use it. He also supported my WHOI application. I thank him and his wife for their hospitality during my stay at Florida State University. I owe a great deal to Frank ('fast Frankie') Millero. He performed the REE speciation calculations for the Bannock brine and provided me with data, figures, scientific discussion and interest in my work. He read the manuscript and supported my WHOI application. David Hawke assisted with the speciation calculations and Barbara Karn kindly let me stay at her apartment during my visit to RSMAS. Ed Sholkovitz offered me the opportunity to work at WHOI for which I am most grateful. I hope that our collaboration this coming year will lead to many interesting scientific results.

Contents

The concept of La anomalies that was introduced in Section 2.2.4. of Chapter 2 was published before in De Baar *et al.* (1991). Section 3.2.6. of Chapter 3 was published before in Hebeda and Schijf (1991). Most of Chapter 4 was submitted for publication in Geochimica et Cosmochimica Acta (Saager *et al.*, 1991). Parts of Chapter 6 were published before in Schijf *et al.* (1991). Parts of Chapters 3-7 will in the near future be submitted for publication in various journals.

Abstract

Life in the oceans mainly occurs in the upper tens of meters of the watercolumn, where sunlight penetrates. This sunlight is used by phytoplankton to combine carbon and nutrients to organic matter, which subsequently serves zooplankton and higher life forms as food. When the plankton dies it slowly settles to the seafloor, meanwhile being decomposed by bacteria. This decomposition requires oxygen, which is extracted directly from the surrounding seawater. If this oxygen would not be constantly replenished, the oceans would soon be completely devoid of oxygen (anoxic). Oxygen is replenished slowly by diffusion and more readily by advection *i.e.* by supply of oxygen-rich water. If advection is locally impeded, then mere diffusion is usually not sufficient to balance the consumption of oxygen and an anoxic basin may be formed. This is the case for instance in the Bannock Basin, eastern Mediterranean, where a volume of brine does not mix with the overlying seawater, and in the Black Sea, where seawater that is supplied at depth through the Bosporus mixes poorly with freshwater that is supplied at the surface by several major rivers.

Very interesting is the behaviour of certain trace metals in the waters of anoxic basins, in particular at the interface between the oxygen-poor and the overlying oxygen-rich waters. Manganese and iron are present in oxygen-rich waters mainly as poorly soluble oxides adsorbed onto particulate matter. When the particulate matter settles across the interface, manganese and iron are reduced to a valency that does not form poorly soluble oxides. As a result, the concentrations of dissolved manganese and iron strongly increase across the interface. This leads to upward diffusion of dissolved manganese and iron into the oxygen-rich waters, where they are once more oxidized and adsorbed onto particulate matter. This cycling closely resembles a process whereby dissolved trace metals are removed from the seawater in the upper part of the watercolumn by adsorption onto particulate matter and released at depth as the particulate matter is decomposed. This process, known as 'scavenging', is the major mechanism for the transport of trace metals from the seawater to the sediment and constitutes an important component of the cycling of trace metals in the oceans. Scavenging is difficult to study, since it occurs on a worldwide scale and on timescales of hundreds to thousands of years. By studying the cycling of trace metals at the interface between oxygen-poor and oxygen-rich waters in anoxic basins, a similar process that is however localized and occurs on considerably shorter timescales, much can indirectly be learned about scavenging.

The rare earth elements or lanthanides are very well suited for this purpose. Their cycling in the oceans seems to be governed by the same mechanisms that govern the cycling of many other trace metals and is in particular closely associated with the cycling of manganese. At the interface between oxygen-poor and oxygen-rich waters in anoxic basins they show a passive cycling that seems to be driven by the cycling of manganese and possibly also by that of iron. Moreover, the element cerium shows an active cycling that is caused by its own oxidation-reduction chemistry, a property that is unique within the rare earth element series. The rare earth elements form a chemically coherent group, yet their chemical properties are not completely the same. Consequently, the cycling of each rare earth element is subtly different from that of all others. Since the chemical properties of the rare earth elements depend in a gradual and more or less predictable way on atomic number, the mechanisms that govern the cycling of the rare earth elements in the ocean and at the interface between oxygen-poor and oxygen-rich waters in anoxic basins can be studied and described in terms of relative rather than absolute behaviour. In fact, the behaviour of the rare earth elements as a group forms a frame of reference for the behaviour of each rare earth element separately. By studying the cycling of the rare earth elements, information can indirectly be obtained about the cycling of trace metals like manganese and iron, for which such a frame of reference is not available.

Samenvatting

Het leven in de oceaan vindt grotendeels plaats in de bovenste tientallen meters van de waterkolom, waar het zonlicht doordringt. Dit zonlicht wordt door plantaardig plankton gebruikt om koolstof en voedingsstoffen te binden tot organisch materiaal dat op zijn beurt dierlijk plankton en hogere levensvormen tot voedsel dient. Als het plankton sterft zakt het langzaam naar de bodem, waarbij het door bacteriën wordt afgebroken. Voor deze afbraak is zuurstof nodig die direct aan het zeewater onttrokken wordt. Als de zuurstof in het zeewater niet voortdurend aangevuld zou worden dan zou de oceaan na korte tijd volledig zuurstofloos (anoxisch) zijn. Zuurstof wordt langzaam aangevuld door diffusie en veel sneller door advectie, dat wil zeggen door aanvoer van zuurstofrijk water. Als advectie plaatselijk wordt gehinderd dan is diffusie alleen vaak niet voldoende om het zuurstofverbruik te compenseren en kan een anoxisch bekken ontstaan. Dit is bijvoorbeeld het geval in het Bannock Basin in de oostelijke Middellandse Zee, waar een hoeveelheid zeer zout water door zijn grote dichtheid niet mengt met het bovenliggende zeewater, en in de Zwarte Zee, waar zeewater dat op diepte wordt aangevoerd via de Bosporus slecht mengt met zoetwater dat aan de oppervlakte wordt aangevoerd door een aantal grote rivieren.

Zeer interessant is het gedrag van bepaalde spoormetalen in het water van anoxische bekkens, met name aan het grensvlak tussen het zuurstofarme en het erboven liggende zuurstofrijke water. Mangaan en ijzer zijn in zuurstofrijk water grotendeels als slecht oplosbare oxiden gebonden aan vaste deeltjes. Als deze deeltjes het grensvlak passeren worden mangaan en ijzer gereduceerd tot een ladingstoestand die geen slecht oplosbare oxiden vormt. Hierdoor neemt de concentratie van opgelost mangaan en ijzer aan het grensvlak sterk toe. Dit leidt tot diffusie van opgelost mangaan en ijzer naar het zuurstofrijke water, waar ze opnieuw oxideren en zich aan vaste deeltjes hechten. Deze kringloop vertoont sterke overeenkomsten met een proces waarbij spoormetalen in het bovenste gedeelte van de waterkolom worden onttrokken aan het zeewater, doordat ze zich hechten aan naar beneden zakkende vaste deeltjes, waarna ze op diepte, waar de vaste deeltjes worden afgebroken, weer worden vrijgegeven. Dit proces, dat bekend staat als 'scavenging', is het belangrijkste mechanisme voor het transport van spoormetalen vanuit het zeewater naar het sediment en vormt een belangrijke schakel in de kringloop van spoormetalen in de oceaan. Scavenging is moeilijk te bestuderen, aangezien het plaatsvindt op wereldwijde schaal en in een tijdsbestek van honderden tot duizenden jaren. Door het bestuderen van de kringloop van spoormetalen aan het grensvlak tussen zuurstofarm en zuurstofrijk water in anoxische bekkens, een vergelijkbaar proces dat echter plaatsvindt op kleine schaal en in een veel korter tijdsbestek, kan indirect veel over scavenging worden geleerd.

De zeldzame aarden of lanthaniden zijn hiervoor bij uitstek geschikt. Hun kringloop in de oceaan lijkt te worden beheerst door dezelfde mechanismen die de kringloop van vele andere spoormetalen beheersen en is in het bijzonder sterk verbonden met de kringloop van mangaan. Aan het grensvlak tussen zuurstofarm en zuurstofrijk water in anoxische bekkens vertonen zij een passieve kringloop die waarschijnlijk gedreven wordt door de kringloop van mangaan en wellicht ook door die van ijzer. Het element cerium vertoont bovendien een actieve kringloop die het gevolg is van zijn eigen oxidatie-reductie chemie, een eigenschap die geen van de overige zeldzame aarden bezit. De zeldzame aarden vormen een chemisch zeer coherente groep, maar hun chemische eigenschappen zijn toch niet geheel hetzelfde. Als een gevolg hiervan verschilt de kringloop van elk van de zeldzame aarden subtiel van die van alle anderen. Doordat de chemische eigenschappen van de zeldzame aarden op een gelijkmatige en min of meer voorspelbare manier afhangen van het atoomnummer, kunnen de mechanismen die de kringloop van de zeldzame aarden in de oceaan en aan het grensvlak tussen zuurstofarm en zuurstofrijk water in anoxische bekkens beheersen worden bestudeerd en beschreven aan de hand van relatief gedrag in plaats van absoluut gedrag. In feite vormt het gedrag van de groep zeldzame aarden als geheel een referentiekader voor het gedrag van elk van de zeldzame aarden afzonderlijk. Door het bestuderen van de kringloop van de zeldzame aarden kan indirect informatie worden verkregen over de kringloop van spoormetalen zoals mangaan en ijzer, voor welke een dergelijk referentiekader ontbreekt.

CHAPTER 1 Introduction

This thesis is about the aqueous geochemistry of the rare earth elements (REE) in two marine anoxic basins, Bannock Basin (eastern Mediterranean) and the Black Sea. Following an introduction into the marine geochemistry of the REE (Chapter 2) and a detailed description of the methods that were used to determine REE concentrations in seawater (Chapter 3), the vertical distributions of Mn, Fe and the REE in the watercolumn of Bannock Basin are discussed in Chapters 4 and 5. REE cycling in the newly discovered suboxic layer of the Black Sea is the subject of Chapters 6 and 7. In this introductory Chapter the contents of the remaining six Chapters are briefly summarized.

Already for several decades the REE are known as an important group of trace elements that can be used to study a variety of geochemical processes (*e.g.* Henderson, 1984). Due to analytical difficulties, the marine geochemistry of the REE has not been actively studied until the early 1980s, when the first accurate and detailed vertical distributions of dissolved REE were published for the eastern North Atlantic Ocean (Elderfield and Greaves, 1982). Chapter 2 reviews what has been learned since then about the marine geochemistry of the REE, in particular with respect to their cycling at the oxic-anoxic interface of marine anoxic basins. Some of the unique properties of the REE, which make them especially suited for studying trace metal scavenging, are also discussed.

Sampling, chemistry, isotope dilution mass spectrometry (IDMS) and data handling are discussed in Chapter 3. In the context of a historical review of the methods available for preconcentrating the REE from rock and seawater samples and for separating them from interfering elements, it is explained why a preconcentration based on the Chelex method of De Baar (1983) was chosen, instead of the probably more convenient and certainly more widely used method of coprecipitation with hydrated Fe(III) oxide. The IDMS method that was used on the Finnigan MAT 261 mass spectrometer is a modification of an IDMS method that was developed for determining REE concentrations in seawater on a VG Isomass 54E mass spectrometer (Greaves *et al.*, 1989). The REE emission sequence on the Finnigan MAT 261 appeared to be very different from that reported by Greaves *et al.* (1989) and called for an entirely new scheme of interference corrections. Since a considerable part of the research period was spent on the IDMS method, it is discussed in great detail.

Chapter 4 describes the vertical distributions of Mn and Fe in the watercolumn of the hypersaline Bannock Basin. Vertical distributions of dissolved Mn, Fe and several other trace metals in the seawater

overlying the brine are used to construct a simple model of trace metal cycling in the eastern Mediterranean Sea in terms of the general circulation of watermasses. Mn and Fe cycling at the seawater-brine interface of Bannock Basin are largely controlled by redox chemistry and Fe sulfide precipitation, in agreement with what is found in many other marine anoxic basins. Mn removal at the interface between two chemically distinct brine layers seems to be caused by uptake into dolomite that forms either *in situ* or in the sediments (De Lange *et al.*, 1990a,b). A similar mechanism is probably responsible for the removal of Fe and the REE at that depth. The vertical distributions of dissolved Fe and sulfide in the Bannock brine are compared with those in the anoxic brines of the Orca Basin (Gulf of Mexico).

The marine geochemistry of the REE is closely related to that of Mn and Fe and Chapter 4 therefore serves as an introduction to Chapter 5, which describes the vertical distributions of dissolved REE in the watercolumn of Bannock Basin. The model of trace metal cycling that was developed in Chapter 4 is applied to the vertical distributions of dissolved REE in the seawater overlying the brine. REE speciation in the brine is calculated with a trace metal speciation computer model. The results of latter calculation are incorporated into the REE scavenging model of Byrne and Kim (1990), in an attempt to elucidate the REE patterns in the brine, which are distinctly different from those in the overlying seawater. Vertical distributions of dissolved REE in the brine are interpreted in terms of the vertical distributions of dissolved Mn and Fe and the model of De Baar *et al.* (1988).

The recent discovery of a broad suboxic layer, forming the transition between oxic and anoxic water in the Black Sea, makes the world's largest anoxic basin a suitable location for attempting to resolve the sequence of reactions that is associated with the bacterial oxidation of organic matter (Froelich *et al.*, 1979; Berner, 1980). In Chapter 6, vertical distributions of dissolved and particulate REE in the Black Sea are discussed in relation to this sequence of reactions. A predominant control by bacterial processes is invoked to explain the unusual vertical distribution of particulate Mn as well as the apparent decoupling of REE and Mn cycling in the suboxic layer. The results of fitting a vertical advection-diffusion model curve to vertical profiles of salinity and potential temperature (Spencer and Brewer, 1971; Goyet *et al.*, 1988) are used to calculate vertical REE fluxes in the watercolumn of the Black Sea, which are subsequently compared with the observed standing crop of particulate REE in the suboxic layer. The exchange of REE between the Black Sea and the Mediterranean Sea through the Bosporus is estimated as a first step towards the construction of a simple REE mass balance for the Black Sea.

During the 1988 Black Sea Expedition a series of mixing

experiments was performed to determine potential rates of Ce and Nd removal in the newly discovered suboxic layer. The results are presented in Chapter 7. Since the idea for these mixing experiments was formed only aboard the research vessel, they had not been prepared beforehand and required some improvisation. Nevertheless, the results are surprisingly interesting, especially in the light of studies of bacterial activity and Mn, Fe and S cycling in the suboxic layer that were performed by others (Millero, 1991; Tebo, 1991).

CHAPTER 2 The marine geochemistry of the REE

2.1. Introduction

The foundations for the science of marine geochemistry were laid in the second half of the 19th century by Forchhammer (1865) and Dittmar (1884) who reported the concentrations of all major and some minor elements in a great many seawater samples from all over the world. In decades thereafter, concentrations in seawater were reported for more and more elements. A large number of metals, commonly known as the trace metals, were found to occur in seawater at exceptionally low concentrations, roughly in the range 10^{-8}-10^{-13} mol/kg. The concentration in seawater of any trace metal represents only a minute fraction of what it would be if the total amount of that trace metal supplied to the oceans during geological time had remained in solution (Krauskopf, 1956). Evidently, the concentration in seawater of trace metals is kept low by some very efficient removal process. To resolve the mechanisms underlying this removal process has become one of the main objectives of marine geochemists.

Krauskopf (1956) estimated the efficacy of several possible removal processes. He calculated and measured the concentrations in seawater of thirteen trace metals in equilibrium with their least soluble salt, compared these to the most accurate measurements of the actual concentrations in seawater available at that time and found seawater to be strongly undersaturated with respect to the least soluble salt in each case. He concluded that the concentrations in seawater of these thirteen trace metals cannot be accounted for by precipitation. From measurements of the amount of adsorption onto a number of important marine solid phases, such as hydrated Mn and Fe oxides, apatite and clay, he further concluded that for some of the trace metals in question concentrations in seawater could instead be accounted for by adsorption onto particulate matter. For the remainder he suggested active uptake by marine organisms to be the major removal process, although he had very little data to substantiate this. New analytical techniques combined with new techniques to avoid contamination during collection and handling of seawater samples have since revealed that for many trace metals seawater is even more undersaturated with respect to the least soluble salt than calculated by Krauskopf (1956). His general conclusion that particulate matter, both organic and inorganic, both living and dead, plays a predominant role in removing trace metals from seawater is now widely accepted.

Turekian (1977) aptly referred to the removal of trace metals from seawater onto particulate matter as 'the great particle

conspiracy', yet 'scavenging' is the more usual term. Scavenging is the combined effect of a variety of processes, such as adsorption onto both organic and inorganic particulate matter, coprecipitation, ion pairing and redox chemistry. Despite many years of studying the marine geochemistry of trace metals with ever more modern techniques, the relative importance of these processes and the exact mechanisms underlying them are as yet largely unknown. As already suggested by Krauskopf (1956), the scavenging of trace metals with different chemical properties is probably dominated by different processes and even the scavenging of a single trace metal is probably not always dominated by the same process, depending on ambient chemical conditions. Clearly, scavenging is a very complicated phenomenon and much research is still needed for it to be completely understood.

One of the best studied trace metals in seawater is thorium (Th) (see for instance the review by Bacon, 1988). Its scavenging, which is dominated by rapid adsorption onto particulate matter, is relatively well understood. The four radioactive Th isotopes that occur in seawater (^{228}Th, ^{230}Th, ^{232}Th and ^{234}Th) all have different vertical distributions, since they derive from different sources and have different half-lives, ranging from tens of days to billions of years. The requirement that any model of Th scavenging must be able to reproduce all these vertical distributions places an important constraint on key model parameters such as Th adsorption-desorption and particle aggregation-disaggregation rates (see also Chapter 7). Attempts to model trace metal scavenging have therefore been much more successful for Th than for other trace metals.

The REE are also very well suited for studying trace metal scavenging, because their unique properties (Sect. 2.2.1.) enable the effects of REE scavenging on REE marine geochemistry to be described in terms of relative abundances rather than absolute concentrations. Moreover, REE scavenging comprises all processes that may contribute to trace metal scavenging in general. While the present understanding of REE scavenging is still far from complete, it may eventually be used to explain and predict the effects of scavenging on the marine geochemistry of other, less closely related trace metals.

An excellent way to study REE scavenging is to observe how it responds to dramatic changes in ambient chemical conditions, such as occur for instance at the interface between oxic and anoxic water in marine anoxic basins. In this thesis I describe and attempt to explain the vertical distributions of REE in two marine anoxic basins, the hypersaline Bannock Basin (eastern Mediterranean) and the Black Sea. Before embarking on this task I introduce in this Chapter several aspects of REE marine geochemistry that pertain to the subject of this thesis. Although this review is necessarily brief, I have tried to make

it comprehensive, yet comprehensible for those who are less familiar with marine geochemistry in general and that of the REE in particular.

2.2. The REE in seawater

2.2.1. Chemical properties of the REE

The rare earth elements (REE) or lanthanides are the elements with atomic numbers 57-71 belonging to Group IIIb of the Periodic Table (convention *cf.* Weast and Astle, 1982), which further includes scandium (Sc), yttrium (Y) and the actinides. Their names and symbols are given in Table 2.1. The REE are not nearly as rare as their name suggests. In fact, their average crustal abundance is not very different from that of cobalt, tin and lead and even substantially higher than that of silver and gold. However, the REE are very evenly distributed within the Earth's crust and significant amounts of them are found only in relatively rare minerals such as monazite, bastnasite and xenotime.

Without doubt the most striking property of the REE is their extreme chemical likeness. As Crookes put it in his lecture at the Royal Institution on Friday evening, 18 February 1887: "These earths form a group to themselves; chemically, they are so much alike that it taxes the utmost skill of the chemist to effect even a partial separation (..)" (Crookes, 1887). As a result of their chemical likeness, the REE always occur together in groups *i.e.* no mineral is known to contain significant amounts of only one REE. In 1794 Gadolin isolated the oxide or 'earth' of an unknown element from a mineral that was later named gadolinite in his honour and called it 'yttria'. In 1803 Hisinger and Berzelius, expecting to isolate yttria from the mineral cerite, instead discovered another earth, which they called 'ceria'. Initially ceria and yttria were believed to be the pure oxides of cerium and yttrium, but around 1840 Mosander demonstrated that several earths containing yet other unknown elements could be isolated from them. As there was no place for these 'rare earth' elements in Mendeleev's Periodic Table, no theoretical limit could be placed on their number. Inorganic chemists relentlessly endeavoured to determine their number by isolating possibly many new REE from the earths discovered by Mosander. In 1907 this culminated in the purification of Lu as last of the naturally occurring REE. The element Pm, which does not occur in nature (Sect. 2.2.2.), was not purified until 1945, when the new technique of ion-exchange chromatography allowed it to be isolated from uranium fission products (Marinsky *et al.*, 1947).

The chemical likeness of the REE is the result of their electronic configuration. As nuclear charge increases from La to Lu, electrons are added to the inner 4f shell rather than to an outer shell (Table 2.1). The

element	symbol	Z	configuration of outer electrons									ionic radius	abundance in mean shales	
			atom						ion (3+)					
			4f	5s	5p	5d	5f	6s	4f	5s	5p	Å	ppm	µmol/kg
lanthanum	La	57		2	6	1		2		2	6	1.061	41	295
cerium	Ce	58	1	2	6	1		2	1	2	6	1.034	83	592
praseodymium	Pr	59	3	2	6			2	2	2	6	1.013	10.1	71.7
neodymium	Nd	60	4	2	6			2	3	2	6	0.995	38	263
promethium	Pm	61	5	2	6			2	4	2	6	0.979	-	-
samarium	Sm	62	6	2	6			2	5	2	6	0.964	7.50	49.9
europium	Eu	63	7	2	6			2	6	2	6	0.950	1.61	10.6
gadolinium	Gd	64	7	2	6	1		2	7	2	6	0.938	6.35	40.4
terbium	Tb	65	9	2	6			2	8	2	6	0.923	1.23	7.74
dysprosium	Dy	66	10	2	6			2	9	2	6	0.908	5.50	33.8
holmium	Ho	67	11	2	6			2	10	2	6	0.894	1.34	8.12
erbium	Er	68	12	2	6			2	11	2	6	0.881	3.75	22.4
thulium	Tm	69	13	2	6			2	12	2	6	0.869	0.63	3.73
ytterbium	Yb	70	14	2	6			2	13	2	6	0.858	3.53	20.4
lutetium	Lu	71	14	2	6	1		2	14	2	6	0.848	0.61	3.49

Table 2.1. Name, symbol and atomic number (Z) of the fifteen rare earth elements (REE). Configuration of the outer electrons is given for the REE atom and for the REE^{3+} ion. Configuration of the inner electrons is $1s^2\ 2s^2\ 2p^6\ 3s^2\ 3p^6\ 3d^{10}\ 4s^2\ 4p^6\ 4d^{10}$ for all REE atoms and REE^{3+} ions. Ionic radius of the REE^{3+} ion is given in Ångstrom (1 Å = 10^{-10} m) for coordination number 6 (Topp, 1965). REE abundances in mean shales from Piper (1974).

4f-electrons are well shielded by 8 electrons in the 5s and 5p shells and therefore not involved in chemical bonding. All REE commonly favour the (III) oxidation state. As a result of imperfect shielding of the 4f-electrons from each other, the ionic radius of the REE^{3+} ions (and also that of differently charged REE cations) decreases gradually with increasing atomic number, an effect that is known as 'lanthanide contraction'. In Table 2.1 the ionic radius of the REE^{3+} ions is given for coordination number 6. Many chemical properties of the REE covary to some extent with ionic radius. For instance, the degree of complexation in seawater of the heavy REE (Gd-Lu), hereafter referred to as HREE, is higher than that of the light REE (La-Eu), hereafter referred to as LREE. More specifically, the coordination number of REE^{3+} ions in aqueous solution changes from about 9 for La to about 8 for Lu along an S-shaped curve with the greatest change near Gd (David, 1991). This coordination number affects both REE speciation and the degree of REE complexation in seawater, which in turn affect REE particle-reactivity *i.e.* their aptness to being scavenged. As a consequence, REE particle-reactivity decreases with increasing atomic number, seemingly also along an S-shaped curve with the greatest change near Gd (Sect. 2.2.5.).

Some of the electrons that are added to the inner 4f shell with increasing nuclear charge from La to Lu have a tendency to enter the more outward 5d shell. For La, Gd and Lu the $4f^{n-1}\ 5d^1$ state is more stable than the $4f^n$ state (Table 2.1). According to Table 2.1 Ce also has an electron in the 5d shell, yet actually its $4f^1\ 5d^1$ state and $4f^2$ state are very close together. Ce readily looses four electrons to form the Ce^{4+} ion, which is relatively stable due to its empty 4f shell. The $4f^8\ 5d^1$ state and the $4f^9$ state of Tb are also very close together, even though according to Table 2.1 it has no electron in the 5d shell. The Tb^{4+} ion, which has a half-filled 4f shell, has been shown to exist, yet Tb(IV) has never been observed in the marine environment. On the other hand, De Baar *et al.* (1985b) did find indications for a negative Tb anomaly in the eastern equatorial Pacific Ocean (see also Sect. 2.2.4.). Other REE may form divalent ions that are relatively stable, such as Eu^{2+} (half-filled 4f shell) and Yb^{2+} (exactly filled 4f shell). In the marine environment, Eu(II) may occur under special circumstances (Sect. 2.2.3.), yet Yb(II) has never been observed.

Actually, a major part of the REE exhibit more than one oxidation state but, as stated before, all commonly favour the (III) oxidation state. Most REE form REE^{3+} ions by loosing two electrons from the 6s shell and one electron from the 4f shell. However, for La, Gd and Lu the third electron resides in the 5d shell and these REE therefore have a significantly lower third ionization potential (Faktor and Hanks, 1969). In Figure 2.1 the sum of the first three ionization potentials of the REE

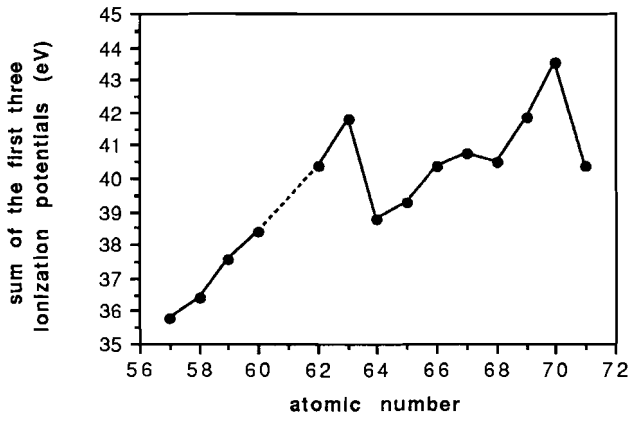

Figure 2.1. Sum of the first three ionization potentials of the REE *versus* atomic number. Note the local minima at Z=57 (La^{3+}, empty 4f shell), Z=64 (Gd^{3+}, half-filled 4f shell) and Z=71 (Lu^{3+}, completely filled 4f shell). Energies in electronvolts (1 eV = $1.6 \cdot 10^{-19}$ J). Data from Faktor and Hanks (1969).

is plotted *versus* atomic number. Local minima are evident at La, Gd and Lu. Again, the corresponding REE^{3+} ions have empty, half-filled and exactly filled 4f shells respectively (Table 2.1). Figure 2.1 is a partial expression of what is known as the 'lanthanide tetrad effect' (Nugent, 1970). A full-fledged lanthanide tetrad effect would also affect the imaginary REE^{3+} ions with quarter-filled (between Nd and Pm) and three-quarter-filled (between Ho and Er) 4f shell. There is some indication in Figure 2.1 for a local minimum between Ho and Er, yet the same cannot be asserted for the imaginary REE^{3+} ion between Nd and Pm, since the sum of the first three ionization potentials was not determined for Pm. The lanthanide tetrad effect may cause the chemical properties of certain REE and hence their particle-reactivity to deviate from a gradual variation with atomic number. For instance, Gd seems slightly more prone to complexation in seawater than adjacent REE. Consequently, the lanthanide tetrad effect may give rise to 'trivalent REE anomalies' (Sect. 2.2.4.).

Summarizing, the REE comprise a coherent group of elements that is very well suited for studying trace metal scavenging in seawater due to (i) their extreme chemical likeness, (ii) lanthanide contraction and (iii) the lanthanide tetrad effect. In nature all REE strictly occur in the (III) oxidation state, except Ce and Eu, which also occur in the (IV) and (II) oxidation state respectively.

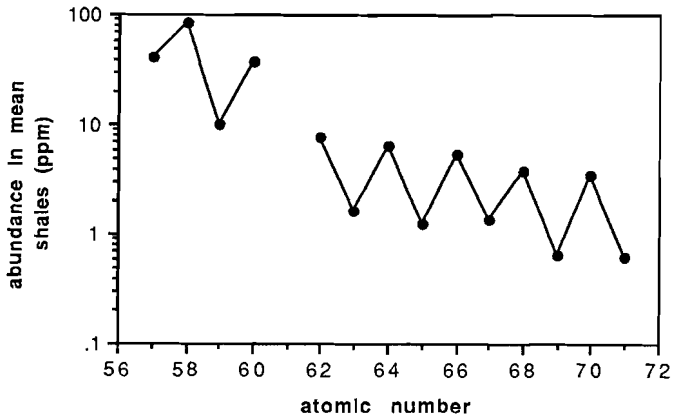

Figure 2.2. The Oddo-Harkins Rule is convincingly illustrated by the REE abundance pattern of mean shales (Piper, 1974). The element Pm (Z=61) is completely absent in nature. Data is given in Table 2.1.

2.2.2. Normalization of REE abundance patterns

During nucleosynthesis the formation of elements with even atomic number is favoured over that of adjacent elements with odd atomic number, since the latter are slightly less stable. Elements with even atomic number are therefore somewhat more abundant in the solar system than adjacent elements with odd atomic number. This universal phenomenon, which is known as the Oddo-Harkins Rule, is convincingly illustrated by the REE abundance pattern of mean shales (Fig. 2.2). The ultimate example is the total absence of the element $_{61}$Pm, which has only short-lived radioisotopes.

A similar sawtooth-shaped abundance pattern emerges when REE concentrations in a seawater sample are plotted *versus* atomic number (Goldberg *et al.*, 1963). The effect of the Oddo-Harkins Rule is so very dominant that it commonly overwhelms the effects of the geochemical REE fractionations that may occur during continental weathering, REE scavenging *etc.* However, the complete resolution of latter effects is essential for understanding REE marine geochemistry, in other words REE abundance patterns cannot be used to their full advantage as a powerful tool for the study of trace metal scavenging unless the effect of the Oddo-Harkins Rule is somehow corrected for. Such a correction or normalization is accomplished by dividing each REE concentration in a seawater sample by the corresponding REE abundance in a suitable standard.

Haskin and Haskin (1966) determined REE abundances in European Shales and the North American Shales Composite (NASC) by neutron activation analysis and compared these with REE abundances in Russian Platform Shales reported earlier by others. They found the three to be equal with respect to REE abundances within analytical and sampling errors and concluded that there is probably very little difference between the REE abundance patterns of shales from different continents. Based on this conclusion Piper (1974) introduced 'mean shales' as a suitable standard for the normalization of marine REE abundance patterns *i.e.* REE abundance patterns of seawater, marine authigenic and biogenic phases *etc.* He defined mean shales simply as the unweighted average of European Shales, NASC and Russian Platform Shales, estimating in an unspecified way those REE abundances that had not been reported by Haskin and Haskin (1966). REE abundances in mean shales as calculated by Piper (1974) are listed in ppm and in μmol/kg in Table 2.1. Gromet *et al.* (1984) determined REE abundances in NASC by isotope dilution mass spectrometry. Differences with the REE abundances reported by Haskin and Haskin (1966) were too small to warrant a recalculation of REE abundances in mean shales.

Mean shales is now the most widely used standard for the normalization of marine REE abundance patterns, since its REE abundance pattern is assumed to best represent the average input of REE into the oceans. For this assumption to be valid it is required that (i) mean shales best represents the continental crust, which is weathered to produce river-transported dissolved and particulate REE, (ii) no significant REE fractionation occurs during weathering of the continental crust and (iii) the abundance pattern of both river-transported dissolved and particulate REE is similar to that of mean shales. It seems that some of these conditions could be circumvented by taking 'mean seawater' or 'mean river water' as the standard for the normalization of marine REE abundance patterns. However, the limited amount of data presently available shows that REE abundance patterns in seawater vary strongly among ocean basins as well as with depth in individual ocean basins (*e.g.* Elderfield and Greaves, 1982; De Baar *et al.*, 1983, 1985a) and that REE abundance patterns in rivers vary strongly with pH and concentration of dissolved organic matter (*e.g.* Elderfield *et al.*, 1990). Consequently, until REE abundance patterns become available for many other ocean basins and rivers, 'mean seawater' or 'mean river water' cannot be unambiguously defined.

Sholkovitz (1988) determined the REE abundance patterns of a large number of shelf and slope sediments, which he argued to be good recorders of the terrigenous input of REE into the oceans, in order to test whether latter input is indeed best represented by mean shales. He found the sediments to be systematically enriched in the LREE relative

to the HREE, their REE abundance patterns showing a La/Lu ratio of 2.0 ± 0.2 when normalized to mean shales. Moreover, he pointed out that the average REE abundance pattern of suspended matter transported by five major rivers (Goldstein and Jacobsen, 1988) showed an average La/Yb ratio of 1.85 when normalized to mean shales. It must be noted that the mean shales normalized La/Yb ratios of suspended matter transported by some minor rivers, which were also analyzed by Goldstein and Jacobsen (1988), ranged from 0.22 (strongly HREE enriched) to 4.6 (strongly LREE enriched). Sholkovitz (1988) concluded that the REE abundance pattern of mean shales is not a good representative of the average REE input into the oceans.

Later he had to partly revoke this conclusion as it appeared that the method which had been used to dissolve the sediments had failed to dissolve a minor heavy mineral fraction, probably mainly consisting of zircon (Sholkovitz, 1990). Gromet *et al.* (1984) suggested that minor phases such as zircon may contain a major part of the total HREE content of shales. In fact, Sholkovitz (1990) found that the undissolved heavy mineral fraction, although representing a mere 0.1-0.3% of the dry sampleweight, contained between 20% and 100% of the total HREE content of the sediments. Reanalysis of the sediments, using another method for their dissolution, led to much lower mean shales normalized La/Lu ratios of 1.33 ± 0.15, in other words the sediments were significantly less different from mean shales than asserted by Sholkovitz (1988). Nevertheless, Sholkovitz (1990) maintained that the REE abundance patterns of slope and shelf sediments as he originally reported them (Sholkovitz, 1988) may still represent the average input of REE into the oceans, if REE fractionation occurs during river transport as a result of segregation of the heavy mineral fraction.

Condie (1991) recently compiled a comprehensive dataset of REE abundance patterns in shales, sediments, river suspended matter and average continental crust, analyzed with a wide variety of methods, and found no reason to abandon shales as a representative of the average input of REE into the oceans. On the other hand, mean shales as defined by Piper (1974) may overestimate the abundances of Tb, Tm and Lu in average continental crust (Murray *et al.*, 1991a; R.L. Korotev, pers. comm. as cited by Murray *et al.*, 1991b).

Clearly, the question what is the most suitable standard for the normalization of marine REE abundance patterns has yet to be settled. Mean shales is certainly a reasonable choice, not in the last place since it facilitates the comparison with previous work, as long as the normalization serves no other purpose than to eliminate the effect of the Oddo-Harkins Rule. However, although the relative behaviour of normalized REE abundance patterns within a dataset does not depend on the choice of standard, any interpretation of individual mean shales

normalized REE patterns in terms of fractionation with respect to the average input of REE into the oceans must apparently be regarded with caution.

Mean shales was used to normalize the REE abundance patterns of all seawater samples presented in this thesis. Plotted on a logarithmic vertical scale the mean shales normalized REE patterns will simply be referred to as 'REE patterns'.

2.2.3. Redox chemistry - Ce and Eu anomalies

Essentially throughout the marine environment all REE, except Ce, are strictly trivalent *i.e.* they strictly occur in the (III) oxidation state (Sect. 2.2.1.). Ce(III) can be oxidized to Ce(IV), yet De Baar *et al.* (1985a) estimated the ratio Ce^{4+}/Ce^{3+} in seawater under normal oceanic conditions (pH = 8.2, pO_2 = 0.2 atm) to be as low as 10^{-17} and suggested that the oxidation does not take place in solution. Instead, Ce^{3+} is presumably oxidized to poorly soluble $Ce(IV)O_2$ on the surface of particulate matter

$$4Ce^{3+} + O_2(g) + 6H_2O \rightarrow 4Ce(IV)O_2(s) + 12H^+ \qquad (2.1)$$

There is no reason to assume that Ce^{3+} is scavenged more strongly than the strictly trivalent REE. However, since adsorptive scavenging is a reversible process (Sect. 2.2.4.), the subsequent irreversible removal of particulate Ce(III) to poorly soluble $Ce(IV)O_2$ causes Ce to be scavenged with much higher efficiency. Consequently, seawater is typically depleted in Ce relative to the adjacent elements La and Pr (*e.g.* Elderfield and Greaves, 1982; De Baar *et al.*, 1985a; Elderfield, 1988).

This relative depletion of Ce is conveniently quantified by the Ce anomaly, Ce/Ce^*, which is defined as the ratio of the measured Ce concentration, normalized to mean shales, and the Ce concentration calculated from a linear interpolation between adjacent elements in the REE pattern. Latter concentration is usually calculated as follows

$$Ce^* = [2(La/La_{sh}) + (Nd/Nd_{sh})]/3 \qquad (2.2)$$

where the subscript sh refers to abundances in mean shales. Nd is used instead of the adjacent element Pr, since the concentration of Pr cannot be determined with IDMS (Chapter 3). The Ce anomaly can then be written as

$$Ce/Ce^* = 3(Ce/Ce_{sh})/[2(La/La_{sh}) + (Nd/Nd_{sh})] \qquad (2.3)$$

Implicitly, the Ce anomaly of mean shales is 1. In keeping with an alternative definition of the Ce anomaly, which uses $\log(Ce/Ce^*)$ rather than Ce/Ce^*, a relative depletion of Ce ($0<Ce/Ce^*<1$) is commonly referred to as a 'negative Ce anomaly' and a relative enrichment of Ce ($Ce/Ce^*>1$) as a 'positive Ce anomaly'.

Ce anomalies occur almost exclusively within the oceanic realm. Only negative Ce anomalies are found in general, positive Ce anomalies being confined to the reducing waters of anoxic basins and the reducing pore waters of anoxic sediments, where reduction of $Ce(IV)O_2$ to more soluble Ce(III) may lead to enrichment of Ce relative to La and Nd (Sect. 2.3.3.). On the other hand, De Baar *et al.* (1983) reported substantial positive Ce anomalies in surface waters of the Sargasso Sea in the western North Atlantic Ocean (33°58'N 58°05'W), which they attributed to horizontal advection of water carrying a positive Ce anomaly, presumably originating in nearby reducing sediments. This observation was recently questioned by Sholkovitz and Schneider (1991), who found no positive Ce anomalies nor evidence for the presence of reducing sediments at two stations in the Sargasso Sea (31°46'N 64°12'W and 30°35'N 63°45'W), occupied in April and May 1989 respectively (Table 3.3). Upon reanalysis of two library samples (Table 3.3) De Baar (1991) in retrospect argued that the positive Ce anomalies reported by De Baar *et al.* (1983) have become rather unlikely. Nowadays it is quite well established that open ocean waters do not exhibit positive Ce anomalies.

The only REE besides Ce that occurs in more than one oxidation state within the marine environment is Eu. Eu(III) can be reduced to Eu(II), yet in solution Eu^{2+} is predicted to be stable only under elevated pressures at temperatures in excess of 250 °C (Sverjensky, 1984). Significant Eu anomalies, defined as

$$Eu/Eu^* = 2(Eu/Eu_{sh})/[(Sm/Sm_{sh}) + (Gd/Gd_{sh})] \qquad (2.4)$$

are therefore not encountered in seawater within the normal range of oceanic conditions, nor under reducing conditions such as found in anoxic basins or in the pore waters of anoxic sediments (Elderfield and Sholkovitz, 1987; De Baar *et al.*, 1988; Sholkovitz and Elderfield, 1988; German and Elderfield, 1989; Sholkovitz *et al.*, 1989).

On the other hand, positive Eu anomalies ranging from ~10 to as high as 70 have been observed in high-temperature fluids ejected by hydrothermal vents along both the Mid-Atlantic Ridge and the East Pacific Rise (Michard *et al.*, 1983; Michard and Albarède, 1986; Michard, 1989; Derry and Jacobsen, 1990), where conditions favouring reduction of Eu(III) to Eu(II) do occur. Since REE concentrations in hydrothermal

of Eu(III) to Eu(II) do occur. Since REE concentrations in hydrothermal fluids are typically 10-10^4 times those in ambient seawater, it has been suggested that hydrothermal vents may account for a substantial fraction of the total input of REE into the oceans. This suggestion seems to be supported by the unusually high mean shales normalized Eu/Sm ratios in seawater (Sect. 2.2.5.). Elderfield (1988) showed that the high Eu/Sm ratio of the hydrothermal endmember may be preserved even after extreme dilution with ambient seawater, allowing it to be detected at great distance from the vent site, provided that Sm and Eu behave conservatively. However, during mixing of the hydrothermal fluids with ambient seawater, hydrothermally derived Fe precipitates as Fe oxyhydroxides. REE are very effectively scavenged onto these Fe oxyhydroxides (Sect. 2.2.5.), obscuring the hydrothermal REE signal away from the vent site (Olivarez and Owen, 1989; German *et al.*, 1990, 1991a). In fact, this scavenging is so effective, that REE depletion relative to ambient seawater REE concentrations was observed near hydrothermal vents in the Pacific Ocean (Klinkhammer *et al.*, 1983). Obviously, Sm and Eu do not behave conservatively during mixing of the hydrothermal fluids with ambient seawater. Consequently, the high mean shales normalized Eu/Sm ratios in seawater cannot be of hydrothermal origin. Instead, they are probably caused by the different degree of complexation of Sm and Eu in seawater. The effect of REE complexation on REE interelement ratios is discussed briefly in Section 2.2.5. and in more detail in Chapter 5.

2.2.4. Complexation - trivalent REE anomalies

In concentrated mixed electrolytes such as seawater, the mutual electrostatical attraction between cations and anions (in this Section and in Chapter 5 the latter will be referred to as 'ligands') may lead to the formation of ion pairs or complexes. Although in the terminology of Millero (1977) the term 'complex' strictly denotes a special type of ion pair, namely one held together by covalent bonds as opposed to electrostatically, throughout this thesis the terms 'ion pairing' and 'complexation' will be regarded as interchangeable. Ion pairing alters both the apparent size and, more importantly, the apparent charge of cations. Depending on the sum of the charges of its constituents, an ion pair can be either positively or negatively charged, or neutral.

In seawater most particulate matter is covered with an organic coating that contains large numbers of carboxylic acid functional groups. The hydroxide part of these groups may loose its proton and become a negatively charged 'surface ligand'. Free trace metal cations may be scavenged from seawater onto particulate matter by forming ion pairs with these (and other) surface ligands. However, trace metals

are often present in seawater mainly as ion pairs with dissolved ligands, rather than as free cations. These ion pairs, which have a net positive charge that is lower than the positive charge of the free cation, will have less affinity for the surface ligands or, if the ion pairs have a net negative charge, will even be repelled by them. Nevertheless, surface ion pairs may still form at the expense of dissolved ion pairs if the affinity of the free trace metal cation for the surface ligands is greater than for the dissolved ligands. The particle-reactivity of any trace metal therefore depends upon its tendency to form ion pairs with surface ligands *versus* its tendency to form ion pairs with dissolved ligands, as well as upon the concentrations of these ligands. Being able to determine trace metal speciation over a wide range of chemical conditions is an essential part of understanding trace metal marine geochemistry. The term 'speciation' denotes the way a trace metal is distributed among its species, including the free cation and all possible surface and dissolved ion pairs. Since very little is as yet known about REE complexation by surface ligands, the discussion in this Section and in Chapter 5 will focus mainly on the speciation of dissolved REE *i.e.* REE complexation by dissolved ligands.

A detailed discussion of ion pairing (*e.g.* Millero, 1977) is far beyond the scope of this thesis, yet the speciation of any trace metal may be calculated from simple thermodynamic principles. In most speciation calculations only ion pairs of the form $M(L_j)_n$ are considered, where M is a free trace metal cation and L_j is an organic or inorganic ligand. Any ion pair $M(L_j)_n$ is formed according to the equilibrium reaction

$$M + nL_j \leftrightarrow M(L_j)_n \qquad (2.5)$$

with equilibrium association constant

$${}_j\beta_n = [M(L_j)_n] / [M]\,[L_j]^n \qquad (2.6)$$

The total concentration M_T of the trace metal is given by the sum of the concentrations of all species

$$M_T = [M] + \sum_{nj} [M(L_j)_n] = [M] + \sum_{nj} ({}_j\beta_n\,[M]\,[L_j]^n) \qquad (2.7)$$

so that the contribution of the free trace metal cation or of any ion pair $M(L_j)_n$ to the total concentration M_T can be expressed in terms of the equilibrium association constants ${}_j\beta_n$

$$[M] / M_T = 1 / \{1 + \sum_{nj} ({}_j\beta_n\,[L_j]^n)\} \qquad (2.8a)$$

$$[M(L_j)_n] / M_T = {}_j\beta_n [L_j]^n / \{1 + \sum_{nj} ({}_j\beta_n [L_j]^n)\} \quad (2.8b)$$

If all equilibrium association constants ${}_j\beta_n$ and all concentrations $[L_j]$ are known, the speciation of the trace metal can be calculated. A detailed discussion is given in Chapter 5.

Turner *et al.* (1981) calculated the speciation of dissolved REE in seawater. At that time, equilibrium association constants had not yet been measured for most REE complexes and therefore had to be estimated by extrapolation and interpolation of available data for other metal complexes. For each ligand Turner *et al.* (1981) reported only the combined contribution of all species containing that particular ligand, without specifying their individual contributions. For instance, the contribution of species containing Cl^- to the speciation of dissolved REE was reported as the combined contribution of $REECl^{2+}$ and $REE(Cl)_2^+$, without specifying the individual contributions of these two species. They found that the REE are present in seawater mostly as ion pairs and that the fraction which is present as free cations decreases along the REE series, from 38% for La to only 5% for Lu. All REE were found to form ion pairs mainly with CO_3^{2-}, while significant fractions of the LREE were found to be present as ion pairs with Cl^- and SO_4^{2-} and of the HREE as ions pairs with OH^-. The REE thus belong to the group of trace metals that have a strong tendency to form ion pairs with CO_3^{2-} or OH^-, which includes trace metals such as Cu, Zn and Pb. Turner *et al.* (1981) suggested that this group of trace metals will have an especially strong tendency to form ion pairs with organic ligands, as has indeed been observed for Cu (Coale and Bruland, 1988) and Zn (Bruland, 1989). Nevertheless, REE complexation by organic ligands was not considered in the speciation calculations, again because the corresponding equilibrium association constants were (and still are) poorly known.

Cantrell and Byrne (1987a) estimated equilibrium association constants for all $REECO_3^+$ and $REE(CO_3)_2^-$ complexes, by fitting the logarithm of measured values for Ce, Eu and Yb to quadratic functions in Z, in analogy with oxalate, fluoride and several organic complexes of the REE, which all seem to show quadratic behaviour when plotted *versus* Z on a logarithmic scale. With the new equilibrium association constants for carbonate complexation they recalculated the speciation of dissolved REE reported by Turner *et al.* (1981). Although the results were largely similar, there were some distinct differences, mainly due to the fact that Turner *et al.* (1981) had not included $REE(CO_3)_2^-$ complexes in their calculations. Cantrell and Byrne (1987a) found that all REE are indeed mostly present in seawater as ion pairs with CO_3^{2-}

and that the fraction that is present as free cations decreases along the REE series from La to Lu. However, they found latter fraction to decrease from 7% for La to a mere 0.3% for Lu, whereas the fraction that is present as ion pairs with CO_3^{2-} was found to increase from 86% for La to 98% for Lu. The speciation of dissolved LREE appeared to be dominated by the $REECO_3^+$ complex and that of dissolved HREE by the $REE(CO_3)_2^-$ complex. The contribution of the $REE(CO_3)_2^-$ complex was found to increase gradually throughout the REE series from La to Lu at the expense of the $REECO_3^+$ complex, with Gd forming nearly equal amounts of both species. Not only complexation by F^-, but also complexation by Cl^-, SO_4^{2-} and OH^- was calculated to contribute insignificantly (<~5%) to the speciation of dissolved REE. These differences demonstrate that it is extremely important to include in the calculations all complexes that may play a role in REE speciation. Unfortunately, dissolved organic ligands can as yet not be included and it is very well possible that, in analogy with Cu and Zn, the REE are present in seawater almost exclusively as organic complexes, in which case the above results merely represent the speciation of the remaining few percent.

According to equations (2.8a) and (2.8b), REE speciation is a function of ligand concentrations $[L_j]$ and equilibrium association constants ${}_j\beta_n$. The concentrations $[L_j]$ in turn depend upon the speciation of the ligands L_j. In this context pH is an important parameter (Baes and Mesmer, 1981; Byrne *et al.*, 1988; Stanley and Byrne, 1990; Byrne and Kim, 1990), as it affects the dissociation of carboxylic acid functional groups as well as of carbonic acid (H_2CO_3) and consequently the concentrations of OH^-, CO_3^{2-} and organic ligands. For trace metals that are mainly complexed in seawater by OH^- and CO_3^{2-} (and therefore presumably also by organic ligands) such as the REE, a small change in ambient pH may have a major effect on speciation (Stanley and Byrne, 1990). The speciation of the ligands L_j also depends upon the presence of other metal cations. Even if the total concentration of a certain ligand is high, its availability for REE complexation may be low in the presence of cations that compete with the REE for that particular ligand (Hering and Morel, 1989).

The constants ${}_j\beta_n$ depend on the chemical properties of both trace metal and ligand (Turner *et al.*, 1981), yet also on external chemical and physical parameters such as temperature (Cantrell and Byrne, 1987b; Byrne *et al.* 1988), ionic strength (Chapter 5) and possibly pressure. Since the speciation of dissolved REE is apparently strongly dominated by carbonate complexation, the constants ${}_{CO_3}\beta_1$ and ${}_{CO_3}\beta_2$ are especially important. However, for most REE latter constants have as yet only been estimated from the quadratic functions of Cantrell and

Byrne (1987a). These functions (fitted to only three datapoints which obviously yields a perfect correlation) may falsely suggest a smooth variation of the $\log_j\beta_n$ with atomic number Z, as indicated by the logarithm of equilibrium association constants for fluoride complexes, which for some REE show small but significant deviations from a quadratic function in Z, even though the overall correlation seems to be quite good (Cantrell and Byrne, 1987a). Such deviations might be explained in terms of the lanthanide tetrad effect. If so, the largest deviations are to be expected for La, Gd and Lu (Sect. 2.2.1.). In fact, recent measurements have yielded values of $co_3\beta_1$ and $co_3\beta_2$ for Gd (Kim *et al.*, 1991) that are distinctly different from the values predicted by Cantrell and Byrne (1987a). The artificial smooth variation of the $\log_j\beta_n$ with Z necessarily imposes a similar smooth variation with Z upon the fraction of the total dissolved REE concentration that is present as free cations and consequently upon REE particle-reactivity (Sect. 2.2.5.), leaving no room for REE anomalies other than those resulting from redox chemistry (Sect. 2.2.3.).

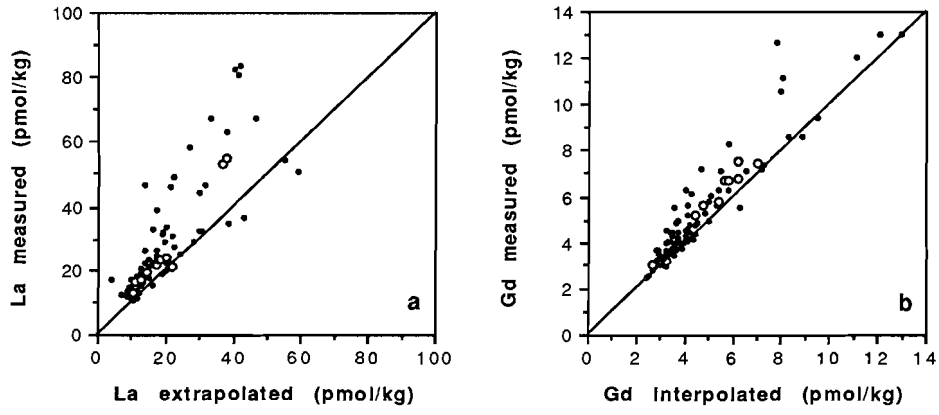

Figure 2.3. Concentrations of dissolved La (a) estimated by extrapolation from Nd and Sm in the REE pattern and of dissolved Gd (b) estimated by interpolation between Eu and Dy in the REE pattern *versus* concentrations actually measured. Data from the eastern North Atlantic Ocean (Elderfield and Greaves, 1982), the western North Atlantic Ocean (De Baar *et al.*, 1983), the eastern equatorial Pacific Ocean (De Baar *et al.*, 1985a,b), the Northwest Indian Ocean (German and Elderfield, 1990), the Cariaco Trench (De Baar *et al.*, 1988) and Saanich Inlet (German and Elderfield, 1989). For samples analyzed with INAA-γ, La was extrapolated from Pr and Sm (De Baar *et al.*, 1983) and Gd was interpolated between Eu and Ho (De Baar *et al.*, 1983, 1985a,b). Open symbols represent data from anoxic waters. Solid lines represent equal estimated and measured concentrations.

Trivalent REE anomalies have actually been reported on several occasions. Masuda and Ikeuchi (1979) found indications for a full-fledged tetrad effect in a single seawater sample from the Japan Sea. De Baar *et al.* (1985b) found positive Gd anomalies and negative Tb anomalies in seawater samples from the eastern equatorial Pacific Ocean, although, in retrospect, these negative Tb anomalies may be an artefact of the mean shales normalization (Sect. 2.2.2.). Concentrations of La and Gd in seawater samples from various marine anoxic basins and open ocean stations are plotted in Figure 2.3 *versus* concentrations estimated by extrapolation or interpolation in the corresponding REE patterns. Clearly, the measured concentrations of La and Gd are in general significantly higher than the estimated concentrations. One could say that these samples are characterized by positive La and Gd anomalies (see also De Baar *et al.*, 1991). On the other hand, the negative Lu anomaly that seems to characterize many seawater samples (see this thesis and various references used in Fig. 2.3) is again probably an artefact of the mean shales normalization (Sect. 2.2.2.).

Improvements to the REE speciation model, for instance including complexation by dissolved organic ligands and organic surface ligands and using measured rather than estimated equilibrium association constants for all REE, may eventually lead to a theoretical basis for trivalent REE anomalies (Byrne and Kim, 1990; Kim *et al.*, 1991). If the positive La anomalies in Figure 2.3 are a real feature rather than some analytical artefact, then a linear interpolation between La and Nd in the REE pattern may not be the best estimate of Ce^* (Sect. 2.2.3.) and the Ce anomaly may have to be redefined. In any case, an accurate model of REE speciation will help to further the understanding of REE marine geochemistry in general and of REE scavenging in particular.

2.2.5. REE scavenging and interelement ratios

REE scavenging is the net effect of a combination of chemical processes that either tend to keep the REE in solution or make them adhere to particulate matter. The REE become more stable in solution by forming complexes with dissolved organic and inorganic ligands, which are abundantly present in seawater. The same process makes them adhere to particulate matter, if complexes are formed not with dissolved ligands, but with ligands that are present as functional groups on the surface of particulate matter (Sect. 2.2.4. and Chapter 5). Where waters containing high concentrations of reduced Mn and Fe come into contact with oxic seawater, such as near hydrothermal vent systems (Klinkhammer *et al.*, 1983; German *et al.*, 1990, 1991a) and at the oxic-anoxic interface of marine anoxic basins (De Baar *et al.*, 1988;

German and Elderfield, 1989), coprecipitation with Mn and Fe oxyhydroxides seems to be the most important mechanism for REE removal. Although undoubtedly latter process also contributes to REE scavenging under normal oceanic conditions, Byrne and Kim (1990) have shown that the main features of open ocean REE patterns can be reproduced with a model of REE scavenging that is based solely on complexation (Chapter 5).

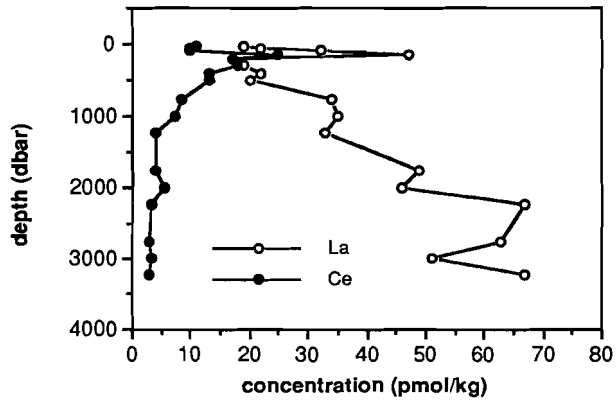

Figure 2.4. Vertical distributions of dissolved La and Ce at a station in the eastern equatorial Pacific Ocean, illustrating the contrasting marine geochemistry of Ce and the trivalent REE. Data from De Baar *et al.* (1985a).

Ce is a unique member of the REE series, since its removal from seawater is not dominated by complexation, yet by its own redox chemistry (Sect. 2.2.3.). As a result, the marine geochemistry of Ce is notably different from that of the trivalent REE and more like that of Mn and Fe, which have a similar tendency to form poorly soluble oxides. Figure 2.4 shows vertical distributions of dissolved La and Ce in the eastern equatorial Pacific Ocean as reported by De Baar *et al.* (1985a). Throughout the watercolumn the concentration of dissolved La increases, whereas that of Ce decreases with depth. The vertical distributions in Figure 2.4 are generally interpreted as follows. La is scavenged mainly in the upper part of the watercolumn, where most of the organic matter is produced (Sect. 2.3.1.), by forming complexes with the ligands that are present on the surface of the organic matter. As the organic matter settles through the watercolumn it is oxidized by bacteria (Sect. 2.3.1. and 2.3.2.) and La is released back into solution.

Ce scavenging on the other hand is dominated by oxidation and precipitation which continues throughout the watercolumn as long as oxic conditions are maintained. Ce is depleted in seawater relative to the trivalent REE, which are less effectively scavenged, and becomes more depleted as it continues to be scavenged with depth, while the trivalent REE are released back into solution. The relative depletion of Ce is clearly visible in the REE pattern as a negative Ce anomaly (Sect. 2.2.3.). The Ce anomaly is a sensitive indicator of the difference in behaviour between Ce and the trivalent REE. Since this difference is completely attributable to Ce redox chemistry, the Ce anomaly enables the marine geochemist to single out redox chemistry from all other processes that contribute to Ce scavenging.

Inasmuch as scavenging of the trivalent REE is dominated by complexation, it is not equally efficient for all of them, due to the variation of some of their chemical properties with atomic number Z (Sect. 2.2.1.). For example, with increasing Z the REE show an increasing tendency to form complexes (Sect. 2.2.4.). The HREE have a stronger tendency to form complexes with dissolved ligands, which makes them more stable in solution, yet at the same time they have a stronger tendency to form complexes with organic surface ligands, which causes them to be removed from seawater. The net effect appears to be that the HREE are scavenged *less* effectively than the LREE (Chapter 5). Consequently, seawater is enriched in the HREE relative to mean shales, in other words seawater HREE/LREE ratios are generally higher than the corresponding HREE/LREE ratios in mean shales.

The gradual variation of chemical properties with Z is mainly caused by lanthanide contraction (Sect. 2.2.1.). The ionic radius in Table 2.1 is a very smooth, almost linear function of Z. Cantrell and Byrne (1987a) suggested that the logarithm of the equilibrium association constants for carbonate complexes is a weakly quadratic, almost linear function of Z. The same seems to hold for the logarithm of the equilibrium association constants for hydroxide complexes, except for major deviations at Z=57 (La) and Z=64 (Gd) which may be attributable to the lanthanide tetrad effect (Sect. 2.2.1.). In fact, the assumption that seawater REE patterns themselves may be approximated with straight lines was used to calculate the trivalent REE anomalies in Figures 2.3a and b. If so, then REE interelement ratios are expected to deviate increasingly from the corresponding ratios in mean shales with increasing difference in Z. However, Elderfield (1988) observed that, whereas the Sm/Nd ratio ($\Delta Z=2$) of seawater samples from the western Mediterranean and the Pacific and Atlantic Oceans could not be distinguished from the Sm/Nd ratio in mean shales, the Eu/Sm ratio ($\Delta Z=1$) of the same samples was persistently higher than its mean shales counterpart. In Section 2.2.3. it was argued that this cannot be

due to worldwide dispersion of hydrothermal fluids containing a large excess of Eu. In that case the Eu/Sm ratio should decrease with increasing distance from the vent site, whereas it appears to be fairly constant throughout the oceans.

Probably, the high Eu/Sm ratio in seawater is caused by more effective scavenging of Sm than of Eu, as a result of subtleties in the Z-dependence of REE chemical properties. It can be shown that the Yb/Er ratio ($\Delta Z=2$) in seawater, like the Sm/Nd ratio, does not deviate appreciably from its mean shales counterpart. The REE patterns are nearly flat at high Z (Dy-Lu) as well as at low Z (La-Sm), hence seawater can only be HREE enriched relative to mean shales if the REE pattern has a substantial positive slope roughly between Eu and Tb, in agreement with the observed high Eu/Sm ratios. Seawater REE patterns thus have an elongated S-shape that strongly reminds of the way the coordination number of REE^{3+} ions in aqueous solution depends on Z (Sect. 2.2.1.). The coordination number partly determines the state of REE cations in solution, affecting both REE hydration and REE complexation (Helm and Merbach, 1991) and therefore indirectly the shape of seawater REE patterns.

HREE/LREE ratios and REE scavenging are apparently intimately related, yet an interpretation of one in terms of the other is by no means straightforward. Scavenging causes the input of REE into the oceans, which on average has a mean shales-like REE pattern (Sect. 2.2.2.), to be redistributed between the dissolved and the particulate reservoir. The REE fractionation that occurs during this redistribution causes seawater to be enriched in the HREE and strongly depleted in Ce. It has therefore often, yet wrongly, been assumed that the REE pattern of marine particulate matter must be characterized by LREE enrichment and a positive Ce anomaly. Notwithstanding the dearth of particulate REE data presently available it can safely be said that particulate matter in general does not show LREE enrichment nor positive Ce anomalies. Murphy and Dymond (1984) found particulate matter from the eastern equatorial Pacific Ocean to have a seawater-like REE pattern, which seems to be in contradiction with the fact that LREE are scavenged more effectively than HREE and that Ce is scavenged more effectively than the strictly trivalent REE. However, when normalized to ambient seawater the particulate matter did show both a positive Ce anomaly and LREE enrichment.

The confusion arises because each REE has a different residence time in seawater. If the input of REE to the oceans has a mean shales-like REE pattern and if the oceans are in steady state with respect to REE concentrations, then implicitly the output of REE to the sediments also has a mean shales-like REE pattern. Hence, since the residence times in seawater of Yb and Ce are longer and shorter respectively than

for instance that of Nd, it follows that $(Yb/Nd)_{sw}>(Yb/Nd)_{sh}$ and $(Ce/Nd)_{sw}<(Ce/Nd)_{sh}$, where the subscripts sw and sh refer to seawater and mean shales respectively, in agreement with what is actually found (De Baar *et al.*, 1985a). The REE are scavenged from seawater that is HREE enriched and although the HREE are less effectively scavenged than the LREE in a relative sense, they may be more effectively scavenged in an absolute sense simply because there is more of them. In the end the two effects should cancel, causing the ouput of REE to the sediments to have a mean shales-like REE pattern on average. Of course, conditions like steady state and the mean shales-like REE pattern of the input of REE into the oceans only apply on a global scale over long periods of time. On a more local scale, for instance in regions where a significant fraction of the REE input into the surface waters is from wind-blown terrigenous debris with an REE pattern that is not mean shales-like (*e.g.* Elderfield and Greaves, 1982) or at the oxic-anoxic interface of marine anoxic basins where REE cycling is extremely rapid, REE patterns of both seawater and particulate matter may deviate considerably from those generally encountered in the open ocean.

In this thesis two REE interelement ratios will be used regularly. One is the Ce/Nd ratio which may replace the Ce anomaly when La data are scanty or inaccurate. The other is the Yb/Nd ratio which was chosen to serve as HREE/LREE ratio rather than the more widely used Er/Nd ratio, since Yb can be measured more accurately than Er (Chapter 3). In general, La and Lu are not used for calculating seawater HREE/LREE ratios because of the analytical problems with La (Chapter 3) and the possible inaccuracy of the Lu abundance in mean shales (Sect. 2.2.4.). The Yb/Nd ratio will be interpreted scarcely and never in a quantitative sense. Interpretations will be limited to assessing its value relative to the Yb/Nd ratio of mean shales as a qualitative measure of the degree of REE complexation and scavenging throughout the watercolumn, focussing on its behaviour at the oxic-anoxic interface.

2.3. REE cycling in marine anoxic basins

2.3.1. Formation of marine anoxic basins

In the photic layer, that part of the watercolumn where sunlight penetrates, phytoplankton produces organic matter by photosynthesis. Bacteria provide in their need for energy by oxidizing this organic matter, thereby consuming oxygen, which is used as the primary electron acceptor. If its consumption by bacteria were not balanced by a steady supply, oxygen would soon become depleted, leading to anoxic *i.e.* reducing conditions throughout the oceans. However, oxygen is

constantly supplied to the surface layer of the oceans by direct exchange with the atmosphere and by photosynthesis. The oxygenated surface seawater is subsequently transported to depth, mainly by advection. Although oxidation continues as the organic matter settles out of the photic layer, most of it takes place within the photic layer itself and the rate of oxidation decreases so strongly with depth that even in the deep Pacific Ocean, where circulation is sluggish, the advective supply of oxygen is sufficient to maintain oxidizing conditions. Nevertheless, exceptional hydrographic circumstances may disturb the subtly poised balance between supply and consumption and cause various degrees of oxygen depletion. As oxygen becomes depleted, the oxidation of organic matter proceeds by a sequence of reactions with other electron acceptors, which are in turn successively depleted until finally organic matter is oxidized by bacteria that reduce sulfate to sulfide (Sect. 2.3.2.). The presence of measurable sulfide ($\geq$ 1 μM), evidence of strongly reducing conditions, is generally taken as the criterion for terming a body of water 'anoxic'. A body of water with both oxygen and sulfide below the normal limits of detection (~10 μM for oxygen) is generally termed 'suboxic'.

Oxygen depletion is usually caused by stagnation of the oxygen supply, which results when a body of water is cut off from circulation. Several hydrographic circumstances may lead to this situation. First, a body of water may be trapped behind a shallow sill, such as occurs for instance in the Framvaren Fjord in southern Norway, the Cariaco Trench off Venezuela and the Saanich Inlet in British Columbia, Canada. In Framvaren Fjord (sill depth 2 m) and in the Cariaco Trench (sill depth 146 m) water below the depth of the sill cannot freely exchange with the open ocean and permanent anoxic conditions prevail below a depth of 18 m and 300 m respectively. Saanich Inlet (sill depth 70 m) is an example of a seasonally anoxic basin. Between late winter and summer anoxic conditions develop gradually in water that is trapped behind the sill. In early autumn the basin is flushed when upwelling along the coast outside the basin causes oxic water to spill over the sill.

Second, a body of water may be separated from the overlying oxic seawater by a pycnocline, a sharp density gradient that is usually the result of a major salinity gradient. Vertical mixing is strongly restricted by the pycnocline and oxygen is supplied to the underlying body of water mainly by diffusion, which is a very slow process. In the Bannock and Tyro Basins in the eastern Mediterranean and in the Orca Basin in the Gulf of Mexico, extreme pycnoclines separate large bodies of anoxic brine, formed by dissolution of evaporite deposits, from the overlying oxic seawater (Chapter 4). The Black Sea is anoxic below a pycnocline that is maintained by the simultaneous inflow of fresh

water from major rivers into the surface layer and of Mediterranean seawater at depth (Chapter 6).

A detailed account of circumstances that lead to the formation of marine anoxic basins was presented by Deuser (1975).

2.3.2. The sequence of oxidation reactions

The oxidation of organic matter can be written in its most simple form as oxidation half-reaction (2.9), with organic matter represented for convenience by CH_2O, the sixth of a glucose molecule

$$CH_2O + H_2O \rightarrow CO_2 + 4H^+ + 4e^- \qquad (2.9)$$

The four electrons on the right hand side of reaction (2.9) are not actually released, but transferred to an electron acceptor or oxidant, a redox element in some oxidized form, by simultaneous reduction of that oxidant. In seawater numerous oxidants are available. Theoretically, these oxidants will be used in order of decreasing $\Delta G°$, the change in free energy per mole of CH_2O. Under oxic conditions, oxygen is the oxidant yielding the largest $\Delta G°$ and the oxidation of organic matter takes the form of reaction (T2.2-1) in Table 2.2. When oxygen is depleted, the oxidation of organic matter continues with the oxidant yielding the next largest $\Delta G°$ and so on, until either all available oxidants or the organic matter itself is depleted. A theoretical sequence of oxidants may be predicted from standard values of $\Delta G°$ for a large number of possible oxidation reactions (Froelich *et al.*, 1979; Berner, 1980). Such a sequence is shown in Table 2.2. When oxygen is depleted, nitrate, Mn oxides, Fe oxides and sulfate successively become the major oxidant. Finally, when even sulfate is depleted, organic matter may decompose directly into carbon dioxide and methane by serving, as it were, as its own oxidant. Latter process is generally referred to as 'disproportionation'.

It must be noted that the free energy changes $\Delta G°$ on which the sequence in Table 2.2 is based are not sharply defined, since for most oxidation reactions the actual oxidant is not precisely known. For instance, for the oxidation of organic matter by Fe(III), $Fe(OH)_3$ was chosen to be the oxidant in reaction (T2.2-5), yet one might also consider a reaction where Fe_2O_3 is the oxidant. However, such a reaction would correspond to a different value of $\Delta G°$. Therefore, each $\Delta G°$ in Table 2.2 represents a range of values, which may overlap with that of the next or previous reaction and a different choice of oxidants may lead to subtle changes in the sequence of oxidation reactions. Nevertheless, broadly speaking the sequence of oxidation reactions is

reaction	ΔG° kJ / (mol CH_2O)	
$CH_2O + O_2 \rightarrow CO_2 + H_2O$	-475	(T2.2-1)
$5CH_2O + 4NO_3^- \rightarrow 2N_2 + 4HCO_3^- + CO_2 + 3H_2O$	-448	(T2.2-2)
$CH_2O + 5H_2O + 11CO_2 + 4CeO_2 \rightarrow 4Ce^{3+} + 12HCO_3^-$	-445	(T2.2-3a)
$CH_2O + 11CO_2 + 4Ce(OH)_4 \rightarrow 4Ce^{3+} + 12HCO_3^- + 3H_2O$	-427	(T2.2-3b)
$CH_2O + 3CO_2 + H_2O + 2MnO_2 \rightarrow 2Mn^{2+} + 4HCO_3^-$	-349	(T2.2-4)
$CH_2O + 7CO_2 + 4Fe(OH)_3 \rightarrow 4Fe^{2+} + 8HCO_3^- + 3H_2O$	-114	(T2.2-5)
$2CH_2O + SO_4^{2-} \rightarrow H_2S + 2HCO_3^-$	-77	(T2.2-6)
$2CH_2O \rightarrow CH_4 + CO_2$	-58	(T2.2-7)

Table 2.2. Theoretical sequence of reactions for the bacterial oxidation of organic matter (CH_2O) according to Berner (1980). Data for reactions (T2.2-3a,b) from Elderfield and Sholkovitz (1987) and from De Baar *et al.* (1988). Sucrose and fine-grained birnessite were taken to represent CH_2O and MnO_2 respectively (Berner, 1980).

well established and has actually been observed in the eastern equatorial Atlantic Ocean, in the pore waters of sediments overlain by oxic seawater (Froelich *et al.*, 1979).

Besides the major oxidants listed in Table 2.2, seawater contains a large number of minor oxidants (Emerson *et al.*, 1979; Murray *et al.*, 1983). These minor oxidants contribute insignificantly to the oxidation of organic matter, yet reversely their simultaneous reduction largely dominates the vertical distributions in marine anoxic basins of the corresponding redox elements, among which are many trace metals (Sect. 2.3.3.). One of these trace metals is Ce, which is the only redox element within the REE series as far as the marine environment is concerned (Sect. 2.2.3.). Two possible oxidation reactions, with $Ce(IV)O_2$ and $Ce(IV)(OH)_4$ as the oxidants, are presented in Table 2.2. Reactions of this kind were already known to chemists at the beginning of this century (Job, 1902, 1903). Elderfield and Sholkovitz (1987) estimated the free energy changes to be $\Delta G°$= -445 kJ/(mol CH_2O) and $\Delta G°$= -427 kJ/(mol CH_2O) for $Ce(IV)O_2$ and $Ce(IV)(OH)_4$ respectively, which ranks both of them below nitrate ($\Delta G°$= -448 kJ/(mol CH_2O)) and above Mn oxides ($\Delta G°$= -349 kJ/(mol CH_2O)). Although this is a logical first step towards resolving the mechanisms underlying Ce cycling at the oxic-anoxic interface of marine anoxic basins, more elaborate thermodynamic modelling is required in order to determine what Ce solid phase is the actual oxidant.

Assuming $Ce(IV)O_2$ to be the oxidant, De Baar *et al.* (1988) attempted to calculate the total dissolved concentrations of Ce above and below the oxic-anoxic interface in the Cariaco Trench. A Ce phase diagram showed that only the Ce^{3+} ion and solid $Ce(IV)O_2$ can exist within the oceanic ranges of $p\varepsilon$ and pH and solid $Ce(IV)(OH)_4$ was therefore rejected as a possible oxidant. They found the calculated equilibrium total dissolved Ce concentrations to be much higher in oxic water and much lower in anoxic water than actually measured concentrations, which would be consistent with kinetic hindrance for oxidative formation of $Ce(IV)O_2$ as well as for its reductive dissolution. Although this is quite reasonable, some solid Ce phase other than $Ce(IV)O_2$ cannot be ruled out. De Baar *et al.* (1988) speculated on the possibility that a solid solution of Ce in Mn and Fe oxyhydroxides is the oxidant. Unfortunately, Mn and Fe oxyhydroxides, let alone solid solutions of Ce in the same, are poorly defined and thermodynamic data regarding their reduction are scarce if not absent.

The fact that it is often uncertain what solid phase or dissolved species is the actual oxidant and that thermodynamic data are scarce, makes thermodynamic modelling extra tedious and the results less meaningful. Therefore, a simpler approach is warranted. One such

approach is to compare the predicted sequence of oxidants in Table 2.2 with the observed sequence of chemical gradients induced by the oxidation reactions (Froelich *et al.*, 1979; Elderfield and Sholkovitz, 1987). For instance, reaction (T2.2-1) leads to decreasing oxygen and increasing nitrate concentrations, reaction (T2.2-4) to increasing concentrations of dissolved Mn and reaction (T2.2-6) to decreasing sulfate and increasing sulfide concentrations. If the sequence of oxidants in Table 2.2 is correct, then the dissolved Ce gradient is roughly expected to be found slightly below the nitrate maximum and well above the dissolved Mn gradient.

As was discussed in Section 2.3.1., the disappearance of oxygen defines the bottom of the oxic layer, while the sulfide gradient defines the top of the anoxic layer. The oxidation reactions of interest thus take place within the suboxic layer, which forms the transition between the oxic and the anoxic layer. In the sediments described by Froelich *et al.* (1979) the suboxic layer was found to have a vertical extent of at least 50 cm. The excellent vertical resolution that may be obtained by squeezing pore water from 0.5-2.0 cm thick slices of sediment made it relatively easy to produce profiles of pH, total CO_2, nitrate/nitrite/ammonium, phosphate, sulfate/sulfide and dissolved Mn and Fe with sufficient detail to resolve the corresponding sequence of gradients. On the other hand, for determining accurate dissolved REE concentrations in pore waters, large sample volumes are needed which cannot be obtained from thin slices of sediment unless they are cut from very large sediment cores. Although such large sediment cores are difficult to process, pore water profiles of dissolved REE with a vertical resolution of ≥2 cm have actually been obtained for sediments overlain by oxic seawater (Elderfield and Sholkovitz, 1987; Sholkovitz *et al.*, 1989). Unfortunately, the sediments were found to be completely anoxic within 1 mm below the seawater-sediment interface.

At the oxic-anoxic interface of marine anoxic basins, where the requirement of large sample volumes can be met without problem, the suboxic layer is generally found to extend over 1-10 m, about ten times the vertical extent of the suboxic layer in the sediments described by Froelich *et al.* (1979). However, the vertical resolution that may be obtained with conventional water sampling systems is usually no better than 5 m, which is still insufficient for the sequence of gradients to be resolved. Even the pump-profiling system mentioned in Chapter 6 has a vertical resolution of no better than 2 m under ideal circumstances. Consequently, a suboxic layer with a much larger vertical extent is needed. Broad suboxic layers have been observed in areas where upwelling leads to very high productivity. German and Elderfield (1990) reported vertical distributions of dissolved REE in such an area, the Northwest Indian Ocean (NWIO). Within the NWIO

suboxic layer, which extends over more than 1000 m and is underlain by ambient seawater, evidence of nitrate reduction was found, together with broad maxima of dissolved Mn and Fe (Saager *et al.*, 1989), yet anoxic conditions do not occur. Notwithstanding the excellent vertical resolution that was obtained, relative to the large vertical extent of the suboxic layer, the sequence of gradients could not be resolved, since it appeared to be compressed within a thin layer below the oxic-suboxic interface. Interpretation of the sequence of gradients was further complicated by horizontal advection of water from different sources at several depths within the suboxic layer, which at some stations gave rise to multiple maxima of dissolved Mn and Ce.

Even when circumstances are seemingly ideal for resolving the sequence of gradients induced by the oxidation of organic matter, it remains a painstaking task for a number of reasons. First, the oxidation of organic matter is not the result of spontaneous chemical reactions, yet the work of bacteria that reside within the suboxic layer. Deuser (1975) pointed out that "(..) it is not clear whether bacterial populations, which are always mixtures of diverse types having specific capabilities, obey or even come close to obeying thermodynamic laws." Consequently, thermodynamic equilibrium is in general not a valid assumption (see also Emerson *et al.*, 1979). The 'specific capabilities' that Deuser referred to is the ability to mediate one of the oxidation reactions in Table 2.2. One could imagine the suboxic layer to be stratified in agreement with the sequence of oxidants in Table 2.2 into a number of sharply defined layers, each layer harbouring a single type of bacteria mediating a specific oxidation reaction. However, it is possible that one type of bacteria can mediate more than one reaction or that circumstances allow various types of bacteria to coexist, so that two or more oxidation reactions occur simultaneously within the same layer, causing gradients to overlap instead of forming a neat sequence.

Second, the sequence of gradients may partly be obscured by chemical reactions that are not related to the oxidation of organic matter. Examples of such reactions are precipitation of Fe sulfides and Mn carbonates, cycling of phosphate along with the cycling of Fe and cycling of Ce along with the cycling of Mn and Fe (Sect. 2.3.3.).

Finally, slow oxidation of reduced species that diffuse upward into the oxic water may cause them to penetrate where they are no longer thermodynamically stable and their gradients to extend far above the depth where the corresponding oxidation reaction is taking place.

In Chapter 6, where an attempt is made to resolve the sequence of oxidation reactions in Table 2.2 from the sequence of gradients

observed in the suboxic layer of the Black Sea, focussing especially on Mn, Fe and Ce, these complications are discussed in more detail.

2.3.3. REE cycling at the oxic-anoxic interface

Based on their vertical distributions in marine anoxic basins trace metals can roughly be divided into two groups (Jacobs and Emerson, 1982). Trace metals in the first group, for instance Cu, Zn and Cd, form poorly soluble sulfides under anoxic (sulfidic) conditions. Consequently, their dissolved concentrations decrease at the oxic-anoxic interface. Deeper into the anoxic water their dissolved concentrations may increase again due to complexation by sulfide anions. Trace metals in the second group, for instance Mn and Fe, are mainly present in oxic seawater as poorly soluble oxides. Under anoxic conditions they are reduced to a more soluble oxidation state. Consequently, their dissolved concentrations increase at the oxic-anoxic interface. Deeper into the anoxic water their dissolved concentrations may decrease again due to oversaturation with respect to their least soluble salt, which may, but need not, be a sulfide.

In view of its marine geochemistry, which is very similar to that of Mn and Fe, one would expect Ce to belong to the second group. In oxic seawater, Ce is presumably mainly present as a poorly soluble oxide, $Ce(IV)O_2$ (Sect. 2.2.3.). Under anoxic conditions Ce(IV) is reduced to Ce(III), which appears to be quite soluble, even in the presence of sulfide. The first reported vertical distribution of dissolved Ce in a marine anoxic basin, the Cariaco Trench off Venezuela (De Baar *et al.*, 1988), was strikingly similar to the vertical distributions of dissolved Mn and Fe, which had previously been reported by Jacobs *et al.* (1987), indicating that Ce indeed belongs to the second group. Concentrations of dissolved Mn, Fe and Ce were all found to increase strongly at the oxic-anoxic interface. Throughout the anoxic water, concentrations of dissolved Mn and Ce remained nearly constant, whereas concentrations of dissolved Fe decreased with depth, most likely as a result of Fe sulfide precipitation. Surprisingly, dissolved concentrations of the other REE were also found to increase substantially at the oxic-anoxic interface. This observation was rather unexpected, since, with the exception of Ce, all REE are strictly trivalent throughout the marine environment (Sect. 2.2.3.) *i.e.* they cannot, like Mn, Fe and Ce, be reduced to a more soluble oxidation state under anoxic conditions.

The remarkable similarities between the vertical distributions of the trivalent REE on the one hand and those of Mn, Ce and, to a lesser extent, Fe on the other hand, led De Baar *et al.* (1988) to propose the following model for the cycling of strictly trivalent REE at the oxic-anoxic interface (Fig. 2.5). Poorly soluble Mn oxides are presumably

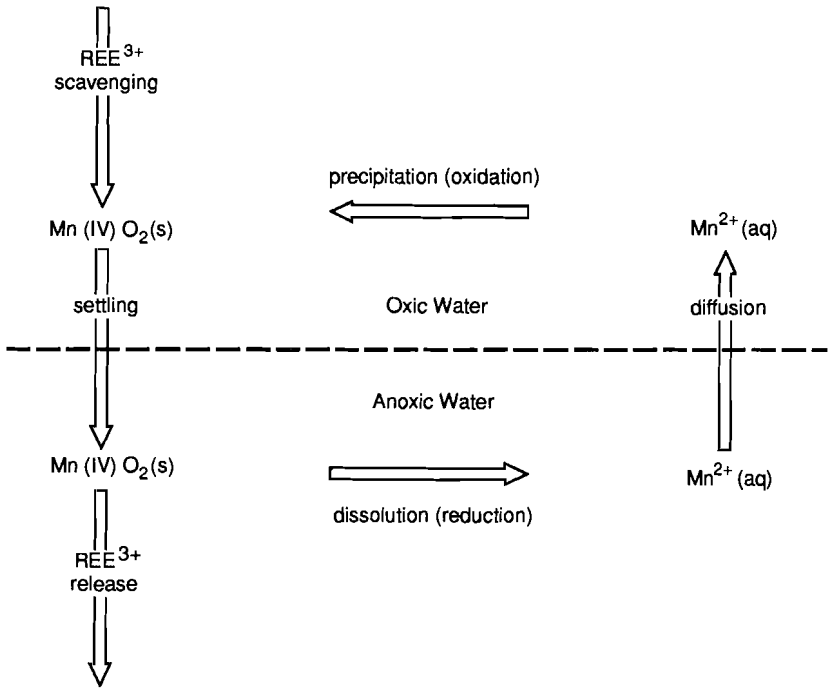

Figure 2.5. Schematic representation of the mechanism that is assumed to underlie the vertical transport of trivalent REE across the oxic-anoxic interface in marine anoxic basins. After De Baar *et al.* (1988). See text for explanation.

present as coatings on the surface of particulate matter that settles through the oxic watercolumn. At the oxic-anoxic interface, Mn(IV) is reduced to Mn(II), causing the Mn oxides to dissolve. The resulting dissolved Mn concentration gradient leads to an upward diffusion of dissolved Mn across the oxic-anoxic interface. In the oxic water, Mn(II) is oxidized again to Mn(IV), which precipitates as Mn oxides. The cycle is closed by renewed settling of the freshly precipitated Mn oxides across the oxic-anoxic interface. Although only Mn cycling is described here and depicted in Figure 2.5, the model applies to the cycling of Fe and Ce as well. In addition, dissolved Fe is removed below the oxic-anoxic interface by precipitation of Fe sulfides. The reduction of Mn, Fe and Ce oxides at the oxic-anoxic interface, and possibly also the oxidation of dissolved Mn, Fe and Ce just above the oxic-anoxic interface, is largely mediated by bacteria. Therefore, the dissolved Mn, Fe and Ce concentration gradients should be vertically ordered roughly in agreement with the sequence of oxidation reactions predicted in

Section 2.3.2. However, in the Cariaco Trench the transition from oxic to anoxic conditions occurs within at most a few meters and the sequence of oxidation reactions cannot be resolved *i.e.* the dissolved Mn, Fe and Ce concentration gradients appear to be coinciding.

The trivalent REE enter the cycle just above the oxic-anoxic interface, where they are scavenged onto the freshly precipitated Mn and Fe (and Ce?) oxides, either by coprecipitation or by adsorption. At the oxic-anoxic interface they are released as the Mn and Fe oxides dissolve, leading to a downward transport that is partly balanced by upward diffusion of dissolved REE across the oxic-anoxic interface as a result of the dissolved concentration gradients (Fig. 2.5). If Ce were strictly trivalent, its cycling at the oxic-anoxic interface would be driven by that of Mn and Fe, just like that of the other trivalent REE and most likely this process actually occurs. However, on top of that, Ce cycling is driven by its own redox chemistry. Consequently, Ce should be cycled more effectively than the strictly trivalent REE and this was in fact observed by De Baar *et al.* (1988). Directly above the oxic-anoxic interface Ce is scavenged more effectively than the trivalent REE, which locally leads to an even more negative Ce anomaly *i.e.* an even larger Ce depletion than in the overlying watercolumn. Directly below the oxic-anoxic interface Ce is released more effectively than the trivalent REE, which causes the Ce anomaly to become less negative, yet rarely leads to positive Ce anomalies (De Baar, 1991). The latter has as yet only been observed in the hypersaline anoxic Bannock Basin, where so much Ce is released below the oxic-anoxic interface that a substantial positive Ce anomaly has developed throughout the upper brine (Chapter 5). Usually no Ce anomaly or a minor negative Ce anomaly is found throughout the anoxic layer, indicating that Ce is present mainly as Ce^{3+} and behaves more or less as the trivalent REE.

Apart from the concomitant concentration gradients of dissolved Mn, Fe and REE at the oxic-anoxic interface, the model of De Baar *et al.* (1988) was supported by the presence, just above the oxic-anoxic interface, of a large standing crop of particulate Mn and Fe, coinciding with distinct concentration minima of the dissolved REE. Vertical distributions of the particulate REE also showed modest concentration maxima just above the oxic-anoxic interface. These observations have recently been confirmed by German and Elderfield (1989), who reported vertical distributions of dissolved and particulate REE in the seasonally anoxic Saanich Inlet.

CHAPTER 3 Methods

3.1. Introduction

In Chapter 2 the significance of studying REE marine geochemistry as a means to learn more about trace metal marine geochemistry and trace metal scavenging in general was discussed in detail. For an adequate study of REE marine geochemistry it is required that REE concentrations in seawater can be determined with great accuracy and precision. However, the determination of the very low concentrations of the REE in seawater, which contains large amounts of interfering elements, defies a simple analytical approach. Much effort was therefore spent during the past 30 years on finding ways of preconcentrating the REE and separating them from the seasalt cations (Sect. 3.2.1.) and other interfering elements (Sect. 3.2.2.).

The number of analytical techniques sensitive enough to determine the very low concentrations of the REE in seawater, without having to preconcentrate excessively large samples, is limited. The only analytical technique available to the pioneers was instrumental neutron activation analysis (INAA) in combination with β-counting (Goldberg *et al.*, 1963; Høgdahl *et al.*, 1968), requiring laborious separation of individual REE radioisotopes. The development of INAA in combination with γ-counting obviated the need for such separations (De Baar, 1983; De Baar *et al.*, 1985a,b). INAA-γ is capable of determining the concentrations of 12 out of the 14 REE that occur in seawater, with reasonable accuracy and precision.

Isotope dilution mass spectrometry (IDMS), which was developed during the same time as INAA-γ, is now the most widely used method for the determination of REE concentrations in seawater. A great advantage of IDMS is that quantitative recovery of the REE from a seawater sample is not essential for an accurate determination of their concentrations *i.e.* there is no need to monitor recovery by means of a yield tracer. On the other hand, since IDMS is only suited for elements with more than one stable isotope, the concentrations of only 10 out of the 14 naturally occurring REE can be determined (Pr, Tb, Ho and Tm have only one stable isotope).

The basic principles of IDMS are explained in many textbooks and publications and will not be repeated in this Chapter. However, a multi-element IDMS analysis of the REE in seawater confronts the operator with a great number of analytical problems that go far beyond the basic principles. Even with a careful choice of the analytical conditions, (multiple) isobaric interferences are inevitable. Some of the REE potentially interfere with each other, either directly or with REE oxide

cations that may form in the source of the mass spectrometer. In addition, seawater contains a number of interfering elements that cannot always be completely separated from the REE. Filament material and configuration of the filament assembly seem to control the REE emission sequence and the emission of REE oxide cations and hence which isobaric interferences are actually encountered in practice (Section 3.2.5.).

The development of the various methods is reviewed in Section 3.2. The final procedure, including sample collection, chemistry and mass spectrometry, is described in Sections 3.3., 3.4. and 3.5.

3.2. Development of the methods: a review

3.2.1. Preconcentration of the REE

Trace metal concentrations in seawater are too low for direct analysis by most analytical techniques. On the other hand, seawater contains large amounts of interfering elements, such as the alkali and alkaline earth elements that make up the seasalt. Any method for the preconcentration of trace metals from seawater should therefore combine a potential for low procedural blanks, a high preconcentration factor and a possibly complete separation of the trace metals from interfering elements.

A well known method for the preconcentration of trace metals from seawater is coprecipitation with hydrated Fe(III) oxide (Burrell, 1965). It is presently the most widely used method for preconcentration of the REE from seawater, since it requires only limited manipulation of the sample and small amounts of reagents, ensuring low and reproducible procedural blanks. A disadvantage of the method is the introduction of relatively large amounts of Fe, which must subsequently be separated from the REE. As an alternative, De Baar (1983) developed a method for preconcentration of the REE from seawater with Bio-Rad Chelex 100 resin, hereafter referred to as 'Chelex'. Preconcentration with Chelex theoretically has the same potential for low procedural blanks as coprecipitation with hydrated Fe(III) oxide, yet the REE are separated from the seasalt cations without introducing large amounts of Fe.

Chelex consists of a cross-linked styrene-divinylbenzene matrix with iminodiacetic acid substituted onto some of its benzene rings (Fig. 3.1a). Proton dissociation reactions of the iminodiacetic acid funtional group are shown in Figure 3.1b. The pH values refer to low ionic strength. When the carboxylic acid functional groups are fully protonated Chelex is referred to as being in the 'hydrogen form' and when they are fully dissociated as being in the 'ammonium form'. Chelex

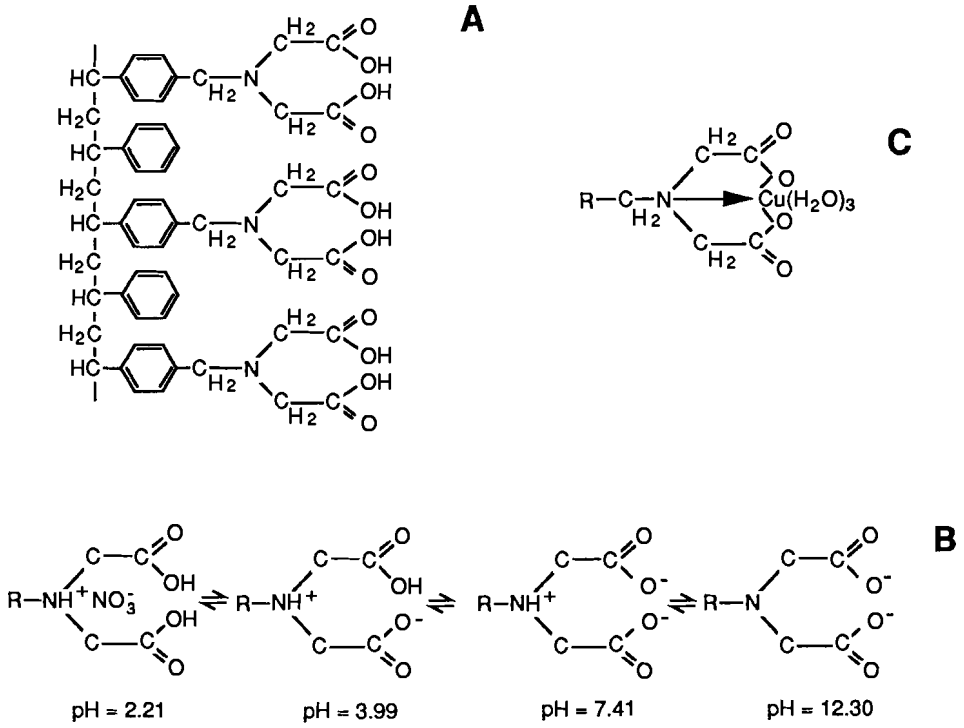

Figure 3.1. Chemical structure of Bio-Rad Chelex 100 resin (A), proton dissociation reactions with increasing pH (B) and two-ring structure of a chelated Cu^{2+} ion (C). After De Baar (1983).

is commonly sold in the 'sodium form', which is the hydrogen form with the protons of the carboxylic acid functional groups replaced by Na^+ ions. The iminodiacetic acid group can bind trace metal cations by ion-exchange (at pH<4) or by chelation (at pH>6) (Luttrell *et al.*, 1971). Complete chelation of the Cu^{2+} ion is shown as an example in Figure 3.1c.

Riley and Taylor (1968) studied the potential of Chelex in the hydrogen form for retaining a large number of trace metals from seawater that was filtered (0.5 μm) but otherwise not pretreated. They found many trace metals to be completely retained by the resin at natural seawater pH (7.7-8.2). Mn and Ce were optimally retained at pH 9.0. The eluate contained minor amounts of Na, K, Mg and Ca, yet the separation was far from complete.

Florence and Batley (1975, 1976), who used a Chelex column to preconcentrate Cu, Zn, Cd and Pb from filtered seawater in the manner

of Riley and Taylor (1968), found that the concentrations of these metals in the column effluent increased considerably after boiling it for 10-15 minutes at pH 0.7. Apparently Cu, Zn, Cd and Pb were partly present in a labile form, which was retained by the resin and partly in a bound form, which was hardly retained by the resin at all. They pointed out that Chelex in the hydrogen form does not attain seawater pH until approximately 1 l of unbuffered seawater has passed through the column, leading to loss of trace metals in the first litre of effluent, and concluded that Chelex should not be used for the preconcentration of trace metals from seawater in the manner of Riley and Taylor (1968). Using Chelex in the sodium form or in the ammonium form improved the retention of the labile fraction, but had hardly any influence on the retention of the bound fraction. They succeeded in converting Cu, Zn, Cd and Pb to the labile form completely before preconcentration by boiling the sample at pH 0.7 for 10-15 minutes and adjusting the pH to 8.1 with reagent grade sodium hydroxide after cooling, yet not without introducing blanks of the order of the natural concentrations of these trace metals.

Paulson (1986) studied the effect of flow rate and sample pretreatment on the retention by a Chelex column of a number of trace metals. He found the retention of Mn, Cu, Cd and Pb to increase with decreasing flow rate and attributed this to slow dissociation of organic trace metal complexes, which are poorly retained by the resin. He also found that a decrease of the bound fraction by some form of sample pretreatment substantially increased recovery, corroborating the results of Florence and Batley (1975, 1976)

Luttrell *et al.* (1971) studied the effect of pH and ionic strength on the retention of Ca and Mg by a column with Chelex in the sodium form. For convenience they expressed retention in terms of V_{max}, the eluent volume needed to drive the maximum concentration of a certain element from the bottom of the column, which is directly related to the equilibrium distribution coefficient D. They found that curves of V_{max} *versus* pH for Ca and Mg show a distinct minimum in the pH range 5.0-6.0 for ionic strengths I>0.1. Based on this result Kingston *et al.* (1978) developed an improved method for the preconcentration of trace metals from high salinity waters such as seawater. Filtered seawater samples were acidified to pH 0.6 with nitric acid to break down colloidal particles during storage. The samples were neutralized with ammonia solution and buffered at pH 5.0-5.5 with ammonium acetate buffer before preconcentration. This pH range is the optimum for retaining most trace metals without retaining large amounts of alkali and alkaline earth elements. Ammonium acetate buffer (1 N, pH 5.2) was found to completely elute Mg and Ca without eluting any Mn (the trace metal with the lowest selectivity coefficient). Excess buffer was

removed with water and trace metals were eluted with 2.5 N nitric acid. This straightforward and successful method was used by Kingston *et al.* (1978) in combination with graphite furnace atomic absorption spectrophotometry (GFAAS) and by Greenberg and Kingston (1982, 1983) in combination with INAA-γ to determine the concentration of a large number of trace metals in seawater.

De Baar (1983) modified the method of Kingston *et al.* (1978), in order to make it suitable for preconcentration of the REE from 10 l seawater samples. Before then, only very little information was available on preconcentration of the REE with Chelex (Christell *et al.*, 1961; Riley and Taylor, 1968; Lee *et al.*, 1977). Samples were buffered at pH 6.0 $\pm$ 0.1 before preconcentration. This pH range is the optimum for retaining the REE without retaining large amounts of Mg and Ca. Chelex columns were operated under forced flow, using a peristaltic pump. The method described in Section 3.5.3. is based on the method that was used by De Baar *et al.* (1988), which in turn is a modification of the method of De Baar (1983). The higher sensitivity of IDMS relative to INAA-γ allows processing 2 l seawater samples under gravity flow (De Baar *et al.*, 1988) rather than 10 l seawater samples under forced flow (De Baar, 1983).

3.2.2. Separation of the REE from Ba

Ba, which is present in seawater at concentrations of 10^{-7}-10^{-8} mol/kg, is a cause of isobaric interferences during IDMS analysis of the REE (Fig. 3.2). Accurate analysis of La is almost impossible in the presence of Ba (Sect. 3.2.5.). The importance of separating the REE from Ba has been emphasized in many publications (Schnetzler *et al.*, 1967; Hooker *et al.*, 1975; Hanson, 1976; Schuhmann and Philpotts, 1979; Thirlwall, 1982; Elderfield and Greaves, 1983; Greaves *et al.*, 1989). During IDMS analysis, Ba interference can neither be eliminated nor corrected for, but only suppressed with great difficulty (Sect. 3.2.5.). Ba must therefore be separated from the REE during preparatory chemistry. A near perfect separation of the REE from Ba is the main objective of the cation-exchange separation that is described in this and the next Section.

Geologists that used IDMS to determine REE abundances in rock and mineral samples were the first to recognize the problem of Ba interference. Schnetzler *et al.* (1967) used a column with Bio-Rad Dowex 50W-X8 cation-exchange resin to separate the REE in rocks and minerals from the bulk solution. The REE were eluted in two fractions, the first roughly containing Gd-Lu and the second La-Eu. No attempts were made to separate the REE from Ba. La could not be analyzed due to Ba interference. Schnetzler *et al.* (1967) stated that a more enriched La

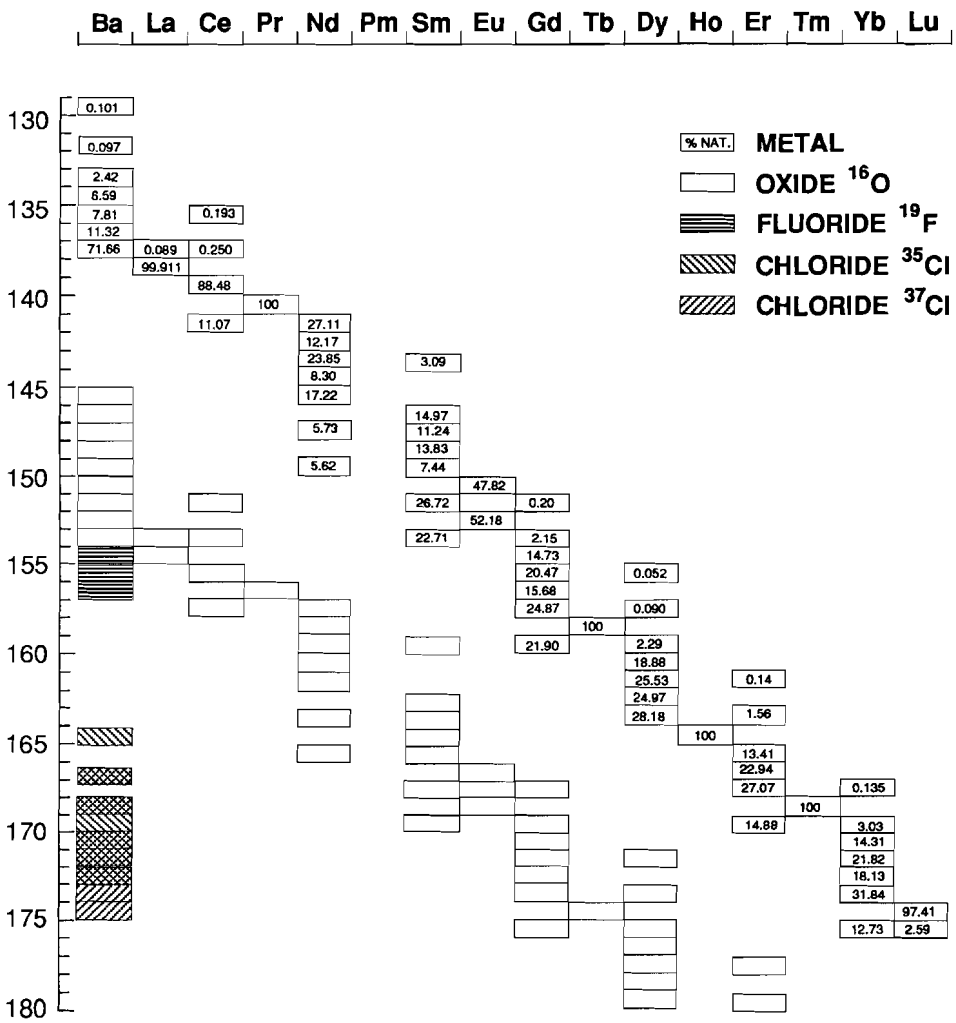

Figure 3.2. Stable isotopes of the REE and their oxides. Also shown are the stable isotopes of Ba and their oxides, fluorides and chlorides. Not all isobaric interferences are actually encountered in practice, due to the REE emission sequence and the reluctance of some REE to form REE oxide cations (Sect. 3.2.5.). After Greaves *et al.* (1989).

spike would be needed if the analysis of La were to attain the accuracy and precision of that of the other REE (their spike solution contained only 2.2% ^{138}La).

Hooker *et al.* (1975) used a column with Bio-Rad AG 1-X8 anion-exchange resin to separate the REE in rocks from the bulk solution as well as from Ba. Sometimes the eluate was passed over the same column again in order to ensure complete removal of Ba. A second column with the same anion-exchange resin was used to separate the REE into a fraction containing Dy-Yb, a fraction containing Ce-Gd and about 50% of the La and a fraction containing the remaining La. These three fractions were analyzed separately (Sect. 3.2.5.). The La spike contained 7.86% ^{138}La. La abundances could successfully be determined for most of the rocks that were analyzed.

Thirlwall (1982) demonstrated that separation of the REE into several fractions is not necessary, as long as a triple-filament assembly is used during IDMS, instead of a single Ta filament. He therefore used the method of Hooker *et al.* (1975) without the second column and analyzed all REE in a single fraction (Sect. 3.2.5.). Furthermore, in order to enhance the separation of the REE from Ba, he passed the eluate of the first column over a smaller version of the first column, rather than passing it over the same column again. This method enabled La abundances to be determined with precisions better than 1%.

Whereas crustal rocks on average contain about ten times more Ba than REE (Weast and Astle, 1982), seawater contains about 10^4 times more Ba than REE. With seawater the problem of Ba interference is therefore much more acute than with rocks and minerals. The first methods for separating the REE in seawater from Ba were based on the methods described above. Elderfield and Greaves (1983) used the method of Hooker *et al.* (1975) with somewhat smaller columns, for seawater samples of 30-50 l, which were preconcentrated by coprecipitation with hydrated Fe(III) oxide. On the first column the REE were separated from Ba, Fe and the seasalt cations. On the second column the REE were separated into three fractions, one containing La and Ce, one containing Nd-Gd and one containing Dy-Yb. Sometimes the REE were separated into a fraction containing La-Eu, one containing Gd and one containing Dy-Yb, in order to facilitate ionization of Gd which had proven difficult for small samples when the separation was less than perfect. Klinkhammer *et al.* (1983) adapted this method for seawater samples of 0.5-2.0 l, yet found that isobaric interferences and small ionbeams made it difficult to determine the concentrations of all 9 REE in every sample (Lu was not analyzed).

Greaves *et al.* (1989) initially applied the method of Thirlwall (1982) to seawater samples of 50 l, which were preconcentrated by coprecipitation with hydrated Fe(III) oxide. It was improved by

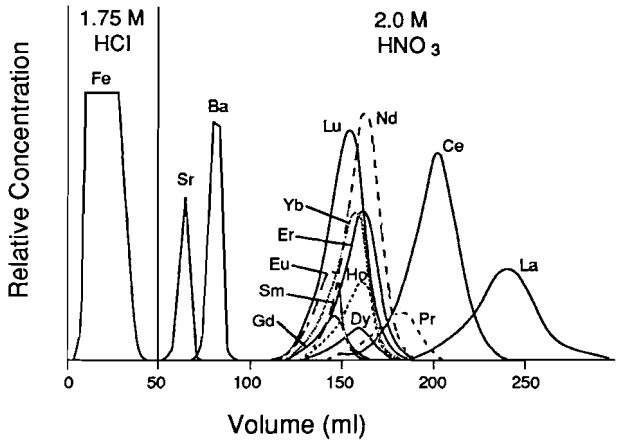

Figure 3.3. Elution curves of Fe, Sr, Ba and the REE for a column (resin bed 12 x 1.0 cm) with AG 50W-X8 resin, 200-400 mesh. The sample, 0.1 g of a ferromanganese nodule with REE concentrations enhanced to allow REE analysis in 2 ml fractions by ICPAES, was loaded in 1.75 N hydrochloric acid. After Greaves *et al.* (1989).

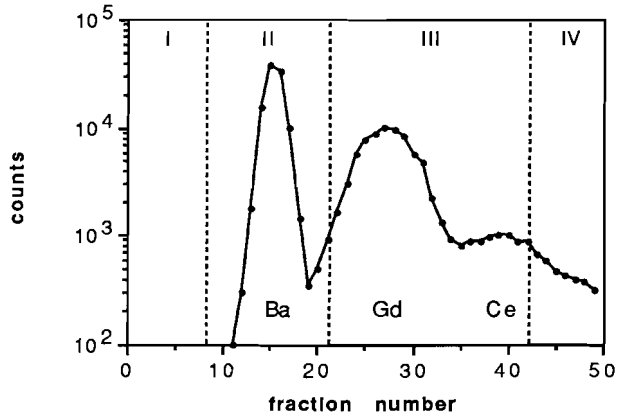

Figure 3.4. Elution curves of Ba, Gd and Ce for a column (resin bed 3.5 x 0.3 cm) with AG 50W-X8 resin, 200-400 mesh, which was loaded with suitable quantities of ^{133}Ba, ^{144}Ce and ^{153}Gd in 0.175 N hydrochloric acid and eluted first with 2 ml 1.75 N hydrochloric acid and then with 2.00 N nitric acid (H.J.W. de Baar, unpublished data). Collected 0.236 ml fractions of acid were analyzed by γ-counting. In the final procedure fractions I-IV were collected as indicated by the dotted lines (Sect. 3.5.4.).

substituting Bio-Rad AG 50W-X8 cation-exchange resin (200-400 mesh) for the anion-exchange resin in the first column. Ba, Fe and the seasalt cations were eluted with 1.75 N hydrochloric acid and the REE with 6 N hydrochloric acid in the manner of Strelow and Jackson (1974). The method was scaled down to process seawater samples of 5 l, yet below 5 l an acceptable analysis of La was no longer possible. Major progress was made by using one column with AG 50W-X8 resin for separating the REE from Ba and Fe as well as into two fractions (one containing Ce-Lu and one containing La and the remainder of the Ce) in a single step (De Baar *et al.*, 1988; Greaves *et al.*, 1989).

3.2.3. Calibration of the AG 50W-X8 columns

The potential of AG 50W-X8 resin for separating the REE from Fe in hydrochloric acid and for separating the REE from Ba in nitric acid was reported by Strelow (1966) and by Strelow (1980) respectively. In hydrochloric acid the REE are eluted in reverse order of atomic number (Strelow, 1960, 1966). In nitric acid Gd has the lowest equilibrium distribution coefficient *i.e.* it is eluted first. Equilibrium distribution coefficients of the other REE increase from Gd to Lu as well as from Gd to La (Strelow *et al.*, 1965).

The elution curve in Figure 3.3 shows the separation of the REE from Fe (in hydrochloric acid) as well as from Ba (in nitric acid). The calibration was performed on a column with a resin bed of 12 x 1.0 cm to allow analysis of collected 2 ml fractions by inductively coupled plasma atomic emission spectrophotometry (ICPAES). As was already demonstrated by Strelow *et al.* (1965) and by Strelow (1980), Ba is eluted well ahead of the REE. The elution curve in Figure 3.4 shows the separation of Ba from Gd and of Gd from Ce on a column with a resin bed of 3.5 x 0.3 cm. Columns of latter dimensions were used by De Baar *et al.* (1988) for separating the REE in 2 l seawater samples from Ba as well as into two fractions, after preconcentration with Chelex (Sect. 3.2.2.).

Next page: **Table 3.1.** Natural REE isotopic ratios and REE isotopic abundances. REE isotopic ratios in the fourth, fifth and sixth column, which were measured on the Finnigan MAT 261 in single-collector peak jumping mode, are the arithmetic mean of twelve corrected scans $\pm 1\sigma$ (see text). * Corrected for isobaric interference. FAR = measured on the Faraday collector. SEM = measured on the secondary electron multiplier. [a] Elderfield and Greaves (1983). [b] Shale and Granites Type REE standard (De Baar, 1983; his Table 2.14.7.). [c] Seawater Type Dilute REE standard (De Baar, 1983; his Table 2.14.8.).

element	ratio	natural [a]	S&G FAR [b]	S&G SEM	STD SEM [c]	numerator isotope	natural abundance (%)
La	138/139	0.0008908	* 0.000912 ± 0.000076	-	-	^{138}La	0.089
Ce	142/140	0.12511	* 0.12596 ± 0.00006	* 0.1245 ± 0.0031	0.1272 ± 0.0011	^{142}Ce	11.07
	138/140	0.002825	-	-	-	^{138}Ce	0.250
						^{140}Ce	88.48
Nd	143/145	1.47221	1.4744 ± 0.0038	1.4398 ± 0.0063	1.4907 ± 0.0049	^{143}Nd	12.17
	142/145	3.2794	-	-	-	^{142}Nd	27.11
	145/150	1.4769	-	-	-	^{145}Nd	8.30
	146/145	2.0733	-	-	-	^{146}Nd	17.22
						^{150}Nd	5.62
Sm	147/149	1.0854	1.0892 ± 0.0003	1.1056 ± 0.0021	1.0989 ± 0.0057	^{147}Sm	14.97
	152/149	1.9348	* 1.9228 ± 0.0009	-	-	^{152}Sm	26.72
Eu	151/153	0.916	0.9178 ± 0.0008	0.9146 ± 0.0051	0.9173 ± 0.0040	^{151}Eu	47.82
Gd	156/155	1.3897	-	-	-	^{156}Gd	20.47
	157/155	1.0645	-	-	-	^{157}Gd	15.68
Dy	162/161	1.35222	-	-	-	^{162}Dy	25.53
	163/161	1.32256	-	-	-	^{163}Dy	24.97
Er	168/167	1.18003	* 1.193 ± 0.032	-	-	^{168}Er	27.07
	170/167	0.6486	* 0.655 ± 0.021	-	-	^{170}Er	14.88
	162/167	0.005928	-	-	-	^{162}Er	0.136
	166/167	1.45641	-	-	-	^{166}Er	13.41
						^{167}Er	22.94
Yb	173/171	1.1272	1.131 ± 0.014	1.117 ± 0.008	-	^{173}Yb	16.13
	174/171	2.22502	2.233 ± 0.018	2.203 ± 0.009	-	^{174}Yb	31.84
	168/171	0.009434	-	-	-	^{168}Yb	0.135
	170/171	0.2117	-	-	-	^{170}Yb	3.03
	176/171	0.8896	-	-	-	^{176}Yb	12.73
						^{171}Yb	14.31
Lu	176/175	0.02659	* 0.02737 ± 0.00046	-	-	^{176}Lu	2.59

element	ratio	spike	REE1 FAR	REE1 SEM	denominator isotope	concentration in spike (pmol/g)
La	138/139	0.072286	-	-	^{139}La	47.025
Ce	142/140	11.43	*11.38 ± 0.03	*11.41 ± 0.11	^{140}Ce	16.630
	138/140	0.00076	-	-		
Nd	143/145	0.00624	0.00632 ± 0.00034	0.00636 ± 0.00006	^{145}Nd	111.38
	142/145	0.0091	-	-		
	150/145	0.0013291	-	-		
	146/145	0.13377	-	-		
Sm	147/149	0.002332	-	0.00208 ± 0.00022	^{149}Sm	34.275
	152/149	0.00497	-	-		
Eu	151/153	0.00561	-	0.00556 ± 0.00052	^{153}Eu	12.423
Gd	156/155	0.00127	-	-	^{155}Gd	27.907
	157/155	0.00283	-	-		
Dy	162/161	0.05203	-	-	^{161}Dy	50.672
	163/161	0.00553	-	-		
Er	168/167	0.05579	-	-	^{167}Er	37.714
	170/167	0.00382	-	-		
	166/167	0.031885	-	-		
	162/167	0†	-	-		
Yb	173/171	0.01423	-	-	^{171}Yb	39.025
	174/171	0.01644	-	-		
	168/171	0.00006	-	-		
	170/171	0.0072	-	-		
	176/171	0.018	-	-		
Lu	176/175	2.48	-	-	^{175}Lu	1.814

Since facilities for calibration of the AG 50W-X8 columns were not available at the Laboratory for Isotope Geology, the elution curve in Figure 3.4 had to be relied upon. Initially the method of De Baar *et al.* (1988) was copied in every detail, in order to ensure that the separation would be exactly as shown in Figure 3.4. Samples were loaded in 0.175 N hydrochloric acid (De Baar *et al.*, 1988), which was collected as a separate 'loading fraction', rather than in 1.75 N hydrochloric acid (Greaves *et al.*, 1989). In 0.175 N hydrochloric acid equilibrium distribution coefficients of the REE are 3-4 orders of magnitude higher than in 1.75 N hydrochloric acid, whereas those of Ca, Sr and Ba are only 1-2 orders of magnitude higher (Strelow, 1960). Consequently, after loading, the REE reside in a narrow band on top of the resin bed. This band may broaden during the separation, but upon elution it will still be narrower than when the sample is loaded in 1.75 N hydrochloric acid. Fe was eluted with 2 ml 1.75 N hydrochloric acid (fraction I), although this is not really necessary when Chelex is used for the preconcentration. Ba was eluted with 3 ml 2 N nitric acid (fraction II). Ce-Lu were eluted with 6 ml 2 N nitric acid (fraction III). Instead of 2 N nitric acid (Greaves *et al.*, 1989), 6.5 N hydrochloric acid was used for eluting La and the remainder of the Ce (fraction IV).

A tentative calibration of the AG 50W-X8 columns was performed, in order to determine whether the separation was indeed as shown in Figure 3.4. A spiked preconcentrated 2 l seawater sample was separated into fractions as described above, the loading fraction and fractions I-III were analyzed by GFAAS and fractions II-IV by IDMS. More than 50% of each of the trace metals Mn, Fe, Co, Ni, Cu and Cd was recovered in the loading fraction and another 45-50% in fraction I. Less than 5% was recovered in fraction II and all were below detection limit (Saager, 1987) in fraction III. All REE were below detection limit (Sect. 3.2.5.) in fraction II. Negligible amounts of Nd and Ce were present in fraction IV, signals decaying rapidly, yet substantial amounts of La were present in fraction III. Since the analysis of La is already very difficult if all La is recovered in fraction IV (Sect. 3.2.5.), any loss of La in fraction III should be avoided. In order to increase the amount of La in fraction IV, fraction III was reduced to 5 ml (Fig. 3.4). Although this also increases the amount of Ce in fraction IV, Ce interference on La was always found

---

Previous page: **Table 3.2.** REE isotopic ratios and concentrations of the enriched REE isotopes in the REE1 spike solution. † Assumed zero. REE isotopic ratios in the fourth and fifth column, which were measured on the Finnigan MAT 261 in single-collector peak jumping mode, are the arithmetic mean of twelve corrected scans ± 1σ (see text). See also Table 3.1.

to be either negligible or correctable (Sect. 3.2.5.).

A second spiked preconcentrated 2 l seawater sample was separated into fractions as before, but now the loading fraction and fraction I were collected and analyzed together, in order to decide whether this combined fraction could be used to determine the concentrations in seawater of some trace metals other than the REE (*e.g.* Mn, Fe, Co, Ni, Cu, Zn, Cd). Unfortunately, severe interference, probably by Mg and Ca, made accurate GFAAS analysis of the combined fraction impossible. The idea was therefore abandoned.

Although tentative calibrations as described above were never repeated, no evidence for major shifts in the elution curves was found during any of the separations that were performed over a period of three years. Nevertheless, the separation between Ba and Gd being rather marginal (Fig. 3.4), it is possible that occasional minor shifts sometimes caused some Gd to be lost in fraction II, or some Ba to be present in fraction III. This could partly account for the poor Gd results (Sect. 3.2.5.). It is unlikely that such minor shifts could cause any Ba to be present in fraction IV.

3.2.4. The isotopically enriched spike solution

The isotopically enriched spike solution REE1 is a diluted mixture of the more concentrated spike solutions L5 and H3. L5 contains La-Gd, enriched in ^{138}La, ^{142}Ce, ^{145}Nd, ^{149}Sm, ^{153}Eu and ^{155}Gd. H3 contains Dy-Lu, enriched in ^{161}Dy, ^{167}Er, ^{171}Yb and ^{176}Lu. REE1 consists of 1.3102 g of L5 and 2.0207 g of H3 diluted with 0.1 N nitric acid to a total weight of 491.7 g. Concentrations of the enriched REE isotopes and relevant abundance ratios of REE isotopes in REE1 are listed in Table 3.2.

In a spike solution like REE1, the natural isotopic ratio A_{jk} of two isotopes j and k of each REE has artificially been changed to B_{jk}, by enrichment of either j or k. Therefore, when a seawater sample is spiked with REE1, the natural isotopic ratio A_{jk} of each REE in the seawater sample is changed to C_{jk}. After adding an amount of REE1 that contains y grams of any REE to an amount of seawater that contains x grams of that REE, x may be calculated from the isotopic ratio C_{jk} of the mixture, which is determined by mass spectrometry. For each REE with given A_{jk} and B_{jk} there is an optimal ratio of x to y for which an error in the measurement of C_{jk} has the smallest effect on the error in the calculation of x. It can be shown (Webster, 1960) that this optimal ratio of x to y corresponds to an isotopic ratio of the mixture

$$C_{jk} = \sqrt{(A_{jk}B_{jk})} \qquad (3.1)$$

Relative concentrations of the REE in L5 and H3 and the composition of

sample	La	Ce	Nd	Sm	Eu	Gd	Dy	Er	Yb	reference	method
STD[a]	515.02	1122.4	827.5	100.04	15.64	256.07	105.4	98.20	90.18	De Baar (1983)	gravimetric
	516.2	1123.3	827.4	100.0	15.85	251.8	106.5	98.2	89.5	De Baar *et al.* (1985b)	IDMS
	-	1140.7	830.3†	-	15.71	-	-	-	-	this work	IDMS
	-	1136.0	831.4†	100.1†	15.71	-	-	-	-	this work	IDMS
	-	1141.4	830.7†	100.7†	-	-	-	-	-	this work	IDMS
CT50[b]	15.47	12.1	14.8	3.27	0.88	4.15	5.36	4.05	3.51	De Baar *et al.* (1988)	IDMS
	-	12.32†	14.82†	3.26†	0.87†	-	-	-	-	this work	IDMS
CT327	16.3	33.3	11.74	2.48	0.66	3.18	3.84	2.97	-	De Baar *et al.* (1988)	IDMS
	-	34.05†	-	-	-	-	-	-	-	this work	IDMS
	16.35†	33.87†	-	-	-	-	-	-	-	this work	IDMS
	-	33.78	-	-	-	-	-	-	-	this work	IDMS
CT697	23.7	57.7	21.2	4.44	1.17	5.79	6.12	4.61	-	De Baar *et al.* (1988)	IDMS
	-	56.89	20.92†	-	-	-	-	-	-	this work	IDMS
	-	56.29†	20.90†	4.34†	1.11†	-	-	-	3.75†	this work	IDMS
CT994	23.2	48.8	18.9	3.98	1.04	-	5.24	3.49	2.94	De Baar *et al.* (1988)	IDMS
	22.69†	49.06†	19.03†	-	1.14†	-	-	-	-	this work	IDMS
OC2-2/3[c]	-	13.71	17.92	3.89	1.00	-	-	-	-	this work	IDMS
49 dbar	12.0	80	-	3.35	0.75	-	-	-	5.1	De Baar *et al.* (1983)	INAA-γ
45 dbar	15.53	14.00	16.01	3.50	0.93	5.10	-	-	-	Sholkovitz and Schneider (1991); their Table 1.I	IDMS
OC2-2/5	-	10.41	16.35	3.45	0.91	-	-	4.58	4.47	this work	IDMS
98 dbar	12.3	42	-	3.0	0.60	-	-	-	3.8	De Baar *et al.* (1983)	INAA-γ
105 dbar	14.88	12.11	15.48	3.46	0.94	5.27	-	-	-	Sholkovitz and Schneider (1991); their Table 1.I	IDMS

REE1 were chosen so that condition (3.1) is nearly satisfied for all REE simultaneously when a 2 l seawater sample with average open ocean REE concentrations is spiked with 0.2-0.3 g of REE1. Adding less or more spike solution to a sample than the optimal amount is commonly referred to as 'underspiking' and 'overspiking' respectively. Underspiking or overspiking leads to magnification of any error in the measurement of C_{jk}. Error magnification was routinely estimated with the computer program REECALC (Sect. 3.5.9.), which projects the statistical error in the measurement of C_{jk} (1σ) on the calculated REE concentration, by means of the isotope dilution curve.

REE1 was stored in a clean 125 ml Teflon FEP drop dispenser bottle with a sealed cap. The drop dispenser bottle was packed in a closed polyethylene (PE) zip-lip bag and kept in a refrigerator, in order to minimize evaporation. Before spiking a series of seawater samples (Sect. 3.5.2.) the weight of the drop dispenser bottle was compared with the last recorded weight of the previous series. Cumulative evaporation of REE1 was found to be negligible over a period of three years.

It has been argued in some publications (Schuhmann and Philpotts, 1979; Thirlwall, 1982; Greaves *et al.*, 1989) that the accuracy of IDMS is mainly dependent on proper calibration of the spike solution, which entails calibration of both the isotopic ratios B_{jk} and the concentrations of the enriched REE isotopes. The isotopic ratios B_{jk} may change as a result of contamination by some natural source of REE. REE1 was always carefully protected from contamination, both during storage and handling. Some of the isotopic ratios B_{jk} were measured during development of the IDMS method. Details of these measurements are presented in Section 3.2.5. The results are listed in Table 3.2. Concentrations of the enriched REE isotopes cannot be measured

---

Opposite page: **Table 3.3.** Spiked REE standards and spiked 2 l seawater samples were analyzed on the SEM (unless indicated otherwise) in single-collector peak jumping mode, in order to determine the accuracy and precision of multi-element IDMS analysis of the REE on the Finnigan MAT 261. Errors were estimated with the computer program REECALC. The STD REE standard and the seawater samples from the Cariaco Trench had been analyzed before on a VG Isomass 54E at the University of Cambridge (UK). † Analyzed on the Faraday collector. [a] Seawater Type Dilute REE standard (De Baar, 1983; his Table 2.14.8.). [b] Seawater samples from the Cariaco Trench (De Baar *et al.*, 1988). Subsamples were taken from the original containers. [c] Seawater samples from station 2 (39°N 67°01'W) of the U.S. R/V *Oceanus* #86/1 cruise to the Sargasso Sea (De Baar *et al.*, 1983). Subsamples were taken from the original containers. Also shown are REE concentrations reported by Sholkovitz and Schneider (1991) for samples from approximately the same area and depth (Chapter 2).

directly. They may change as a result of evaporation of the spike solution, yet, as stated before, evaporation of REE1 was found to be negligible.

REE1 was indirectly calibrated by IDMS analysis of spiked REE standards and seawater samples that had been analyzed before in other laboratories (Sect. 3.2.5.). The results (Table 3.3) suggested that there was no reason to doubt the certified values of REE isotopic ratios and REE isotopic concentrations in REE1.

3.2.5. Isotope dilution mass spectrometry

The first methods for multi-element IDMS analysis of the REE were developed for the determination of REE abundances in rocks and minerals. Hooker *et al.* (1975) separated the REE into three fractions (Sect. 3.2.2.), which were loaded on single Ta filaments. Since three analyses had to be performed for each sample, the method was very time consuming and had some potential for operator error. Furthermore, even with the REE separated into three fractions, isobaric interferences were only partly eliminated, especially when the separation was less than perfect.

Thirlwall (1982) recognized these and other disadvantages of the method of Hooker *et al.* (1975). He analyzed the REE on a VG Isomass 54E mass spectrometer in a single fraction, which he loaded on the side filaments of a triple-filament assembly that consisted of a Re centre filament and two Ta side filaments. The use of a single REE fraction precluded the need for an additional laborious separation, yet confronted the operator with the full suite of isobaric interferences. These were minimized by a careful choice of filament temperatures for each REE. Remaining isobaric interferences were corrected for by monitoring the interfering element at a suitable mass.

Greaves *et al.* (1989) used a combination of the methods of Hooker *et al.* (1975) and Thirlwall (1982) for IDMS analysis of the REE in seawater on a VG Isomass 54E. Initially the Ce-Lu fraction was analyzed in the manner of Thirlwall (1982), loading it on the side filaments of a triple-filament assembly, while the La-Ce fraction was analyzed separately on a single Ta filament. In the final (fully automated) procedure both fractions were loaded on the same triple-filament assembly, the La-Ce fraction on the Re centre filament and the Ce-Lu fraction on the Ta side filaments, so that only one position on the sample magazine was needed per sample.

The method for multi-element IDMS analysis of the REE in seawater on the Finnigan MAT 261 mass spectrometer, which is described in the remainder of this Section, was based on the method of Greaves *et al.* (1989). The double-filament assemblies of the Finnigan

MAT 261 consist of two identical Re filaments of rectangular U-shape, placed directly opposite each other, so that their surfaces are parallel and have a distance of about 0.5 mm between them. One filament, the evaporation filament, is meant to contain the sample, while the other filament, the ionization filament, is meant to remain empty. The initial intention was to follow the method of Greaves *et al.* (1989) as closely as possible. Therefore, the two REE fractions were loaded on the same double-filament assembly, the La-Ce fraction on the ionization filament and the Ce-Lu fraction on the evaporation filament. However, the high temperature of the ionization filament during La analysis, the small distance between the filaments and the long time needed for the Ba signal to decay (see below), caused untimely evaporation of some of the LREE, leading to loss of sample and Ce interference on La. This approach was therefore abandoned. It was decided to analyze the La-Ce fraction on a separate double-filament assembly, which also led to a higher and more stable La signal.

Analytical conditions for multi-element IDMS analysis of the REE on the Finnigan MAT 261 were determined with an REE standard. The REE mass spectrum was repeatedly scanned between mass 130 and mass 180 at an ionization temperature of 1700 °C, each time increasing the current through the evaporation filament by 0.1 A. Whenever the next REE appeared in the mass spectrum, the current through the evaporation filament was written down (Table 3.5). The following REE emission sequence was found

Ce - Eu - Nd - Sm - Yb - Er - Dy - Lu - GdO (3.2)

which is distinctly different from the REE emission sequence reported by Greaves *et al.* (1989)

Eu - Yb - Sm - (Ce) - Nd - Er - Dy - GdO - Lu (3.3)

for the VG Isomass 54E. The parentheses refer to the fact that Ce was only analyzed on the side filaments if its analysis on the centre filament had failed. La was not included in (3.2) and (3.3), since it was always analyzed separately. The difference between (3.2) and (3.3) may be due to the fact that Greaves *et al.* (1989) used Ta filaments rather than Re filaments, which yields a different workfunction w for the formation of REE^+ ions (Sect. 3.2.6.). The REE emission sequence on the Finnigan MAT 261 gives rise to isobaric interferences that are less important on the VG Isomass 54E, such as Yb interference on Er, GdO and Lu.

Another cause of isobaric interferences is the emission of REE oxide cations. This is normally suppressed by high ionization

temperatures, but on the Finnigan MAT 261 raising the ionization temperature invariably leads to untimely emission of REE that are yet to be analyzed, probably due to the close juxtaposition of filaments in the double-filament assemblies. The REE emission sequence (3.2) and the copious emission of REE oxide cations called for modification of the scheme of interference corrections that was developed by Thirlwall (1982). Details of the modified scheme are discussed below and summarized in Table 3.5.

After the analytical conditions had been determined, data acquisition routines were written for each REE. The Finnigan MAT 261 at the Laboratory for Isotope Geology is equipped with nine Faraday collectors in fixed positions. The elements that can be analyzed in multi-collector mode are Sr, Nd and Pb. All other elements can only be analyzed in single-collector peak jumping mode *i.e.* by sequential rather than by simultaneous integration of signals. Signals on the Faraday collector were integrated for eight seconds. Before each integration four seconds of idle time allowed for relaxation of the amplifier in order to avoid memory effects from the previous signal. Data was collected in three blocks of five scans. During a scan, each of the isotopic ratios specified in the data acquisition routine was measured once. All scans were corrected for the baseline, which was integrated for 32 seconds after every block, as well as for long term drift of the REE signals. Latter correction causes one scan to be lost per block. Therefore, final isotopic ratios are the arithmetic mean of twelve corrected scans.

Isotopic ratios of the REE in an REE standard (S&G) and in the REE1 spike solution were measured in order to test the data acquisition routines, to determine the accuracy of isotopic ratio measurements on the Faraday collector in single-collector peak jumping mode and to determine the effect of isobaric interferences. The amount of REE loaded on the filament was much larger than the amount of REE in a 2 l seawater sample. The results are presented in Tables 3.1 and 3.2. Accuracy with respect to certified values is 1-3%, which is well outside the statistical error (1σ) in most cases.

It appeared that when smaller amounts of REE were loaded on the filament, the Faraday collector was not sensitive enough to determine isotopic ratios of the less abundant REE with acceptable accuracy and precision. Therefore, all data acquisition routines were rewritten for the secondary electron multiplier (SEM). In order to test these new data acquisition routines, isotopic ratios of the REE in two REE standards (S&G and STD) and in the REE1 spike solution were measured. The amount of REE loaded on the filament was approximately equal to the amount of REE in a 2 l seawater sample. The results are presented in Tables 3.1 and 3.2. Accuracy with respect to certified values is 1-3%,

well outside the statistical error (1σ), similar to what was found before.

Next, a spiked REE standard (STD) and spiked 2 l seawater samples were analyzed, in order to determine the accuracy and precision of multi-element IDMS analysis of the REE on the Finnigan MAT 261. The REE standard was analyzed in triplicate. In Table 3.3 the results are compared with the certified REE concentrations in the standard (De Baar, 1983), which was made up gravimetrically, and with the results of an earlier IDMS analysis that was performed on a VG Isomass 54E (De Baar *et al.*, 1985b). Four samples from the Cariaco Trench, with different REE concentrations, were analyzed after preconcentration with Chelex (Sect. 3.5.3.) and separation of the REE from Ba and into two fractions (Sect. 3.5.4.). One of the samples was analyzed in duplicate and another in triplicate. In Table 3.3 the results are compared with concentrations reported by De Baar *et al.* (1988), who analyzed the same samples on a VG Isomass 54E. Precision, as calculated from duplicate and triplicate analyses, was better than 0.5% in all cases. Accuracy with respect to certified values and the results of earlier measurements was usually better than 2%, which is quite satisfactory for marine geochemical purposes. Error magnification was probably negligible, since the accuracy of the measurement of REE concentrations is very similar to the accuracy of the measurement of REE isotopic ratios.

Because of technical problems with the SEM most of the analyses in Table 3.3 were performed on the Faraday collector in single-collector peak jumping mode. Therefore, concentrations of the HREE

element	blank (pmol)	blank (pmol) Greaves *et al.* (1989)
Ce	0.308 ± 0.010	0.034
Nd	0.071 ± 0.010	0.010
Sm	0.018 ± 0.005	0.0013
Lu	0.0030 ± 0.0026	0.0005

Table. 3.4. Procedural blanks were determined for some REE as described in Chapter 7. Nd procedural blank is the arithmetic mean of two independent measurements. Also shown are procedural blanks reported by Greaves *et al.* (1989).

element	evaporation current (A)	ionization temperature (°C)	isotopic ratios measured	isobaric interferences
Ce(O)	0.5-0.8	1700	142/140 (158/156) 145/140 (161/156)	 Nd
Eu	0.7-1.5	1900-2000	151/153 154/153	 (BaO)
Nd	1.7-1.9	1700	143/145	
Sm	1.8-2.1	1700	147/149	
Yb	2.0-2.2	1700	173/171 174/171	(GdO)† (GdO)†
Er	2.1-2.3	1700	168/167 170/167 171/167 163/167	 Yb (SmO)
Dy	2.1-2.4	1700	162/161 163/161 166/161 167/161	 (NdO) Er
Lu	2.3-2.5	1700	176/175 171/175	 Yb
GdO	2.5-2.8	1500-1700	172/171 173/171	(Yb)† (Yb)†
LaO	1.8-2.1	1700	154/155 153/155 156/155	 (BaO) CeO

Opposite page: **Table 3.5.** Analytical conditions for multi-element IDMS analysis of the REE on the Finnigan MAT 261. Evaporation current ranges indicate that evaporation currents were not always the same for all samples. REE isotopic ratios that were measured and isobaric interferences that were generally encountered are shown in the fourth and fifth column respectively. Isobaric interferences in parentheses were monitored but not corrected for. † Yb interference on GdO and GdO interference on Yb could not be corrected for, since there are no free masses at which GdO and Yb can be monitored (Fig. 3.2).

---

could not be determined. After the problems with the SEM had been solved, the use of the Faraday collector was abandoned altogether.

The results in Table 3.3 show that the accuracy of multi-element IDMS analysis of the REE is about 2%. Therefore, the detection limit of IDMS may be defined as the amount of any REE that changes the isotopic ratio B_{jk} of that REE in a certain amount of spike solution by more than 2%. This detection limit may be calculated for any amount of spike solution. For instance, the detection limit for Nd, using the smallest amount of spike solution that can accurately be weighed (~0.01 g), is 0.14 pg (0.001 pmol). The smaller the amount of spike solution, the smaller the detection limit, yet ultimately the detection limit is determined by the smallest amount of spike solution on which a measurement of REE isotopic ratios can be performed with acceptable accuracy and precision.

Procedural blanks were determined for some REE as described in Chapter 7. The results are presented in Table 3.4. The errors that were estimated from the statistical errors in the isotopic ratios (1σ) by the computer program REECALC (Sect. 3.5.9.) are as high as 90% for Lu and indicate that error magnification was substantial, most likely as a result of severe overspiking. The procedural blanks for Sm and Lu are equal to those reported by Greaves *et al.* (1989) within these errors, yet the procedural blanks for Ce and Nd are higher by a factor of 5-10. The higher procedural blanks may be caused by the fact that preconcentration with Chelex was used, whereas Greaves *et al.* (1989) used coprecipitation with hydrated Fe(III) oxide. Although, theoretically, both techniques have a potential for low procedural blanks (Sect. 3.2.2.), preconcentration with Chelex requires large amounts of reagents and considerable manipulation of the samples. Since REE reagent blanks are assumed to be well below detection limit (Sect. 3.4.1.), sample manipulation is probably the most important source of procedural blanks. On the other hand, precision of the procedural blanks was found to be very poor due to the error magnification. The difference with the procedural blanks reported by

Greaves *et al.* (1989) may therefore be less significant than suggested by the errors in Table 3.4.

In the remainder of this Section details of the analysis are discussed for each of the 10 REE that may be analyzed by IDMS.

La. La has two stable isotopes, ^{138}La and ^{139}La, with natural abundances of 0.089% and 99.911% respectively (Fig. 3.2). The minor isotope ^{138}La is interfered with by ^{138}Ba, which has a natural abundance of 71.66%. The abundance of ^{138}La in REE1, which contains one of the best commercially available La spikes, is a mere 6.7%. According to (3.1), a sample that is optimally spiked with REE1 has a 138/139 ratio of 0.008024. Accurate measurement of such unfavourable isotopic ratios is difficult even when there are no isobaric interferences. The 138/139 ratio of an optimally spiked sample may be increased by overspiking, but only at the expense of substantial error magnification (Sect. 3.2.4.).

Commonly, Ba emission is very unstable and the Ba signal fluctuates rapidly. Consequently, in single-collector peak jumping mode it is not possible to determine the 137/139 ratio, which is needed to correct La for Ba interference, with the necessary precision. It may seem that Ba interference could be eliminated by complete separation of Ba from La during preparatory chemistry, yet despite the fact that such a separation can be performed to perfection (Fig. 3.3) Ba is nearly always present during La analysis. Greaves *et al.* (1989) suggested that this residual Ba originates in the source of the VG Isomass 54E, more specifically in the borosilicate glass beads of the filament supports. However, any Ba that is not emitted by the filaments will either hit the extraction plate (Sect. 3.5.5.) or leave the source completely out of focus and never reach the SEM. It is therefore more likely that Ba is emitted by the filaments. Even zone-refined Re ribbon contains elements such as Fe, Mo, Al, Co, Cr and Ni at ppm levels. In order to remove such impurities, all filaments were baked for about 15 minutes at a temperature of about 1600 °C (3.5 A) and a vacuum of 10^{-5} mbar, before loading the samples (Sect. 3.5.5.). Finnigan MAT recommends temperatures of 1400-1700 °C and possibly long baking times for removing Ba from the filaments. Apparently a temperature of 1600 °C and a baking time of 15 minutes are not sufficient to remove Ba completely, yet at a vacuum of 10^{-5} mbar higher temperatures and longer baking times lead to oxidation of the Re ribbon and hence to deterioration of the filament.

As it is apparently not possible to eliminate Ba interference, methods were applied to suppress it. Oxygen was introduced into the source during La analysis ($5 \cdot 10^{-7}$ mbar oxygen partial pressure), using the gas bleed system decribed in Section 3.2.6. In the presence of oxygen La is primarily emitted as LaO^+ ions, whereas Ba is still mainly emitted as Ba^+ ions. BaO interference on LaO is therefore much less severe than Ba interference on La. Ba is emitted at a lower temperature than La, so that it could be monitored while La was not yet present in the mass spectrum. As soon as the Ba signal had decayed below the background, the bleeding valve was opened, the evaporation temperature was gently raised until a stable LaO signal was established and La analysis was started. La concentrations were calculated from the 154/155 ratio (Table 3.5). BaO was monitored at mass 153. Since even the slightest BaO interference could not be corrected for, the 154/155 ratio was not accepted until the

$^{137}Ba^{16}O$ signal could no longer be distinguished from the background. Occasionally, the 154/155 ratio had to be corrected for a minor CeO interference. Even when La was analyzed in the presence of oxygen, it would typically take 1-5 hours before BaO was no longer present in the mass spectrum. Attempts to determine La concentrations were successful for about 75% of the samples that were analyzed.

Ce. Ce has four stable isotopes (Fig. 3.2). Ce concentrations were calculated from the 142/140 ratio, which was corrected for Nd interference by monitoring ^{145}Nd (Table 3.5). Ce was often emitted mainly as CeO^+ ions. Ce concentrations were therefore often calculated from the 158/156 ratio, which was corrected for NdO interference by monitoring NdO at mass 161 (Table 3.5). Comparison of Ce concentrations calculated from the 158/156 and from the 142/140 ratio for the same sample showed $^{140}Ce^{18}O$ interference on $^{142}Ce^{16}O$ to be negligible.

Eu. Eu has two stable isotopes (Fig. 3.2), ^{151}Eu and ^{153}Eu, which are interfered with by $^{135}Ba^{16}O$ and $^{137}Ba^{16}O$ respectively. Eu concentrations were calculated from the 151/153 ratio (Table 3.5). Thirlwall (1982) and Greaves *et al.* (1989) suppressed the BaO signal with a very high temperature of the Re centre filament. However, due to the close juxtaposition of filaments in the double-filament assemblies of the Finnigan MAT 261, it is not possible to raise the ionization temperature without causing untimely evaporation of REE that are yet to be analyzed. Unfortunately, raising the ionization temperature seems to be the only way to suppress BaO interference on Eu. The ionization temperature was therefore raised to 1900-2000 °C during Eu analysis (Table 3.5), while monitoring BaO at mass 154. The BaO signal would increase strongly at first, yet immediately decay below the background. Eu was started as soon as a stable Eu signal was established. The ionization temperature was lowered directly upon completion of the Eu analysis to prevent untimely emission of Sm and Yb. No more than two attempts to analyze Eu were made for each sample.

Nd. Nd has seven stable isotopes (Fig. 3.2). Nd concentrations were calculated from the 143/145 ratio without further corrections (Table 3.5). NdO emission was often observed during analysis of the HREE.

Sm. Sm has seven stable isotopes (Fig. 3.2). Sm concentrations were calculated from the 147/149 ratio without further corrections (Table 3.5). SmO emission was sometimes observed during analysis of the HREE.

Yb. Yb has seven stable isotopes (Fig. 3.2). Yb concentrations were calculated from the 173/171 ratio as well as from the 174/171 ratio and the results were compared (Table 3.5). The difference was usually less than 5% of the highest concentration, yet sometimes as high as 10%, probably due to GdO interference, which cannot be corrected for since there is no free mass at which GdO can be monitored (Fig. 3.2). As suggested by Schuhmann and Philpotts (1979), a weighted average was taken of the Yb concentrations calculated from the 173/171 ratio and from the 174/171 ratio, giving more weight to the latter, since ^{174}Yb is the most abundant isotope and least interfered with by GdO. Greaves *et al.* (1989) suggested that ^{173}Yb is interfered with by $^{138}Ba^{35}Cl$ and deemed it preferable to measure the 172/171 ratio instead of the 173/171 ratio. Unfortunately, GdO interference on ^{172}Yb is even stronger than on ^{173}Yb.

Er. Er has six stable isotopes (Fig. 3.2). Er concentrations were calculated from the

168/167 ratio as well as from the 170/167 ratio, which were corrected for Yb interference on ^{168}Er and ^{170}Er by monitoring ^{171}Yb, and the results were compared (Table 3.5). The difference was usually less than 5% of the highest concentration. Discrepancies may arise because Yb is interfered with by GdO, which makes the correction for Yb interference inaccurate. Moreover, SmO interference on ^{168}Er and ^{170}Er cannot be corrected for, since there is no free mass at which SmO can be monitored (Fig. 3.2). A weighted average was taken of the Er concentrations calculated from the 168/167 ratio and from the 170/167 ratio, giving more weight to the former, since ^{168}Er is the most abundant isotope and least interfered with by Yb.

Dy. Dy has 7 stable isotopes (Fig. 3.2). ^{161}Dy is interfered with by $^{145}Nd^{16}O$. ^{162}Dy is interfered with by $^{146}Nd^{16}O$ and by ^{162}Er. ^{163}Dy is interfered with by $^{147}Sm^{16}O$. NdO interference on Dy was corrected for by monitoring $^{150}Nd^{16}O$, which is in turn interfered with by $^{150}Sm^{16}O$ and by ^{166}Er. Er interference on Dy and NdO was corrected for by monitoring ^{167}Er, which is in turn interfered with by $^{151}Eu^{16}O$, yet latter isobaric interference was never encountered in practice. SmO interference could not be corrected for, since there is no free mass at which SmO can be monitored. Dy concentrations were calculated from the 162/161 ratio as well as from the 163/161 ratio, which were corrected for all these complex isobaric interferences by the computer program DYCALC (Sect. 3.5.9.), and the results were compared (Table 3.5). The corrections failed if SmO was present during Dy analysis. If the difference was less than 5% of the highest concentration, the arithmetic mean of the two concentrations was accepted as the final Dy concentration. Unfortunately, due to SmO interference and the often very copious emission of NdO^+ ions, which could not be suppressed by raising the ionization temperature (see **Eu.**), Dy concentrations could only rarely be determined.

Lu. Lu has two stable isotopes, ^{175}Lu and ^{176}Lu (Fig. 3.2). It was suggested in some publications (Hooker *et al.*, 1975; Hanson, 1976; Thirlwall, 1982) that Lu analysis may be difficult or impossible due to TbO interference on ^{175}Lu, which cannot be corrected for, since Tb has only one stable isotope. However, emission of REE oxide cations was never observed for elements heavier than Sm (except for Gd). Lu concentrations were calculated from the 176/175 ratio, which was corrected for Yb interference by monitoring ^{171}Yb (Table 3.5). The correction was often inaccurate as a result of GdO interference on Yb.

Gd. Gd has seven stable isotopes (Fig. 3.2) and is emitted mainly as GdO^+ ions. The total emission of Gd is extremely low and Gd isotopic ratios are therefore hard to measure, even when there are no interferences. Unfortunately, the REE emission sequence (3.2) on the Finnigan MAT 261 causes Yb to be emitted at a much higher temperature. GdO interferes with all seven isotopes of Yb (and *vice versa*). These isobaric interferences cannot be corrected for, since there is no free mass at which either GdO or Yb can be monitored (Fig. 3.2). Gd concentrations were calculated from the 172/171 ratio as well as from the 173/171 ratio and the results were compared (Table 3.5). If the difference was less than 5% of the highest concentration, the arithmetic mean of the two concentrations was accepted as the final Gd concentration. Since Yb was usually emitted with much higher efficiency than GdO, Gd concentrations could only rarely be determined, whereas Yb could often be successfully analyzed, albeit with limited accuracy and precision.

3.2.6. A gas bleed system for suppressing isobaric interferences

La was mostly analyzed in the presence of oxygen. Pure oxygen was introduced into the source by means of a gas bleed system based on a commercial design (Anonymus, 1986). It was injected in the vicinity of the double-filament assembly through a capillary, out of a 5 l container filled with pure oxygen at a pressure of about 10 mbar. The gasflow was controlled by means of a bleeding valve (Varian 951-5106). The tip of the capillary was at a distance of about 5 cm from the double-filament assembly. The gas bleed system was also used for introducing CCl_2F_2-gas (freon) into the source. Freon suppresses the emission of REE oxide cations. The exact mechanism is not clearly understood, yet Hebeda and Schijf (1991) suggested that the surface of the filament is covered with molecules of freon and its derivatives, yielding a higher workfunction w, which determines the efficiency of positive ion emission (Schuhmann and Philpotts, 1979)

$$n^+/n_0 \propto \exp[e(w-\phi)/kT] \qquad (3.4)$$

where n^+ and n_0 are the number of positive ions and neutral atoms emitted per unit time respectively, e is the electron charge, ϕ the ionization potential of element n, k the Boltzmann constant and T absolute temperature. In general, the value of the workfunction w depends on the material and nature of the emitting surface. If $w<\phi$ the ratio n^+/n_0 may be increased by raising the temperature of the filament, yet this leads to rapid consumption of the sample.

Hebeda and Schijf (1991) used pure Ba nitrate and REE nitrate standards to determine the effect of freon on the emission of Ba, La, Ce, Nd and Gd. The results are now briefly reviewed. Freon partial pressures were measured with an ionization gauge that was located between the source and the turbomolecular pump. Freon partial pressures in the source were therefore higher.

Ba. Under optimal conditions, BaO^+ emission comprised less than 0.1% of the total Ba emission. Ba^+ emission was strongly suppressed with increasing freon partial pressure (Fig. 3.5a), whereas BaF^+ emission was strongly enhanced. At about $5 \cdot 10^{-7}$ mbar freon partial pressure, BaF^+ emission was higher than Ba^+ emission by a factor of 20 and equalled the Ba^+ emission at zero freon partial pressure. At the same time there was no evidence for any BaO^+ (or $BaCl^+$) emission *i.e.* Ba was emitted almost completely as BaF^+ ions.

La. Under optimal conditions, LaO^+ emission comprised about 85% of the total La emission. Figure 3.5b shows that, contrary to what was found for Ba (Fig. 3.5a), both La^+ and LaO^+ emission increased with increasing freon partial pressure. However, when the freon partial pressure exceeded $5 \cdot 10^{-7}$ mbar LaO^+ emission decreased again, while La^+

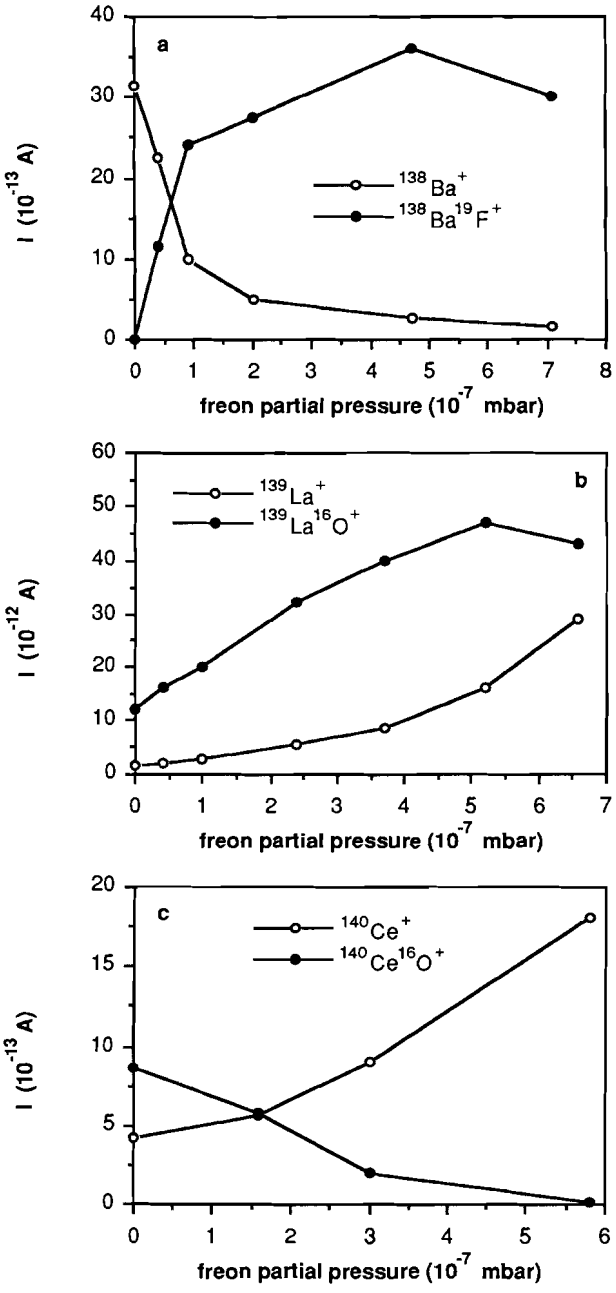

Figure 3.5. Ion current of Ba and BaF (a), La and LaO (b) and Ce and CeO (c) as a function of freon partial pressure. After Hebeda and Schijf (1991).

emission continued to increase strongly. At $6.5 \cdot 10^{-7}$ mbar freon partial pressure, LaO^+ emission comprised only 60% of the total La emission, whereas La^+ emission had increased by a factor of 16 with respect to the La^+ emission at zero freon partial pressure. Higher freon partial pressures, which might further suppress LaO^+ emission, are not advisable since they could cause the source to spark.

Ce and Nd. Freon had a similar effect on the emission of Ce (Fig. 3.5c) and on that of Nd (not shown). Ce^+ and Nd^+ emission was strongly enhanced, whereas CeO^+ and NdO^+ emission was strongly suppressed with increasing freon partial pressure. No evidence for any CeF^+ or NdF^+ emission was found.

Gd. Under optimal conditions, GdO^+ emission comprised about 50% of the total Gd emission. During IDMS analysis of seawater samples, Gd is almost completely emitted as GdO^+ ions, probably due to the presence of some organic residue. The Gd signal could barely be distinguished from the background on the SEM, even with 500 ng of Gd loaded on the filament. At $4 \cdot 10^{-7}$ mbar freon partial pressure Gd^+ emission was higher by a factor of 40 than the Gd^+ emission at zero freon partial pressure (Fig. 3.6). At the same time the GdO signal could no longer be distinguished from the background, whereas a minor emission of GdF^+ ions was observed.

The results in Figures 3.5 and 3.6 suggest an alternative method for suppressing Ba interference on La. In the presence of freon (*e.g.* $6 \cdot 10^{-7}$ mbar freon partial pressure) La is emitted mainly as La^+ ions, whereas Ba is emitted almost completely as BaF^+ ions. Ba interference on La would thus be much less severe than in the absence of freon. La concentrations could then be calculated from the 138/139 and Ba could be monitored at mass 137. Ce emission also increases in the presence of freon (Fig. 3.5b), yet Ce interference on La can adequately be

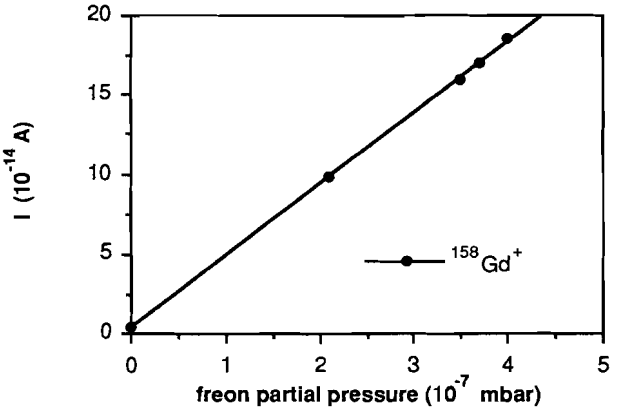

Figure 3.6. Ion current of Gd as a function of freon partial pressure. After Hebeda and Schijf (1991).

corrected for by monitoring ^{140}Ce. If freon and oxygen are equally successful in suppressing Ba interference on La, it is more convenient to use freon, since it also suppresses interferences by a number of REE oxides on Dy and Gd. Moreover, Re ribbon is rapidly oxidized in the presence of oxygen, especially at higher temperatures, which leads to deterioration and eventually to breakage of the filaments.

At $6 \cdot 10^{-7}$ mbar freon partial pressure the emission of NdO^+ ions is strongly suppressed (Hebeda and Schijf, 1991), so that NdO interference on Dy would strongly be suppressed as well. Moreover, in analogy with La, Ce, Nd and Gd, freon may enhance the emission of Dy^+ ions.

At the same freon partial pressure Gd is almost completely emitted as Gd^+ ions. Gd concentrations could thus be calculated from the 156/155 ratio as well as from the 157/155 ratio. CeO and PrO would not interfere, because CeO emission and presumably also PrO emission is strongly suppressed in the presence of freon. LaO and BaF also would not interfere, because La is not present on the filament, whereas the Ba signal has decayed below the background at this high temperature. Finally, Gd is no longer emitted as GdO^+ ions, which would strongly suppress GdO interference on Yb. Instead, GdF would probably interfere with Yb, yet this isobaric interference could be corrected for by monitoring $^{158}Gd^{19}F$.

All these results refer to pure Ba nitrate and REE nitrate standards and therefore need not apply to multi-element IDMS analysis of the REE in seawater. The effect of freon on the emission of the REE has yet to be tested for real samples, which consist of a mixture of all REE, probably not pure REE nitrates, and may also contain impurities such as organic matter.

3.3. Sample collection

Seawater samples were collected with 12 l or 30 l GoFlo bottles, mounted on a coated or stainless steel CTD Rosette frame. At the beginning of each cruise the GoFlo bottles were cleaned by filling them with reagent grade 0.1 N nitric acid and rinsing them with demineralized water after 10-20 hours. A CTD profile was recorded during the downcast, mostly together with a profile of light transmission or oxygen. Seawater samples were collected during the upcast and pressure-filtered aboard ship inside a containerized class 100 clean air laboratory, within 1-2 hours after collection.

Two types of filtration unit were used for filtering large volumes of seawater. Large filtration units (Fig. 3.7) were used for filtering the contents of 30 l GoFlo bottles. The PE top-piece, fitted with a Teflon

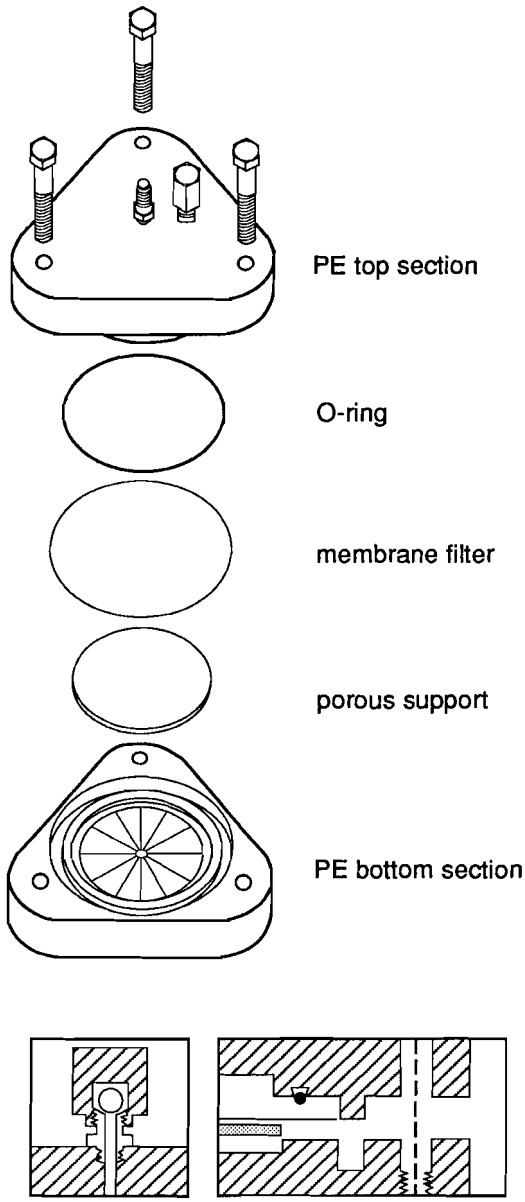

Figure 3.7. Schematic drawing of a large filtration unit for filtering the contents of 30 l GoFlo bottles. Vent valve (bottom left) and O-ring seal with 'dirt-barrier' groove and tongue (bottom right) are shown in detail. After De Baar (1983).

TFE vent valve to remove air from the filtration unit and with a PE inlet, and the PE bottom-piece, fitted with a PE outlet, are clamped together with three Nylon screws. A round porous PE plate, mounted in the bottom-piece, supports a 142 mm diameter polycarbonate membrane filter (Nuclepore). The membrane filter is pressed onto the support by a Teflon FEP coated rubber O-ring, which is contained by a groove in the top-piece. Smaller filtration units of the same general design were used for filtering the contents of 12 l GoFlo bottles. The Teflon TFE top-piece and bottom-piece of these smaller units are screwed together directly, rather than clamped together with screws. The smaller units are therefore more rigid and resistant against leakage and the number of parts per unit is reduced. The round porous PE plate of the smaller units supports a 47 mm diameter polycarbonate membrane filter (Nuclepore).

Filtration units were assembled after rinsing the various parts thoroughly with Milli-Q water. A porous PE filter support was mounted in the bottom-piece of each filtration unit. A clean preweighed polycarbonate membrane filter (Sect. 3.4.2.) was carefully centered on each filter support, the top-piece screwed on tightly and a 30 cm long piece of Teflon FEP tube connected to the outlet. The filtration units were placed on a workbench inside the clean air laboratory container and connected to the Teflon FEP filtration lines.

As soon as the CTD Rosette frame was on deck, small samples were taken from each GoFlo bottle for determination of oxygen and nutrient concentrations. The GoFlo bottles were then lifted off the CTD Rosette frame, mounted in racks on the outside of the clean air laboratory container and connected to a silicon rubber nitrogen pressure line on top and to a Teflon FEP filtration line at the bottom. A 1 bar nitrogen overpressure was applied to each GoFlo bottle in turn to start filtration. The first 1-2 litres of seawater were used to rinse filtration units and sample bottles. The latter were subsequently placed under the filtration units and filled. Seawater samples for REE analysis and for GFAAS analysis (Chapter 4) were collected in clean 2 l or 5 l and in clean 250 ml low-density PE narrow-mouth bottles respectively. Occasionally, unfiltered seawater samples were collected by disconnecting the filtration unit and filling a sample bottle directly from the GoFlo bottle after rinsing it with the unfiltered seawater. Remaining contents of the GoFlo bottles were filtered and discarded.

After removing excess seasalt with Milli-Q water, filters were carefully taken out of the filtration units with Teflon TFE tweezers, sealed in PE zip-lip bags and stored in a freezer at -20 °C. Filtration units were taken apart, the parts rinsed with Milli-Q water and stored under 3Q 0.1 N nitric acid (Sect. 3.4.1.). GoFlo bottles were

disconnected, thoroughly rinsed with demineralized water and mounted on the Rosette frame.

Unfiltered surface seawater samples were collected from a rubber boat in clean 2 l or 5 l low-density PE narrow-mouth bottles, navigating against the wind at very low speed, at least half a mile from the R/V in order to avoid contamination by the ship's exhaust and metal hull. Samples were collected wearing PE gloves, approximately half a meter below the sea surface, after rinsing the sample bottle with surface seawater three times. Sample bottles were opened after submersion and closed before taking them out of the water to prevent contamination by particulate matter floating on the sea surface. Samples were not filtered since facilities for clean filtration of small sample volumes were not available.

All filtered and unfiltered seawater samples were acidified to pH 2 inside a class 100 laminar flow clean hood, by addition of 1 ml of 3Q 6.5 N hydrochloric acid (Sect. 3.4.1.) per litre of seawater, in order to slow down oxidation and to inhibit microbial activity and adsorption of trace metals onto the walls of the sample bottle. Sample bottles were covered with PE bags to protect them from dust.

3.4. Cleaning of reagents and laboratory ware

3.4.1. Reagents

Concentrated reagent grade reagents were cleaned by repeated subboiling distillation in a pure quartz still. Quartz-distilled reagents will hereafter be referred to as '1Q', '2Q' or '3Q' reagents, depending on the number of quartz-distillation steps they had undergone. Quartz-distilled concentrated reagents were diluted and further cleaned if necessary. Acids were stored in clean Teflon FEP bottles or in clean Teflon FEP wash bottles (Kuehner *et al.* 1972), since low-density PE was found to release trace metals when in contact with acids. Milli-Q water was stored in clean low-density PE wash bottles. All other reagents were stored in clean low-density PE narrow-mouth bottles. Reagent bottles were covered with PE bags to protect them from dust.

The pure quartz still was described by Kuehner *et al.* (1972). A 1 l low-density PE separatory funnel serves as a reservoir. Connections between the still and the liquid level control and between the reservoir and the liquid level control consist of Teflon FEP tubing. The temperature of the electric heating coils is controlled by an 8-position stepwise temperature control unit (P.M. Tamson, HOMEF LA-05). Hydrochloric acid was distilled at position 8. Nitric acid was distilled at position 5 to avoid excessive formation of nitrous fumes. Acetic acid and ammonia solution were distilled at position 3-4. Liquid levels in

the reservoir, inside the still and in the bottle were checked regularly during distillation. The still was rinsed with reagent before each new distillation step. Before changing to another reagent, the system was rinsed thoroughly with Milli-Q water. The first 200 ml of reagent collected during distillation were used to rinse the bottle and poured back into the reservoir.

A Chelex column, similar to the Chelex columns that were used for preconcentration of the REE (Sect. 3.5.1.), was used for final cleaning of buffers and dilute ammonia solution. It was prepared for use as described in Section 3.5.3. The resin bed was stirred only if the column had not been used for a long time. Reagents were always cleaned in the order ammonia solution - dilute buffer - concentrated buffer. The first 200 ml of reagent collected were used to rinse the bottle and poured back into the reservoir. Ammonium acetate buffer was not collected until the resin bed had resumed its normal length and the effluent had the right pH (5.3 and 6.1 for dilute and concentrated ammonium acetate buffer respectively).

Only procedural blanks were determined for the REE (Sect. 3.2.5.). Since direct determination of REE reagent blanks by IDMS is very time consuming, REE reagent blanks were not determined directly. Instead, reagent blanks were determined for Mn, Fe, Ni, Cu, Zn and Cd by GFAAS analysis of a small amount of reagent. These trace metals (especially Fe and Zn) are much more prone to contamination than the REE, in other words reagents with a low blank for all of these trace metals are likely to contain negligible amounts of REE. Approximately 30 ml of reagent was evaporated in the evaporator pots (Sect. 3.5.1.) in a 30 ml Teflon PFA vial. The dry residue was redissolved in 1 ml of 3Q 0.1 N nitric acid for GFAAS analysis. Reagent blanks were always near detection limit (Saager, 1987) for all trace metals that were analyzed, except for Fe in 3Q 6.5 N hydrochloric acid (*cf.* Kuehner *et al.*, 1972). Fe seems to form volatile compounds with chlorine and is therefore hard to separate from hydrochloric acid by distillation (J.C. van Belle, pers. comm.). REE are not likely to form such volatile compounds and special treatment of the hydrochloric acid (for instance additional cleaning with an anion-exchange resin) was deemed unnecessary. Reagent blanks were always determined shortly after cleaning the reagents, so that any suspect batch could be subjected to extra quartz-distillation or Chelex cleaning before use.

In the remainder of this Section, details of the preparation and cleaning are discussed for each reagent that was used during sample collection and preparatory chemistry.

Water. Demineralized water from the Free University demi-system was purified by a Milli-Q system (Millipore ZD20 230 74) to produce water of 18 MΩ•cm resistivity (at

25 °C). Milli-Q water was stored in low-density PE wash bottles for rinsing small objects and for use as reagent. It was never stored in large quantities in order to prevent contamination as a result of prolonged storage. Whenever large quantities were needed (for instance for diluting reagents or rinsing large objects) it was taken directly from the Milli-Q system. Trace metal blanks were always below detection limit and quartz-distillation of Milli-Q water was therefore deemed unnecessary.

Acetic acid. Acetic acid was only used for preparing ammonium acetate buffer. Reagent grade 17 N (96%) acetic acid was cleaned by twofold subboiling distillation. Final normality was determined from specific gravity by accurately weighing 50 ml of the 2Q acetic acid on an analytical balance (Sartorius 1608 MP6), normalizing the weight to 50 ml of Milli-Q water in order to correct for temperature effects.

Ammonia solution. Clean ammonia solution (9 N) was prepared by subboiling distillation of a 2:1 mixture of reagent grade 13.4 N (25%) ammonia solution and Milli-Q water. Final normality was determined from specific gravity as described for acetic acid. The 1Q 9 N ammonia solution was diluted to 1 N with Milli-Q water on an analytical balance (Mettler PM 4600) and further cleaned by passing it twice over the Chelex column.

Ammonium acetate buffer. Dilute (1 N) ammonium acetate buffer was obtained by weighing 1Q 9 N ammonia solution and 2Q 17 N acetic acid into a low-density PE narrow-mouth bottle and diluting with Milli-Q water. In order to avoid excessive production of heat, the ammonia solution was diluted with the required amount of water before adding the acetic acid. The pH was adjusted to 5.3 by dropwise addition of ammonia solution or acetic acid. The dilute buffer was cleaned by passing it twice over the Chelex column, followed by a final pH check. Concentrated (~6 N) ammonium acetate buffer was obtained by weighing 1Q 9 N ammonia solution and 2Q 17 N acetic acid into a low-density PE wide-mouth bottle. The acetic acid and the ammonia solution were first stored overnight in a freezer at -20 °C. The cold ammonia solution was poured onto the frozen acetic acid, while cooling the wide-mouth bottle continuously in a water bath, in order to counteract the excessive production of heat. The pH was adjusted to 6.1 by dropwise addition of acetic acid or ammonia solution. The concentrated buffer was cleaned by passing it twice over the Chelex column, followed by a final pH check.

Hydrochloric acid. Clean hydrochloric acid is routinely produced at the Laboratory for Isotope Geology (IGO) by subboiling distillation of a 1:1 mixture of reagent grade 12 N (37%) hydrochloric acid and Milli-Q water in a fully automated pure quartz still. The clean hydrochloric acid is collected in a 25 l high-density PE container. After distillation its normality is adjusted to 6.5 ± 0.2 by addition of hydrochloric acid or Milli-Q water and repeated titration with 0.1 M potassium hydroxide, using methyl red as indicator. This hydrochloric acid was used for cleaning laboratory ware (Sect. 3.4.2.) and for preparing 3Q hydrochloric acid of various normalities and will hereafter be referred to as 'IGO hydrochloric acid'. IGO hydrochloric acid was further cleaned by threefold subboiling distillation. Final normality was determined from specific gravity as described for acetic acid. Part of the 3Q 6.5 N hydrochloric acid was diluted to ~1.75 N with Milli-Q water on an analytical balance (Sartorius 1608 MP6). The normality was further adjusted to 1.75 ± 0.01 by dropwise addition of water or hydrochloric acid and repeated titration with 0.1 M potassium hydroxide, using methyl red as indicator. Sometimes, batches of the 3Q 6.5 N

hydrochloric acid were diluted with Milli-Q water to other normalities for various purposes, such as cleaning of laboratory ware (Sect. 3.4.2.).

Nitric acid. Reagent grade 14.4 N (65%) nitric acid was cleaned by threefold subboiling distillation. The resulting 3Q 14.4 N nitric acid has a bright yellow colour due to the dissolution of nitrous oxides during the distillation process. Final normality was determined from specific gravity as described for acetic acid. Part of it was diluted roughly 140 and 4 times with Milli-Q water to 0.1 N and 3.5 N respectively. Another part of it was diluted to ~2 N with Milli-Q water on an analytical balance (Sartorius 1608 MP6). The normality was further adjusted to 2.00 ± 0.05 by dropwise addition of water or nitric acid and repeated titration with 0.1 M potassium hydroxide, using methyl red as indicator.

3.4.2. Laboratory ware

Teflon and PE bottles were filled with IGO hydrochloric acid and placed in a 100 l water bath at 60 °C for 24 hours. The water bath was heated by an immersion circulator (JULABO EM/1). The bottles were taken out of the water bath to cool in horizontal position, so that the warm acid was in contact with the inside of the caps. After another 24 hours the bottles were emptied and rinsed with Milli-Q water. Small Teflon and PE objects were cleaned in a low-density PE wide-mouth bottle filled with IGO hydrochloric acid. The wide-mouth bottle was placed in the 100 l water bath at 60 °C for 24 hours. After the acid had cooled, the objects were taken out and rinsed with Milli-Q water. Teflon PFA vials and caps were cleaned in a 3 l Pyrex glass beaker filled with reagent grade 7 N nitric acid. The acid was heated to 80 °C on a hot plate for at least 5 hours. Vials and caps were taken out of the warm acid with large Teflon TFE tongs, rinsed with Milli-Q water and stored under 3Q 0.1 N nitric acid in low-density PE wide-mouth bottles. Laboratory ware that cannot stand cleaning in warm acid, such as pipette tips, porous PE frits and polypropylene analytical funnels, was soaked in cold IGO hydrochloric acid for a few days, rinsed with Milli-Q water and stored under 3Q 0.1 N nitric acid in low-density PE wide-mouth bottles. All objects stored under 3Q 0.1 N nitric acid were taken out of the storage bottles with large Teflon TFE tongs shortly before use, rinsed with Milli-Q water and dried inside a class 100 laminar flow bench.

Teflon FEP capillary tube, cut into pieces of a few centimeters length, was used as pipette tip for the micropipette (Sect. 3.5.6.). The pieces were placed in large centrifuge tubes filled with cold IGO hydrochloric acid and centrifuged for a short time to replace all the air inside the capillary. They were then soaked in the hydrochloric acid for one night, rinsed by repeatedly centrifuging them in large centrifuge tubes filled with Milli-Q water and dried on a hot plate in a clean Teflon TFE beaker.

Polycarbonate membrane filters were soaked in cold 3Q 1 N hydrochloric acid for one night, rinsed with Milli-Q water and soaked in cold 3Q 1 N nitric acid for another night. The filters were repeatedly rinsed with Milli-Q water to remove all traces of acid, dried inside a class 100 laminar flow bench and weighed on an analytical balance (Sartorius 2842) inside the clean air laboratory before packing them separately in clean, coded, polycarbonate petri dishes. The filters were handled with Teflon TFE tweezers only.

3.5. The final procedure

3.5.1. Clean air laboratory and clean techniques

All preparatory chemistry was performed inside the class 100 clean air laboratory of the Laboratory for Isotope Geology. Clean labcoat, cap and clogs were worn at all times. Clean sleeve covers and PE gloves were worn during the most critical stages. Cleaning of reagents, preconditioning and elution of the Chelex columns and the AG 50W-X8 separation were performed inside a class 100 laminar flow bench in the clean air laboratory. Seawater samples were passed over the Chelex columns outside the laminar flow bench. Evaporation of column eluates and small amounts of reagents and cleaning of laboratory ware were also performed outside the laminar flow bench. Spiking of the seawater samples (Sect. 3.5.2.) was performed inside a temperature controlled weighing room in the clean air laboratory.

In the remainder of this Section the Chelex and AG 50W-X8 columns, the evaporator pots and the use of adjustable pipettes and pH indicator sticks are briefly discussed.

Columns. Dry Bio-Rad Chelex 100 resin (200-400 mesh, sodium form) and dry Bio-Rad AG 50W-X8 cation-exchange resin (200-400 mesh, hydrogen form) were cleaned by soaking in cold 3Q 6.5 N hydrochloric acid for 48 hours, stirring the slurry gently with a Teflon TFE coated stirring bar on a magnetic stirrer. Every 6-12 hours stirring was interrupted and the resin allowed to settle. The hydrochloric acid was decanted, discarded and replaced with a clean batch. The final batch was replaced with Milli-Q water and the slurry was transferred to the columns with a clean, one-piece molded PE disposable transfer pipette. After transferring the resin it was rinsed with Milli-Q water from a wash bottle. When they were not used, the columns were connected in pairs with silicon rubber tubes and stored with Milli-Q water on top of the resin bed to prevent it from desiccating. The Chelex resin and the AG 50W-X8 resin were never replaced over a period of three years.

The Chelex columns (Fig. 3.8) consist of a 200 mm long, $^5/_8$" internal diameter, low-density PE '$CaCl_2$ drying tube' (Cole Parmer, T-6377-80), with a tapered fitting at one end. A porous PE frit in the tapered fitting supports the 7 cm long resin bed and the open end of the column is covered with a low-density PE dustcover. Before assembling the

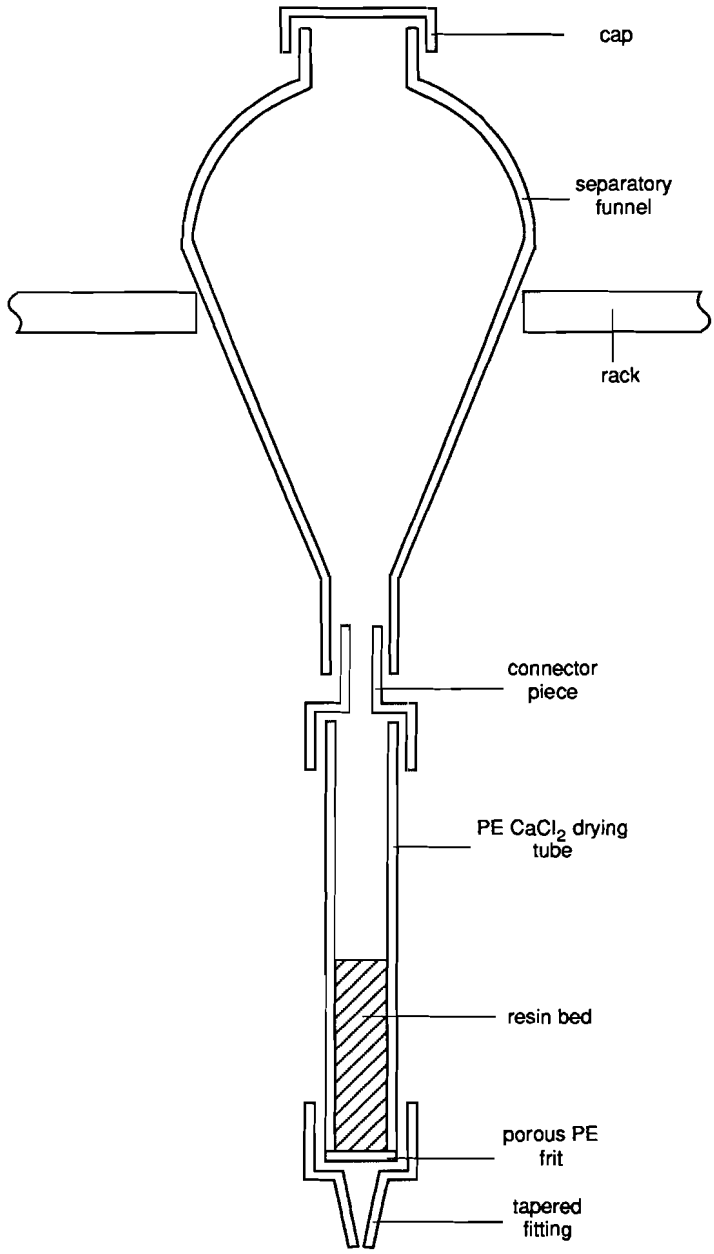

Figure 3.8. Schematic drawing of a Chelex column connected to a Teflon separatory funnel, which serves as a reservoir.

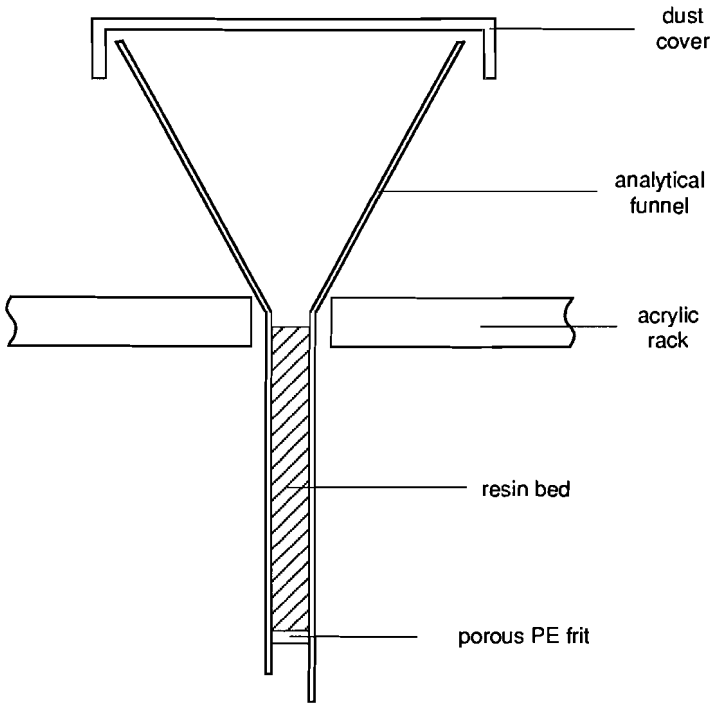

Figure 3.9. Schematic drawing of a small AG 50W-X8 column (resin bed 3.5 x 0.3 cm).

columns, all parts were cleaned separately (Sect. 3.4.2.). Twelve columns are mounted together in an acrylic rack inside the laminar flow bench. Seawater was passed over the columns out of 1 l Teflon FEP separatory funnels, which serve as a reservoir and are mounted in a large rack outside the laminar flow bench. Columns and separatory funnels are joined by Teflon TFE connector pieces (Fig. 3.8).

The AG 50W-X8 columns (Fig. 3.9) consist of a polycarbonate analytical funnel with a straight stem (Just Plastics, Art. 147). The stem has an internal diameter of 3 mm and a length of 45 mm. The 35 mm long resin bed is supported by a porous PE frit, 1 mm above the bottom of the stem. The funnels are covered with polycarbonate petri dishes to protect them from dust. Twelve columns are mounted together in an acrylic rack. Before assembling the columns, all parts were cleaned separately (Sect. 3.4.2.).

Adjustable pipettes. Reagents were pipetted onto the resin beds of the columns with adjustable pipettes (Labsystems Finnpipette 4007040, 200-1000 µl and 4007050, 1-5 ml) with disposable low-density PE tips, unless stated otherwise. A new batch of reagent was not pipetted until the previous batch had passed over the column completely, in

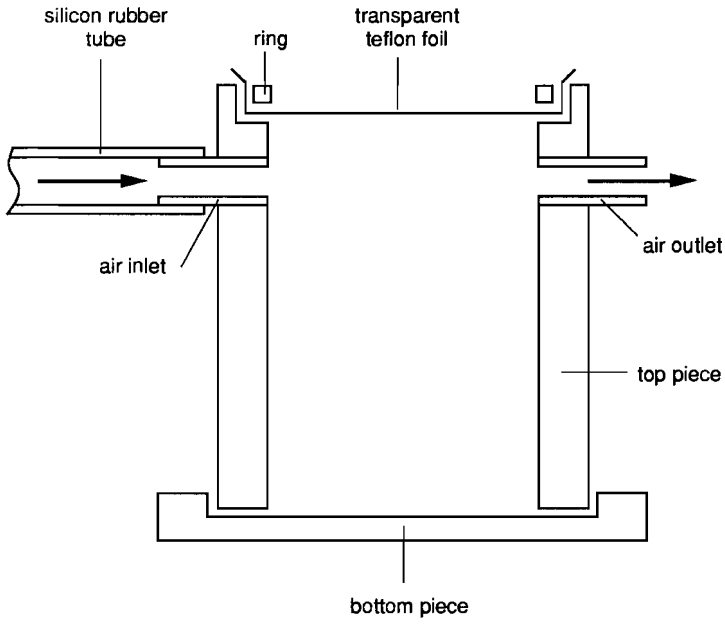

Figure 3.10. Schematic drawing of an evaporator pot. Arrows indicate flow of clean air over the vial (not shown).

order to prevent mixing of reagents. Only the highest purity reagents (Sect. 3.4.1.) were used at all times.

Reagents were never pipetted directly from the reagent bottle. Instead, a small amount of reagent was poured into a 30 ml Teflon PFA vial and pipetted from the vial. Pipette tips were taken out of the storage bottle using large Teflon TFE tongs, rinsed with Milli-Q water, mounted on the pipette and rinsed again by pipetting and discarding Milli-Q water three times from a 30 ml Teflon PFA vial (which was used exclusively for this purpose). Before use the pipette tip was rinsed with reagent by pipetting and discarding it three times from a 30 ml Teflon PFA vial.

Evaporator pots. All evaporations were performed in special evaporator pots (Fig. 3.10), consisting of a hollow Teflon TFE cylinder, one end of which is covered with transparent Teflon foil. The cylinder is placed with the open end down on a Teflon TFE bottomplate. Each evaporator pot can hold several 5 ml or 30 ml Teflon PFA vials.

Vials were placed on the Teflon TFE bottomplate and covered with the cylinder. The evaporator pot with the vials was placed under an infrared (IR) lamp, which creates a

temperature inside the evaporator pot of 70-80 °C. Fumes were removed by constantly flushing the evaporator pots with clean air (Fig. 3.10), which was pumped from the laminar flow bench by an electric pump (Verder N022 AT.18) through a pourous PE prefilter and then through a 0.2 µm mini capsule filter (Gelman Sciences No. 12122).

pH indicator sticks. pH was determined with non-bleeding pH indicator sticks (Merck Spezialindikator 9542.0001 and 9543.0001 and Merck Acilit-indikator 9531.0001). In order to avoid contamination, the pH indicator sticks were never dipped directly into the sample or reagent bottle. Instead, the pH of reagents and 2 l seawater samples was determined by dipping the pH indicator sticks into a small amount of the reagent or sample that had been poured into a 5 ml Teflon PFA vial. After each pH determination the vial was carefully rinsed with demineralized water. pH of small seawater samples (see for instance Chapter 7) was determined by putting a small drop of sample on the pH indicator stick with an adjustable pipette (Labsystems Finnpipette 4007020, 5-50 µl), using a clean pipette tip for each sample. Column effluent pH was checked by catching a drop of effluent on the pH indicator stick.

3.5.2. Spiking of the seawater samples

Twelve seawater samples were transferred to dry, clean 2 l low-density PE narrow-mouth bottles, which had been weighed on an analytical balance (Mettler PM 4600) with a precision of ±0.5 g. After rinsing and filling the preweighed bottles with the seawater samples, sampleweights were determined by weighing the bottles on the same balance again. Approximately 30 drops (~0.2 g) of REE1 spike solution (Sect. 3.2.4.) were added to each sample. A little air was first squeezed from the Teflon FEP drop dispenser bottle in upright position, so that the flow of drops could easily be stopped during transfer of the spike solution. This prevents little drops of spike solution from sticking to the outside of the dispenser. Spikeweights were determined by weighing the drop dispenser bottle on an analytical balance (Sartorius 2842) with a precision of ±0.0005 g, immediately before and after transfer of the spike solution. If a drop did stick to the outside of the dispenser after transfer of the spike solution, the drop dispenser bottle was quickly weighed and then weighed again after removing the drop with a piece of tissue or filterpaper. Sample bottles were shaken vigorously for a few seconds and left to equilibrate for at least 24 hours.

3.5.3. The Chelex preconcentration

First day. The silicon rubber tubes (Sect. 3.5.1.) were removed and each column was filled to the top with Milli-Q water. A slurry was formed by stirring the resin firmly with a clean flexible Teflon TFE rod, in order to remove air bubbles and to prevent coagulation of the resin. After the resin had settled and all the Milli-Q water had passed over

the column, the length of each resin bed was checked and clean resin was added if necessary. The resin bed was cleaned with 45 ml of 6.5 N hydrochloric acid, in three batches of 15 ml, rinsed with 45 ml of Milli-Q water, in nine batches of 5 ml and preconditioned with 30 ml of 1 N ammonia solution, in three batches of 10 ml. All column effluent was discarded. The columns were connected in pairs with the silicon rubber tubes and a fourth batch of 10 ml ammonia solution was left on the resin bed overnight to prevent it from desiccating.

Second day. The silicon rubber tubes were removed and after the ammonia solution on the resin bed had passed over the column a final batch of 5 ml ammonia solution was pipetted onto the resin bed. The resin bed had by then expanded to almost twice its initial length and its colour had become a bright yellow, except for a small part near the bottom.

Shortly before passing it over the column, the sample was neutralized with 1 N ammonia solution and buffered at pH 5.9 by adding 5 ml of 6 N ammonium acetate buffer, followed by a final pH check. The dustcovers (Sect. 3.5.1.) were removed and the columns were connected to the reservoirs (Fig. 3.8) in the rack outside the laminar flow bench. No more than 500 ml of sample was poured into the reservoir at first, in order to allow the resin bed to resume its normal length. Effluent pH was checked regularly, until it reached the sample pH of 5.9. It usually reached this value after about 500 ml of seawater had passed over the column. The reservoirs were then completely filled. It would typically take about 10 hours for a 2 l sample to pass over the column completely. The effluent was collected in low-density PE narrow-mouth bottles and discarded the next day. The empty sample bottles were rinsed three times with Milli-Q water, dried and stored for future use.

Third day. After discarding the effluent, the bottles were rinsed with demineralized water and stored. The reservoirs were rinsed three times with Milli-Q water and placed in the rack outside the laminar flow bench to dry. The columns were transferred to the acrylic rack inside the laminar flow bench and the dustcovers were replaced.

Major elements (specifically Mg and Ca) were eluted with 45 ml of 1 N ammonium acetate buffer, in three batches of 15 ml. Excess buffer was removed with 45 ml of Milli-Q water, in nine batches of 5 ml. The resin bed expanded again slightly during this last step and the effluent pH was about 4.7 due to acetic acid originating from the ammonium acetate buffer. All column effluent was discarded. Trace metals (including the REE) were eluted with 22 ml of 3.5 N nitric acid into a clean 30 ml Teflon PFA vial. The resin bed shrinks during this step, releasing interstitial fluid, so that the final volume of fluid in the vial is about 30 ml. The eluates were evaporated in the evaporator pots (Sect. 3.5.1.). The columns were rinsed with about 50 ml of Milli-Q water and connected in pairs with the silicon rubber tubes. A small amount of Milli-Q water was left on the resin bed to prevent it from desiccating during storage.

After evaporation of the eluates, the vials usually contained a substantial amount of salt, probably ammonium salts that were formed from the ammonium acetate buffer. One day before the AG 50W-X8 separation (Sect. 3.5.4.), 1 ml of 3Q 6.5 N hydrochloric acid was added to each vial. The vials were then closed and placed in the evaporator pots under the IR lamps for about 24 hours.

3.5.4. The AG 50W-X8 separation

First day. The silicon rubber tubes were removed and the reservoirs of the funnels were filled with Milli-Q water. A slurry was formed by stirring the resin firmly with a clean flexible Teflon TFE rod, in order to remove small air bubbles, which may severely reduce the flowrate. After the resin had settled and all Milli-Q water had passed over the column, the length of each resin bed was checked and clean resin was added if necessary. The resin bed was cleaned with 10 ml of 6.5 N hydrochloric acid, in two batches of 5 ml, which makes it shrink to about two thirds of its initial length. Excess acid was removed with 5 ml of Milli-Q water, in five batches of 1 ml. At this point large air bubbles may get trapped at the top of the stem, between the Milli-Q water in the reservoir and the resin bed, blocking it completely. These air bubbles were removed by hitting the funnel on top with the back of the large Teflon TFE tongs. The shock makes the air bubble float to the surface. This somewhat crude method is preferable to touching the clean resin bed with the Teflon TFE rod. As soon as the first batch of water had passed over the column, the resin bed would resume its normal length and remain that way throughout the rest of the procedure. The average flowrate is 2.0 ± 0.5 ml/h, yet hydrochloric acid passes over the column more quickly than Milli-Q water.

The vials under the evaporator pots (Sect. 3.5.3.) were opened so that the contents would evaporate before the next morning.

Second day. The resin bed was preconditioned with 1.5 ml of 0.175 N hydrochloric acid, in three batches of 0.5 ml, which was prepared in small quantities just before use by tenfold dilution of 3Q 1.75 N hydrochloric acid with Milli-Q water, using a 1 ml adjustable pipette. All column effluent was discarded.

The dry and warm samples were redissolved in 1 ml of 0.175 N hydrochloric acid and poured onto the resin bed directly from the vial to minimize contamination. In order to transfer the sample as quantitatively as possible, the sample vials were carefully rinsed with another 1 ml of 0.175 N hydrochloric acid, which was also poured onto the resin bed directly from the vial. The sample was washed onto the resin bed with 0.5 ml of 0.175 N hydrochloric acid. Major elements and trace metals (Sect. 3.2.3.) were eluted with 2 ml of 1.75 N hydrochloric acid and discarded. Ba was eluted with 3 ml of 2.0 N nitric acid and also discarded. At this point clean 5 ml Teflon PFA vials with conic bottoms were placed under each column. Nd-Lu and part of the Ce were eluted with 5 ml of 2.0 N nitric acid. The eluates were evaporated in the evaporator pots (Sect. 3.5.1.).

Third day. La and the remainder of the Ce were eluted with 6 ml of 6.5 N hydrochloric acid into clean 5 ml Teflon PFA vials with conic bottoms, which can just hold 6 ml of fluid. The eluates were evaporated in the evaporator pots (Sect. 3.5.1.). The columns were rinsed with 10 ml of Milli-Q water, connected in pairs with the silicon rubber tubes and stored with a few ml of Milli-Q water on the resin bed to prevent it from desiccating during storage.

After evaporation of the eluates the vials with the Ce-Lu fraction sometimes contained a barely visible yellow spot, probably consisting of traces of resin. The vial with the La-Ce fraction usually did not

contain any visible residue. Before loading the fractions on the filaments (Sect. 3.5.5.) they were redissolved in 0.5-1.0 ml of 3Q 14.4 N nitric acid. The vials were closed and placed in the evaporator pots under the IR lamps for 24 hours, in order to decompose any organic residue (*e.g.* traces of resin) and to convert REE chlorides to REE nitrates. Unlike REE chlorides, REE nitrates give rise to very stable REE emission in the mass spectrometer. Incomplete conversion from chlorides to nitrates may also result in untimely emission of REE (Sect. 3.5.8.). Any organic residue in the REE fractions may cause problems during loading (Sect. 3.5.6.), deterioration of the source vacuum when the temperature of the filaments is raised (Sect. 3.5.8.) and severe blackening of the stainless steel extraction plates (Sect. 3.5.5.).

3.5.5. Filaments and extraction plates

Old filaments were completely removed from the filament inserts with metal tweezers and the tips of the filament inserts were polished. Long strips of zone-refined Re ribbon (0.0012" x 0.030") were cut into pieces of approximately 2 cm length. Each filament insert was placed in a filament welding gauge (Fig. 3.11) together with a piece of the Re ribbon. The welding gauge bends the piece of ribbon in a rectangular U-shape and keeps it in place so that the ends of the ribbon can easily be spotwelded onto the tips of the filament insert (Fig. 3.11). In this way 26 filaments were made, for 13 double-filament assemblies (Fig. 3.12).

The filaments were cleaned for about 15-20 minutes in a boiling soap solution in order to remove fat and fingerprints. Excess detergent was removed by boiling the filaments in pure Milli-Q water for another 15-20 minutes. The filaments were dried in a large oven at 100 °C. After cleaning, the filament inserts were touched only with metal tweezers or wearing clean gloves. The filaments were subsequently baked in a vacuum-oven for about 15 minutes at a temperature of 1600 °C and a vacuum of 10^{-5} mbar, in order to remove impurities that may be present in the Re ribbon. The current through the filaments was raised slowly at first in order to prevent deterioration of the vacuum. When they were still barely glowing, the filaments were counted through a window in the door of the vacuum-oven, to make sure that none of them were broken during spotwelding or cleaning. After baking, the filaments were left to cool under vacuum for one hour. The baked filaments were stored in a stainless steel box to protect them from dust.

Each of the 13 double-filament assemblies on the sample magazine is covered with a stainless steel extraction plate (Fig. 3.12). Each extraction plate contains a vertical slit, ensuring that the ions leave the sample magazine as a reasonably well defined beam. The

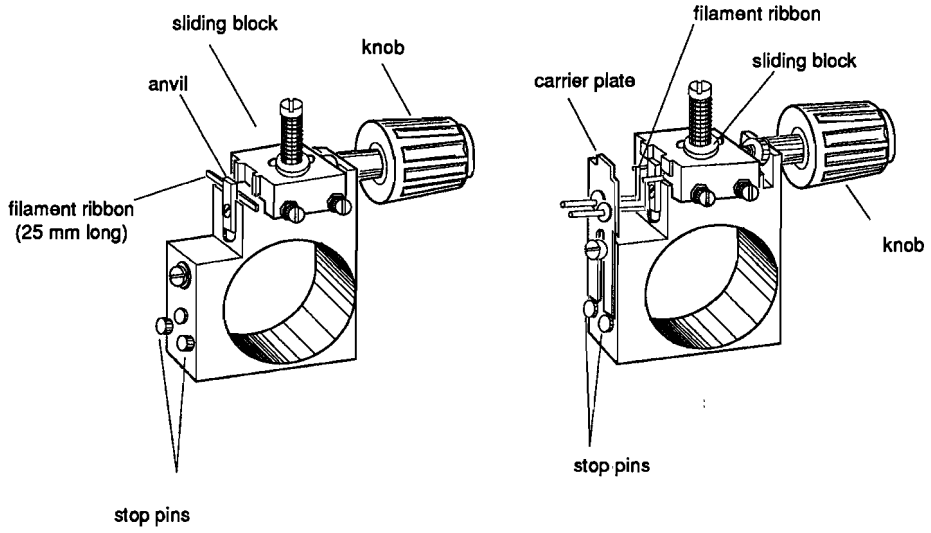

Figure 3.11. Filament welding gauge with a piece of Re ribbon (left) and with a filament insert mounted and the Re ribbon bent (right).

extraction plate also protects the double-filament assembly and separates the samples, to prevent them from contaminating each other during analysis. The extraction plates were often severely blackened, probably as a result of charring of organic matter (*e.g.* resin) that may be present on the filaments (Sect. 3.5.4.). Therefore, the extraction plates were cleaned before assembling the sample magazine (Sect. 3.5.6.). The extraction plates were polished with an ordinary toothbrush using tapwater and liquid abrasive. The extraction plates were subsequently rinsed with tap water, boiled in a soap solution for 15-20 minutes, then in Milli-Q water for another 15-20 minutes and finally dried in a large oven at 100 °C.

3.5.6. Loading the REE fractions on the filaments

The REE fractions were loaded on the filaments inside a class 100 laminar flow clean hood. All stainless steel surfaces were touched only with tweezers or wearing gloves. Half of the filaments were mounted on one side of the sample magazine. The magazine was then mounted horizontally on a sample application device, which allows the magazine to be rotated, connecting each filament in turn with a current source.

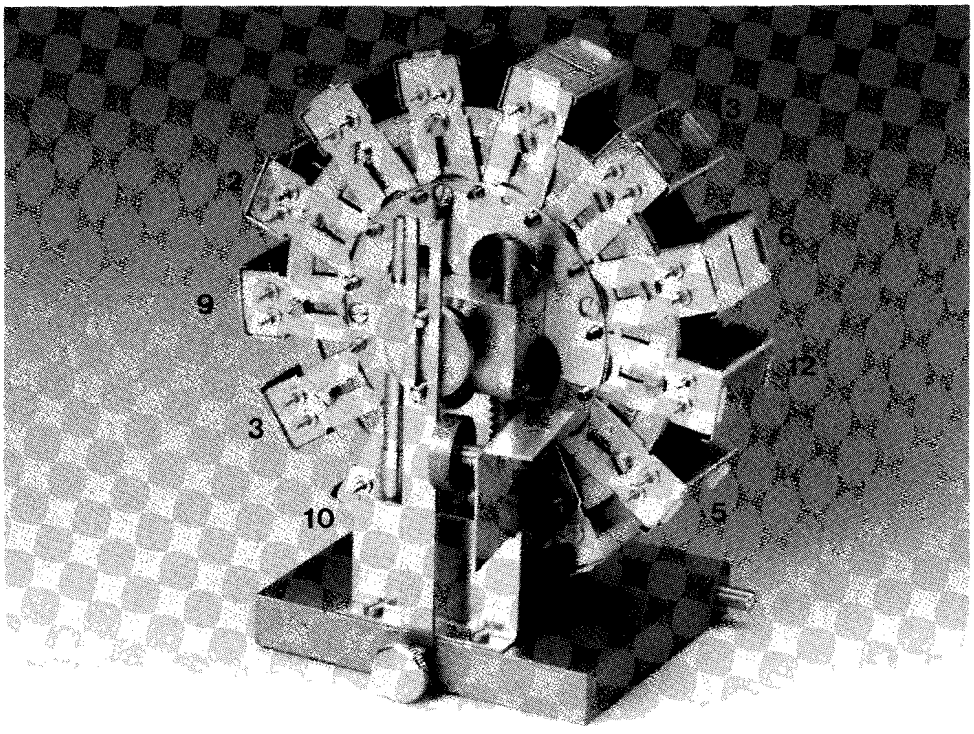
8
3
12
6
9
12
3
10
5

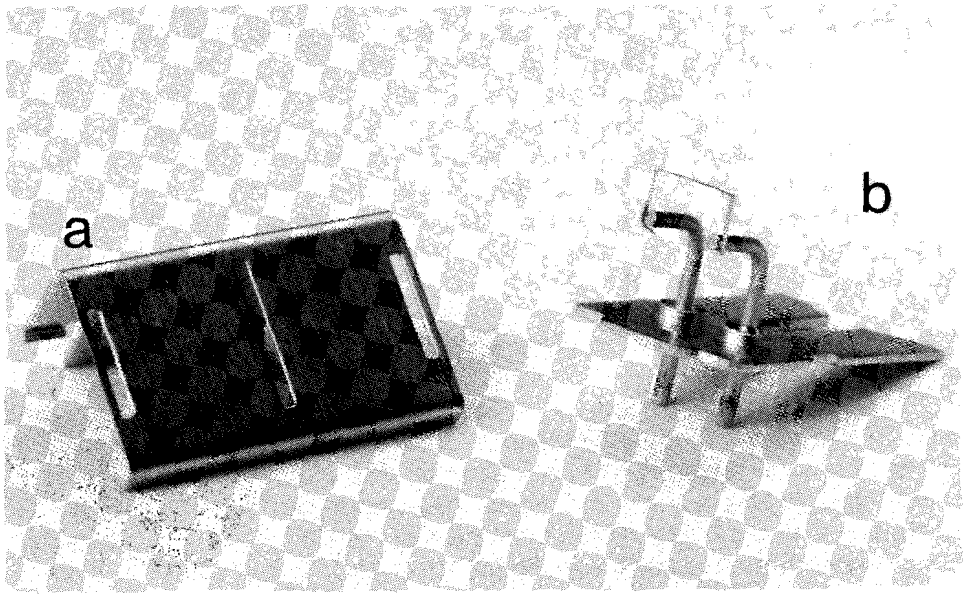
a
b

The sample positions are numbered along the periphery of the magazine in such a way, that there is always a third sample between two successive sample positions (Fig. 3.12). Consequently, all samples have been connected to the current source once, after two full rotations of the magazine, rotating it two positions at a time.

Twelve La-Ce fractions, or twelve Ce-Lu fractions, were loaded in turn on the evaporation filaments of sample positions 2-13 (Fig. 3.12). Shortly before loading it on a filament, each REE fraction was redissolved in 3 µl of 3Q 0.1 N nitric acid, which was transferred to the vial with a micropipette. The tip of the micropipette was first rinsed three times with Milli-Q water and three times with the nitric acid. A current of 0.5 A was sent through the filament and the dissolved fraction was taken up with the micropipette and loaded on the filament, exactly in the middle, in small drops of 0.3-0.5 µl. Each drop was left to dry completely before loading the next one. After the last drop had dried, the current was increased to 1.2 A for three minutes and then to 1.5 A for another three minutes to evaporate all remaining nitric acid. A small white or yellow spot would appear on the filament and sometimes visible fumes escaped. The current was further increased, for just a few seconds, until the filament emitted a dull red glow. The current was never increased above 2 A. The dull red glow is best seen with the lights in the room turned off. The high temperature causes a Re/REE oxide matrix to be formed, which yields an optimal workfunction w for stable REE emission (Sect. 3.2.6.). The same procedure was used for all twelve REE fractions, each time replacing the tip of the micropipette with a clean one.

Finally, the evaporation filament of sample position 1 was loaded with 2 µl of a Nd nitrate standard solution, containing 1 µg of Nd, which was used for calibration of the mass spectrometer (Sect. 3.5.7.). The tip of the micropipette was first rinsed three times with Milli-Q water and three times with the Nd nitrate standard solution. The Nd nitrate standard was loaded as described above for the REE fractions.

When all filaments were loaded, an empty ionization filament was mounted opposite each evaporation filament and the double-filament assemblies were covered with the extraction plates. It was checked that all filaments were visible through the slits from the outside and that all filaments were parallel, not too close together or touching each other. The sample magazine was then mounted in the source of the mass

---

Opposite page: **Figure 3.12.** Top: Sample magazine of the Finnigan MAT 261. Numbering indicates the order in which the samples are analyzed. Bottom: Extraction plate (a). Filament insert with Re filament (b).

spectrometer. The source was evacuated overnight to a vacuum of better than 10^{-7} mbar by a turbomolecular pump. The next morning the cold trap overhead the source was filled with liquid nitrogen (not if the gas bleed system was used) in order to obtain a vacuum of better than 10^{-8} mbar. The valve between the source and the beamtube was opened and calibration of the mass spectrometer was started.

3.5.7. Calibration of the mass spectrometer

The magnetic field of the mass spectrometer is calibrated *versus* mass, by finding the optimal settings of magnetic field and accelerating voltage for a few masses within the mass range of interest and fitting a theoretical curve to these settings. Masses that are selected for calibrating the magnetic field must not be too close together, in order to prevent oscillation of the calibration curve and to ensure accuracy of the calibration over the full mass range of interest (mass 130-180). One of the Faraday collectors (Sect. 3.2.5.) serves as reference collector for calibration of the other Faraday collectors as well as for calibration of the SEM. The calibration curves for the other Faraday collectors are calculated by the computer from their known distance to the reference collector. The calibration curve for the SEM is calculated by the computer from the calibration curve for the reference collector by means of a conversion factor, which is calibrated separately.

When the computer is instructed to set the magnetic field so that the signal corresponding to a certain mass may be detected by the Faraday collector or by the SEM, it refers to the calibration curve. If the calibration curve is inaccurate, then the signal may not be optimally focussed or it may not be detected at all. In the first case, the computer may be instructed to perform a 'peak centre' routine. The computer then changes the settings until the signal is optimally focussed again, compares these new settings with the settings that were given by the calibration curve and stores the difference as a temporary correction to the calibration curve for that particular mass. The correction is updated whenever that same mass is peak centered.

When the computer is instructed to set the magnetic field so that the signal corresponding to a previously peak centered mass may be detected by the Faraday collector or by the SEM, it will apply the latest correction to the calibration curve. If all masses that are specified in the data acquisition routines (Table 3.5) are regularly peak centered during REE analysis, then the corresponding signals will continue to be optimally focussed, even when the electronics of the mass spectrometer are drifting due to unstable room conditions.

Calibration of the mass spectrometer was started as soon as a

vacuum of better than 10^{-8} mbar was established in the source (Sect. 3.5.6.). ^{23}Na and ^{39}K were used for the low-mass end of the calibration curve. Na and K were always present on the filaments. ^{187}Re was used for the high-mass end of the calibration curve and the intermediate mass range was covered by ^{142}Nd, ^{146}Nd and ^{150}Nd. Signals of ^{23}Na and ^{39}K were produced by sending a current of 2.5-3.0 A through the ionization filament of the double-filament array on which the Nd nitrate standard was loaded. Increasing the current to 5 A produced a ^{187}Re signal of about 30-50 mV. The ionization temperature was then lowered to 1700 °C (4.1-4.3 A) and signals of ^{142}Nd, ^{146}Nd and ^{150}Nd were produced by sending a current of 1.8-2.0 A through the evaporation filament. Each signal was identified visually from the mass spectrum on the reference collector and focussed by adjusting the magnetic field and the lens settings manually until an optimal signal was obtained. Calibration of the corresponding mass was then performed automatically by the computer. Masses were calibrated in the order 39-23-187-142-145-150. Masses 39, 23 and 187 were calibrated only once, while the calibration of masses 142-145-150 usually had to be repeated several times (in the same order), before a satisfactory result was obtained. After the calibration, all seven Nd isotopes were peak centered in order of increasing mass, so as to minimize the magnet's hysteresis. This was repeated twice. Finally, the conversion factor for calculating the SEM calibration curve from the calibration curve of the reference collector was calibrated and the SEM peakshape was checked and optimized if necessary by adjusting the SEM deflection voltage.

Calibration of the mass spectrometer would typically take about one hour. In general, it had to be repeated every other day, depending on room conditions (stable temperature, humidity *etc.*).

3.5.8. REE analysis of a seawater sample

When the gas bleed system was used (Sect. 3.2.6.), the bleeding valve was opened gradually, meanwhile monitoring the source vacuum on the ionization gauge, until the desired oxygen or freon partial pressure was established.

The temperature of the ionization filament was raised in steps of 0.2 A, meanwhile monitoring the source vacuum on the ionization gauge. The vacuum may suddenly deteriorate as the temperature increases, if organic matter is present on the evaporation filament. Ba was monitored on the SEM at mass 138 and the ionization temperature was further raised until a significant Ba signal was detected (usually at 3.0-3.5 A). After the Ba emission had stabilized, the signal was focussed by manually adjusting the lens settings and the vertical

position of the double-filament assembly. The ionization temperature was then raised to 1700 °C (4.1-4.3 A). At this point small Ce signals or CeO signals would sometimes be present in the mass spectrum. Mostly these signals were very unstable and decayed rapidly and were probably caused by poor conversion of REE chlorides to REE nitrates (Sect. 3.5.4.). If however these Ce or CeO signals were stable and strong enough, they were used for further optimization of the focus.

Subsequently, the evaporation temperature was slowly raised, meanwhile monitoring the major isotope of the first REE to be emitted (Ce), until all signals were large enough (≥10 mV) for the SEM to determine isotopic ratios with acceptable precision (Sect. 3.2.5.). REE signals were rarely raised above 25-30 mV, since such strong signals often decay rapidly or are associated with major isobaric interference. Only the ^{139}La signal was commonly raised above 100 mV, in order to obtain a possibly high ^{138}La signal (although still <<10 mV) and to stimulate prompt decay of the Ba signal. This is possible (as long as La emission remains stable), since the La-Ce fraction does not contain interfering elements with higher emission temperatures.

The desired data acquisition routine was selected and after final focussing of the signals, data acquisition was started. The signal on the SEM was continuously plotted on a stripchart recorder, so that the operator could take immediate action if the signals became unstable, or if they increased or decreased too rapidly. After the computer had completed data acquisition with acceptable precision, the evaporation temperature (and if necessary also the ionization temperature) was raised again, until strong and stable signals of the next REE in the REE emission sequence (3.2) were established. In this way all REE were analyzed successively.

Data is printed in a data report, which contains final isotopic ratios with the corresponding statistical errors (1σ) as well as twelve corrected scans (Sect. 3.2.5.). Each scan contains all the isotopic ratios that are specified in the data acquisition routine (Table 3.5) as well as the ioncurrent of the major REE isotope (expressed in Volts).

3.5.9. Data processing

Three computer programs were written in Turbo Pascal 3.0 for processing the REE isotopic ratio data that result from the REE analyses on the mass spectrometer. All data were taken directly from the data report (Sect. 3.5.8.), either in the form of one final REE isotopic ratio with the corresponding statistical error (1σ), or, in case correction for isobaric interference was required, in the form of twelve corrected scans (Sect. 3.2.5.).

The program DYCALC corrects Dy isotopic ratios for the complex

isobaric interferences that are associated with the analysis of Dy (Sect. 3.2.5.). The 162/161 ratio is corrected for Er and NdO interference and the 163/161 ratio for NdO interference. The correction is performed for each scan separately. The arithmetic mean of the twelve corrected scans is calculated together with the statistical error (1σ).

The program SCANCOR is similar to the program DYCALC and corrects isotopic ratios of several other REE for isobaric interferences. On request SCANCOR can correct the 138/139 ratio of La for Ce interference, the 142/140 ratio of Ce for Nd interference and finally the 168/167 ratio and the 170/167 ratio of Er as well as the 176/175 ratio of Lu for Yb interference. SCANCOR can also correct the 151/153 ratio of Eu for BaO or BaF interference, yet this option was never used in practice (Sect. 3.2.5.). Again, the corrections are performed for each scan separately. The arithmetic mean of the twelve corrected scans is calculated together with the statistical error (1σ).

The program REECALC calculates REE concentrations from the final corrected REE isotopic ratios C_{jk} in the spiked seawater sample (Sect. 3.2.4.). REECALC also estimates the error in the calculated REE concentrations from the statistical errors in the isotopic ratios (1σ), by calculating the REE concentrations corresponding to $C_{jk} + 1\sigma$ and $C_{jk} - 1\sigma$. The differences between either of these two REE concentrations and the REE concentration calculated from C_{jk} are compared and the largest difference is accepted as the error. These errors are not representative of the precision of multi-element IDMS analysis of the REE in seawater on the Finnigan MAT 261, yet merely a qualitative measure of the error magnification that may result from overspiking or underspiking of the seawater sample (Sect. 3.2.4.). Finally, from the calculated REE concentrations REECALC calculates all REE isotopic ratios in the spiked seawater sample that are necessary for interference corrections but not directly measured by the mass spectrometer during REE analysis.

If two isotopic ratios are available for calculating the REE concentration, then REE concentrations are calculated from both and presented together with the relative difference between them as well as with their arithmetic mean or weighted average (Sect. 3.2.5.). The error corresponding to the arithmetic mean or weighted average is calculated from the errors that are estimated for the two REE concentrations. If for Er or Yb the relative difference between the two REE concentrations exceeds 5%, REECALC offers the possibility to use either of them or their weighted average for the calculation of Er and Yb isotopic ratios that are necessary for interference corrections.

CHAPTER 4 Vertical distributions of Mn and Fe in the anoxic brines of Bannock Basin

4.1. Introduction

In 1983 and 1984 two anoxic basins were discovered in the eastern Mediterranean Sea, which were called Tyro Basin and Bannock Basin after the respective research vessels (Jongsma *et al.*, 1983; De Lange and Ten Haven, 1983; Scientific staff of cruise *Bannock* 1984-12, 1985). Actually, the basins appeared to be filled with anoxic brines, formed by dissolution of outcropping or underlying Messinian evaporites (Ten Haven *et al.*, 1985; Corselli and Aghib, 1987; Camerlenghi, 1990). The only previously known examples of basins containing brines were deeps in the Red Sea (Degens and Ross, 1969) and Orca Basin in the northern Gulf of Mexico (Shokes *et al.*, 1977), yet Tyro Basin and Bannock Basin are very different from both of these. The Tyro and Bannock brines are cold brines, unlike the Red Sea brines, which are hot brines. Moreover, whereas the Orca brine contains a maximum of 3 µM sulfide, sulfide contrations as high as 2.7 mM were reported for the Tyro and Bannock brines (Bregant *et al.*, 1990; Luther *et al.*, 1990), second in the world only to Framvaren Fjord (South Norway), where sulfide concentrations of 7 mM were found in anoxic water of normal seawater salinity (Skei, 1983). The extraordinary combination of high salinity and high sulfide levels provides unique conditions for a study of trace metal cycling (Saager *et al.*, 1991).

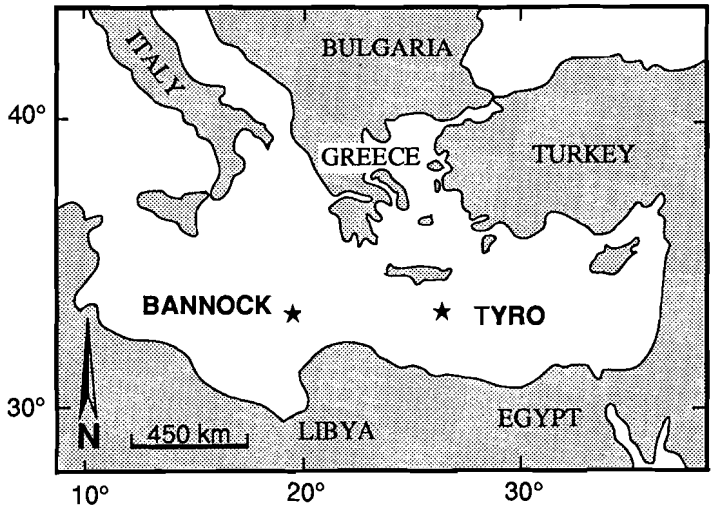

Figure 4.1. Map of the eastern Mediterranean Sea. Bannock Basin (34°18'N 20°02'E) and Tyro Basin (33°54'N 26°02'E) are indicated with solid stars.

Although Tyro Basin and Bannock Basin are filled with anoxic brines of similar origin, there is a number of significant differences between them. First, Tyro Basin is located in the Levantine basin, whereas Bannock Basin is located in the Ionian basin (Fig. 4.1). The Levantine basin and the Ionian basin are separated by a sill in the Strait of Crete, which may partly impede the exchange of deep water. Since deep water in the Levantine basin and in the Ionian basin may be formed in different regions (Sect. 4.2.1.), the Tyro and Bannock brines may be in contact with deep water masses of slightly different chemical composition.

Second, Tyro Basin and Bannock Basin were formed by different processes (Sect. 4.2.2.). As a result, their morphology is different. In the Tyro area only one basin, the Tyro Basin, was found to contain anoxic brine, whereas the Bannock area consists of a conglomerate of sub-basins, which were named after various local winds (Fig. 4.2).

Third, the Tyro brine and the Bannock brine have a different chemical composition (Bregant *et al.*, 1990; De Lange *et al.*, 1990a,b). De Lange *et al.* (1990a,b) demonstrated that this may largely be attributed to the composition of the evaporites from which they derive. Apparently, the Bannock brine was formed by dissolution of a late stage evaporite, whereas the Tyro brine was formed by dissolution of an early stage evaporite. Furthermore, it was shown that the chemical composition of the brine was probably affected by secondary alteration processes (Sect. 4.2.2.). Such processes may have affected the chemical compositions of the Tyro and Bannock brines to different extents. Secondary alteration of the Bannock brine has led to a distinct two-layered structure, with a slightly different chemical composition in each layer (Sect. 4.2.2.). The interface between the upper brine and the lower brine will hereafter be referred to as the 'second interface'. In the Tyro brine no multi-layered structure was observed, in fact it appears to be completely homogeneous, both physically and chemically.

Apart from the newly discovered anoxic basins in the eastern Mediterranean, the Mediterranean Sea itself has long been recognized as a very interesting environment for studying trace metal cycling. It has been shown that the correlations, characteristic of open ocean waters, between several trace metals on the one hand and the nutrients nitrate, phosphate and silicate on the other hand (Bruland, 1983), are either modest or absent in the Mediterranean Sea (Kremling and Petersen, 1981; Spivack *et al.*, 1983; Laumond *et al.*, 1984; Boyle *et al.*, 1985; Statham *et al.*, 1985; Huynh Ngoc and Whitehead, 1986; Copin-Montegut *et al.*, 1986; Van Geen *et al.*, 1988; Sherrell and Boyle, 1988; Morley *et al.*, 1991, Saager *et al.*, 1991). Concentrations of most trace metals were found to be largely homogeneous throughout the watercolumn, showing neither depletion in the surface waters nor enrichment in the

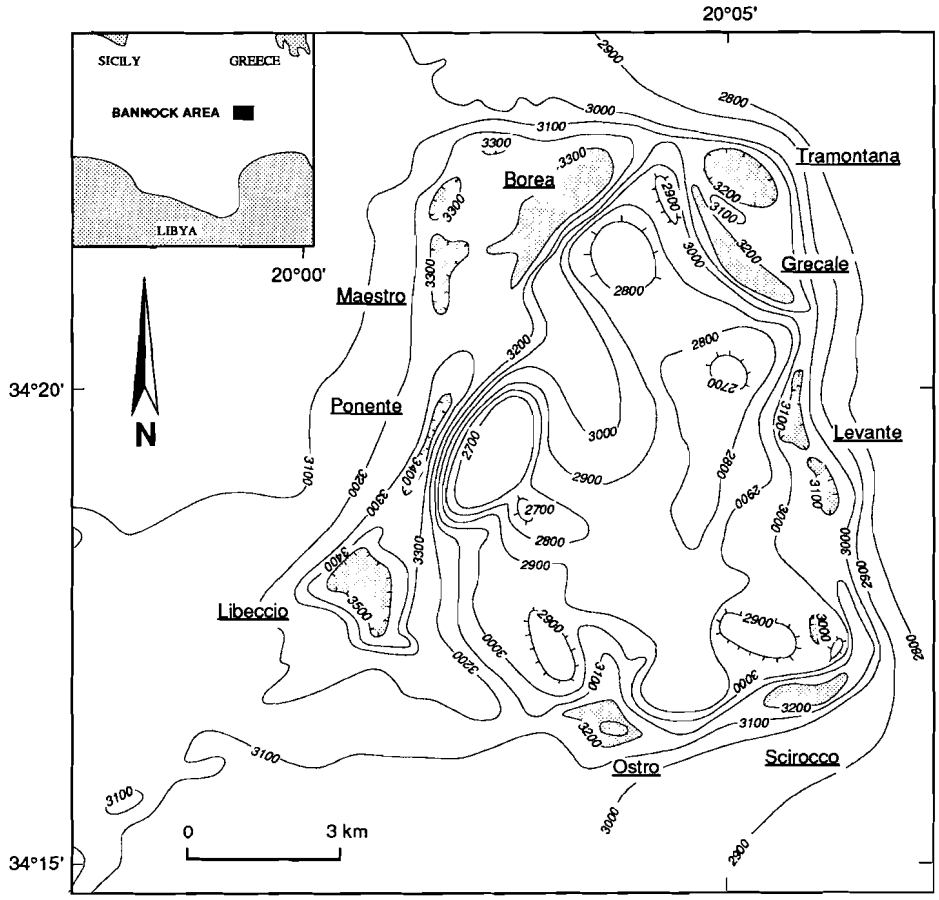

Figure 4.2. Detailed map of the Bannock area showing the various sub-basins. Anoxic brines are indicated by shading. All data in Chapters 4 and 5 are from the Libeccio sub-basin, which is referred to in the text as 'Bannock Basin'.

deep water. In contrast, studies of dissolved aluminium in the Mediterranean Sea have revealed a strong correlation with silicate (Mackenzie *et al.*, 1978; Hydes *et al.*, 1988), whereas no such correlation is commonly found in open ocean waters (Orians and Bruland, 1986).

The Mediterranean Sea is characterized by very low nutrient concentrations and very low productivity (Sect. 4.2.3.) and has been described as the most impoverished large body of water in the world. Salinity is high as a result of excessive net evaporation. The water budget is dominated by exchange of water through the Strait of Gibraltar. For this reason most studies of trace metal cycling in the Mediterranean Sea have been focussed on the western Mediterranean and the Alboran Sea. Spivack *et al.* (1983) used measurements of surface water trace metal concentrations across most of the Mediterranean Sea to estimate the exchange of trace metals through the Strait of Gibraltar. Their calculations suggested that the Strait of Gibraltar is a net sink of several trace metals to the Mediterranean Sea. Various sources of trace metals have been proposed to balance the loss, such as trace metal enriched coastal waters outside the Mediterranean Sea that are entrained by the inflow of Atlantic surface water (Boyle *et al.*, 1985; Sherrell and Boyle, 1988; Van Geen *et al.*, 1988), atmospheric input (Spivack *et al.*, 1983; Buat-Ménard *et al.*, 1989) and non-steady-state behaviour due to anthropogenic trace metal discharges (Béthoux *et al.*, 1990). On the other hand, Boyle *et al.* (1985) and Sherrell and Boyle (1988) proposed that sluggish removal of trace metals from the surface waters due to inefficient recirculation of nutrients could account for the observed vertical distributions of trace metals and that external sources need not necessarily be invoked. In order to obtain a complete database for testing these assumptions, it is imperative that more attention is given to other parts of the Mediterranean Sea. Vertical distributions of trace metals in the Mediterranean seawater overlying the Tyro and Bannock brines are very interesting in this respect (Saager *et al.*, 1991).

In the period 1986-1988 Tyro Basin and Bannock Basin were the subject of four scientific cruises. Seawater samples for analysis of the REE and other trace metals were collected from both basins during the 1987 Anoxic Basin Chemistry (ABC) Cruise aboard Dutch R/V *Tyro*. The discussion in this Chapter is limited to the vertical distributions of Mn and Fe in Bannock Basin. Vertical distributions of Mn and Fe in Tyro Basin (De Baar *et al.*, 1987; De Lange *et al.*, 1990a,b,c; Saager *et al.*, 1991) will only be referred to for comparison, when appropriate. The discussion is divided into two parts, one dealing with the overlying seawater and the other dealing with the brine, with special focus on the seawater-brine interface, and forms the groundwork for the discussion of the vertical distributions of dissolved REE in Bannock Basin (Chapter 5). All data presented in this Chapter and in Chapter 5 are from a station in the deepest part of the main body of sub-basins, the Libeccio sub-basin (Fig. 4.2). This station will hereafter simply be referred to as 'Bannock Basin'.

4.2. Bannock Basin

4.2.1. Hydrography of the overlying seawater

The hydrography of the eastern Mediterranean was recently reviewed by Malanotte-Rizzoli and Hecht (1988). Emphasizing the many contradictory observations in the literature they showed that very little has as yet been established concerning general circulation, the number of watermasses and their origin. Nevertheless, some facts seem to be generally accepted. First, virtually all exchange of deep water between the eastern and the western Mediterranean is prevented by the sill in the Strait of Sicily. Second, three distinct watermasses have been identified in the eastern Mediterranean. These watermasses can clearly be distinguished in the salinity profile for the overlying seawater that was recorded at Bannock Basin during the 1987 ABC Cruise (Fig. 4.3a,b).

Atlantic Surface Water (ASW) enters the Mediterranean Sea through the Strait of Gibraltar and penetrates as far as the easternmost Mediterranean. In the western Mediterranean, a thin layer of hot, highly saline water, formed at the very surface by extensive evaporation during summer, prevents early dissipation of ASW. In winter, depletion of ASW occurs near the Strait of Sicily. At Bannock Basin ASW extends from the surface down to about 60 dbar. Salinity is variable in the range 38.4-38.6 psu (Fig. 4.3b). The salinity maximum of 38.55 psu at about 25 dbar is probably associated with the core of ASW. Malanotte-Rizzoli and Hecht (1988) reported a salinity of 38.6 psu for ASW near the Strait of Crete. Temperature decreases rapidly from 19.1 °C at the surface to 15.3 °C at 60 dbar (Fig. 4.3c).

Levantine Intermediate Water (LIW) is present between 60 and 400-600 dbar, with a salinity maximum of 38.90 psu at about 200 dbar (Fig. 4.3a), in excellent agreement with the value given by Malanotte-Rizzoli and Hecht (1988) for LIW near the Strait of Crete. Temperature decreases gradually from 15.3 °C to 13.9 °C. LIW originates in the Levantine basin, as its name implies. The exact formation area is not known, but the region between Rhodes and Cyprus is favoured in most publications. Optimal conditions for the formation of LIW are created in winter, when cold, dry masses of continental polar or arctic air, crossing the eastern Mediterranean, intensively cool the surface waters and increase their salinity by evaporation (Ovchinnikov and Plakhin, 1984). LIW then spreads across the Mediterranean Sea to the west, where it becomes a major component of the Mediterranean outflow through the Strait of Gibraltar (Wüst, 1961).

Deep water is found below about 600 dbar, with a temperature of 13.6 °C and a salinity of 38.66 psu (Fig 4.3a,c). There have been

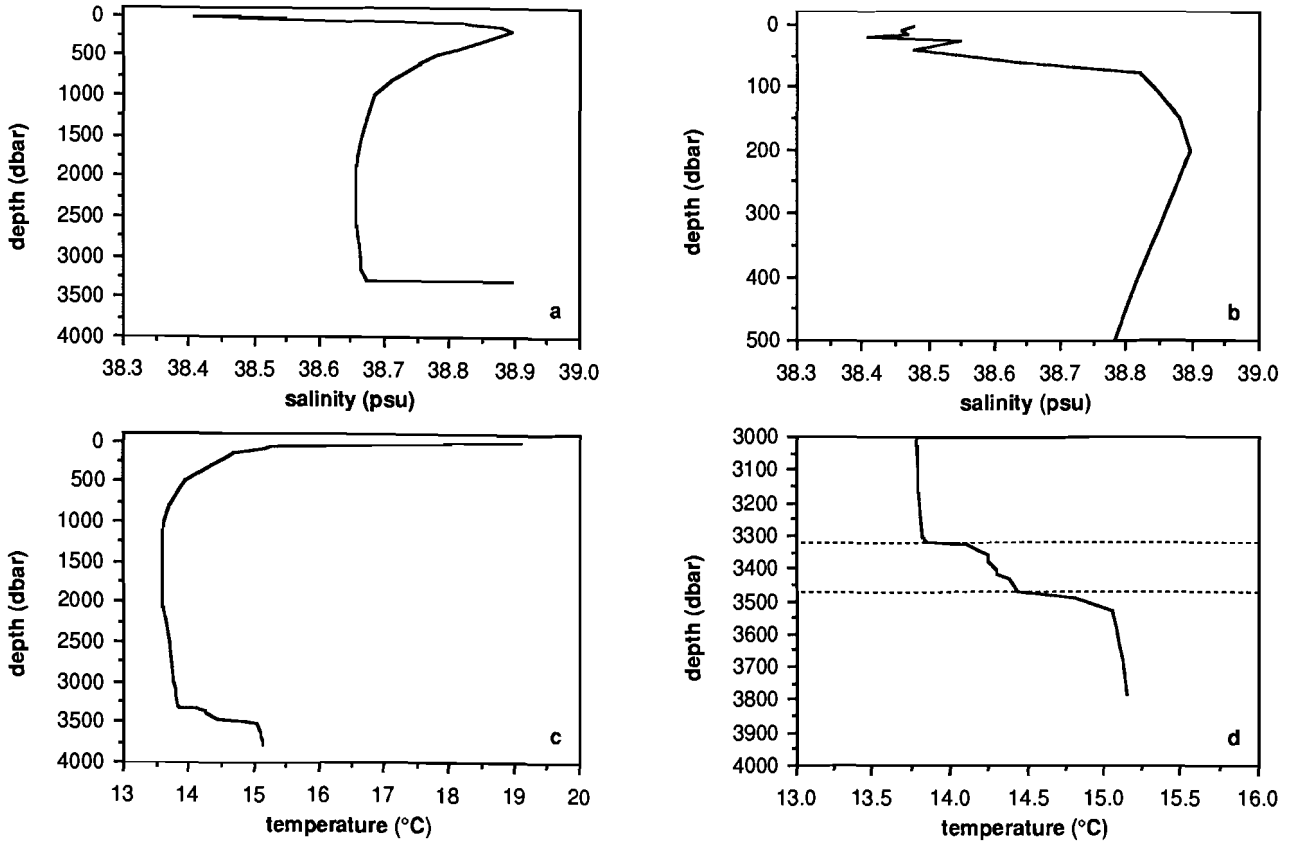

Figure 4.3. Salinity profile (a) with detail of the top 500 dbar (b). Salinity is expressed in practical salinity units (psu). Temperature profile (c) with detail of the brine (d). Seawater-brine interface and second interface are indicated with dashed lines. All data from Hydes *et al.* (1988).

attempts to distinguish as many as three distinct deep water masses, yet Malanotte-Rizzoli and Hecht (1988) found no firm hydrographical grounds to do so and preferred to treat the entire watercolumn below 600 dbar as a single watermass. The watercolumn below 600 dbar at Bannock Basin will hereafter be referred to as 'Eastern Mediterranean Deep Water' (EMDW). Various contradictory observations suggest different formation areas for deep water. Plakhin (1971) proposed that each basin in the Mediterranean Sea is the formation area of its own characteristic deep water, with the exception of the Ionian Sea, where deep water is of Adriatic origin. The northern and central parts of the Adriatic Sea and the Aegean Sea are often mentioned as important deep water formation areas for the eastern Mediterranean, although in part of the Aegean Sea deep water formation may be impeded by low salinity Black Sea water coming from the Sea of Marmara (Plakhin, 1972). Winter is the most propitious season for the formation of deep water (Plakhin, 1972), as it is for the formation of LIW.

4.2.2. The brine

At Bannock Basin the watercolumn between 3323 dbar and the bottom at 3784 dbar is occupied by anoxic brine. The transition from overlying seawater to brine is associated with sharp gradients of salinity (Fig. 4.3a) and temperature (Fig. 4.3c). It is difficult to determine salinity in the brine accurately. Bregant *et al.* (1990) estimated brine salinity with a salinometer after diluting brine samples volumetrically to approximately seawater salinity. They reported a salinity of 325 psu, which is nearly ten times the salinity of the overlying seawater. However, this estimate does not take into account that seawater and the brine have different compositions. Boldrin and Rabitti (1990) measured brine conductivity, using a special conductivity sensor with an extended range. In the Bannock brine they found a conductivity of about 177 mS/cm, nearly four times that of the overlying seawater.

The formation of Bannock Basin itself, like the formation of the Bannock brine, is directly related to the dissolution of Messinian evaporites (Camerlenghi, 1990). In contrast, the formation of Tyro Basin (Camerlenghi, 1990) and Orca Basin (Addy and Behrens, 1980) is not related to the formation of their respective brines. Bannock Basin is located on the Mediterranean Ridge, which is an accretionary prism, forming in response to the convergence between the African and European plates. In this region, direct contact between seawater and Messinian evaporites occurs when tensional cracks are created on the crest of anticlines upon initial folding of the sediments close to the deformation front. Subsequent dissolution of the underlying Messinian

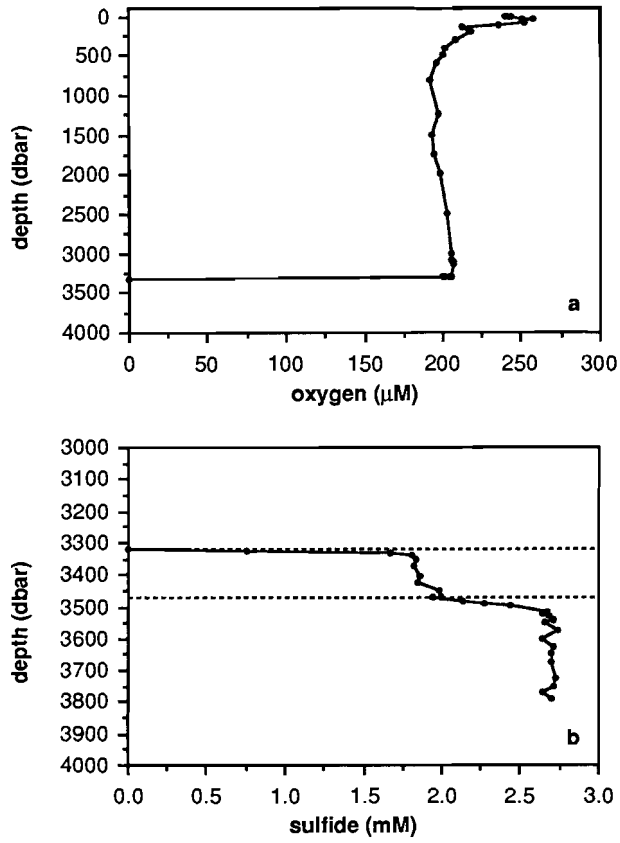

Figure 4.4. Oxygen profile (a). Sulfide profile in the brine (b). Seawater-brine interface and second interface are indicated with dashed lines. Oxygen data from Hydes *et al.* (1988). Sulfide data from Luther *et al.* (1990).

evaporites causes collapse of the sediments and inversion of relief (Camerlenghi, 1990). This process is the origin of the so called 'cobblestone topography', which characterizes the general area (Scientific staff of cruise *Bannock* 1984-12, 1985). As the Bannock Basin deepened, Messinian evaporites were eventually exposed at the base of its walls, establishing the proper conditions for formation of a brine lake. Evidence from the sediments indicates that such exposure of Messinian evaporites and the onset of permanent anoxic conditions occurred as early as 180,000 years ago.

By dissolution of Messinian evaporites a brine was formed with a salinity nearly ten times that of the overlying seawater and a density of about 1.2 kg/dm^3 (Bregant *et al.*, 1990; De Lange *et al.*, 1990a). The resulting density gradient at the seawater-brine interface is the sharpest known in the world today (De Lange *et al.*, 1990c). Due to the density gradient, mixing between the brine and the overlying seawater is strongly restricted and decomposition of organic matter has caused total depletion of oxygen in the brine (Fig. 4.4a), by the mechanism that was discussed in Chapter 2. Sulphate reduction takes place in the brine as signified by the presence of sulfide (Fig. 4.4b) at concentrations of up to 2.7 mM (Luther *et al.*, 1990; Bregant *et al.*, 1990), which makes the Bannock brine the second most sulfidic body of water in the world (Sect. 4.1.). The decomposition of organic matter in the brine and its implications for the vertical distributions of sulfide, organic carbon and the major nutrients is discussed in more detail in Section 4.2.3.

The concentrations of most elements change dramatically at the seawater-brine interface. For some elements the change can be attributed directly to the dissolution of Messinian evaporites. Higher concentrations may lead to oversaturation with respect to solid phases. Moreover, solubility products and equilibrium association constants (Chapters 2 and 5) are strongly affected by the extreme ionic strength, increasing or further decreasing the solubility of elements in the brine. Finally, the large shift in the redox potential at the seawater-brine interface causes redox sensitive elements to be reduced to lower oxidation states within the brine, which may be either more soluble or less soluble than the oxidation states that prevail in the overlying seawater. Consequently, the concentrations of elements in the brine are determined by a very intricate system of interrelated equilibria. The situation is complicated even more by the fact that equilibrium may often not be reached as a result of kinetic hindrance. Finally, steady state within the brine may not be a valid assumption.

The most conspicuous feature of the Bannock brine is its two-layered structure, which is clearly portrayed by the temperature profile (Fig. 4.3d). A temperature profile of this kind is typically formed when a linear, stable salinity gradient is heated uniformly from below at a constant rate (Boldrin and Rabitti, 1990). From estimates of the geothermal flux Boldrin and Rabitti (1990) calculated that it would take at least 4500 years to establish the observed temperature profile, assuming that the geothermal flux is the only source of heat and that heat transfer is limited to molecular diffusion. A minimum time of only 150 years was calculated for the Tyro brine, which is at a lower temperature than the Bannock brine, has a much smaller volume and does not show a multi-layered structure. This difference is in apparent contrast with the conclusions of Stenni and Longinelli (1990), who

inferred from measurements of $\delta^{18}O(H_2O)$ that the Bannock and Tyro brines have approximately the same age.

The major constituents of the brine, Na and Cl, do not show a change of concentration at the second interface, nor does ammonium (Sect. 4.2.3.). However, concentrations of most major ions either significantly increase (*e.g.* K^+, Mg^{2+}, SO_4^{2-}, Br^-), or significantly decrease (*e.g.* Ca^{2+}, Ba^{2+}) across the second interface (De Lange *et al.*, 1990a). Total alkalinity (Bregant *et al.*, 1990) and phosphate (Sect. 4.2.3.) show a distinct maximum, whereas Mn and Fe (Sect. 4.4.1.) and the REE (Chapter 5) show a distinct minimum at the second interface. De Lange *et al.* (1990a) demonstrated that the lower concentrations of K^+ and Br^- in the upper brine are perfectly consistent with a slightly higher dilution with ambient seawater. After correcting for this excess dilution, the upper brine is still enriched in Ca^{2+} and depleted in Mg^{2+} and SO_4^{2-} relative to the lower brine. De Lange *et al.* (1990a,b) argued that this observation may be explained by secondary alteration of the brine, specifically recrystallization of Ca carbonates (dolomitization) and simultaneous precipitation of gypsum as in equation (4.1)

$$Mg^{2+} + (1+x)SO_4^{2-} + (2+x)CaCO_3 + (2+2x)H_2O \rightarrow$$

$$Mg,Ca(CO_3)_2\downarrow + (1+x)CaSO_4{\cdot}2H_2O\downarrow + xCO_3^{2-} \qquad (4.1)$$

During the alteration process Mg^{2+} is removed from the brine and Ca^{2+} is released. Part of the Ca^{2+} subsequently precipitates with SO_4^{2-} to form gypsum. Large gypsum crystals were indeed recovered from the sediments underlying Bannock Basin (Scientific staff of cruise *Bannock* 1984-12, 1985; Corselli and Aghib, 1987). Precipitation of gypsum is the limiting factor for the concentration of Ca^{2+}. Similarly, precipitation of $BaSO_4$ is the limiting factor for the concentration of Ba^{2+}. De Lange *et al.* (1990b) suggested that the major part of the alteration process occurred before outflow of the brine into the Bannock Basin. A different degree of pre-outflow alteration could account for the differences in chemical composition between the upper and the lower brine.

On the other hand, some anomalies at the second interface, such as the phosphate maximum (Sect. 4.2.3.), the alkalinity maximum and the Mn minimum (Sect. 4.4.1.), can best be explained by *in situ* dolomitization and precipitation of gypsum. For instance, the alkalinity maximum is probably caused by the release of CO_3^{2-}, which rapidly equilibrates to form HCO_3^-. The Mn minimum is indicative of a removal process, probably related to the precipitation of some solid phase. The

ionic radius of Mn^{2+} is nearly equal to that of Ca^{2+}. Mn^{2+} is known to replace Ca^{2+} readily in the crystal lattice of Ca solid phases (see for instance Middelburg *et al.*, 1987). Therefore, *in situ* precipitation of both dolomite and gypsum could account for the observed Mn minimum. The Mn content of gypsum (6 ppm) *versus* that of dolomite (550 ppm) suggests that the latter is the more likely candidate (De Lange *et al.*, 1990b).

4.2.3. Nutrients

Profiles of the major nutrients are shown in Figures 4.5 and 4.6. The phosphate (PO_4^{3-}) profile in the overlying seawater (Fig. 4.5a) is similar to phosphate profiles in the open ocean. Concentrations are low at the surface, where phosphate is taken up in organic matter due to biological activity, and rapidly increase with depth below the surface as the organic matter decomposes. Despite considerable scatter in the data, a maximum can be resolved at about 1000 dbar. Throughout the overlying seawater concentrations are 5-10 times lower than in the open Atlantic Ocean. The same is true for nitrate and silicate (Fig. 4.5c and 4.6a). This depletion of major nutrients is characteristic of the Mediterranean Sea and a direct result of general circulation. Atlantic Surface Water (ASW), depleted in major nutrients, enters the Mediterranean Sea through the Strait of Gibraltar. The inflow is balanced by an outflow through the Strait of Gibraltar into the North Atlantic, probably mainly consisting of Levantine Intermediate Water (LIW), which is enriched in major nutrients relative to ASW. Since the magnitudes of inflow and outflow are nearly equal, the Strait of Gibraltar is a net sink of major nutrients to the Mediterranean Sea. Another reason is probably the low age of the deep water (Béthoux, 1980). Flushing seems to be sufficiently rapid to prevent the building up of high phosphate concentrations (Boyle *et al.*, 1985; Sherrell and Boyle, 1988).

At the seawater-brine interface concentrations of phosphate increase by about two orders of magnitude, with a pronounced maximum at the second interface (Fig. 4.5b). The higher concentrations of phosphate in the brine are caused by decomposition of organic matter, also signified by elevated concentrations of DOC (Henneke and De Lange, 1990). However, it is not exactly known where this decomposition takes place (Bregant *et al.*, 1990). Organic matter settling from the productive layer may accumulate at the density gradient and be oxidized as a result of bacterial activity. This seems to be supported both by a POC maximum (Henneke and De Lange, 1990) and an extreme light transmission minimum (Rabitti and Boldrin, 1989) at the seawater-brine interface. A DOC minimum just above the seawater-

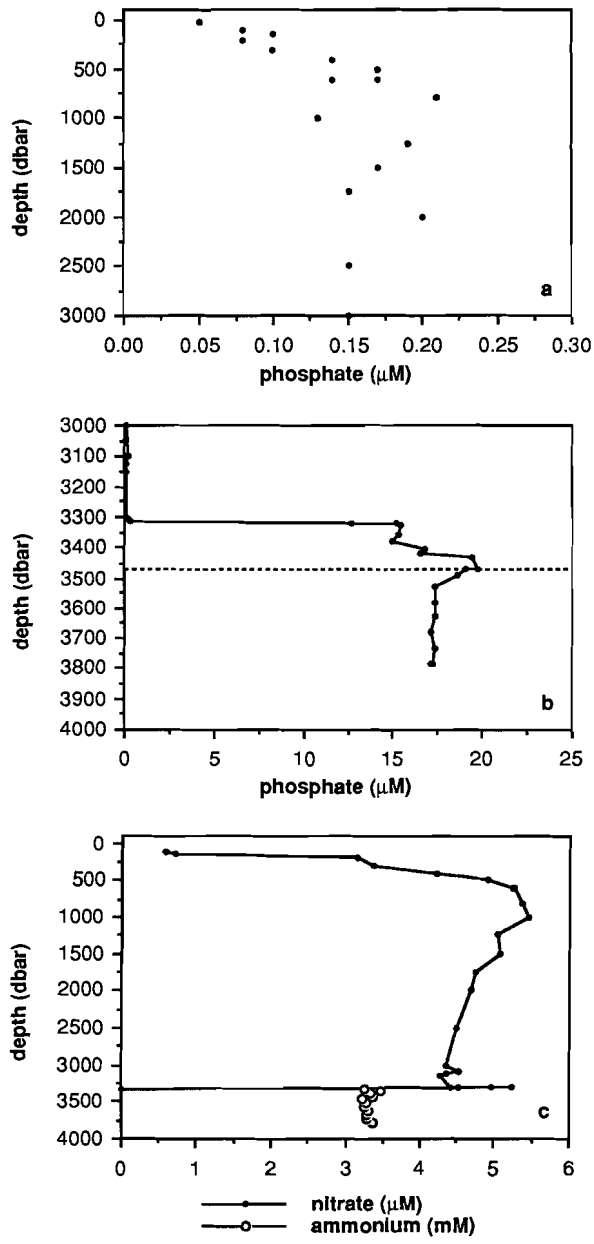

Figure 4.5. Phosphate profile in the overlying seawater (a) and in the brine (b). Second interface is indicated with a dashed line. Profiles of nitrate and ammonium (c). Ammonium data from Bregant *et al.* (1990). All other data from Hydes *et al.* (1988).

brine interface suggests that conversion of DOC back to POC, possibly also as a result of bacterial activity, may account for part of the POC maximum. Erba *et al.* (1987) proposed that gelatinous pellicles, which were detected in several sediment cores from the Tyro and Bannock Basins, are formed by bacteria at the seawater-brine interface. Copious presence of bacteria, at the seawater-brine interface (De Domenico and De Domenico, 1989) as well as in the gelatinous pellicles (Erba, 1989), was later confirmed. Decomposition of organic matter may also take place within the sediment, leading to production of phosphate and subsequent upward diffusion into the brine.

The phosphate maximum at the second interface can be accounted for by *in situ* recrystallization of calcium carbonates (dolomitization) and simultaneous precipitation of gypsum (Sect. 4.2.2.), as proposed by De Lange *et al.* (1990b), since the phosphate content of calcium carbonates is known to decrease upon such recrystallization. The absence of a light transmission minimum indicates that the density gradient at the second interface is not sufficient to cause accumulation of organic matter (Rabitti and Boldrin, 1989; Boldrin and Rabitti, 1990). Consequently, decomposition of organic matter is not likely to take place only at the second interface and cannot explain the phosphate maximum.

The nitrate (NO_3^-) profile in the overlying seawater (Fig. 4.5c) is similar to that of phosphate, with low concentrations at the surface, increasing rapidly with depth below the surface to a maximum at about 1000 dbar. Concentrations increase just above the seawater-brine interface. This may be caused either by enhanced decomposition of organic matter accumulating at the density gradient, or by oxidation of ammonium diffusing upward into the oxic seawater. However, the apparent absence of a nitrite (NO_2^-) maximum at the seawater-brine interface indicates that oxidation of ammonium is of minor importance. At the seawater-brine interface concentrations abruptly decrease to zero as nitrate is reduced, replacing oxygen as electron acceptor in the decomposition of organic matter (Chapter 2).

The concentration of ammonium (NH_4^+) is constant at 3.3 mM throughout the brine (Fig. 4.5c). Ammonium is a reaction product of the oxidation of organic matter by sulfate, which is simultaneously reduced to sulfide (Froelich *et al.*, 1979). Since sulfate is the ultimate electron acceptor, the fact that ammonium immediately reaches its maximum concentration at the seawater-brine interface indicates that the sequence of oxidation reactions (Chapter 2) is completed within a very limited range of depths. Notwithstanding the substantial scatter in the data, concentrations of DOC and POC also seem to be constant throughout the brine (Henneke and De Lange, 1990). These observations are in apparent contradiction with a localized decomposition of organic

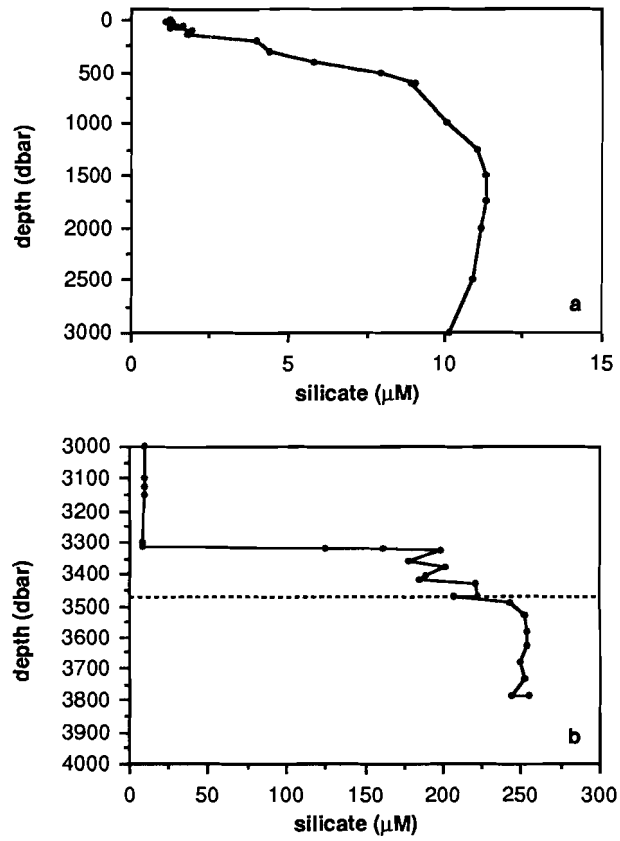

Figure 4.6. Silicate profile in the overlying seawater (a) and in the brine (b). Second interface is indicated with a dashed line. Data from Hydes *et al.* (1988).

matter, either in the sediments or at the seawater-brine interface, unless oxidation rates are extremely low relative to the rate of vertical mixing in the brine. In any case, in view of the vertical distributions of ammonium, DOC and POC in the brine, a similar vertical distribution would be expected for sulfide, yet it was shown in Section 4.2.2. that concentrations of sulfide follow the two-layered structure of the brine, increasing at the second interface from about 2 mM in the upper brine to about 3 mM in the lower brine. Calculations based on the concentration of ammonium in the brine and the stoichiometry of the oxidation reaction, assuming a normal Redfield ratio for organic matter (Redfield *et al.*, 1963), which may very well not be a valid assumption, predict concentrations of sulfide that are 5-10 times higher than the

concentrations actually observed (Bregant *et al.*, 1990; Luther *et al.*, 1990). This indicates that the vertical distribution of sulfide is ultimately determined by some removal process, probably related to the precipitation of Fe sulfide (Saager *et al.*, 1991).

The silicate profile in the overlying seawater (Fig. 4.6a) is similar to silicate profiles in the open ocean, with low concentrations at the surface, increasing with depth to a broad maximum at 1500-2000 dbar, signifying that silicate is remineralized at greater depth than the labile nutrients phosphate and nitrate. Concentrations in the brine are about a factor of 20 higher than in the overlying seawater and follow the two-layered structure of the brine, increasing near the second interface from 180-200 μM in the upper brine to 250 μM in the lower brine (Fig. 4.6b). Release of silicate in the brine may be caused either by dissolution of opaline material settling from the productive layer, or by dissolution of opaline material within the sediments and subsequent upward diffusion of silicate into the brine (Shokes *et al.*, 1977). The increase of silicate concentrations across the second interface suggests that silicate concentrations in the brine are limited by precipitation of some solid phase.

4.3. Methods

During the 1987 ABC Cruise seawater and brine samples for trace metal analysis were collected aboard Dutch R/V *Tyro* at Bannock Basin and at Tyro Basin (Fig. 4.1). Samples were collected as described in Chapter 3, using 12 l GoFlo bottles, 0.4 μm polycarbonate membrane filters (Nuclepore, ø47 mm) and storing the filtered seawater and brine samples in clean 250 ml, 1 l and 2 l low-density PE narrow-mouth bottles. At Bannock Basin filters were only kept for a number of samples within the upper brine. Dissolved and particulate Mn and Fe were analyzed by GFAAS. Analyses of dissolved Mn in brine samples were performed on a Perkin Elmer 5000 AAS, in combination with a HGA400 graphite furnace and an AS40 autosampler. All other analyses were performed on a Perkin Elmer 1100 AAS, in combination with the same type of graphite furnace and autosampler.

Dissolved Mn. Brine samples were analyzed by GFAAS, using direct injection after suitable dilution with Milli-Q water and standard addition. Detection limit was 100 nmol/kg and precision of the analyses was about 5% at the 5 μmol/kg level. Seawater samples were preconcentrated with Chelex, using the procedure described in Chapter 3 modified for samples of approximately 200 ml (Saager, 1987), and analyzed by GFAAS. Standard calibration curves in 3Q 0.1 N nitric acid were used, since a comparison with standard addition showed no matrix effects. Detection limit was 35 pmol/kg and precision of the analyses

was about 5% at the 2 nmol/kg level. Procedural blanks were below detection limit.

Dissolved Fe. Both seawater and brine samples were preconcentrated with APDC-DDDC/chloroform solvent extraction (Bruland *et al.*, 1979) and analyzed by GFAAS. Extracted standard calibration curves were used to compensate for matrix effects and extraction efficiencies. Detection limit was 0.2 nmol/kg and precision of the analyses was about 5% at the 2 nmol/kg level. Concentrations were corrected for low but significant procedural blanks. Samples with concentrations beyond the linear part of the calibration curve were reanalyzed after suitable dilution with 3Q 0.1 N nitric acid, using standard calibration curves in 3Q 0.1 N nitric acid. These samples were corrected for extraction efficiencies, which were generally estimated to be >80% from a comparison of the extracted standard calibration curves with the standard calibration curves in 3Q 0.1 N nitric, not taking into account any matrix effects.

Particulate Mn and Fe. Filters were leached for 2 hours in 3Q 7.0 N nitric acid. The leachates were evaporated in the evaporator pots (Chapter 3), redissolved in 3Q 0.1 N nitric acid and preconcentrated with APDC-DDDC/chloroform solvent extraction (Bruland *et al.*, 1979) modified for very small samples. Extracts were analyzed for Fe by GFAAS, after suitable dilution with 3Q 0.1 N nitric acid, using standard calibration curves in 3Q 0.1 N nitric acid. Samples were corrected for extraction efficiency, which was estimated to be >80% from a comparison of an extracted standard calibration curve with the standard calibration curves in 3Q 0.1 N nitric, not taking into account any matrix effects. Detection limit was about 0.1 nmol/kg. Since the extraction efficiency for Mn was estimated to be zero, Mn concentrations were determined by GFAAS analysis of the extracted samples, after suitable dilution with 3Q 0.1 N nitric acid, using standard calibration curves in 3Q 0.1 N nitric acid. Detection limit was about 2 pmol/kg. Precision of the analyses was about 5%. Accuracy of the analyses is limited by uncertainties in the amount of seawater or brine that was passed over the filters. A sampleweight of 10,000 g was assumed for the calculation of all particulate concentrations. Procedural blanks were below detection limit.

4.4. Results

4.4.1. Dissolved Mn and Fe

Concentrations of dissolved Mn and Fe are presented in Table 4.1. All trace metal concentrations in this Chapter and in Chapter 5 were calculated with respect to sampleweight rather than samplevolume and

depth (dbar)	Mn (nmol/kg)	Fe (nmol/kg)	depth (dbar)	Mn (nmol/kg)	Fe (nmol/kg)
0	-	5.84	3310	2.17	1.97
10	3.45	1.07	3315	2.16	0.95
16	-	2.67	3323	4490	106
25	3.24	6.04	3329	5290	82.8
40	-	1.35	3359	4640	23.3
60	-	2.49	3377	4760	-
80	-	0.87	3403	5220	16.2
101	-	1.24	3420	4820	29.4
149	-	1.62	3420		27.5
200	0.66	1.63	3430	3790	10.8
300	-	2.26	3430		10.1
400	-	1.88	3468	2870	12.3
801	-	0.72	3468		10.4
801		0.40	3470	2570	10.0
1000	0.06	0.67	3470		10.2
1500	-	0.60	3491	2910	9.59
1751	-	1.53	3529	3780	22.8
2000	0.09	-	3580	3750	20.5
2999	0.19	1.30	3628	3480	12.9
3101	-	2.49	3679	4070	19.8
3151	0.54	0.62	3730	3870	16.5
3151		0.75	3784	3620	19.5
3306	0.87	0.70			

Table 4.1. Concentrations of dissolved Mn and Fe. Seawater-brine interface, second interface and bottom at approximately 3323 dbar, 3470 dbar and 3784 dbar respectively. Dashes (-) signify that the sample was not analyzed (Mn) or suspected of contamination (Fe).

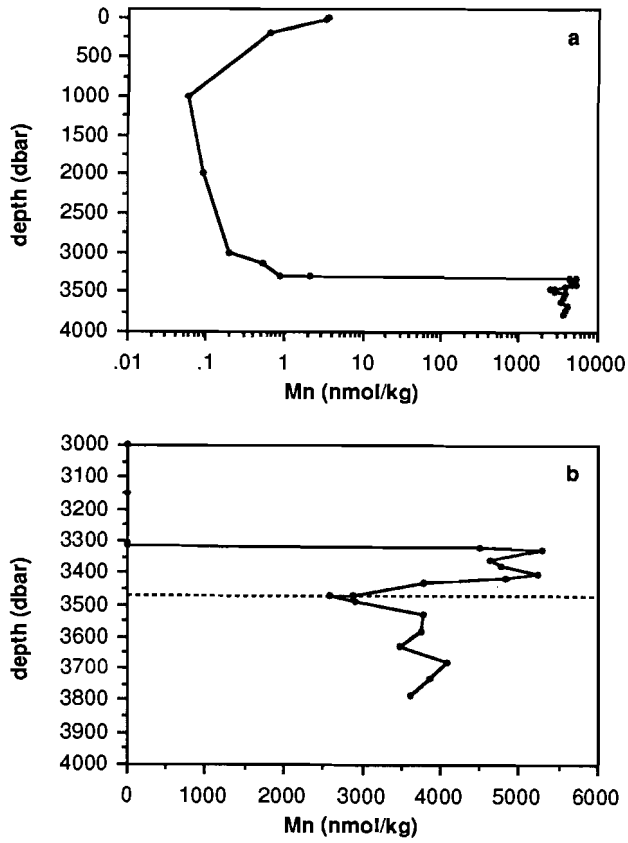

Figure 4.7. Vertical distribution of dissolved Mn (a). Note the logarithmic scale. Vertical distribution of dissolved Mn in the brine (b). Second interface is indicated with a dashed line.

are therefore expressed in mol/kg. Although in seawater the units mol/kg and mol/l are virtually exchangeable, the conversion of concentrations in the brine from mol/kg to mol/l is non-trivial and was not attempted. The conversion of pressure data to actual depths in m was discussed by Boldrin and Rabitti (1990). Such a conversion was also not attempted here and all depths are expressed in dbar. At Bannock Basin the bottom is at 3784 dbar and the seawater-brine interface at 3323 dbar. The second interface occurs at about 3470 dbar. In several Figures the seawater-brine interface and the second interface are indicated by dashed lines.

The vertical distribution of dissolved Mn in the overlying seawater (Fig. 4.7a) is primarily controlled by scavenging and surface input, in agreement with what was previously reported for the Mediterranean Sea (Kremling and Petersen, 1981; Statham *et al.*, 1985; Morley *et al.*, 1991). Concentrations are elevated near the surface, decreasing rapidly to a minimum at about 1000 dbar. Below 1000 dbar concentrations increase gradually and then more strongly below 3000 dbar towards the seawater-brine interface. Kremling and Petersen (1981) generally found somewhat higher concentrations at several stations in the eastern Mediterranean. This could be due to spatial or temporal variation, yet the possibility of some residual contamination cannot be excluded, especially since the concentrations which they found for other trace metals at stations in the western Mediterranean are significantly higher than those reported by Boyle *et al.* (1985). Statham *et al.* (1985) reported a vertical distribution of dissolved Mn in the Alboran Sea, similar to that in Figure 4.7a, with concentrations of 3-4 nmol/kg at the surface, rapidly scavenged below the surface to <0.5 nmol/kg in the deep water. Morley *et al.* (1991) recently determined vertical distributions of dissolved Mn at a large number of stations in the Golfe du Lion (western Mediterranean). At stations away from the shelf they found surface water Mn concentrations of 2-4 nmol/kg, rapidly scavenged below the surface to 0.1-0.2 nmol/kg in the deep water.

At the seawater-brine interface dissolved Mn concentrations increase by three to four orders of magnitude (Fig. 4.7b, Table 4.1). In the lower brine concentrations are approximately 20% lower than in the upper brine, with a distinct minimum at the second interface. This seems in excellent agreement with observations recently reported by De Lange *et al.* (1990a,b,c), yet a detailed comparison is not possible due to their omission of a datatable. Concentrations in the brine are intermediate between concentrations in the anoxic waters of the Cariaco Trench (Jacobs *et al.*, 1987) and the Black Sea (Lewis and Landing, 1991). Concentrations in the anoxic Orca brine are almost two orders of magnitude higher (Trefry *et al.*, 1984).

The vertical distribution of dissolved Fe in the overlying seawater (Fig. 4.8a) is apparently determined to a large extent by the vertical sequence of watermasses (Sect. 4.2.1.). The same seems to be true for Ni, Cu and Cd (Saager *et al.*, 1991) and for the REE (Chapter 5). In the ASW, between the surface and 60 dbar, concentrations are elevated and variable (Table 4.1). Although the variability in dissolved Fe concentrations in the ASW resembles the variability in salinity (Fig. 4.3b), a direct correlation between the two could not be established. Sherrell and Boyle (1988) reported Fe concentrations for a large number of surface samples collected throughout the Alboran Sea.

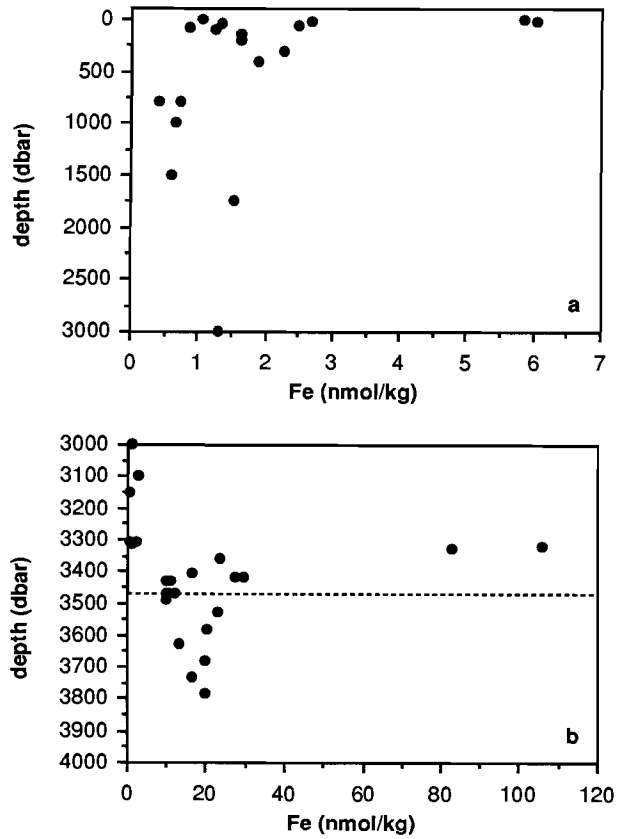

Figure 4.8. Vertical distribution of dissolved Fe in the overlying seawater (a) and in the brine (b).

Outside the direct influence of the Atlantic inflow plume they found surface water Fe concentrations of 4-7 nmol/kg.

In the LIW, between 60 and about 600 dbar, dissolved Fe concentrations show a gentle maximum (Fig. 4.8a), similar to, although not quite coinciding with, the salinity maximum (Fig. 4.3a). Below 600 dbar concentrations are low, varying between approximately 0.5 and 1.5 nmol/kg. A possible increase of concentrations towards the seawater-brine interface, as was observed for dissolved Mn, cannot be resolved within the uncertainty of the data. Morley *et al.* (1991) determined one vertical distribution of dissolved Fe at a station away from the shelf in the Golfe du Lion. Concentrations do not exceed 4 nmol/kg and are

generally within the range 1.5-2.5 nmol/kg, with no apparent structure throughout the watercolumn.

At the seawater-brine interface concentrations increase by two orders of magnitude (Fig. 4.8b), decreasing rapidly directly below the seawater-brine interface and then more gradually thoughout the upper brine to a minimum of about 10 nmol/kg near the second interface. Throughout the lower brine concentrations vary around 20 nmol/kg. The concentration at the seawater-brine interface is of the same order of magnitude as maximum concentrations in the anoxic waters of the Black Sea (Lewis and Landing, 1991) and the Cariaco Trench (Jacobs *et al.*, 1987), more than an order of magnitude lower than the maximum concentration in the anoxic waters of Framvaren Fjord (Haraldsson and Westerlund, 1988) and more than two orders of magnitude lower than the maximum concentration in the anoxic Orca brine (Trefry *et al.*, 1984), where sulfide concentrations do not exceed 3 μM. The vertical distribution of dissolved Fe in the Bannock brine is remarkably similar to the vertical distributions of dissolved REE presented in Chapter 5. The apparent minimum near the second interface is also very similar to that of Mn (Fig. 4.7b), although Mn and Fe have distinctly different vertical distributions in the upper brine.

4.4.2. Particulate Mn and Fe

Pressure-filtration of seawater and brine samples as described in Section 4.3. does not guarantee quantitative sampling of particulate matter. First, the outlet of a GoFlo bottle is located a few centimeters above its bottom. Consequently, during filtration part of the particulate matter may collect at the bottom of the GoFlo bottle and thus escape

depth (dbar)	cast/bottle	Mn (pmol/kg)	Fe (nmol/kg)
3323	ABC44/10	18.6	13.0
3323	ABC44/12	15.0	22.8
3323	ABC44/14	55.0	47.7
3359	ABC44/18	280	16.5
3403	ABC44/20	241	7.59
3420	ABC44/22	224	4.59
3470	ABC44/24	234	6.55

Table 4.2. Concentrations of particulate Mn and Fe. Seawater-brine interface, second interface and bottom at approximately 3323 dbar, 3470 dbar and 3784 dbar respectively.

filtration. This will probably affect the yield of larger particles more than that of smaller ones, since the former settle much faster. Second, although it was assumed in the calculation of particulate Mn and Fe concentrations that the full contents of the GoFlo bottle were passed over the filter for every sample (Sect. 4.3.), this is in fact not certain. The particulate Mn and Fe concentrations in Table 4.2 must therefore be regarded as lower limits.

The vertical distribution of particulate Mn (Fig. 4.9a) displays low concentrations at the seawater-brine interface, increasing by approximately an order of magnitude in the upper brine. Throughout the upper brine concentrations vary around 250 pmol/kg. The three samples from the seawater-brine interface (Table 4.2) were collected during the same hydrocast in different GoFlo bottles, fired one after the other. A particulate Mn maximum, such as found near the oxic-anoxic

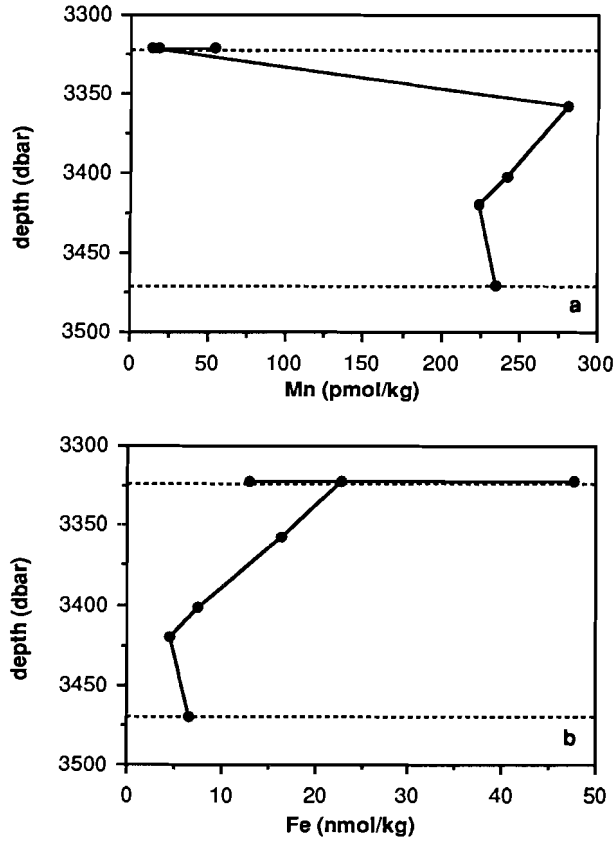

Figure 4.9. Vertical distributions of particulate Mn (a) and Fe (b) in the upper brine. Seawater-brine interface and second interface are indicated by dashed lines.

interface of many anoxic basins (Spencer and Brewer, 1971; Trefry *et al.*, 1984; Jacobs *et al.*, 1985; De Baar *et al.*, 1988; German and Elderfield, 1989; Lewis and Landing, 1991), was probably missed as a result of poor vertical resolution. These particulate Mn maxima are usually very pronounced, with strong gradients directly above and below. Saager *et al.* (1991) did find a particulate Mn maximum near the seawater-brine interface of the Tyro Basin.

The vertical distribution of particulate Fe is presented in Figure 4.9b. Concentrations are variable at the seawater-brine interface, between 10 and 50 nmol/kg. As for Mn, a clear particulate Fe maximum cannot be resolved. Below the interface concentrations appear to decrease with depth. Concentrations vary around 6 nmol/kg throughout the lower part of the upper brine.

4.5. Discussion

4.5.1. The overlying seawater

Spivack *et al.* (1983) estimated trace metal (Ni, Cu, Cd) exchange through the Strait of Gibraltar from water exchange and trace metal concentrations in the inflow and outflow. Since trace metal concentrations in the outflow had not been determined directly, they assumed them to be equal to trace metal concentrations in eastern Mediterranean surface waters. Eastern Mediterranean surface waters are the source of LIW, which in turn, after having spread to the western Mediterranean, becomes a major component of the Mediterranean outflow (Sect. 4.2.1.). Direct measurements by Boyle *et al.* (1985) showed this rather bold assumption to be surprisingly accurate, in other words trace metal concentrations in the Mediterranean outflow indeed appear to be largely preformed in the eastern Mediterranean and during their transfer from east to west the trace metals in question appear to behave conservatively. This is all the more remarkable, since, considering the extremely low rate at which LIW spreads across the Mediterranean (Malanotte-Rizzoli and Hecht, 1988), there would be ample time for trace metal concentrations to increase as a result of the decomposition of organic matter, or to decrease as a result of scavenging.

Surface water concentrations of some trace metals (Al, Ni, Cu, Cd) were found to increase gradually from the western to the eastern Mediterranean (Spivack *et al.*, 1983; Hydes *et al.*, 1988). The most likely explanation seems to be, that ASW, on its journey from west to east, is progressively enriched in some trace metals by continuous atmospheric input. Trace metal concentrations do not change any further as the

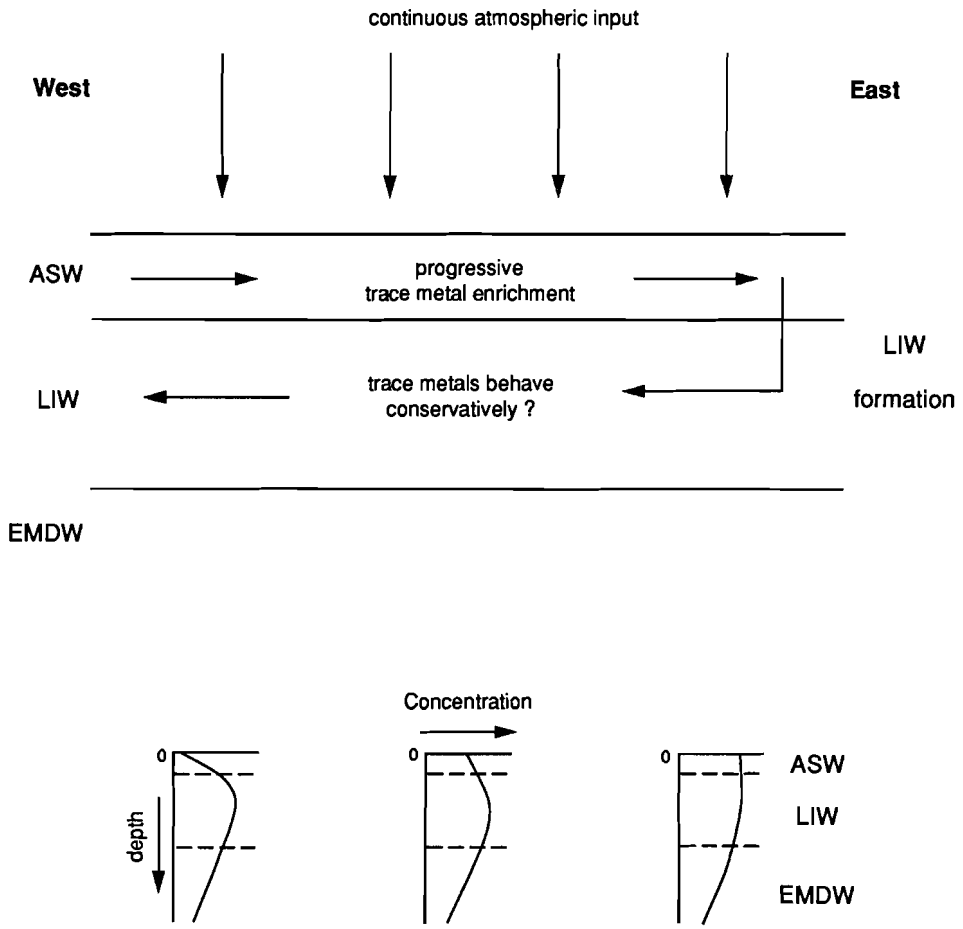

Figure 4.10. Schematic representation of the circulation of watermasses in the Mediterranean Sea. ASW, flowing from west to east, is progressively enriched in trace metals as a result of aeolian input. Trace metal concentrations do not change any further as ASW sinks to form LIW and returns from east to west. Approximate vertical distributions of dissolved trace metals are sketched for the western, central and eastern Mediterranean (bottom left to right).

enriched surface water sinks to form LIW in the easternmost Mediterranean and subsequently returns to the west (Fig. 4.10).

Accordingly, vertical distributions of dissolved trace metals in the western Mediterranean will show low concentrations at the surface

and elevated concentrations in the LIW, approximately below 100 dbar. Vertical distributions showing these features were indeed found for a number of trace metals (Boyle *et al.*, 1985; Statham *et al.*, 1985; Copin-Montegut *et al.*, 1986). In the eastern Mediterranean, LIW is also expected to be enriched in trace metals relative to ASW, although the difference will be less, since ASW is already more enriched than in the western Mediterranean (Fig. 4.10). The vertical distribution of dissolved Fe at Bannock Basin (Fig. 4.8a) shows a maximum near 300 dbar, approximately coinciding with the salinity maximum associated with LIW (Fig. 4.3b), in agreement with this prediction. A similar maximum was observed in the vertical distributions of Ni, Cu and Cd (Saager *et al.*, 1991). Nevertheless, Fe concentrations directly below the surface are higher than in the LIW maximum. Assuming that the shallow samples were not contaminated, elevated concentrations may result from local inputs. Alternatively, in contrast with other trace metals, Fe may be scavenged during transfer of LIW from the eastern to the western Mediterranean. This could explain the vertical Fe distribution, determined by Morley *et al.* (1991) at a station in the Golfe du Lion, which shows no apparent structure throughout the watercolumn.

The qualitative model described here and represented graphically in Figure 4.10 explains vertical distributions of trace metals in terms of general circulation in the Mediterranean Sea. The most important assumption is that trace metals behave conservatively during transport of LIW from east to west (Spivack *et al.*, 1983; Boyle *et al.*, 1985). The model therefore best applies to trace metals which are the least particle-reactive, such as Cd, Ni (Saager *et al.*, 1991) and the HREE (Chapter 5). Vertical distributions of dissolved Fe show deviations from those predicted by the model which can at least partly be attributed to scavenging. The model is certainly not applicable to trace metals which are highly particle-reactive, as is clearly demonstrated by Mn in Figure 4.7a. Only a limited number of samples in the overlying seawater was analyzed for Mn and the resulting vertical distribution (Fig. 4.7a) does not reveal whether LIW is associated with a Mn maximum. However, the vertical distribution appears to be controlled by an input of Mn at the surface and considerable scavenging throughout the upper part of the watercolumn. Scavenging will tend to obscure any features in the vertical distribution related to the vertical sequence of watermasses.

The substantial effect of atmospheric input on the vertical distribution of some trace metals in the Mediterranean Sea is exemplified by Al. Surface water concentrations of Al increase from the western to the eastern Mediterranean (Mackenzie *et al.*, 1976; Hydes *et al.*, 1988). This enrichment cannot be explained by fluxes from

the sediments, since sediments are not a source of Al (Mackin and Aller, 1984). Hydes *et al.* (1988) showed that rivers may be a source of Al, but not a dominant one. They further showed, using estimates of atmospheric inputs (Ganor and Mamane, 1982; Loÿe-Pilot *et al.*, 1986) and assuming that 5% of the atmospheric Al is readily soluble in seawater, that an aeolian source can account for the observed surface water enrichments. Moreover, sediment trap experiments and analyses of aerosols by Buat-Ménard *et al.* (1989) indicated that, in the Mediterranean Sea, atmospheric input of Al is balanced by the flux of particulate Al in the watercolumn. Continuous concentration of surface waters by extensive evaporation and entrainment of relatively enriched LIW in the relatively depleted ASW may also contribute to the progressive enrichment of ASW. However, since the Strait of Gibraltar is in general a net sink of trace metals to the Mediterranean Sea, such a process cannot ultimately be maintained without an external source (Sect. 4.1.). At least for Al and Mn, atmospheric input seems to be the most important external source. The origin and hence the chemical composition of the atmospheric input in the Mediterranean Sea strongly depends on the prevailing wind direction (Tomadin *et al.*, 1984). One of the major contributors is Saharan dust (Ganor and Mamane, 1982; Loÿe-Pilot *et al.*, 1986), which contains lower amounts of Fe and higher amounts of Al, Mn, Ni and Cu than dust of northern provenance (Tomadin *et al.*, 1984).

A comparison of surface water concentrations of dissolved Mn at Bannock Basin with surface water concentrations previously reported for the western Mediterranean (Kremling and Petersen, 1981; Morley *et al.*, 1991) reveals no systematic trend. Since surface water Mn concentrations are the net result of atmospheric input and scavenging, this does not necessarily mean that surface waters are not enriched in Mn by continuous atmospheric input, yet probably reflects that vertical distributions of dissolved Mn in the surface waters are primarily controlled by scavenging. Morley *et al.* (1991) found large seasonal variations in surface water Mn concentrations in the Golfe du Lion, which they attributed to seasonal variations in Mn scavenging or in Mn mobilization from particulate matter. At Bannock basin, where samples were collected in May and June, the mobilization of Mn from wind-blown dust may well be caused for a large part by photoreduction of solid Mn(IV) or by photoinhibition of the bacterially mediated oxidation of Mn^{2+} (Sunda *et al.*, 1983; Sunda and Huntsman, 1988).

In contrast with LIW, very little is known about the formation areas and general circulation of Mediterranean deep water (Sect. 4.2.1.). The mechanism of deep water formation seems to be similar to that of LIW formation (Plakhin, 1971, 1972). On that ground it may be possible to extend the qualitative model in order to explain the vertical

distribution of trace metals in EMDW. Concentrations of dissolved Fe in EMDW are lower than in both ASW and LIW. If trace metal concentrations in EMDW are preformed, in analogy with LIW, then surface water Fe concentrations in EMDW formation areas are much lower than at Bannock Basin. It is well known that Mediterranean deep water has a short residence time. Malanotte-Rizzoli and Hecht (1988) mentioned 150 years as the renewal time of deep water in the eastern Mediterranean. Béthoux (1980) reported the ages of eastern and western Mediterranean deep water to be 70 years and 15 years respectively. Latter age seems hard to reconcile with the fact that LIW retains its identity throughout the western Mediterranean. In any case, short residence times should ensure that trace metal concentrations in EMDW are not very different from the concentrations in the surface waters of its formation areas. The northern and central parts of the Adriatic Sea are generally favoured as deep water formation area for the Ionian Basin (Malanotte-Rizzoli and Hecht, 1988). Although no data are available for the Adriatic Sea, it is highly unlikely that surface water trace metal concentrations will be in the range indicated by concentrations in EMDW, since this region is surrounded by densely populated and industrialized coasts. Anthropogenic sources are probably of minor significance for Fe, yet for trace metals that are expected to be enriched as a result of industrial pollution (Cd, Cu) concentrations in EMDW are also considerably lower than in ASW and LIW (Saager *et al.*, 1991). Obviously, a complete understanding of vertical distributions of trace metals in the Mediterranean Sea is not possible without more detailed information on general circulation and better constraints on various trace metal sources and sinks.

4.5.2. The brine

The activities of free ions in the brine are mostly unknown due to the high ionic strength. It is therefore very hard to calculate trace metal speciation or the state of saturation of trace metals with respect to their least soluble solid phase (Van der Weijden *et al.*, 1990). For this reason the present discussion of vertical distributions of Mn and Fe in the brine is limited to general observations and remarks.

The brine can be divided into three regions as implied by its two-layered structure: the upper brine, the lower brine and the interface between the two (the second interface). At the second interface the vertical distributions of dissolved Mn and Fe are characterized by distinct minima. De Lange *et al.* (1990a,b) argued that the pronounced Mn minimum is the result of incorporation of Mn^{2+} into dolomite, which precipitates during *in situ* alteration of the brine (Sect. 4.2.2.). The

term *in situ* alteration was used by De Lange *et al.* (1990b) as opposed to pre-outflow alteration and refers to dolomitization and simultaneous precipitation of gypsum as in reaction (4.1) at the second interface, either within the brine or at the edges of the basin. The model of De Lange *et al.* (1990a,b) is substantiated by several observations. First, it qualitatively explains anomalies in the vertical distributions of a number of major and minor elements at the second interface (Sect. 4.2.2.). Second, large gypsum crystals were found in the sediments underlying Bannock Basin (Scientific staff of cruise Bannock 1984-12, 1985; Corselli and Aghib, 1987). Third, samples of dolomite recovered from Bannock Basin contain approximately 550 ppm of Mn (De Lange *et al.*, 1990b).

The Fe minimum at the second interface is less discernable than the concomitant minima of Mn and the REE (Chapter 5), as a result of considerable scatter in the data. Nevertheless, the four samples nearest the second interface (3430-3490 dbar) have the lowest dissolved Fe concentrations of all brine samples (Table 4.1). Fe removal at the second interface may well be caused by the same process that is responsible for the Mn minimum. The ionic radius of Fe^{2+} is nearly equal to that of Mn^{2+} and Ca^{2+}, so that precipitation of both dolomite (*e.g.* Banner *et al.*, 1988) and gypsum could account for the removal of Fe at the second interface (Sect. 4.2.2.). This assumption cannot be supported by direct evidence, since no Fe content was reported for the dolomite and gypsum samples that were recovered from the brine. Another process that could account for the Fe minimum is precipitation of some Fe sulfide solid phase. However, it is not clear why such precipitation should take place predominantly at the second interface.

The lower brine is largely homogeneous with respect to temperature (Fig. 4.3d) and concentrations of major and minor elements, indicating that it is well mixed. The concentration of Fe in the lower brine is probably limited by precipitation of some Fe sulfide solid phase. Jacobs and Emerson (1982) found that greigite (Fe_3S_4) is the most likely candidate in anoxic water of normal salinity, yet in anoxic brine it may not be. An interesting result is the difference between the Mn concentrations in the upper brine and in the lower brine (Fig. 4.7b). The higher Mn concentration in the upper brine cannot have been caused by pre-outflow alteration (Sect. 4.2.2.). De Lange *et al.* (1990b) showed that the upper brine has undergone more extensive pre-outflow alteration which would lead to a lower Mn concentration than in the lower brine. Instead, throughout the brine the Mn concentration is probably limited by precipitation of some Mn solid phase. It is not very likely that this solid phase is a Mn carbonate, because the carbonate concentration does not increase significantly across the second interface (Bregant *et al.*, 1990; De Lange *et al.*, 1990a,b), nor is

carbonate significantly more complexed in the upper brine (Chapter 5). Still, a dominant control by precipitation of a Mn carbonate cannot be ruled out. Possibly, the Mn concentration in the brine is limited by precipitation of some Mn sulfide solid phase (Jacobs and Emerson, 1982). At the second interface sulfide concentrations increase from 1.8 mM to 2.7 mM (Fig. 4.4b), whereas Mn concentrations decrease from 4.9 µmol/kg to 3.7 µmol/kg (Table 4.1). Therefore, the concentration product for alabandite (MnS) in the upper brine (4.9 x 1.8 = 8.8) is not very different from that in the lower brine (3.7 x 2.7 = 10.0). Of course, for a proper calculation ion activity products (IAPs) and solubility products should be considered, yet these are hard to determine in the brine because of the high ionic strength. Nevertheless, the opposite behaviour of Mn and sulfide at the second interface (not regarding the Mn minimum) and the similar ionic strengths of the two brine layers (Chapter 5) suggest that Mn sulfide IAPs are fairly constant throughout the brine. The same was observed for Ba^{2+} and SO_4^{2-} (De Lange *et al.*, 1990b). Secondary alteration as in reaction (4.1) controls the vertical distribution of SO_4^{2-}, which in turn controls the vertical distribution of Ba^{2+}. Similarly, the sulfide profile may control the vertical distribution of dissolved Mn, although it is difficult to decide what exactly controls the sulfide profile.

The temperature profile in the upper brine (Fig. 4.3d) is characterized by a multi-layered structure (Boldrin and Rabitti, 1990), indicating that it is less well mixed than the lower brine. The vertical distributions of dissolved Mn and Fe are very different. Fe concentrations decrease rapidly below the seawater-brine interface and then more gradually to the minimum at the second interface. In contrast, Mn concentrations are rather constant throughout the upper brine. De Lange *et al.* (1990a,b,c) sampled the brine with high resolution and found a dissolved Mn maximum of 6-8 µM at the seawater-brine interface that cannot be resolved from the data in Table 4.1 and that was also not observed by De Baar *et al.* (1987). The vertical distributions of dissolved Mn and Fe are not linear between the source at the seawater-brine interface and the sink at the second interface. This indicates that the vertical distributions of dissolved Mn and Fe in the upper brine are not controlled simply by diffusion, yet that Mn and Fe are removed throughout the upper brine, most likely by precipitation of some solid phase. For Fe this solid phase is probably an Fe sulfide.

In Figure 4.11 the sulfide profile and vertical distribution of dissolved Fe in the Bannock brine are compared with those in the Orca brine (Wiesenburg *et al.*, 1985). The most striking difference, not regarding actual concentrations, is the interchange, as it were, of Fe and sulfide behaviour. Wiesenburg *et al.* (1985) assumed that the high salinity of the Orca brine decreases bacterial activity, thereby

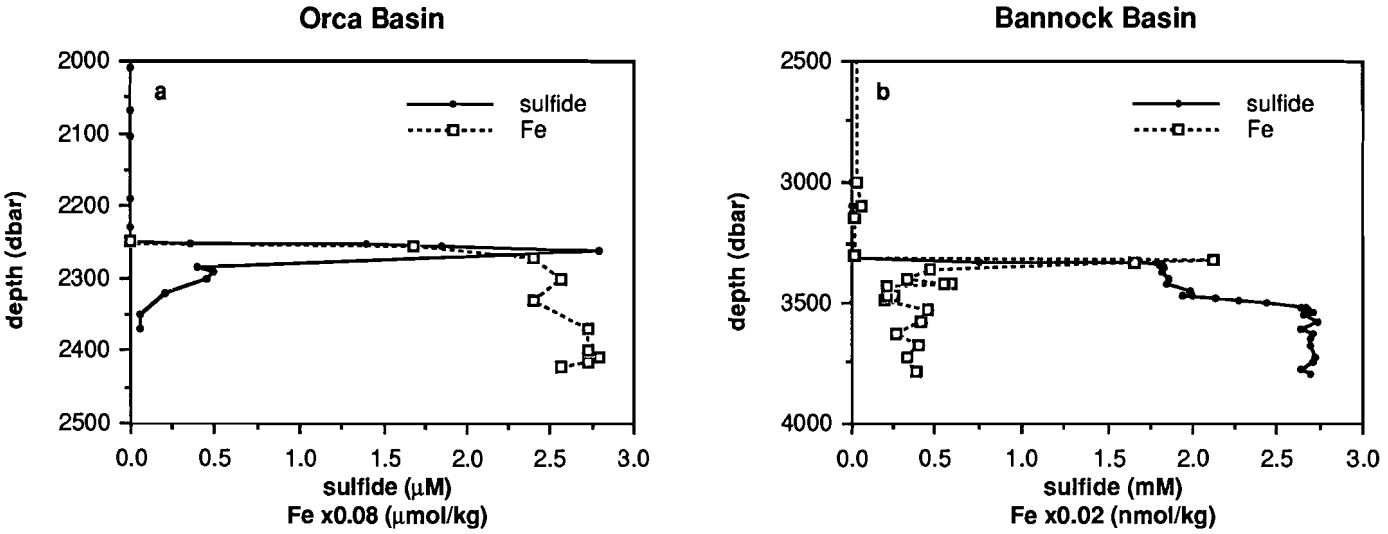

Figure 4.11. Sulfide profiles and vertical distributions of dissolved Fe in the Orca and Bannock brines. Sulfide data for Bannock Basin from Luther *et al.* (1990). Sulfide profile and vertical distribution of dissolved Fe in the Orca brine after Wiesenburg *et al.* (1985).

impeding the reduction of sulfate to sulfide. Consequently, sulfide would be the limiting species in Fe sulfide precipitation. However, sulfide concentrations in the Bannock brine, which are the second highest ever reported for a marine anoxic basin, do not support a decreased bacterial activity. Therefore, assuming that the rate of sulfate reduction is equal for Bannock Basin and Orca Basin, the difference is probably best explained in terms of Fe input to the brine. Figure 4.11 suggests that the input of Fe to the Orca brine is orders of magnitude higher than the input of Fe to the Bannock brine. One source of soluble Fe to the Orca Basin could be turbidites, which have been observed within the sulfidic black mud underlying the Orca brine as graded layers of gray mud. This gray mud is representative of the surrounding continental slope and contains a leachable Fe concentration of 1675 ppm (Addy and Behrens, 1980). On the other hand, turbidites have also been reported for both Bannock and Tyro Basin (Camerlenghi, 1990). Although Erba (1989) inferred from differences in gelatinous pellicles that turbidites occur more frequently in Tyro Basin than in Bannock Basin, the sulfide profiles and vertical distributions of dissolved Fe are very similar in both brines (Luther *et al.*, 1990; Saager *et al.*, 1991). Moreover, there is no evidence that sediments surrounding Orca Basin would contain much more leachable Fe than those surrounding Bannock and Tyro Basin.

Alternatively, the Bannock and Tyro brines are formed by dissolution of Messinian evaporites, outcropping on the walls of the respective basins (Camerlenghi, 1990), whereas pore water salinity profiles in sediments underlying the Orca brine indicate, that the Orca brine probably enters the basin as a brine flow originating outside the basin and flowing along the seafloor (Shokes *et al.*, 1977; Addy and Behrens, 1980). Recently, such a brine flow feeding the Orca Basin was indeed discovered (Brooks *et al.*, 1990). Therefore, it is possible that the Orca brine is already enriched in Fe before entering the basin and before the onset of sulfate reduction.

Interpretation of the vertical distributions of particulate Mn and Fe at Bannock Basin is difficult, since particulate concentrations were only determined for the upper brine. Particulate concentrations of Mn and Fe throughout the Bannock brine as well as in the overlying seawater were reported by Van der Sloot *et al.* (1990). They collected brine and seawater samples in ten 30 l Niskin bottles, mounted on a CTD Rosette frame. Three hydrocasts were needed to fill a 1 m^3 container. Particulate matter was recovered by processing the full contents of this container in a continuous-flow ultracentrifuge, operated at 0.8-1.0 dm^3/min and 10,000 g, and analyzed by INAA-γ. The resulting concentrations thus refer to total particulate trace metals,

whereas the particulate Mn and Fe concentrations in Table 4.2 refer to a fraction leachable in 7.0 N nitric acid (Sect. 4.3.). Apparently Van der Sloot *et al.* (1990) took no precautions to prevent oxidation of the brine samples, neither during sampling, nor during processing in the continuous-flow ultracentrifuge. The remarkably high particulate Mn concentrations that they reported for the lower Bannock brine may therefore be due to partial oxidation of the dissolved Mn standing stock during processing of the samples.

At 5 dbar Van der Sloot *et al.* (1990) found particulate Mn and Fe concentrations of 13 pmol/kg and 4 nmol/kg respectively. Open ocean vertical distributions of particulate Mn and Fe (Sherrell, 1989) show that concentrations vary widely throughout the watercolumn. Hence, any single sample is probably not representative of the Mediterranean seawater overlying the Bannock brine. The only other concentrations of particulate Mn and Fe in the overlying seawater reported by Van der Sloot *et al.* (1990) are 46 pmol/kg and 8 nmol/kg respectively, at 2500 dbar. Taking these concentrations as upper limits, it appears that concentrations of particulate Mn are a factor of 5 higher in the brine than in the overlying seawater. This is in agreement with the vertical distribution of particulate Mn at Tyro Basin (Saager *et al.*, 1991), where concentrations of particulate trace metals were determined for the overlying seawater as well as for the brine. On the other hand, concentrations of dissolved Fe in the Bannock brine do not seem to be significantly different from those in the overlying seawater, except near the seawater-brine interface, whereas at Tyro Basin they increase by a factor of 5-10 (Saager *et al.*, 1991).

Higher concentrations of particulate trace metals in the brine may be the result of trace metal sulfide precipitation, yet it may also be the result of the higher density of the brine, leading to lower sinking rates, a longer residence time and consequently higher concentrations of particulate matter. Van der Sloot *et al.* (1990) found particles enriched in Fe, Cu, Zn and S at the seawater-brine interface of Tyro Basin. This could indicate that precipitation of Fe sulfide and other trace metal sulfides (Saager *et al.*, 1991) is taking place *in situ* at the seawater-brine interface, either in the watercolumn or near the edges of the basin. However, in view of the sampling methods used by Van der Sloot *et al.* (1990), the nature and origin of these trace metal enriched particles is uncertain and they may not be an actual constituent of particulate matter at the seawater-brine interface. No particles were found that specifically contain elevated concentrations of Mn. More detailed and accurate vertical distributions of particulate trace metals are necessary for a complete discussion of trace metal cycling within the brine.

4.5.3. The seawater-brine interface

Adopting the model of Mn cycling at the oxic-anoxic interface of marine anoxic basins presented in Chapter 2, an attempt is made in this Section to calculate and balance Mn fluxes across the seawater-brine interface of Bannock Basin. A comparison of temperature profiles recorded during cruises in two successive years indicates that the density gradient at the seawater-brine interface is an extremely stable feature (Boldrin and Rabitti, 1990). Mixing between the brine and the overlying seawater is strongly restricted by the density gradient.

In view of this and in order to symplify the calculations it is assumed that vertical advection across the seawater-brine interface is negligible and that the upward flux of dissolved Mn is dominated by either molecular diffusion or eddy diffusion. In either case the magnitude of the upward flux of dissolved Mn can be estimated using Fick's Law

$$J = - D (\partial C/\partial z) \qquad (4.2)$$

where J is the upward diffusive flux in mol m^{-2} s^{-1}, D the diffusion coefficient in m^2/s and $\partial C/\partial z$ the concentration gradient in mol/m^4. The concentration gradient $\partial C/dz$ may be derived from the vertical distribution of dissolved Mn at the seawater-brine interface. Cycling of Mn at the seawater-brine interface seems to be determined by the same processes as that of Fe, specifically initial reductive dissolution of particulate Mn that settles along the seawater-brine interface and subsequent precipitation of some Mn solid phase, possibly a Mn sulfide, in the brine. Therefore, a dissolved Mn maximum at the seawater-brine interface, similar to the dissolved Fe maximum, may be expected. Such a maximum was indeed observed by De Lange *et al.* (1990a,b,c), who determined the dissolved Mn concentration gradient at the seawater-brine interface to be 135 nM/cm = $1.35 \cdot 10^{-2}$ mol/m^4.

The diffusion coefficient D is a more difficult matter. De Lange *et al.* (1990c) showed that, after correcting for cross-coupling of diffusive fluxes, the vertical distributions of Cl, Na and Mg are consistent with a major control by molecular diffusion. They concluded that, although the possibility of turbulent dispersion (which may be caused by friction as a result of horizontal advection of EMDW along the seawater-brine interface) cannot be ruled out, the vertical distribution of dissolved Mn at the interface also suggests a dominant control by molecular diffusion. Ullman *et al.* (1990) used the molecular diffusion coefficient of I^- at the temperature of the brine as given by Li and Gregory (1974) to calculate the upward diffusion of I^- across the

seawater-brine interface. Similarly, the upward diffusive flux of dissolved Mn can be calculated using (4.2) and the molecular diffusion coefficient of Mn^{2+}, which was reported by Li and Gregory (1974) to be $5.75 \cdot 10^{-10}$ m^2/s. The molecular diffusion coefficient at 18°C is used rather than that at the true temperature of the brine, yet the correction is not very large. The upward diffusive flux of dissolved Mn then becomes $7.8 \cdot 10^{-12}$ mol m^{-2} s^{-1}. However, this flux may be much larger if vertical advection or turbulent dispersion occur at the seawater-brine interface. Wiesenburg *et al.* (1985) used an eddy diffusion coefficient "determined from the temperature and salinity gradient" of 10^{-5} m^2/s for calculation of fluxes across the seawater-brine interface at Orca Basin.

Assuming steady state, the upward diffusive flux of Mn should be balanced by precipitation of Mn oxides directly above the seawater-brine interface, causing a downward flux of particulate Mn into the brine. Several assumptions will be made before calculating this downward flux: (i) The upward diffusive flux of dissolved Mn is completely oxidized immediately upon entering the overlying seawater. (ii) The resulting freshly precipitated Mn solid phases settle across the seawater-brine interface and completely dissolve immediately upon entering the brine. (iii) The settling velocity of freshly precipitated Mn solid phases is $6 \cdot 10^{-5}$ m/s, a value derived for the open ocean from sediment trap experiments (Sherrell, 1989). According to assumption (ii) the freshly precipitated Mn solid phases completely dissolve immediately upon entering the brine, hence this settling velocity need not be corrected for the density of the brine. (iv) Particle transport involves only settling. Particle diffusion will not be considered. (v) The maximum concentration of particulate Mn is equal to the particulate Mn concentration in the brine, namely 250 pmol/kg = $2.5 \cdot 10^{-7}$ mol/m^3. Although the vertical distribution of particulate Mn at Tyro Basin shows a particulate Mn maximum near the seawater-brine interface (Saager *et al.*, 1991), in agreement with what was found near the oxic-anoxic interface of many marine anoxic basins, such a maximum was not observed near the seawater-brine interface of Bannock Basin (Sect. 4.4.2). Taking all these assumptions into account, the downward flux of particulate Mn is $15 \cdot 10^{-12}$ mol m^{-2} s^{-1}. Within the uncertainty of the calculation this is equal to the upward diffusive flux of dissolved Mn, in other words the downward particulate flux is large enough to balance the upward diffusive flux and an additional flux of Mn from the sediments need not be invoked.

Some of the above assumptions may be questioned. Assumption (i), implying fast oxidation kinetics of Mn(II), seems in disagreement with the general assumption of slow oxidation kinetics of Mn(II) in

seawater (Sung and Morgan, 1981; Bruland, 1983). On the other hand, Mn oxidation can be fast when microbially mediated as was shown by Tebo (1991) for Mn oxidation in the suboxic zone of the Black Sea. In view of the copious presence of bacteria (De Domenico and De Domenico, 1989), there is a distinct possibility that Mn oxidation at the seawater-brine interface is also microbially mediated. Nonetheless, the very short residence time of Mediterranean deep water (Béthoux, 1980; Malanotte-Rizzoli and Hecht, 1988) may cause some dissolved Mn to escape oxidation, as indicated by the increase of dissolved Mn concentrations below 3000 dbar towards the seawater-brine interface. Although all Mn that diffuses out of the brine will eventually be oxidized, the resulting Mn oxides need not settle back into the brine. In fact, a substantial fraction of the Mn oxides that precipitate directly above the brine interface may be transported away from the basin if the horizontal advection of EMDW along the seawater-brine interface is strong. Neither a flux of Mn oxides escaping into the overlying seawater, nor a flux of Mn solid phases escaping into the brine was considered in the calculations (see also Saager *et al.*, 1991).

The flux calculations presented here are largely based on the observed vertical distributions of dissolved and particulate Mn, assuming steady state within the brine and rapid kinetics for all reactions involved. Clearly, a more detailed vertical distribution of particulate Mn and a better knowledge of the mechanisms underlying Mn cycling at the seawater-brine interface as well as of general circulation in the eastern Mediterranean is needed to calculate the fluxes with greater accuracy.

4.6. Conclusions

Conclusion 1. The cycling of some trace metals in the Mediterranean Sea seems to be related to the general circulation of watermasses. A simple model was proposed in Section 4.5.1. to account for the observed vertical distributions of dissolved Fe and several other trace metals (Saager *et al.*, 1991) in ASW and LIW. ASW is progressively enriched in trace metals by continuous atmospheric input, while flowing from the Strait of Gibraltar to the east. In the easternmost Mediterranean ASW sinks to form LIW and trace metal concentrations are assumed to remain constant during transport of LIW back to the Strait of Gibraltar (Spivack *et al.*, 1983; Boyle *et al.*, 1985). Vertical distributions of trace metals for which latter assumption is valid are reasonably well described by the model. On the other hand, the vertical distribution of dissolved Mn is primarily controlled by surface input and scavenging.

Conclusion 2. Throughout the brine, concentrations of dissolved

Mn and Fe seem to be limited by precipitation of Mn and Fe solid phases. For Fe this solid phase is most likely an Fe sulfide. For Mn it may either be a Mn carbonate or a Mn sulfide. At the second interface Mn is removed by *in situ* alteration, specifically dolomitization, as indicated by the high Mn content of dolomite samples recovered from Bannock Basin (De Lange *et al.*, 1990a,b). Although the Fe content of these dolomite samples was not reported, the similar ionic radius of Mn^{2+} and Fe^{2+} suggests that the same process may account for the dissolved Fe minimum at the second interface. In the Orca brine sulfide concentrations rather than concentrations of dissolved Fe are limited by precipitation of some Fe sulfide solid phase. High sulfide concentrations in the Bannock brine indicate that bacterial activity, responsible for the reduction of sulfate to sulfide, is not decreased by the high salinity. Therefore, the low sulfide concentrations in the Orca brine are probably due to a much higher input of soluble Fe.

Conclusion 3. Simple calculations suggest that the upward diffusive flux of dissolved Mn across the seawater-brine interface is balanced by the downward flux of particulate Mn. Assuming steady state within the brine, no other Mn fluxes are required to sustain Mn cycling at the seawater-brine interface.

CHAPTER 5 Vertical distributions of dissolved REE in the anoxic brines of Bannock Basin

5.1. Introduction

In Chapter 2 two processes were presented that may contribute to REE scavenging in the open ocean. First, the REE form complexes with ligands that are present as functional groups on the surface of organic matter. Second, the REE are adsorbed onto or coprecipitate with Mn and Fe oxyhydroxydes that form coatings on the surface of particulate matter. Although the first process is probably more important in surface waters, where fresh organic matter is constantly produced, and the second process in deep waters, where particulate matter is coated with Mn and Fe oxyhydroxides as it sinks, in the open ocean the two are hard to study independently and their individual contributions to REE scavenging are hard to determine.

On the other hand, directly above the oxic-anoxic interface of marine anoxic basins, where reduced Mn and Fe constantly diffuse upwards into the oxic water and precipitate as Mn and Fe oxyhydroxides (Chapters 2 and 4), REE scavenging appears to be completely dominated by the second process (De Baar *et al.*, 1988; German and Elderfield, 1989). Therefore, marine anoxic basins provide an excellent opportunity to study REE scavenging by Mn and Fe oxyhydroxides without major interference from other processes. Bannock and Tyro Basin are unique in this respect, since the brines combine anoxia with a very high ionic strength (Chapter 4), which is likely to have a strong effect on the equilibrium association constants of REE complexes (Chapter 2). Consequently, not only REE scavenging by Mn and Fe oxyhydroxides but also REE speciation and hence REE particle-reactivity in general will be affected by the rapid chemical changes at the seawater-brine interface. By comparing vertical distributions of the REE in Bannock and Tyro Basin with those in marine anoxic basins where the anoxic water has normal seawater ionic strength and by comparing REE patterns in the brine with those in the overlying seawater, it may be possible to determine the effect of solution composition on REE speciation as well as the effect of REE speciation on REE scavenging.

During the 1987 Anoxic Basin Chemistry (ABC) Cruise samples for the determination of REE concentrations were collected from both Bannock and Tyro Basin. The hydrography of Bannock and Tyro Basin was elaborately discussed in Chapter 4. The Bannock brine consists of two chemically distinct layers, which makes Bannock Basin potentially more interesting than Tyro Basin. Moreover, the Bannock brine is more than two and a half times thicker than the Tyro brine, allowing it to be

sampled in greater detail. In this Chapter vertical REE distributions in Bannock Basin are discussed in relation to the vertical distributions of Mn and Fe that were presented in Chapter 4. REE speciation in the brine as well as in the overlying seawater is calculated with a computer model of trace metal speciation in seawater and subsequently incorporated into a model of REE scavenging that was developed by Byrne and Kim (1990). With latter model Byrne and Kim (1990) were able to reproduce some prominent features of seawater REE patterns, such as HREE enrichment and La and Gd anomalies (Chapter 2). Actual REE patterns in the brine, which were found to be very different from those in the overlying seawater, are compared with REE patterns predicted by the model as a stringent test of the model's capability to reproduce REE patterns over a wide range of chemical conditions.

5.2. Methods

Sample collection was described in Chapter 4. Brine subsamples of approximately 200 ml were diluted with Milli-Q water to a total volume of 2 l before adding the spike, in order to obtain a solution with the ionic strength of seawater. The ion-exchange and chelating properties of Chelex strongly depend on the ionic strength of the sample (Chapter 3). The 2 l tenfold diluted brine samples were spiked with 0.2-0.3 g of REE1 spike solution. Filters were not analyzed for particulate REE concentrations.

Concentrations of La-Eu could be determined for almost all samples. La was analyzed on a separate double-filament assembly for all samples, except initially for 3470 dbar and 3730 dbar, yet these two samples were later reanalyzed with La loaded on a separate double-filament assembly. In order to suppress Ba interference, La analysis was mostly performed in the presence of oxygen. Yb interference on GdO and NdO interference on Dy impeded the determination of reliable Gd and Dy concentrations for all but a few samples. The method of suppressing these interferences with freon (Sect. 3.2.6.) was not yet available at that time. As a result of isobaric interferences as well as small and unstable ionbeams the analysis of one or more of the HREE (Er-Lu) failed for about 50% of the samples.

On average, REE concentrations in the brine are between 3 times higher (Lu) and 50 times higher (Ce) than in the overlying seawater (Table 5.1), so that REE concentrations in the tenfold diluted brine samples are between 3 times lower and 5 times higher than in the seawater samples. Assuming that all REE are optimally spiked in the seawater samples, using the same amount of spike solution for the tenfold diluted brine samples leads to overspiking of the HREE and underspiking of La and Ce, which in turn causes loss of accuracy and

precision (Chapter 3). Nevertheless, the errors estimated by REECALC are typically 1-2% for Ce-Sm, 2-5% for Eu-Yb and 5-7% for La and Lu, showing no systematic variation with REE concentrations throughout the watercolumn, which indicates that the degree of overspiking or underspiking was not large enough to cause significant error magnification.

Duplicate analyses were performed on two brine samples (3470 dbar and 3730 dbar). Except for the rather inferior La duplicate of the 3470 dbar sample (Table 5.1), which is probably the result of Ba interference, differences between duplicates are less than 1-10% of the highest concentration. The duplicates in Table 5.1 seem to be somewhat poorer than the duplicates on standards and seawater samples presented in Chapters 3 and 6, yet this may be due to the unusual character of the brine samples. In any case, they should not be considered as an indication of the general accuracy and precision of the IDMS method.

5.3. Results

5.3.1. Vertical distributions of dissolved REE

Dissolved REE concentrations are presented in Table 5.1, together with the Ce anomaly (Ce/Ce^*) and REE abundances in mean shales. The 603 dbar sample was not included in any of the Figures. High concentrations of the LREE (especially Ce) as well as very high concentrations of Mn, Fe, Ni, Cu, Zn and Cd (P.M. Saager, unpublished data) suggest that it was contaminated, most likely during sampling.

Vertical distributions of dissolved REE are shown in Figures 5.1 and 5.2, except for Gd and Dy. Concentrations of the LREE, which are elevated at the surface, decrease rapidly with depth, whereas concentrations of the HREE increase with depth below the surface to a maximum near 200 dbar (Fig. 5.1). Below 200 dbar the concentrations of all REE decrease gradually with depth to a minimum at 1500-2000 dbar. REE concentrations increase again slightly with depth towards the seawater-brine interface.

REE concentrations at the seawater-brine interface are the highest ever observed in the watercolumn of a marine anoxic basin (De Baar *et al.*, 1988; German and Elderfield, 1989; Schijf *et al.*, 1991) and comparable only to REE concentrations reported for pore waters of reducing sediments at depths of 30-40 cm below the sediment-seawater interface (Elderfield and Sholkovitz, 1987; Sholkovitz *et al.*, 1989). Concentrations of the trivalent REE increase 9-40 times across the seawater-brine interface, whereas Ce concentrations increase by a

depth (dbar)	La	Ce	Nd	Sm	Eu	Gd	Dy	Er	Yb	Lu	Ce/Ce*
0	31.16	31.30	30.42	6.84	1.74	-	-	7.84	-	0.91	0.485
25	30.11	25.90	27.78	6.29	1.68	-	-	8.08	7.71	0.97	0.424
41	-	22.40	26.77	6.05	1.68	-	-	8.08	7.73	0.94	-
80	30.68	19.02	26.28	5.91	1.59	-	-	8.57	-	1.08	0.313
200	27.97	16.35	26.45	6.05	-	-	-	8.92	8.25	1.09	0.286
603	(27.09)	(20.18)	(26.63)	(5.95)	(1.65)	-	-	(8.03)	(7.85)	(1.04)	(0.359)
1000	22.20	12.24	22.63	5.23	1.46	-	-	7.31	7.20	1.07	0.262
1250	23.16	11.93	21.80	4.94	1.35	-	-	7.07	6.97	-	0.252
1501	20.73	10.27	20.11	4.48	1.25	-	-	6.88	6.49	0.89	0.240
2000	19.99	9.98	21.49	4.76	1.32	-	-	6.95	6.79	0.95	0.233
2998	24.25	10.08	21.20	4.79	1.31	-	-	-	6.87	-	0.208
3300	26.86	11.95	23.41	5.43	1.48	-	-	-	7.25	1.02	0.223
3306	24.91	10.17	21.87	4.92	1.40	-	-	7.32	7.07	1.06	0.204
3310	-	10.84	22.99	5.19	1.44	-	-	-	7.14	-	-
3315	25.46	10.13	22.95	5.10	1.43	-	-	-	7.09	-	0.198
3323	1038	3750	970.1	179	42.9	197	144	94.3	75.9	9.27	1.772
3329	415.8	1523	359.6	75.0	19.2	-	-	48.0	45.5	7.09	1.844
3359	292.2	860.1	211.8	43.3	11.4	-	-	29.7	-	3.64	1.564
3377	303.7	904.8	221.1	46.2	11.8	56.6	48.2	27.4	-	3.40	1.581
3420	223.9	564.3	145.1	32.0	8.35	-	-	-	24.8	2.86	1.382
3470	177.8	431.2	113.5	25.3	-	-	-	19.4	17.4	2.63	1.335
3470	140.6	424.6	111.2	24.3	6.44	-	-	-	-	-	1.564
3491	193.3	476.2	128.0	27.4	7.47	-	-	22.0	20.6	2.75	1.343
3529	321.6	615.6	218.9	45.3	12.0	-	-	41.8	32.3	-	1.035
3580	310.0	638.2	233.5	48.6	12.6	-	-	42.8	34.5	3.58	1.082
3628	363.8	599.0	216.0	44.8	12.0	-	-	39.8	31.5	3.31	0.923
3730	326.4	671.2	240.0	48.4	12.5	-	-	-	-	-	1.088
3730	318.2	603.0	219.6	45.2	11.4	55.1	-	35.6	-	3.73	1.021
3784	330.1	581.7	210.1	43.5	11.7	-	-	34.0	32.3	3.79	0.971
shales	295	592	263	49.9	10.6	40.4	33.8	22.4	20.4	3.49	1.000

factor of 370 as a result of Ce redox chemistry (Chapter 2). In Figure 5.3 REE enrichment (or depletion) at the surface, relative to REE concentrations at 41 dbar, is plotted *versus* REE enrichment at the seawater-brine interface, relative to REE concentrations at 3306 dbar. These enrichments show a strong linear correlation for the trivalent REE, which rank along the regression line roughly in the order of decreasing atomic number. La, which would be expected from such a ranking to show the highest enrichments among the trivalent REE, instead shows an enrichment at the surface comparable to that of Eu and an enrichment at the seawater-brine interface comparable to that of Nd. This is a further demonstration of the anomalous behaviour of La also discussed in Chapter 2. Nevertheless, the enrichment at the seawater-brine interface generally decreases with increasing atomic number, consistent with an increasing degree of REE complexation and concomitant decrease of REE particle-reactivity with increasing atomic number (Chapter 2). The anomalous position of Ce in Figure 5.3 is again the result of Ce redox chemistry.

Below the seawater-brine interface REE concentrations decrease rapidly to a minimum at the second interface (Fig. 5.2). A similar minimum was observed in Chapter 4 for Mn and possibly also for Fe. Below the second interface REE concentrations increase again to about twice the concentrations in the minimum and then remain constant throughout the lower brine. In contrast, upon initial increase Er concentrations decrease throughout the lower brine, leading to an apparent maximum of Er below the second interface. Since there is no reason why such a conspicuous feature should be found only for Er, it is probably the result of an analytical artefact.

5.3.2. The Ce anomaly and the Ce/Nd ratio

The vertical distribution of the Ce anomaly is shown in Figure 5.4a. The negative Ce anomaly in the Mediterranean seawater overlying the brine is characteristic of all open ocean waters (Chapter 2). At the surface, where LREE concentrations are elevated, the depletion of Ce relative to La and Nd is about twofold. The vertical distributions of dissolved REE in Figure 5.1 indicate that the LREE are actively scavenged below the surface. At the same time the distinct increase of

---

Opposite page: **Table 5.1.** REE concentrations (pmol/kg) and Ce anomaly (Ce/Ce^*) in Bannock Basin. The 603 dbar sample was probably contaminated and therefore not included in any of the Figures (see text). REE abundances in mean shales (µmol/kg) from Piper (1974).

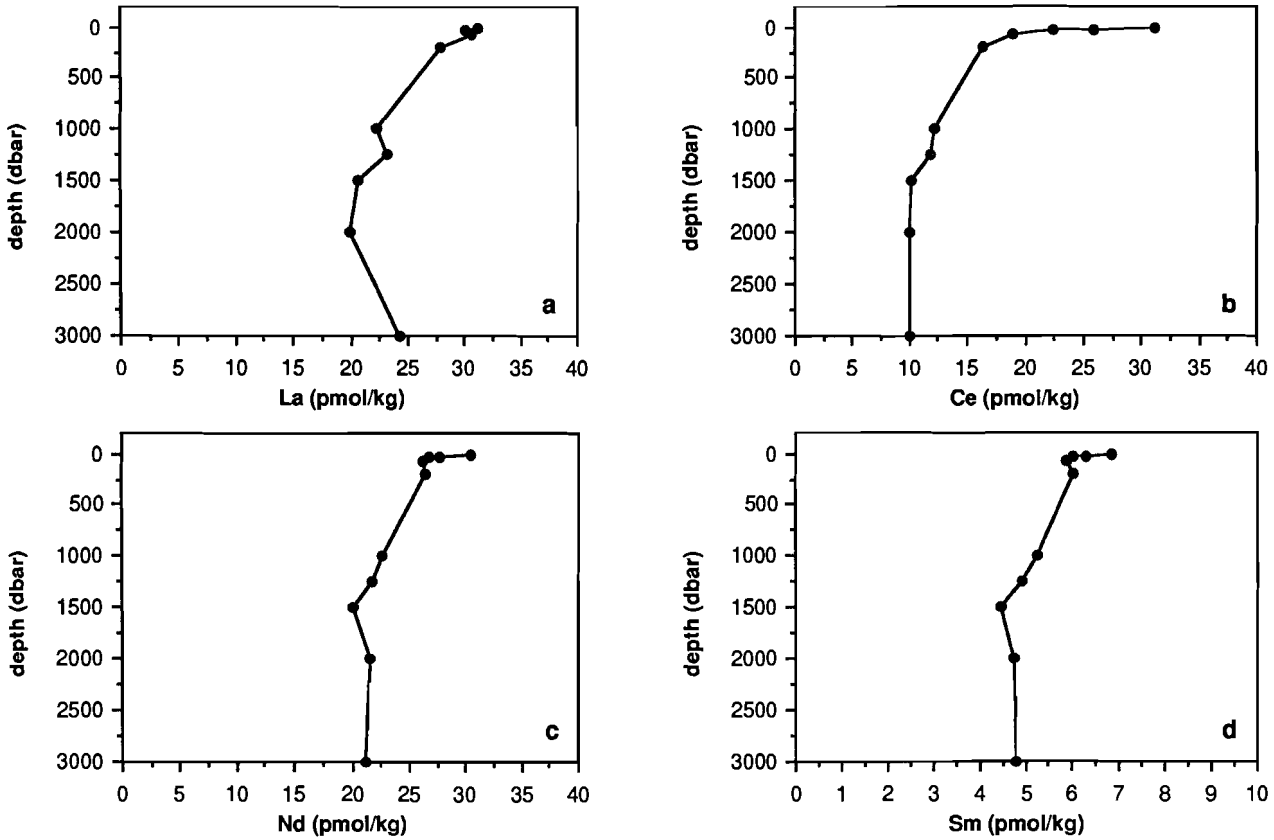
depth (dbar)
0
500
1000
1500
2000
2500
3000
0 5 10 15 20 25 30 35 40
La (pmol/kg)
a
Ce (pmol/kg)
b
Nd (pmol/kg)
c
0 1 2 3 4 5 6 7 8 9 10
Sm (pmol/kg)
d

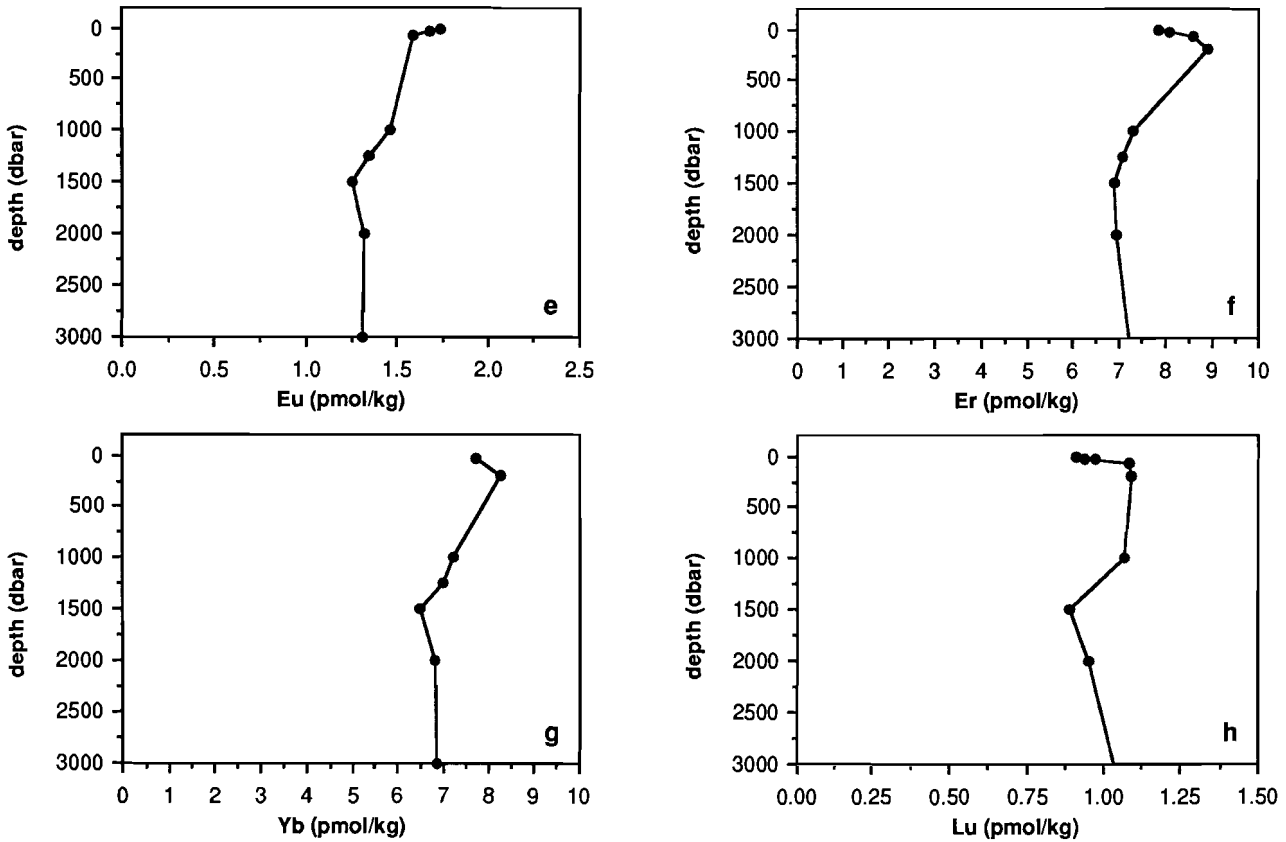

Figure 5.1. Vertical distributions of dissolved REE in the Mediterranean seawater overlying the Bannock brine. Insufficient data is available for Gd and Dy to present reasonable vertical distributions.

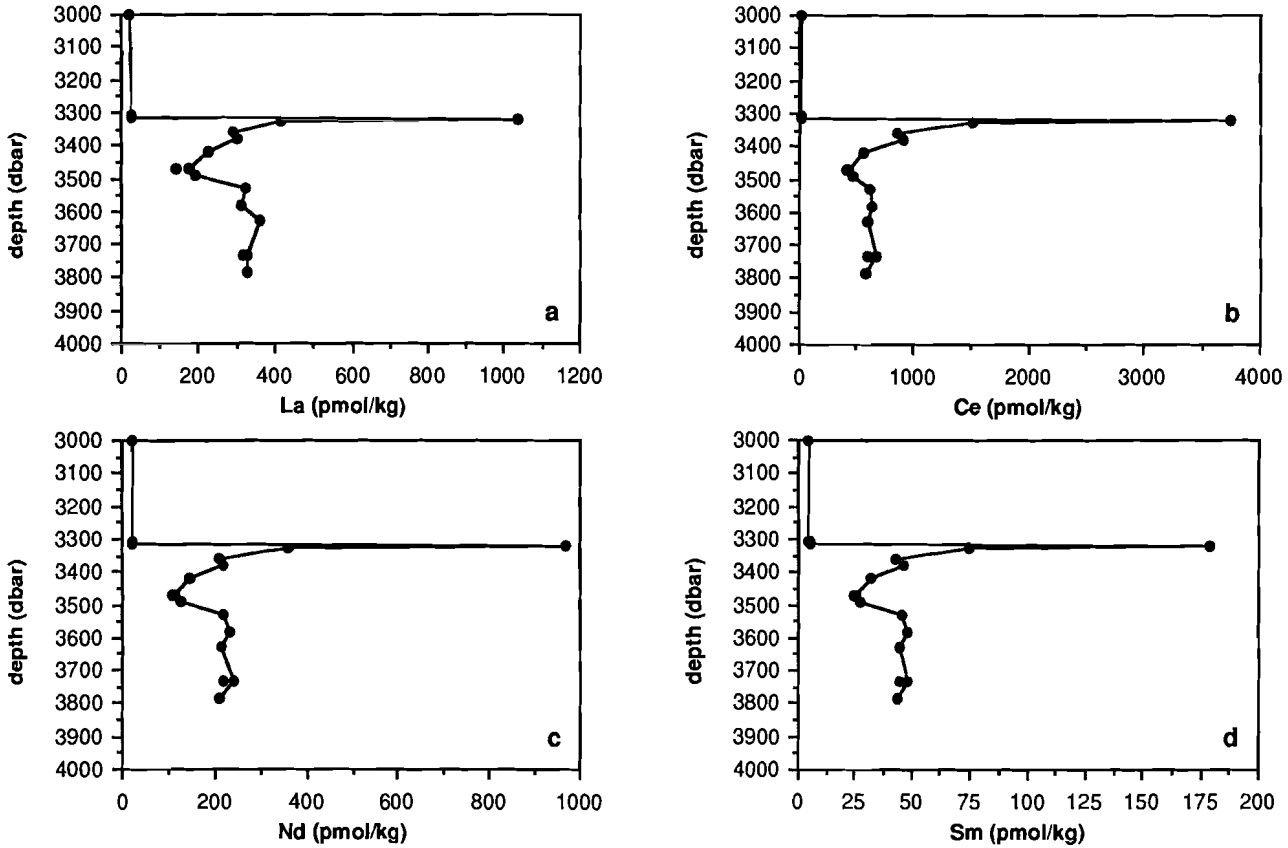
depth (dbar)
3000
3100
3200
3300
3400
3500
3600
3700
3800
3900
4000
0
200
400
600
800
1000
1200
La (pmol/kg)
a
depth (dbar)
0
1000
2000
3000
4000
Ce (pmol/kg)
b
depth (dbar)
0
200
400
600
800
1000
Nd (pmol/kg)
c
depth (dbar)
0
25
50
75
100
125
150
175
200
Sm (pmol/kg)
d

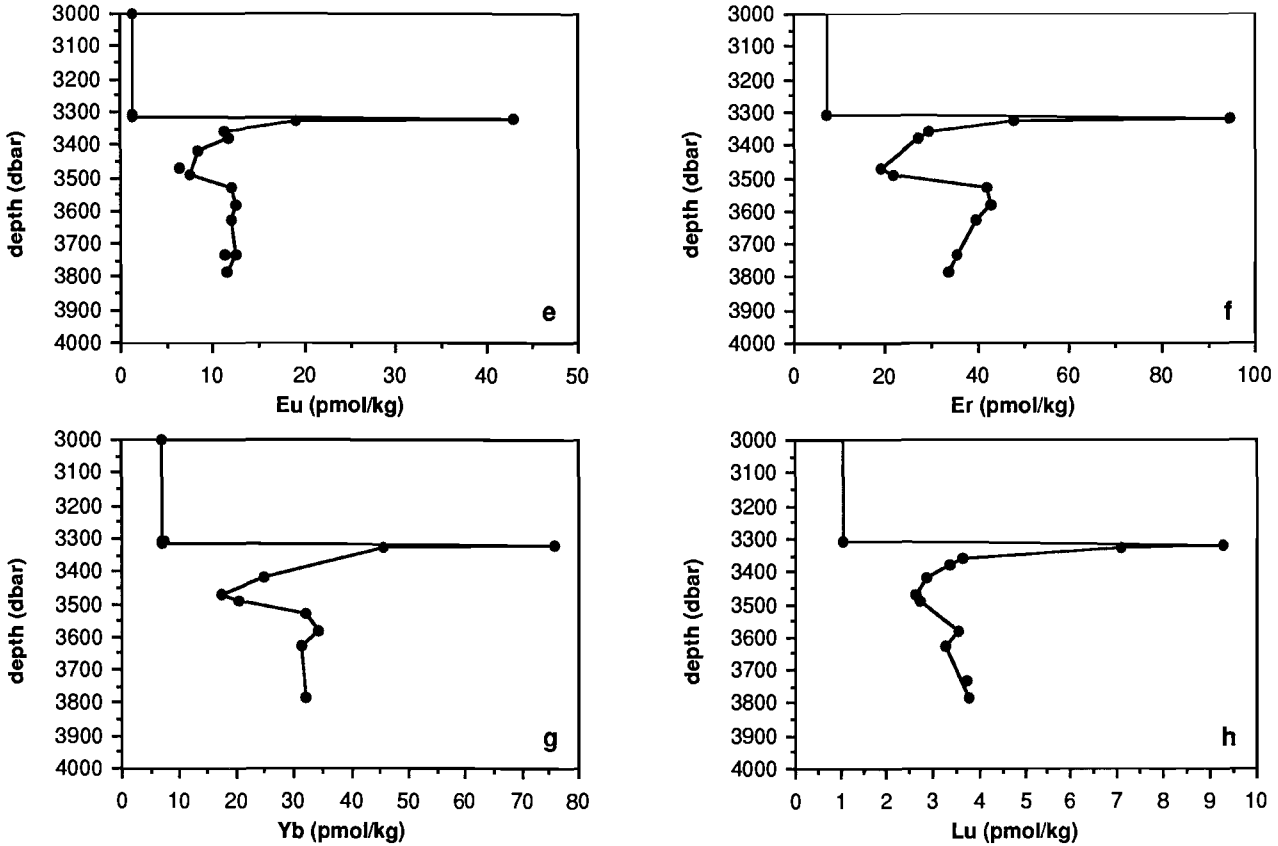

Figure 5.2. Vertical distributions of dissolved REE in the Bannock brine. Seawater-brine interface and second interface at approximately 3323 dbar and 3470 dbar respectively. Insufficient data is available for Gd and Dy to present reasonable vertical distributions.

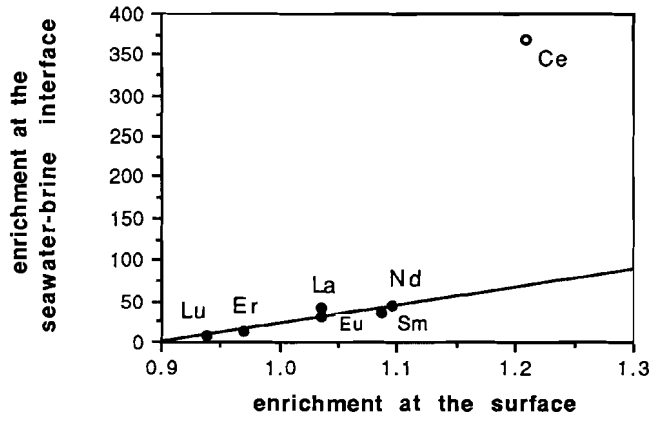

Figure 5.3. REE enrichment at the surface *versus* REE enrichment at the seawater-brine interface, relative to REE concentrations at 41 dbar and 3306 dbar respectively. The enrichments show a strong linear correlation for the trivalent REE (closed symbols). Ce behaves anomalously as a result of its own redox chemistry (open symbol).

the relative Ce depletion from twofold at the surface to fourfold at 200 dbar indicates that, as expected, Ce is more effectively scavenged than the trivalent REE. Below 200 dbar the relative Ce depletion gradually increases from fourfold to fivefold just above the seawater-brine interface.

The enrichment of Ce at the seawater-brine interface is almost a factor of 10 higher than that of La and Nd, which in turn show the highest enrichments among the trivalent REE (Fig. 5.3). The preferential release of Ce at the seawater-brine interface leads to positive Ce anomalies in the upper brine. At the seawater-brine interface itself the enrichment of Ce relative to La and Nd is about twofold (Fig. 5.4b). Apart from very pronounced positive Ce anomalies that were reported by De Baar *et al.* (1983) for surface waters from the western North Atlantic Ocean, positive Ce anomalies have never before been observed in the open ocean nor in marine anoxic basins. In retrospect De Baar

---

Opposite page: **Figure 5.4.** Vertical distributions of the Ce anomaly (Ce/Ce^*) in the total watercolumn (a) and in the brine (b). Dashed line indicates the Ce anomaly in mean shales, which is 1 by definition. Vertical distribution of the Ce/Nd ratio in the brine (c). Dashed line indicates the Ce/Nd ratio in mean shales (~2.25). Seawater-brine interface and second interface at approximately 3323 dbar and 3470 dbar respectively.

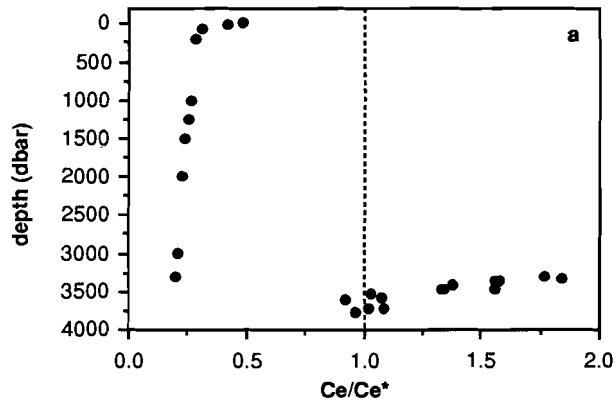
a
depth (dbar)
0
500
1000
1500
2000
2500
3000
3500
4000
0.0
0.5
1.0
1.5
2.0
Ce/Ce*

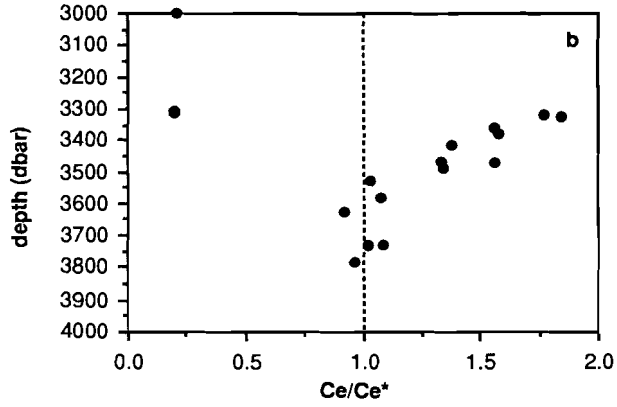
b
depth (dbar)
3000
3100
3200
3300
3400
3500
3600
3700
3800
3900
4000
0.0
0.5
1.0
1.5
2.0
Ce/Ce*

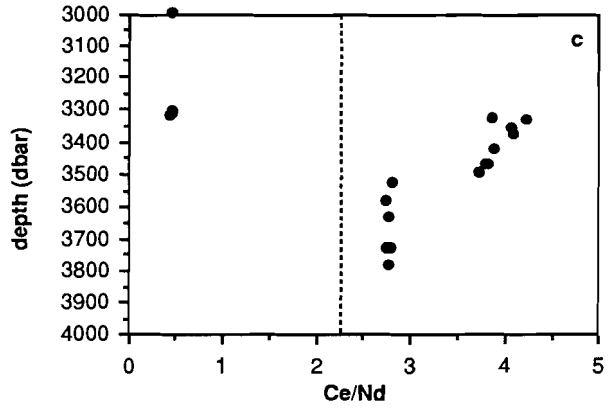
c
depth (dbar)
3000
3100
3200
3300
3400
3500
3600
3700
3800
3900
4000
0
1
2
3
4
5
Ce/Nd

(1991) argued that the observations of De Baar *et al.* (1983) may be called in question and that the occurrence of positive Ce anomalies in oxic open ocean waters is altogether unlikely (Chapter 2).

Throughout the upper brine concentrations of all REE decrease rapidly (Fig. 5.2), suggesting that the REE are actively scavenged below the seawater-brine interface. Again, the Ce anomaly indicates that this scavenging is more effective for Ce than for the trivalent REE (Fig. 5.4b). At the second interface the Ce anomaly abruptly disappears. No Ce anomaly, neither positive nor negative, is found throughout the lower brine. The absence of a Ce anomaly suggests that Ce is mainly present as Ce(III) and that its distribution between particulate matter and solution is controlled by the same processes as that of the trivalent REE.

In contrast with the Ce anomaly, the Ce/Nd ratio in the lower brine is not equal to, but distinctly higher than, its mean shales counterpart (Fig. 5.4c), suggesting that fractionation occurs among the trivalent REE and hence that at high ionic strength the REE are still complexed and not all to the same degree. In Section 5.3.4. this observation is further discussed in terms of the REE patterns in the brine.

5.3.3. The Yb/Nd ratio

The Mediterranean seawater overlying the brine shows the HREE enrichment that is characteristic of open ocean waters as indicated by the Yb/Nd ratio (Fig. 5.5a). Below the surface the Yb/Nd ratio increases with depth. Below 200 dbar down to the seawater-brine interface it remains virtually constant. From the vertical distributions of the REE (Fig. 5.1) and from the behaviour of Ce (Fig. 5.4a) it was inferred (Sect. 5.3.2.) that the REE are actively scavenged below the surface. The fact that Yb is less effectively scavenged than Nd could explain the increase of the Yb/Nd ratio with depth just below the surface. Actually, the situation is more complicated. Nd is enriched at the surface, its concentration decreasing with depth, whereas the concentration of Yb increases with depth between the surface and 200 dbar (Sect. 5.3.1.). This is equally consistent with an increase of the Yb/Nd ratio with depth, yet calls for a more sophisticated explanation than simply an REE input at the surface that is scavenged by settling particles (Elderfield and Greaves, 1982).

At the seawater-brine interface the Yb/Nd ratio abruptly decreases to its value in mean shales, as a result of the larger release of Nd relative to Yb (Fig. 5.3). Tentatively, it might be argued that the higher particle-reactivity of Nd should lead to its enrichment in particulate matter, so that a complete release of particulate REE upon

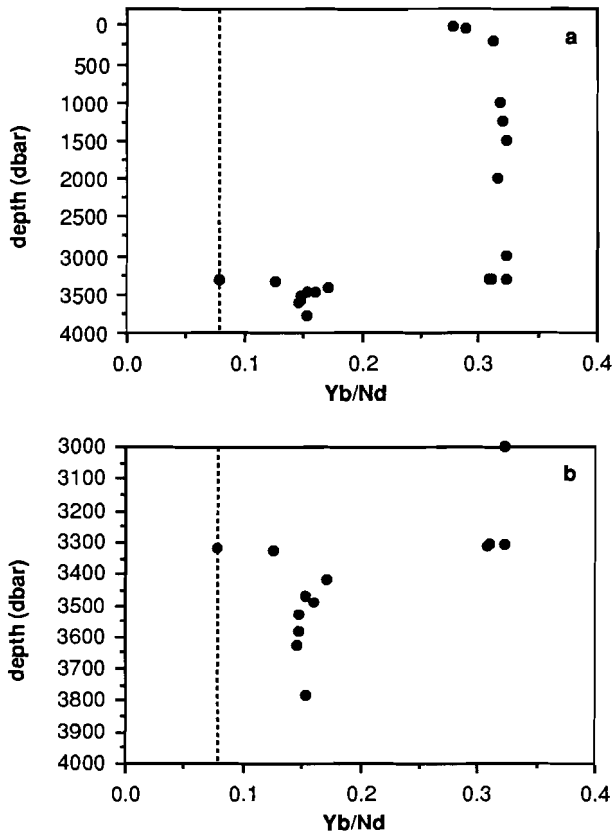

Figure 5.5. Vertical distributions of the Yb/Nd ratio (a) with detail of the brine (b). Dashed line indicates the Yb/Nd ratio in mean shales (~0.078). Seawater-brine interface and second interface at approximately 3323 dbar and 3470 dbar respectively.

dissolution of the Mn and Fe oxyhydroxides that sink into the anoxic water would lead to a net decrease of the dissolved Yb/Nd ratio at the seawater-brine interface. However, as was explained in Chapter 2, this is not quite what happens. Directly above the seawater-brine interface the REE are strongly scavenged from seawater that is substantially HREE enriched (Fig. 5.5a). Although the LREE are scavenged more effectively than the HREE, the HREE are relatively more abundant, which may cause them to be scavenged about as effectively as the LREE. Therefore, particulate matter directly above the seawater-brine interface may actually have a mean shales-like REE pattern. Complete

release of particulate REE at the seawater-brine interface would then lead to a dissolved Yb/Nd ratio equal to that of mean shales, as observed.

It was suggested in Section 5.3.2. that the decrease of REE concentrations with depth (Fig. 5.2) and the behaviour of the Ce anomaly (Fig. 5.4a,b) in the upper brine is indicative of some scavenging process. This suggestion seems to be supported by the increase of the Yb/Nd ratio below the seawater-brine interface. Apparently Nd is scavenged more effectively than Yb, implying as before (Sect. 5.3.2.) that fractionation of the trivalent REE and hence REE complexation are still important at high ionic strenght. Apart from its increase below the seawater-brine interface, the Yb/Nd ratio is constant throughout the brine, with no conspicuous change at the second interface.

5.3.4. REE patterns

A qualitative impression of how the REE behave throughout the watercolumn relative to each other and in the brine relative to the overlying seawater is obtained by comparing some selected REE patterns (Fig. 5.6). REE patterns in the overlying seawater show the pronounced negative Ce anomaly and HREE enrichment characteristic of open ocean waters, as already observed in Sections 5.3.2. and 5.3.3.

REE patterns in the upper brine are characterized by a positive Ce anomaly and little HREE enrichment. The REE pattern at the seawater-brine interface (3323 dbar) shows some indication of a positive Gd anomaly. The sample at the second interface (3470 dbar) shows a pronounced enrichment of La relative to Nd, which is shared by all brine samples, except for the two samples nearest the seawater-brine interface. This La enrichment is not observed in the overlying seawater, which suggests that it is the result of a true La anomaly that may change as a result of ambient chemical conditions, rather than an analytical artefact caused by Ba interference (Chapters 2 and 3).

The REE pattern at 3628 dbar typifies the lower brine, since REE concentrations are almost constant throughout this brine layer. It largely overlaps with the REE pattern at 3377 dbar (upper brine) except for Ce, Er and Yb. The HREE are more strongly enriched in the lower brine than in the upper brine, but less than in the overlying seawater. Throughout the lower brine there is no Ce anomaly. Ce thus falls on the line that connects La and Nd in the REE pattern, yet, since La is enriched relative to Nd throughout the brine, the Ce/Nd ratio in the lower brine is still distinctly above the Ce/Nd ratio in mean shales (Fig. 5.4c).

REE patterns in the brine are very different from those in the overlying seawater, which are characteristic of open ocean REE patterns. The REE pattern at the seawater-brine interface very much

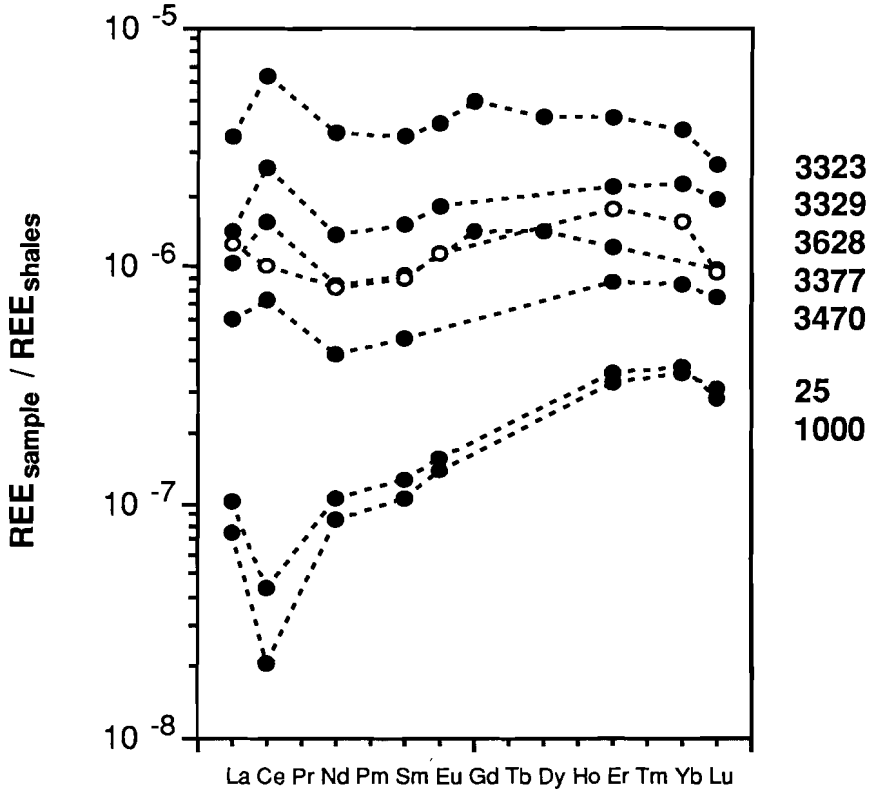

Figure 5.6. REE patterns for selected samples in the upper brine, in the lower brine and in the overlying seawater. Corresponding depths in dbar indicated at the right hand side of each pattern. REE pattern at 3628 dbar drawn with open symbols for comparison with REE pattern at 3377 dbar.

resembles that of mean shales, except for the positive Ce anomaly, showing neither HREE nor LREE enrichment. The enrichment of La and Ce relative to Nd is a very distinctive feature of REE patterns in the lower brine and causes them to have a minimum near Nd. At the same time they have a maximum near Er and nearly equal mean shales normalized concentrations for La, Gd and Lu. In the second part of this Chapter an attempt is made to reproduce such an REE pattern from calculations of REE speciation in the brine, which are incorporated into the model of REE scavenging developed by Byrne and Kim (1990).

5.4. REE scavenging

5.4.1. General framework and assumptions

The oceanic residence time τ_M of a trace metal M is a direct measure of how effectively it is removed from seawater relative to other trace metals. Oceanic residence times are defined with respect to the total input of trace metal M into the oceans (or sometimes with respect to a specific input such as rivers or hydrothermal vents) in terms of its total concentration in seawater A_M (mol/kg) and the rate of its total input into the oceans $(\partial A_M/\partial t)_{in}$ (mol kg^{-1} y^{-1})

$$\tau_M = A_M / (\partial A_M/\partial t)_{in} \qquad (5.1)$$

Unfortunately, the mechanisms of trace metal input into the ocean are poorly understood and the relative importance of various sources is not well known. Input rates $(\partial A_M/\partial t)_{in}$ are therefore hard to determine. Alternatively, if it is assumed that the oceans are at steady state with respect to A_M (*i.e.* $dA_M/dt = (\partial A_M/\partial t)_{in} - (\partial A_M/\partial t)_{out} = 0$), then the total input rate $(\partial A_M/\partial t)_{in}$ is equal to the total output rate $(\partial A_M/\partial t)_{out}$. Scavenging onto marine particulate matter is the dominant process for removing trace metals from seawater and the output rate $(\partial A_M/\partial t)_{out}$ may therefore be calculated from models of trace metal scavenging.

Early attempts to calculate trace metal scavenging rates were made by Craig (1974) and Schindler (1975). Craig (1974) directly estimated the rate of *in situ* scavenging for Cu, Sb, Sc and Ni, by fitting a vertical advection-diffusion scavenging model to their deep water vertical distributions at a North Pacific Geosecs-I station, assuming the scavenging process to be first order in concentration. The oceanic residence times of these four trace metals with respect to scavenging were subsequently calculated from the estimated scavenging rates. An advantage of this approach is that any specific knowledge of the mechanisms that underlie the scavenging process is not required.

Schindler (1975) calculated trace metal oceanic residence times from a model of trace metal scavenging. He assumed that the mechanism underlying adsorption of trace metals onto particulate matter is complexation by hydroxide functional groups on the metal oxide surfaces of this particulate matter. Such a mechanism qualitatively explains the observation that trace metal adsorption onto metal oxide surfaces increases from zero to 100% within a narrow range of pH and that this critical pH range coincides with the region where hydroxide complexes of the trace metals in question are formed. Schindler (1975) found a good correlation between the equilibrium

formation constants of metal complexes with hydroxide functional groups on silica surfaces and the corresponding hydrolysis constants in solution for a large number of trace metals. He therefore considered scavenging to be the combined effect of complexation by *inorganic* surface functional groups and complexation by dissolved *inorganic* ligands, taking suspended amorphous silica as the model surface. He calculated the residence time with respect to scavenging for a number of trace metals from the ratio of the total amount of trace metal (free, complexed and adsorbed onto surfaces) and the amount of trace metal that is adsorbed within the residence time of the amorphous silica. Although the validity of the model is limited by a number of important simplifications (complexation by organic ligands was disregarded, equilibrium complexation constants at other than seawater conditions were used, suspended amorphous silica is probably not a good representative of marine particulate matter *etc.*) he found for most trace metals good agreement between calculated residence times and residence times that had been reported earlier by Goldberg (1965). However, the latter were of doubtful quality and the validity of Schindler's results is further limited by the fact that he overestimated the total concentrations of all trace metals included in his calculations and hence the values of A_M in (5.1) by one to three orders of magnitude.

Balistrieri *et al.* (1981) found a correlation between equilibrium formation constants of trace metal complexes with organic ligands containing carboxylic acid functional groups and the corresponding equilibrium constants for trace metal hydrolysis that bore great resemblance to the correlation reported by Schindler (1975) between equilibrium formation constants of trace metal complexes with hydroxide functional groups on silica surfaces (silanol groups) and equilibrium constants for trace metal hydrolysis. Apparently the ligand properties of the hydroxide functional group are not very dependent on the nature of the substrate to which it is attached or even on whether it is attached at all. From a comparison of two theoretical correlations, based on an 'organic coating' and a 'silica surface' scavenging model respectively, with the correlations actually observed, Balistrieri *et al.* (1981) concluded that the 'organic coating' model predicts the carboxylic acid-hydrolysis correlation better, than the 'silica surface' model predicts the silanol-hydrolysis correlation. These observations led Balistrieri *et al.* (1981) to propose that the carboxylic acid functional groups of organic coatings on the surface of particulate matter, rather than hydroxide functional groups on metal oxide surfaces, are responsible for the adsorption of trace metals onto particulate matter. It must be noted that all the above correlations were observed under experimental conditions using model surfaces and

ideal solutions of the organic ligands. Balistrieri and Murray (1984) found no correlation between the capacity of interfacial sediment for binding any of a large number of trace metals and the first hydrolysis constants of these metals in seawater.

Byrne and Kim (1990) performed laboratory experiments to determine distribution coefficients for the distribution of REE between seawater and various surfaces. They observed that scavenging by various silica phases (glass beads, acid-washed diatoms, silica gel) would typically lead to LREE enrichment in seawater. On the other hand, glass beads which had obtained an organic coating through immersion in Tampa Bay for one week showed a greater affinity for LREE than for HREE. A greater affinity for LREE was also found for all other surfaces used in the experiments (*e.g.* MnO_2, calcite, aragonite and α-FeOOH), but the fact that organic coatings are a ubiquitous feature of marine particulate matter led Byrne and Kim (1990) to support the conclusion of Balistrieri *et al.* (1981).

By assuming that scavenging is the combined effect of complexation by *organic* surface functional groups and complexation by dissolved *inorganic* ligands, Byrne and Kim (1990) arrived at an expression for the input normalized concentration of the REE in seawater. Their starting point was an expression for the oceanic residence time τ_M of a trace metal M, which was obtained by rewriting the expression of Schindler (1975) in terms of D_M, the solid/solution distribution coefficient of trace metal M in seawater (mol M per kg solid/mol M per kg solution), τ_P, the oceanic residence time of particulate matter and ϕ_P, the concentration of particulate matter in seawater (kg solid/kg solution)

$$\tau_M = \tau_P(1 + D_M^{-1}\phi_P^{-1}) \qquad (5.2)$$

Byrne and Kim (1990) subsequently focussed on the oceanic residence times of the REE. For the REE $\tau_M \gg \tau_P$ (Elderfield and Greaves, 1982; De Baar *et al.*, 1985a) so that $\tau_M - \tau_P \approx \tau_M$ and (5.2) may be simplified to

$$\tau_M = \tau_P D_M^{-1}\phi_P^{-1} \qquad (5.3)$$

By substituting (5.1) for the residence time τ_M in (5.3) and rearranging, an expression is obtained for A_M, the total amount of REE in seawater, in terms of the rate of their input into the oceans $(\partial A_M/\partial t)_{in}$ and the factor $\tau_P D_M^{-1}\phi_P^{-1}$, which is indirectly related to REE complexation

$$A_M = (\partial A_M/\partial t)_{in}\, \tau_P D_M^{-1}\phi_P^{-1} \qquad (5.4a)$$

When both sides are divided by $(\partial A_M/\partial t)_{in}$, (5.4a) becomes

$$A_M^* = A_M/(\partial A_M/\partial t)_{in} = \tau_P D_M^{-1} \phi_P^{-1} \quad (5.4b)$$

where A_M^* is the 'input normalized' concentration of the REE in seawater. As was discussed in Chapter 2, the average input of REE into the oceans is assumed to have a mean shales-like REE pattern *i.e.* for the REE 'input normalized' is equal to 'mean shales normalized' and A_M^* is simply the mean shales normalized REE concentration in seawater. A_M^* depends exclusively on the factor D_M^{-1}, since τ_P and ϕ_P are independent of atomic number. It is however more convenient to consider the factor $D_M^{-1}\phi_P^{-1}$, which is

$$D_M^{-1}\phi_P^{-1} = M_T/M_S = (M_T/[M]) \,/\, (M_S/[M]) \quad (5.5)$$

by definition. M_T is the total dissolved REE concentration, [M] is the concentration of free dissolved REE and M_S is the concentration of REE adsorbed onto particulate matter. M_T is the sum of the free dissolved REE concentration [M] = $[M^{3+}]$ and the concentrations of all dissolved REE complexes. Byrne and Kim (1990) considered the first and second carbonate complex of the REE as well as the minor REE complexes with chloride, sulfate, fluoride and hydroxide anions

$$M_T = [M^{3+}] + [MCl^{2+}] + [MSO_4^+] + [MF^{2+}] +$$

$$+ [MOH^{2+}] + [MCO_3^+] + [M(CO_3)_2^-] \quad (5.6)$$

A very high equilibrium association constant for the Ce phosphate complex was reported by Mayer and Schwartz (1950), suggesting that the phosphate complex is the major Ce species in seawater. Based on this incorrect assumption is was argued by Liu *et al.* (1988) that Ce anomalies in marine carbonates are a sensitive indicator of redox conditions in the paleo-ocean. Byrne and Bingler (1989) and Byrne *et al.* (1991) recently showed that the equilibrium association constant reported by Mayer and Schwartz (1950) is the result of incorrect interpretation of an otherwise excellent dataset. The Ce phosphate complex need not be considered when calculating Ce speciation in seawater, yet it may be important in fresh waters that contain little carbonate (Byrne *et al.*, 1991).

Equation (5.6) may be rewritten to obtain the numerator on the right hand side of (5.5)

$$M_T / [M] = B_0 + \beta_1^* [H^+]^{-1} + {}_{CO_3}\beta_1[CO_3^{2-}] + {}_{CO_3}\beta_2[CO_3^{2-}]^2 =$$

$$= 1 + \Sigma_{nj}({}_j\beta_n[L_j]^n) \qquad (5.7a)$$

where $[L_j]$ is the concentration of dissolved ligand L_j in seawater and

$$B_0 = 1 + {}_{Cl}\beta_1[Cl^-] + {}_{SO_4}\beta_1[SO_4^{2-}] + {}_F\beta_1[F^-] \qquad (5.7b)$$

The constants ${}_j\beta_n$ in (5.7a) and (5.7b) are the equilibrium association constants for REE complexes with dissolved ligands L_j at the ionic strength of seawater

$${}_j\beta_n = [M(L_j)_n][M^{3+}]^{-1}[L_j]^{-n} \qquad (5.7c)$$

and β_1^* is the first REE hydrolysis constant at the ionic strength of seawater

$$\beta_1^* = [MOH^{2+}][M^{3+}]^{-1}[H^+] \qquad (5.7d)$$

Equation (5.5) may be written more conveniently by taking the logarithm of both sides, substituting (5.7a) for the numerator on the right hand side and using a simple expression for the denominator

$$\log(D_M^{-1}\phi_P^{-1}) = \log\{1 + \Sigma_{nj}({}_j\beta_n[L_j]^n)\} - \log\{\Sigma_i(K_i \cdot [{}_sL_i])\} \qquad (5.8)$$

where K_i are the equilibrium association constants for REE complexes with organic surface ligands at the ionic strength of seawater and $[{}_sL_i]$ is the concentration of organic surface ligand ${}_sL_i$ (mol per kg solution).

Byrne and Kim (1990) further simplified the second term on the right hand side of (5.8) by assuming that REE complexation with organic surface ligands is dominated by carboxylic acid functional groups and that the equilibrium association constants K_i are independent of the type of carboxylic acid, $K_i = \mathbf{K}$. Equation (5.8) then changes into

$$\log(D_M^{-1}\phi_P^{-1}) = \log\{1 + \Sigma_{nj}({}_j\beta_n[L_j]^n)\} - \log(\mathbf{K}\Sigma_i[{}_sL_i]) =$$

$$= \log\{1 + \Sigma_{nj}({}_j\beta_n[L_j]^n)\} - \log(\mathbf{K}) + \text{constant} \qquad (5.9)$$

where the constant is independent of atomic number since the organic surface ligand concentrations $[{}_sL_i]$ are independent of atomic number. Equation (5.4b) shows that, except for a factor τ_P which is independent

of atomic number, the left hand side of (5.9) is equal to A_M^*, the mean shales normalized concentration of the REE in seawater. Consequently, when the right hand side of (5.9), except for the constant, is calculated for each REE and plotted *versus* atomic number, the resulting curve should resemble a seawater REE pattern.

5.4.2. The calculation of REE speciation

In solutions of ionic strength I>0, thermodynamic equilibria and thermodynamic equilibrium constants are expressed in terms of activities rather than concentrations of the reactants. The activity a_i of a free (uncomplexed) dissolved species i and its concentration $[i]_F$ are related by the activity coefficient $\gamma_F(i)$

$$a_i = [i]_F \gamma_F(i) \qquad (5.10a)$$

The activity a_i is also related to the total concentration $[i]_T$ of i by the total activity coefficient $\gamma_T(i)$

$$a_i = [i]_T \gamma_T(i) \qquad (5.10b)$$

which results in an expression for the total activity coefficient

$$\gamma_T(i) = \{[i]_F / [i]_T\} \times \gamma_F(i) \qquad (5.11)$$

In a hypothetical (infinitely dilute) solution of zero ionic strength all the activity coefficients $\gamma(i)$ are equal to 1 and activities and concentrations are interchangeable. For solutions of ionic strength I>0, such as seawater, equilibrium constants may only be compared after converting all concentrations to activities, using values of $\gamma(i)$ at that particular ionic strength. Consequently, the stoichiometric equilibrium association constants ${}_j\beta_n$ at the ionic strength of seawater in (5.7c) are directly related to the thermodynamic equilibrium association constants ${}_jK_n$ at zero ionic strength

$${}_j\beta_n = {}_jK_n \{\gamma_F(M)\ \gamma_F{}^n(L_j) / \gamma_F(M(L_j)_n)\} \qquad (5.12)$$

From (5.7a) an expression is obtained for the fraction of the total dissolved REE concentration that is present as free REE cations

$$[M] / M_T = \{1 + \Sigma_{nj} ({}_j\beta_n [L_j]^n)\}^{-1} \qquad (5.13)$$

By combining (5.13) and (5.7c) an expression is obtained for the fraction

of the total dissolved REE concentration that is complexed by n ions of a ligand L_j

$$[M(L_j)_n] / M_T = {}_j\beta_n [L_j]^n / \{1 + \Sigma_{nj} ({}_j\beta_n[L_j]^n)\} \qquad (5.14)$$

If the ${}_j\beta_n$ are known or if the $\gamma_F(i)$ are known so that the ${}_j\beta_n$ may be calculated from the ${}_jK_n$ then the fractions $[M]/M_T$ and $[M(L_j)_n]/M_T$ can be solved from (5.13) and (5.14) respectively by a series of iterations (Millero and Schreiber, 1982; Cantrell and Byrne, 1987a; Byrne *et al.*, 1988; Stanley and Byrne, 1990; Byrne and Kim, 1990). For highly complex solutions such as seawater, such calculations can only be performed with the help of a computer. A variety of computer programs has been developed, using a number of different solution algorithms.

Two computer programs were available for trace metal speciation calculations: EASEQL and WATEQX. All calculations of REE speciation in seawater presented here were performed with EASEQL, which is an interactive version (release 2.0) of MINEQL. The solution algorithm was adequately described elsewhere (Morel and Morgan, 1972) and will not be discussed here. WATEQX, which is based on a different solution algorithm (Van Gaans, 1989), was used by De Baar *et al.* (1988) to model the speciation and redox chemistry of Ce in the anoxic Cariaco Trench.

The major difficulty of calculating trace metal speciation at high ionic strength is the calculation of the stoichiometric equilibrium association constants ${}_j\beta_n$ from the thermodynamic equilibrium association constants ${}_jK_n$ *i.e.* the calculation of the activity coefficients $\gamma_F(i)$. Both EASEQL and WATEQX use the equations of Pitzer (1973) and Pitzer and Mayorga (1973) (see also Millero and Schreiber, 1982) to extrapolate the ${}_jK_n$, which are read from a database, to the ionic strength of interest. WATEQX calculates the ionic strength of the initial solution and extrapolates all ${}_jK_n$ to that ionic strength. At each iteration it recalculates the ionic strength and extrapolates the ${}_jK_n$ to this new value. EASEQL assumes ionic strength to be independent of the speciation of the solution components. The ionic strength of the initial solution must be calculated and entered by the user. EASEQL then extrapolates all ${}_jK_n$ to this ionic strength and uses the resulting ${}_j\beta_n$ throughout the calculations.

The extrapolation of the ${}_jK_n$ by means of the equations of Pitzer (1973) and Pitzer and Mayorga (1973) is not reliable above I=0.7. The ${}_jK_n$ can therefore barely be extrapolated to the ionic strenght of seawater, but certainly not to the ionic strength of the brine which is about 7. However, EASEQL offers the possibility of changing the ${}_jK_n$ interactively for each species separately. The program may be 'fooled' by entering ${}_j\beta_n$ at the ionic strength of interest that are calculated separately by some method that is more reliable than the Pitzer equations, as if they were

the ${}_jK_n$. When I=0 is entered as the ionic strength of the initial solution, regardless of its true ionic strength, EASEQL will use the correctly extrapolated ${}_jK_n$ throughout the calculations, without extrapolating them itself.

The seawater and brine compositions that were used in the present speciation calculations are listed in Table 5.2. The equilibrium association constants ${}_j\beta_n$ at the ionic strength of seawater were kindly calculated by F.J. Millero (pers. comm.). They are largely equal to the constants that were used by Stanley and Byrne (1990) and by Byrne *et al.* (1988). Average major element composition of the two brine layers was partly provided by G.J. de Lange (pers. comm.), partly taken from De Lange *et al.* (1990b) and converted to molal units (mol/kg) by F.J. Millero (pers. comm.). Latter conversion is non-trivial in the brine, which has a density of about 1.2 kg/l (De Lange *et al.*, 1990b). REE speciation in the brine was calculated at an assumed pH of 8.

REE speciation in seawater is presented in Table 5.3 and in Figure 5.7. The contribution of each species to REE speciation is presented as a fraction of the total dissolved REE concentration. The REE speciation in Figure 5.7 is largely equal to that presented by Stanley and Byrne (1990), showing the minor contribution of all species but the first and second carbonate complex. Moreover, it shows the characteristic distribution of the REE between the first and the second carbonate complex, the first being more important for the LREE and the second for

	seawater	upper brine	lower brine
I	0.68	7.04	7.24
pH	8.2	8	8
Na^+	0.468	4.65	4.71
K^+	0.010	0.140	0.142
Mg^{2+}	0.0532	0.685	0.723
Ca^{2+}	0.0104	0.0250	0.0180
Cl^-	0.55	5.96	6.03
CO_3^{2-}	0.00229	0.00470	0.00460
SO_4^{2-}	0.0282	0.1160	0.1510

Table 5.2. Average major element composition for seawater of 0.68 m ionic strength. Average concentrations of the major elements in the Bannock brine (De Lange *et al.*, 1990b; G.J. de Lange, pers. comm.) were converted to mol/kg by F.J. Millero (pers. comm.). pH in the brine was assumed to be 8 (see text).

REE	REE^{3+}	$REESO_4^+$	$REECl^{2+}$	$REEOH^{2+}$	$REEHCO_3^{2+}$	$REECO_3^+$	$REE(CO_3)_2^-$
seawater							
La	5.6	2.4	2.5	0.7	0.3	64.5	24.0
Ce(III)	4.1	2.1	1.9	2.5	0.2	62.6	26.6
Pr	3.4	1.6	1.5	2.1	0.1	60.8	30.5
Nd	2.6	1.2	1.2	2.1	0.1	59.4	33.4
Sm	1.6	0.8	0.7	1.6	-	54.2	41.1
Eu	1.2	1.2	0.5	1.3	-	50.7	45.1
Gd	1.0	0.7	0.4	0.9	-	46.9	50.1
Tb	0.8	0.3	0.3	1.2	-	43.7	53.7
Dy	0.6	0.2	0.3	1.1	-	38.9	58.9
Ho	0.5	0.2	0.2	1.0	-	34.8	63.3
Er	0.4	0.2	0.2	0.9	-	31.8	66.5
Tm	0.3	0.1	0.1	0.8	-	27.6	71.1
Yb	0.3	0.1	0.1	0.8	-	24.1	74.6
Lu	0.2	0.1	0.1	0.7	-	20.6	78.3
upper brine							
La	43.5	21.0	4.0	-	-	30.7	0.8
Ce(III)	39.6	21.1	3.5	-	0.1	34.7	1.0
Pr	37.1	19.0	3.3	-	0.1	39.1	1.4
Nd	33.1	16.9	3.1	-	0.1	45.0	1.8
Sm	25.1	14.6	2.4	-	0.1	54.8	3.0
Eu	18.0	16.6	2.1	-	0.1	59.5	3.7
Gd	16.7	11.6	2.0	-	0.1	64.8	4.8
Tb	13.1	9.7	1.8	-	0.1	69.2	6.1
Dy	11.0	8.0	1.7	-	0.1	71.7	7.5
Ho	10.4	7.4	1.5	-	0.1	71.6	9.0
Er	9.1	6.6	1.4	-	0.1	72.1	10.7
Tm	8.3	5.2	1.3	-	0.1	72.0	13.1
Yb	7.9	4.8	1.0	-	0.1	71.0	15.2
Lu	7.4	4.0	0.6	-	0.1	69.6	18.3
lower brine							
La	42.3	25.9	3.4	-	-	27.7	0.7
Ce(III)	38.5	26.2	3.0	-	-	31.4	0.9
Pr	36.5	23.7	2.9	-	-	35.7	1.2
Nd	32.8	21.4	2.7	-	-	41.6	1.5
Sm	25.2	18.7	2.1	-	0.1	51.3	2.6
Eu	17.9	21.2	1.9	-	0.1	55.7	3.2
Gd	17.0	15.2	1.8	-	-	61.7	4.3
Tb	13.4	12.8	1.6	-	0.1	66.7	5.4
Dy	11.3	10.6	1.5	-	0.1	69.7	6.8
Ho	10.8	9.9	1.4	-	0.1	69.7	8.1
Er	9.4	8.9	1.3	-	0.1	70.6	9.7
Tm	8.6	7.0	1.2	-	0.1	71.1	12.0
Yb	8.3	6.6	0.9	-	0.1	70.2	13.9
Lu	7.8	5.4	0.5	-	0.1	69.3	16.9

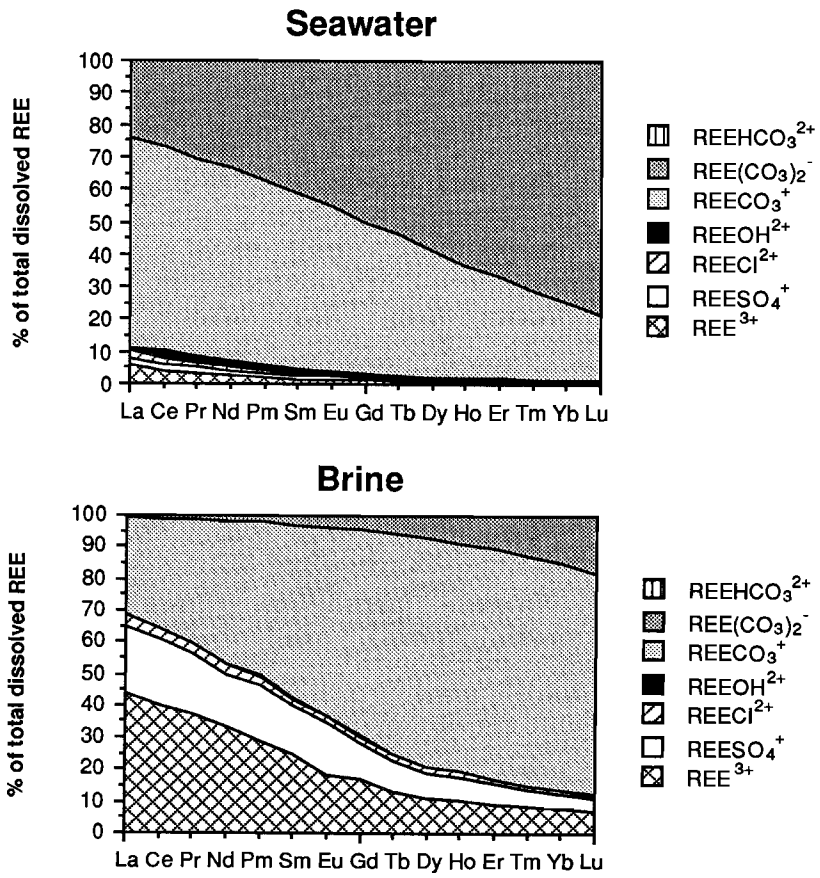

Figure 5.7. REE speciation in the overlying seawater and in the brine. The contribution of each species is indicated as a percentage of the total dissolved REE concentration. Species contributing less than about 1% cannot be resolved in the Figure.

Opposite page: **Table 5.3.** REE speciation in average seawater, in the upper Bannock brine and in the lower Bannock brine. Contribution of each species is expressed as a percentage of the total dissolved REE concentration. Dashes indicate contributions smaller than 0.1%. REE speciation in average seawater was calculated with the EASEQL computer model. REE speciation in the Bannock brine was kindly calculated by F.J. Millero (pers. comm.) in the manner of Millero (1992).

the HREE, with Gd forming about equal amounts of both. The bicarbonate complex was included in the calculations instead of the fluoride complex, yet both complexes seems to contribute equally to REE speciation in seawater and the contribution of the other species is not affected.

REE speciation in the brine was kindly calculated by F.J. Millero (pers. comm.). Briefly, the speciation of the major elements at the ionic strength of the brine is calculated separately, in order to determine the concentration of the free dissolved anion for each of the ligands that are considered in (5.6), except for the fluoride complex which as before was replaced by the bicarbonate complex. REE speciation was calculated from these concentrations with equations (5.13) and (5.14), simply by hand, using equilibrium association constants ${}_j\beta_n$ at the ionic strength of the brine that were calculated as described by Millero (1992). The results are presented in Table 5.3 for both the upper and the lower brine. REE speciation in the two brine layers is very similar and in Figure 5.7 only REE speciation in the upper brine is shown. Apparently, in the brine the contribution of the free REE ion and the minor REE complexes increases at the expense of the second carbonate complex. This is mainly caused by the decrease of the concentration of the free carbonate anion as a result of extensive complexation by Mg and Ca, which are both abundantly present in the brine (Table 5.2). The effect is strongest for the second carbonate complex for reasons given in Chapter 2. Although the absolute effect is largest for the LREE, the relative effect is largest for the HREE, for which the second carbonate complex is the most important species in seawater (Fig. 5.7). The fraction of free HREE ions in the brine is increased by a factor of about 40 relative to seawater, whereas that of the LREE is increased only by a factor of about 7 (Table 5.3).

5.4.3. Theoretical REE patterns

The term $\log(M_T/[M])$ on the right hand side of (5.9) can directly be calculated from the REE speciation presented in Table 5.3, by taking the logarithm of the reciprocal of the fraction of free dissolved REE ions for each REE. In Figure 5.8 these numbers are plotted versus atomic number for four values of pH. For pH 7.3, 7.6 and 7.9 REE speciation was actually calculated only for La, Ce, Nd, Sm, Eu, Er, Yb and Lu, since EASEQL can only calculate REE speciation for 8 different REE at a time. For all other REE the value of $\log(M_T/[M])$ was determined by interpolation. The term $\log(\mathbf{K})$ on the right hand side of (5.9) was calculated as suggested by Byrne and Kim (1990). Equilibrium association constants K_i for REE complexes with 15 monocarboxylic acids taken form Martell and Smith (1977) are plotted *versus* atomic

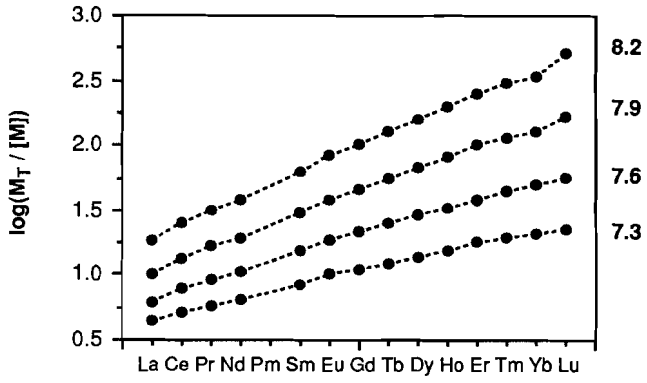

Figure 5.8. Values of $\log(M_T/[M])$, the first term in (5.9), for four values of pH as indicated at the right hand side of each curve. For pH 7.3, 7.6 and 7.9, $\log(M_T/[M])$ was calculated with the EASEQL computer model for La, Ce, Nd, Sm, Eu, Er, Yb and Lu and determined by interpolation for all other REE.

number in Figure 5.9. The solid curve, which represents log(**K**), connects the averages of the 15 constants for each REE.

Theoretical REE patterns for seawater at four values of pH, constructed by subtracting the curve in Figure 5.9 from each of the curves in Figure 5.8, are shown in Figure 5.10. Clearly, the REE pattern at the normal seawater pH of 8.2 reproduces some prominent features of seawater REE patterns, such as HREE enrichment and La and Gd anomalies (Chapter 2). With decreasing pH, HREE enrichment decreases and the theoretical REE patterns become more like that of mean shales. As before, this is caused by the lower concentration of the free carbonate anion. At lower pH, the speciation of dissolved carbonate is increasingly dominated by the bicarbonate anion, for which the REE have no great affinity (Fig. 5.7).

The term $\log(M_T/[M])$ was calculated for the brine from REE speciation in the upper brine (Table 5.3) as was described for seawater. A theoretical REE pattern for the brine was then constructed by subtracting the curve in Figure 5.9. It was thereby implicitly assumed that the term log(**K**) is not affected by the high ionic strength of the brine. This is a valid assumption for two reasons. First, it was found by Schindler (1975) and Balistrieri *et al.* (1981) that the ligand properties of the hydroxide functional group are not very dependent on whether it is present as the free dissolved anion or attached to either organic matter or metal oxide surfaces. Second, it was shown by Millero (pers.

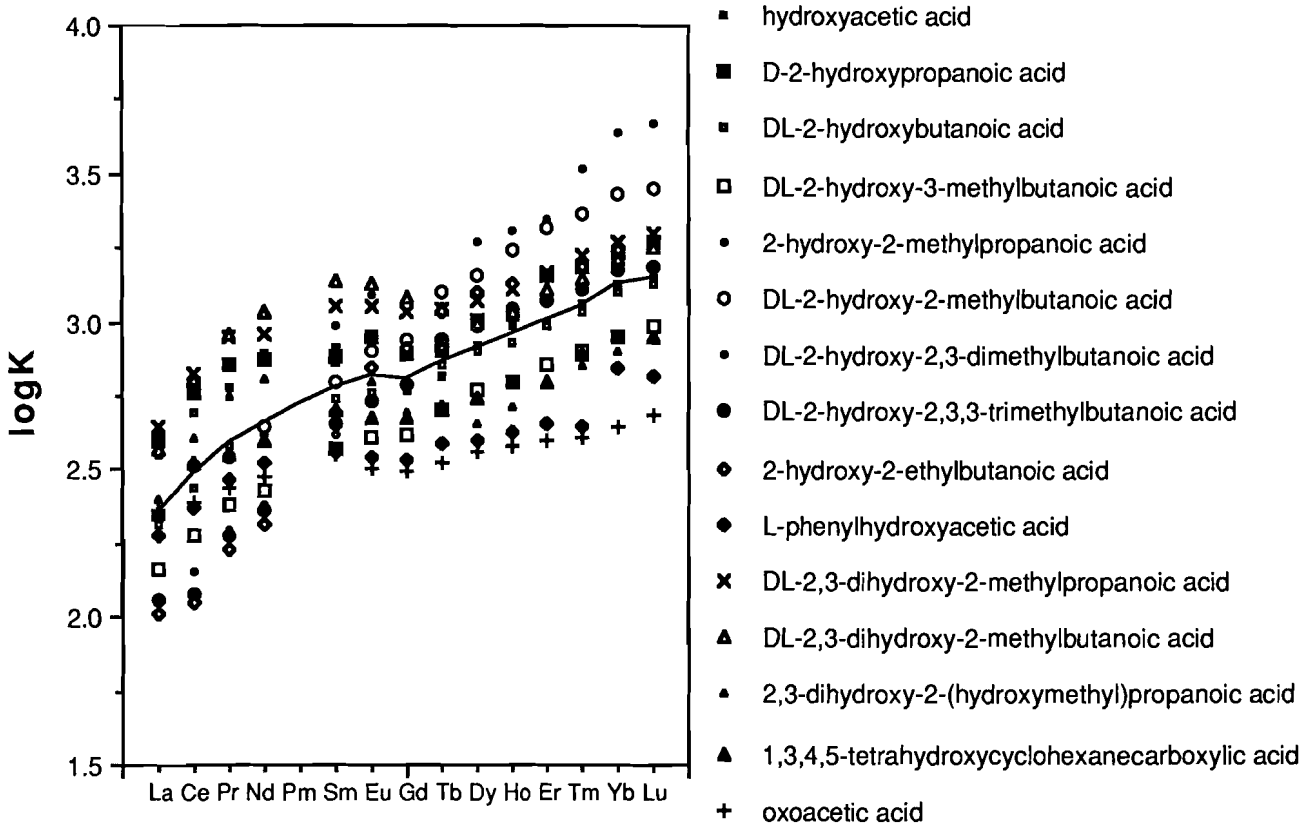

Figure 5.9. Logarithm of equilibrium association constants **K** for REE complexes with 15 monocarboxylic acids. The averages of the 15 equilibrium constants for each REE are connected by the solid curve, which represents the second term in (5.9). Data from Martell and Smith (1977).

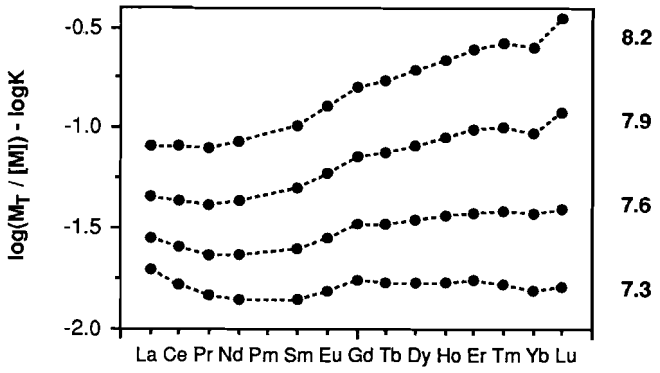

Figure 5.10. Theoretical REE patterns, constructed by subtracting the curve in Figure 5.9 from each of the curves in Figure 5.8, for four values of pH as indicated at the right hand side of each pattern.

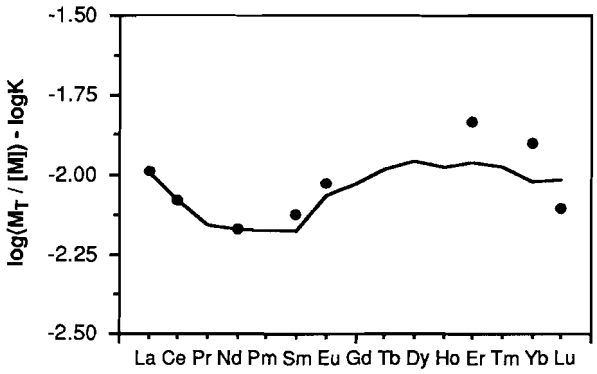

Figure 5.11. Theoretical REE pattern in the brine (solid curve). The term $\log(M_T/[M])$ was calculated from the REE speciation in the brine (Table 5.3). The term log(K) was taken from Fig. 5.9 and was assumed not to be affected by the high ionic strength of the brine (see text). The closed symbols (•) represent the REE pattern actually measured at 3628 dbar. To facilitate the comparison, the REE pattern at 3628 dbar was vertically shifted until its mean shales normalized La concentration was equal to that of the theoretical REE pattern.

comm.) that the equilibrium association constants for REE complexes with the free dissolved hydroxide anion are hardly affected by the high ionic strength of the brine.

The theoretical REE pattern for the brine is shown as a solid curve in Figure 5.11. It is compared with the REE pattern actually measured at 3628 dbar. To facilitate the comparison, the REE pattern at 3628 dbar was vertically shifted until its mean shales normalized La concentration was equal to that of the theoretical REE pattern. An REE pattern from the lower brine was chosen, since the lower brine does not show a Ce anomaly (Sect. 5.3.2.), in other words Ce behaves exactly like the trivalent REE and its distribution between particulate matter and the brine can thus be fully described with the model of Byrne and Kim (1990). Ce anomalies such as occur in the upper brine are the result of Ce redox chemistry, which is not included in the model of Byrne and Kim (1990).

5.5 Discussion

5.5.1. The overlying seawater

The vertical distributions of the REE in the Mediterranean seawater overlying the Bannock brine are the first to be reported for the eastern Mediterranean. Until now, publications on REE in the Mediterranean Sea have mainly been focussed on the western Mediterranean, more specifically on the outflow of Mediterranean water into the North Atlantic Ocean. The only published value of REE concentrations in the eastern Mediterranean is for a mixture of equal volumes of unfiltered surface seawater from five stations in the central and eastern basins (Spivack and Wasserburg, 1988). For this mixture they reported a total Nd concentration of 31.45 pmol/kg, which is in good agreement with the dissolved Nd concentration of 30.42 pmol/kg in the surface waters at Bannock Basin (Table 5.1).

The two most conspicuous features of the vertical distributions of dissolved REE in the Mediterranean seawater overlying the brine are the LREE surface maxima and the HREE maxima at 200 dbar. The latter coincide with the salinity maximum at that depth, which is associated with the presence of Levantine Intermediate Water (LIW), suggesting that the HREE maxima may be explained in terms of the simple model of trace metal cycling in the eastern Mediterranean that was presented in Chapter 4 (Fig. 4.10). According to that model, Atlantic Surface Water (ASW), entering the Mediterranean Sea through the Strait of Gibraltar, is progressively enriched in dissolved trace metals as it flows eastward, as a result of continuous aeolian input. In winter, in the far eastern part of the Mediterranean Sea, ASW sinks down to form LIW,

which subsequently returns to the west, being transported at depths between 60 and 600 dbar. If the REE behave conservatively during the transport of LIW to the west, then, at the longitude of Bannock Basin, LIW will cause a dissolved REE maximum within that same depth range, since the surface water that is the source of LIW originates to the east of Bannock Basin and is therefore more enriched in dissolved REE than the surface water at Bannock Basin (Fig. 4.10). The fact that the maximum at 200 dbar is the most prominent for the HREE is consistent with their relatively low particle-reactivity.

For the LREE, which are more particle-reactive than the HREE, the maximum at 200 dbar is obscured by pronounced surface maxima and active scavenging below the surface (Fig. 5.1). This is in apparent disagreement with vertical distributions of dissolved REE reported for the western Mediterranean by Greaves *et al.* (1991), which show a maximum at 175-250 dbar for all REE, except Ce. Greaves *et al.* (1991) suggested these REE maxima to be preformed from cold surface waters during the formation of Western Mediterranean Intermediate Water (WMIW). Their explanation is conceptually the same as the model presented for the eastern Mediterranean in Chapter 4, yet for a detailed comparison of the vertical distributions of dissolved REE in Bannock Basin with those reported by Greaves *et al.* (1991) a model is needed of the general circulation of watermasses in the western Mediterranean, which is much more complex than in the eastern Mediterranean (Wüst, 1961; Van Geen *et al.*, 1988). Elderfield and Greaves (1982) reported vertical distributions of dissolved REE at a station in the eastern North Atlantic Ocean to the west of the Strait of Gibraltar, where they found subsurface maxima at 200 dbar depth only for Er and Yb and surface enrichment for most other REE. Vertical distributions of dissolved REE reported by Greaves *et al.* (1991) for a station in the North Atlantic Ocean much closer to the Strait of Gibraltar showed no conspicuous behaviour near the surface for any of the REE.

The pronounced surface maxima of the LREE at Bannock Basin are a clear indication of the aeolian input that is causing the gradual enrichment of ASW on its journey to the east. The fact that the HREE do not show a surface maximum seems to be in contradiction with their lower particle-reactivity, which tends to make them more soluble in seawater than the LREE. In any case, the aerosols in question are likely to have an REE pattern that is less HREE enriched than that of the surface seawater. Saharan dust is a good candidate for aeolian deposition in the Mediterranean area. Elderfield and Greaves (1982) invoked deposition of Saharan dust to explain the REE pattern of surface waters at their station in the eastern North Atlantic Ocean. However, both this surface water and Saharan dust and are characterized by a distinct negative Eu anomaly (Rahn, 1976) which is not observed at

Bannock Basin. Although most Saharan dust is blown to the west as a result of the prevailing wind direction, part of it will also be blown to the north and northeast (Ganor and Mamane, 1982; Loÿe-Pilot *et al.*, 1986) This dust may have another provenance than the dust that affected the surface water REE patterns at the station of Elderfield and Greaves (1982). It may therefore have a different mineralogical composition and hence a different REE pattern. Alternatively, during the time of collection of the samples (May-June) prevailing winds come mostly from the north and northwest (Malanotte-Rizzoli and Hecht, 1988) and the aeolian input may instead derive from the European continent.

The extreme surface maximum of Ce and the pronounced gradient indicate that Ce is more effectively dissolved at the surface and more effectively scavenged below the surface than the trivalent LREE. Ce surface maxima leading to less negative Ce anomalies (*cf.* Fig. 5.4) were attributed by Moffett (1990) and by Sholkovitz and Schneider (1991) to photoinhibition of microbially mediated Ce oxidation, which causes it to be less effectively removed than in the deep oxic watercolumn, and to photoreduction of Ce(IV). Both processes may have been active in the eastern Mediterranean at the time of sampling (May-June) when there was a lot of sunlight. However, explaining the Ce surface maximum at Bannock Basin in terms of photoinhibition of Ce oxidation requires a source of dissolved Ce(III) that is poorly removed from the surface waters as the sunlight inhibits its oxidation to solid $Ce(IV)O_2$ by bacteria. On the other hand, photoreduction of Ce(IV) requires a source of solid Ce(IV) which is rapidly dissolved as sunlight enhances its reduction to more soluble Ce(III). The latter is consistent with aeolian input, which is an essential component of the model of trace metal cycling in the eastern Mediterranean that was presented in Chapter 4.

5.4.3. The brine

The two most conspicuous features of the vertical distributions of dissolved REE in the Bannock brine are the maximum at the seawater-brine interface and the minimum at the second interface. The former is caused by release of REE that are adsorbed onto Mn and Fe oxyhydroxides as these oxyhydroxides dissolve in the anoxic water. The minimum at the second interface is apparently caused by active removal of the REE at that depth. As was also argued for Mn and Fe in Chapter 4, this removal is probably the result of incorporation into dolomite that precipitates at the second interface, either *in situ* or in the sediment. Although there is no direct evidence for this process (dolomite samples recovered from the brine were not analyzed for REE

abundances), REE are known to occur in dolomites at sufficient levels to account for such a removal process (Banner *et al.*, 1988).

The vertical distributions of dissolved REE are not linear between the source at the seawater-brine interface and the sink at the second interface, which indicates that they are not controlled simply by diffusion, yet that additional removal of REE is taking place throughout the upper brine. One process that might account for this removal is coprecipitation with or adsorption onto Fe sulfides, as also suggested by the great similarity of the vertical distributions of dissolved REE and dissolved Fe in the upper brine. Again, there is no evidence for such a process, although Brookins (1989) stated that "Under very alkaline, sulfur-rich, carbonate-poor conditions, some heavy lanthanides may be incorporated into metal sulfides".

The REE pattern in the brine is amazingly well reproduced by the model of Byrne and Kim (1990). This indicates that latter model is capable of accurately describing the effects of REE scavenging even for the extreme chemical conditions in the Bannock brine. The model REE pattern has a minimum near Nd and a maximum near Ho-Er as was also observed for the REE patterns in the brine (Fig. 5.6). The mean shales normalized concentrations of La, Ce and Nd are perfectly reproduced, which confirms that Ce is behaving exactly like the trivalent REE. At Sm-Eu the model curve falls somewhat below the measured REE pattern yet the steep slope between Sm and Eu is accurately reproduced, which confirmes that the high mean shales normalized Eu/Sm ratio that is also observed in seawater is caused by complexation and not by dispersion of Eu enriched hydrothermal waters (Chapter 2). For the HREE the measured REE pattern is less accurately reproduced, yet this may be due to the relatively poor accuracy of the HREE measurements (Sect. 5.2.). It was already stated that the flatness of the HREE pattern is caused by the increasing particle-reactivity of the HREE, which is caused by the decreasing importance of the second carbonate complex, which in turn is caused by the decreasing concentration of the free carbonate anion. It was argued that the latter is brought about either by extensive complexation of dissolved carbonate by Mg and Ca, which are abundantly present in the brine, or by a very low pH. A pH in the brine of 6.50-6.55 on the NBS-scale was reported by Bregant *et al.* (1990), yet these measurements must be regarded with some caution because of the problems that arise when measuring pH in solutions of high ionic strength (Knauss *et al.*, 1990, 1991; Mesmer, 1991). Therefore, the pH in the brine was chosen to be 8 (Millero, pers. comm.), equal to that of the overlying seawater. If the pH in the brine is indeed much lower than 8, then this would tend to reduce the concentration of the free carbonate anion even further, which in turn would cause the theoretical REE pattern to become even more like that of mean shales.

5.6 Conclusions

Conclusion 1. Vertical distributions of dissolved REE in the Mediterranean seawater overlying the Bannock brine can be explained in terms of the simple model of trace metal cycling that was presented in Chapter 4 (Fig. 4.10). The HREE show a distinct maximum at about 200 dbar, which probably derives from REE enriched surface water that originates in the far eastern part of the basin and is transported to the west as LIW (Chapter 4). This signal is best preserved for the HREE, since these behave the most conservatively. For the LREE, which are the most particle-reactive, the maximum at 200 dbar is obscured by scavenging throughout the upper part of the watercolumn from high concentrations at the surface to a minimum at about 1500 dbar. The pronounced surface maximum of Ce may be caused by photoreduction of Ce(IV), with wind-blown dust as a possible source.

Conclusion 2. Dissolved REE concentrations at the seawater-brine interface are the highest ever reported for the watercolumn of a marine anoxic basin. Below the seawater-brine interface REE concentrations decrease rapidly to a minimum at the second interface. This minimum is presumably caused by incorporation of REE into dolomite, such as proposed for both Mn and Fe in Chapter 4. The decrease of REE concentrations from the seawater-brine interface down to the second interface is not linear with depth, signifying additional removal of REE throughout the upper brine rather than simple diffusion. The similarity between the vertical distributions of the REE and that of Fe suggests that latter removal is the result of adsorption onto or coprecipitation with Fe sulfides.

Conclusion 3. Considering the many assumptions that have to be made when using the REE scavenging model of Byrne and Kim (1990) to predict REE patterns in the brine, the agreement between the model predictions and REE patterns that were actually observed in the brine is surprising. Apparently REE speciation is not directly affected by the high ionic strength of the brine, yet rather indirectly by the effect of ionic strength on the speciation of the major inorganic ligands, in particular that of the carbonate anion. The REE, which have a strong affinity for the carbonate anion, are in general less strongly complexed *i.e.* they become relatively more particle-reactive if the concentration of free carbonate decreases. In the brine the latter results from excessive complexation of carbonate by Mg and Ca, which are abundantly present. The effect is strongest for the second carbonate complex of the REE and hence for the HREE, causing the brine to be substantially less HREE enriched than the overlying seawater.

CHAPTER 6 Vertical REE distributions in the Black Sea

6.1. Introduction

The discovery of a broad suboxic layer overlying the anoxic water in the Black Sea was without doubt the most exciting result of the 1988 Black Sea Expedition. The oxic-anoxic interface had undergone radical changes since the last U.S. cruises in 1969 (R/V *Atlantis II*) and 1975 (R/V *Chain*). At a station in the centre of the western gyre the first appearance of sulfide in the watercolumn had risen by as much as 30 m and was overlain by a 10-40 m thick layer within which oxygen concentrations did not exceed 5 μM (Murray *et al.*, 1989; Murray and Izdar, 1989). In some publications the possibility that the upper boundary of the anoxic layer was rising had already been mentioned (Deuser, 1970; Zhorov *et al.*, 1982; Fashchuk and Ayzatullin, 1986), yet the hydrographical results of the 1969 and 1975 cruises were nearly identical. Although the anoxic water has often been reported to be overlain by a layer were oxygen and sulfide coexist at low levels (<15 μM), the so called 'C layer' (see for instance Fashchuk and Ayzatullin, 1986), the suboxic layer was a completely new and unexpected phenomenon. Possible explanations for its formation are discussed in Sections 6.2.1. and 6.5.2.

The large vertical extent of the suboxic layer offers a unique opportunity to study REE cycling with respect to the sequence of oxidation reactions induced by the depletion of oxygen (Chapter 2). Moreover, since the suboxic layer is underlain by anoxic water, the full suite of oxidation reactions is expected to be encountered.

During the 1988 Black Sea Expedition the newly discovered suboxic layer was sampled extensively. In this Chapter vertical distributions of dissolved and particulate REE are reported for a station in the centre of the Black Sea. The only previous report on vertical REE distributions in the Black Sea was by Kolesov *et al.* (1975). They determined REE concentrations by INAA-γ in 5 unfiltered seawater samples between the surface and a depth of 1720 m from a station in the easternmost Black Sea (42°17'N 40°26'E). Concentrations ranged from 200 pmol/kg for Lu to 6000 pmol/kg for Ce at a depth of 10 m and no clear structure could be resolved from the vertical distributions. Apparently no precautions were taken to prevent contamination of the samples. Apart from the remote location of the station, the exceptionally high concentrations suggest that a detailed comparison with the present data is inappropriate.

Part of this Chapter has already been published (Schijf *et al.*, 1991). Schijf *et al.* (1991) compared their vertical REE distributions to

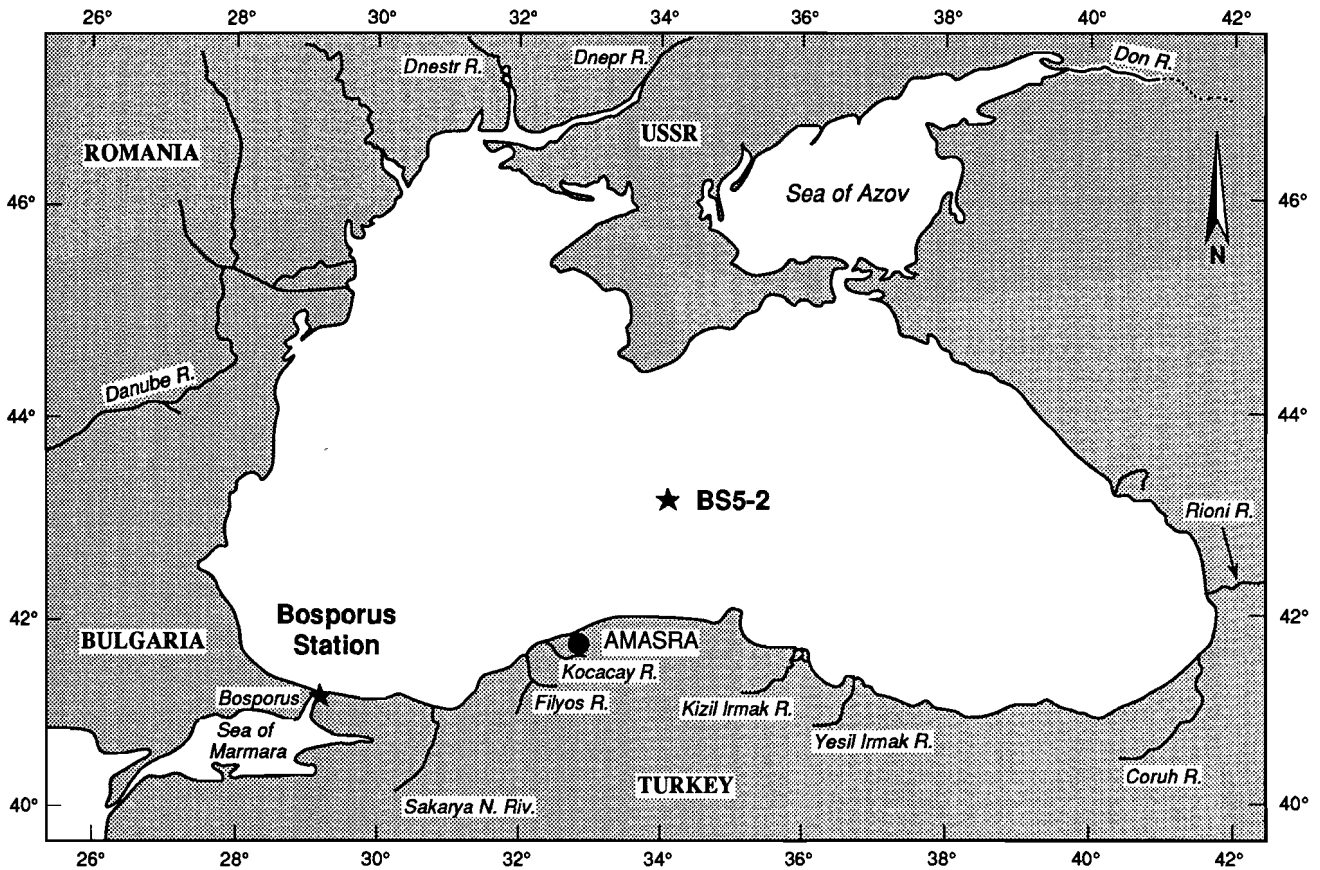
26°
28°
30°
32°
34°
36°
38°
40°
42°
46°
44°
42°
40°
Dnestr R.
Dnepr R.
Don R.
ROMANIA
USSR
Sea of Azov
N
Danube R.
★ BS5-2
Rioni R.
Bosporus Station
BULGARIA
AMASRA
Kocacay R.
Bosporus
Filyos R.
Kizil Irmak R.
Sea of Marmara
Yesil Irmak R.
Coruh R.
TURKEY
Sakarya N. Riv.

a vertical distribution of dissolved Mn (Lewis and Landing, 1991). However, samples for Mn analysis were collected during Leg 3, whereas samples for REE analysis were collected during Leg 5, one month later, albeit at almost exactly the same location (BS3-6, 43°04'N 34°00'E and BS5-2, 43°06'N 34°00'E respectively). Oxygen data from the new pump-profiling system suggest that the suboxic layer may have undergone significant changes during this time and that it was also highly variable during Leg 5 itself (Sect. 6.2.1.). A direct comparison of data from different Legs, even of data corresponding to the same location, would be invalidated by such changes. In order to determine whether the vertical distribution of dissolved Mn had changed during the period between Leg 3 and Leg 5, some samples that had already been analyzed for REE were analyzed for Mn (Sect. 6.2.3.).

In this Chapter a simple evolutionary model is proposed for the suboxic layer in the Black Sea. An attempt is made to determine how the formation of the suboxic layer has affected the cycling of Mn, Fe and the REE at the former oxic-anoxic interface. New data, including vertical distributions of particulate REE at station BS5-2, contribute to a more complete understanding of REE cycling within the suboxic layer. Spencer and Brewer (1971) attempted to explain the vertical distribution of dissolved Mn in terms of a vertical advection-diffusion model. Their approach is used to calculate vertical REE fluxes within the watercolumn. REE fluxes through the Bosporus, which may form an important component in an REE mass balance for the Black Sea, are estimated from a hydrographical model and vertical distributions of dissolved REE at a station near the exit of the Bosporus.

6.2. The Black Sea

6.2.1. Hydrography

The Black Sea is the largest permanently anoxic basin in the world (420.000 km^2). Fresh water is supplied to the Black Sea by a large number of rivers. Total river input into the Black Sea amounts to about 350 km^3/yr, more than half of it (200 km^3/yr) coming from the Danube (Sorokin, 1983). The only source of seawater to the Black Sea is the Mediterranean Sea. The Dardanelles connect the Mediterranean Sea to the Sea of Marmara, which is in turn connected to the Black Sea by

---

Opposite page: **Figure 6.1.** Map of the Black Sea. Station BS5-2 (43°06'N 34°00'E) and the Bosporus station (41°17'N 29°10'E), occupied during Leg 5 of the 1988 Black Sea Expedition, are indicated with a solid star.

the Bosporus (Fig. 6.1). The sill depths on the Sea of Marmara end and on the Black Sea end of the Bosporus are approximately 35 m and 50 m respectively.

A southerly flow of surface water from the Black Sea through the Bosporus is caused by the difference in sea level between the Black Sea and the Sea of Marmara (Gunnerson and Özturgut, 1974). This difference is largest during summer as a result of enhanced freshwater discharge to the Black Sea. The flow of surface water is occasionally reversed for one or more days during periods of southerly winds. A strong northerly undercurrent was already known to exist in ancient times by fishermen, who had their boats towed against the top current towards the Black Sea by lowering baskets into the deep water of the Bosporus. A large number of publications addressed the question whether or not water from the Mediterranean Sea transported by this undercurrent actually reaches the Black Sea.

Ullyott and Ilgaz (1946) assumed that the sill near the exit of the Bosporus prevents the undercurrent from penetrating the Black Sea and that all Mediterranean water is returned to the Sea of Marmara after mixing with water flowing out of the Black Sea through the Bosporus. According to Pektas (1956) the situation described by Ullyott and Ilgaz (1946) occurs only during summer when the difference in sea level between the Black Sea and the Sea of Marmara is largest. In his view, Mediterranean water does flow into the Black Sea during winter, dispersing at a level of 150-200 m and preventing mixing between surface and deep water by maintaining the salinity gradient. Bogdanova (1961) demonstrated that Mediterranean water flows into the Black Sea throughout the year (except during periods of southerly winds). In the Bosporus, Mediterranean water mixes with Black Sea water from the warm surface layer or from the cold intermediate layer (see below). Upon reaching the Black Sea it can sink to any depth depending on the resulting density.

Profiles of salinity, potential temperature and σ_θ at the Bosporus station (Fig. 6.1) are shown in Figure 6.2. Three watermasses can be identified from the profile of σ_θ, separated by strong density gradients. The high salinity (35-36 ppt = parts per thousand) and temperature (14.0-14.3 °C) of the lowermost layer confirm its Mediterranean origin. The salinity of the upper two layers is almost equal and the density gradient between them is caused by an abrupt decrease in potential temperature from 24.9 to 7.6 °C. The profiles of salinity, potential temperature and σ_θ between the surface and 50 dbar are nearly identical to those at station BS5-2 (Fig. 6.3). A comparison of the profiles in Figures 6.2 and 6.3 shows that the middle layer at the Bosporus station is the so called cold intermediate layer (CIL). This

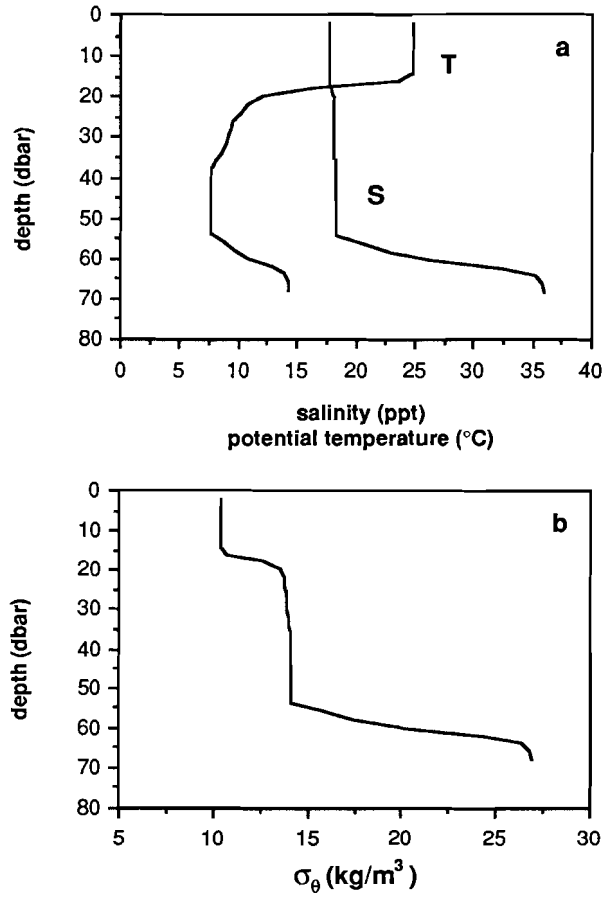

Figure 6.2. Profiles of salinity and potential temperature at the Bosporus station (a). Salinity in ppt = parts per thousand. Profile of σ_θ at the Bosporus station (b). Profiles were recorded on 27 July 1988 (White *et al.*, 1989).

watermass, bounded by the 8 °C isotherms, is found throughout the Black Sea (Tolmazin, 1985; Murray and Izdar, 1989; Murray *et al.*, 1989) and can clearly be identified between 35 and 75 dbar at station BS5-2. The occurrence of water from the CIL at the Bosporus station seems to contradict the conclusions of Bogdanova (1961), who stated that 'during the pile up in the summer months only the surface waters flow out through the Bosporus'. Although the station is located near the exit of the Bosporus and not in the Bosporus itself, it is unlikely that the sill

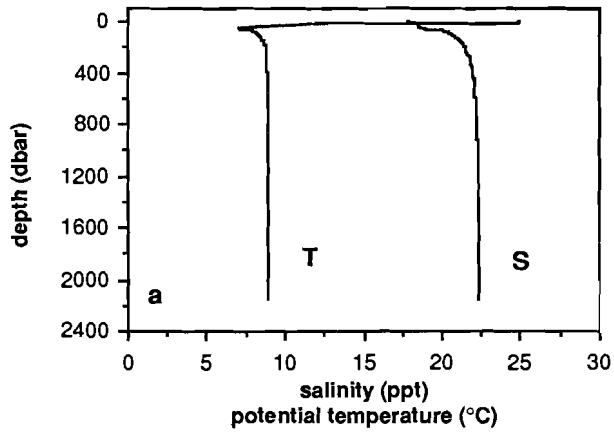
depth (dbar)
0
400
800
1200
1600
2000
2400
T
S
a
0
5
10
15
20
25
30
salinity (ppt)
potential temperature (°C)

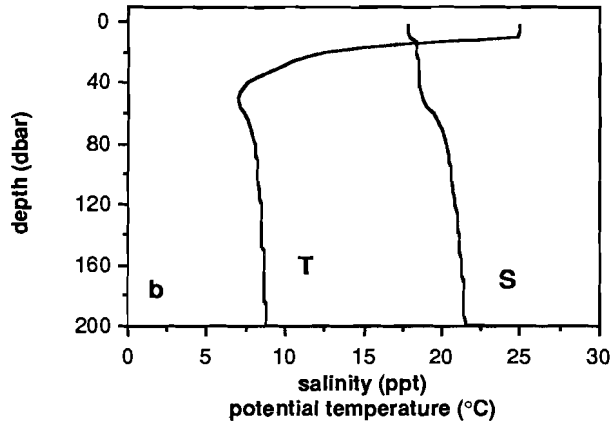
depth (dbar)
0
40
80
120
160
200
T
S
b
0
5
10
15
20
25
30
salinity (ppt)
potential temperature (°C)

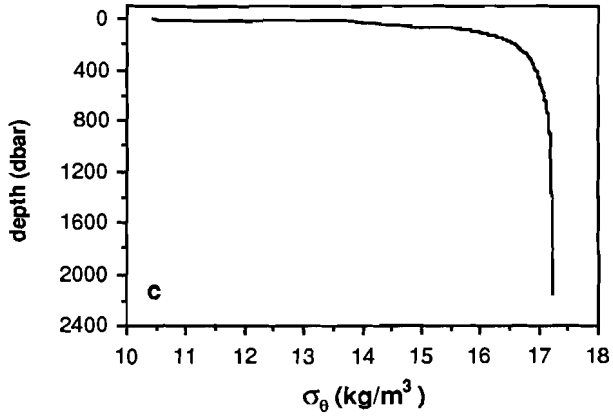
depth (dbar)
0
400
800
1200
1600
2000
2400
c
10
11
12
13
14
15
16
17
18
σ_θ (kg/m^3)

could prevent colder water from flowing into the Bosporus, since the density gradient separating the upper two layers is situated well above the depth of the sill (Fig. 6.2b).

The balance between fresh water input, evaporation and the restricted outflow of surface water through the Bosporus on the one hand and the input of high salinity Mediterranean water into the deep Black Sea on the other hand maintains a substantial halocline (Fig. 6.3a) separating the relatively fresh surface water (~18 ppt) from the more saline deep water (22.3 ppt). In accordance with the model presented in Chapter 2, restricted mixing across the ensuing density gradient (Fig. 6.3c) has caused permanently anoxic conditions to develop in the deep water some 3000 years ago (Sorokin, 1983).

By comparison of hydrographic data collected at approximately the same location during the 1988 Black Sea Expedition and the 1975 R/V *Chain* Cruise, Murray *et al.* (1989) and Murray and Izdar (1989) found that since 1975 temperature had increased by 0.1 °C in the depth interval 100-200 m and salinity by 0.1 ppt in the depth interval 50-200 m, causing a 20 m upward shift of the isopycnal surfaces. They proposed that the observed changes are directly related to artificial reduction of the river input into the Black Sea (Tolmazin, 1985), which may have led to a greater inflow of Mediterranean water through the Bosporus and hence to shoaling of the halocline. Further reduction of the river input would eventually result in "a Mediterranean-style circulation for the Black Sea" (Murray *et al.*, 1989). This explanation is somewhat questionable. Tolmazin (1985) reported that Soviet water management projects, leading to reduction of the river input, were initiated in the early 1950s and that the annual input of the major rivers Don, Kuban, Dniepr and Dniestr had already been reduced by 20-40% in 1975. Therefore, hydrographic changes might have been observed in 1975, yet Murray *et al.* (1989) found no differences between hydrographic data collected at approximately the same location during the 1969 R/V *Atlantis II* Cruise and the 1975 R/V *Chain* Cruise. On the other hand, Kempe *et al.* (1990) showed that hydrographic changes, such as occurred between 1975 and 1988, did occur during the 1969 R/V *Atlantis II* Cruise as well as during the 1984 R/V *Piri Reis* Cruise on timescales of weeks to months. Moreover, they showed that at station BS1-HC10 (41°26'N 41°20'E) of the 1988 Black Sea Expedition the isopycnal surfaces had shifted *down* since 1975. They argued that the isopycnal surfaces may at any time be both extremely warped and

---

Opposite page: **Figure 6.3.** Salinity profile at station BS5-2 (a). Salinity in ppt = parts per thousand. Profile of potential temperature at station BS5-2 (b). Profile of σ_θ at station BS5-2 (c). Profiles were recorded on 22 July 1988 (White *et al.*, 1989).

highly variable, due to internal waves and interannual changes in the intensity of Black Sea surface currents. Nevertheless, Murray *et al.* (1989) and Murray and Izdar (1989) proposed that the hydrographic changes between 1975 and 1988 may indirectly have led to formation of the suboxic layer. If these hydrographic changes are no more than recurrent fluctuations, it is not clear why a strongly developed suboxic layer has never been observed before. Instead, the suboxic layer seems to be a persistent feature and therefore related to hydrographic changes of a more permanent nature.

The surface current pattern of the Black Sea is dominated by a large cyclonic gyre in the western basin and two large cyclonic gyres and a smaller anticyclonic gyre in the eastern basin (Sorokin, 1983). Within each of the cyclonic gyres the isopycnal surfaces are generally dome-shaped *i.e.* they are elevated near the centre of the gyre and sloping down towards the edges. Since hydrographic and chemical isosurfaces (for instance the upper boundary of the anoxic layer) broadly coincide with isopycnal surfaces, it is essential that data from different stations, or even from different casts at the same station, are compared as a function of σ_θ rather than depth.

Figure 6.4a shows profiles of oxygen and sulfide, recorded with the new pump-profiling system (Murray *et al.*, 1989; Friederich *et al.*, 1990) at station BS3-6 and BS5-2 between 10 June and 25 July 1988. The profiles are shown between the isopycnals σ_T = 14.00 and σ_T = 17.00, encompassing the entire suboxic layer. The profiles are plotted *versus* σ_T rather than σ_θ, since values of σ_θ are not available for the pumpcasts. The difference between σ_T and σ_θ is however minor, amounting to about 0.002 units near the lower boundary of the suboxic layer (White *et al.*, 1989).

Figure 6.4a demonstrates that the sulfide profile was very stable during the period 10 June - 25 July 1988. In this Chapter the 2 μM

Opposite page: **Figure 6.4.** Profiles of oxygen (o) and sulfide (•) *versus* σ_T (a). Profiles of sulfide were recorded with the pump-profiling system on 10 and 13 June (station BS3-6) and on 16, 18, 21 and 25 July 1988 (station BS5-2). Oxygen concentrations were determined on discrete samples collected with the pump-profiling system on 13 June and on 18, 21 and 25 July 1988. Profiles of oxygen and sulfide *versus* σ_T recorded on 13 June (station BS3-6), 29 June (station BS4-14) and on 18 July 1988 (station BS5-2) (b). Profiles of nitrate *versus* σ_T recorded with the pump-profiling system on 10 and 13 June (station BS3-6), 29 June (Station BS4-14) and on 16, 18, 21 and 25 July 1988 (station BS5-2) (c). All data from Friederich *et al.* (1990).

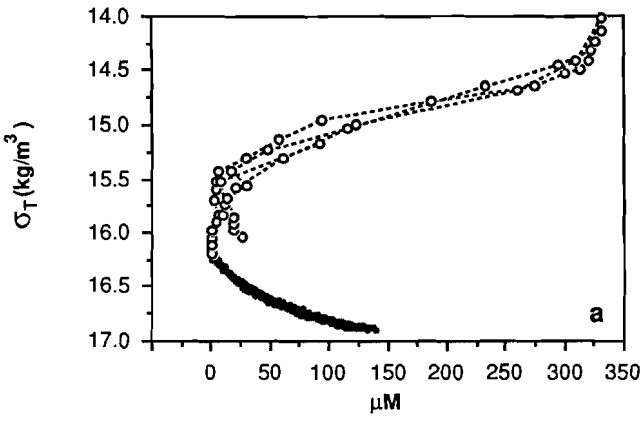
14.0
14.5
15.0
15.5
16.0
16.5
17.0
σT(kg/m3)
0
50
100
150
200
250
300
350
µM
a

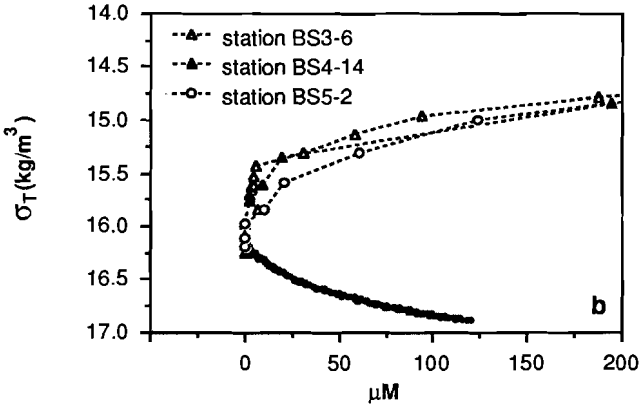
station BS3-6
station BS4-14
station BS5-2
14.0
14.5
15.0
15.5
16.0
16.5
17.0
σT(kg/m3)
0
50
100
150
200
µM
b

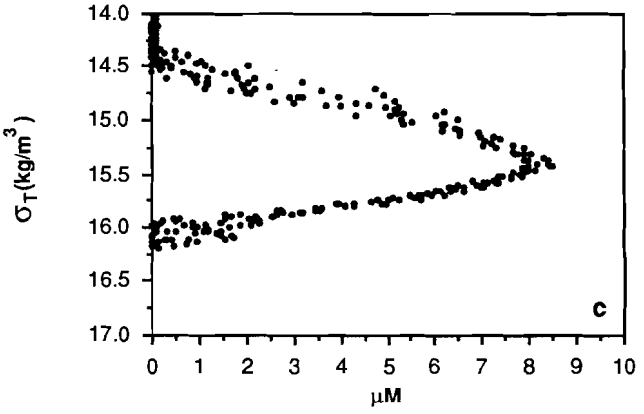
14.0
14.5
15.0
15.5
16.0
16.5
17.0
σT(kg/m3)
0
1
2
3
4
5
6
7
8
9
10
µM
c

sulfide level, coinciding on average with the isopycnal σ_T = 16.22, is taken as the upper boundary of the anoxic layer. According to Murray *et al.* (1989), the upper boundary of the anoxic layer at station BS3-2 (32°00'E 42°50'N) coincides with the isopycnal σ_θ = 16.32, whereas it coincided with the isopycnal σ_θ = 16.39 in 1969. The 30 m upward shift of the boundary since 1969 is partly accounted for by the upward shift of 20 m of the isopycnals and partly by an upward shift of the boundary relative to σ_θ (0.07 units, corresponding to about 10 m at the depth of the boundary). Pumpcasts performed at station BS3-2 (Friederich *et al.*, 1990) indicate that the isopycnal σ_T = 16.32 coincides on average with the 10 μM sulfide level.

On the other hand, the oxygen profiles in Figure 6.4a show considerable variation during the period 10 June - 25 July 1988. The variation is so large that a broad suboxic layer could not always be clearly resolved during Leg 5. Figure 6.4b shows profiles of sulfide and oxygen *versus* σ_T, recorded at the same location during three consecutive Legs on 13 June (station BS3-6), 29 June (station BS4-14, 43°05'N 34°01'E) and 18 July (station BS5-2). It seems that, whereas the sulfide profile is very stable, the oxygen concentrations in the suboxic layer are gradually increasing, in other words that the suboxic layer is eroding and therefore merely a transient feature. However, profiles of nitrate *versus* σ_T (Fig. 6.4c), recorded during each of the aforementioned pumpcasts, show no evidence of erosion of the suboxic layer. Oxygen concentrations were partly determined by the colorimetric method of Broenkow and Cline (1969), which is especially suited for concentrations below 50 μM, and partly by Winkler titration (Carpenter, 1965), which becomes unreliable below 20-30 μM. The fact that Winkler titration was sometimes used for determining oxygen concentrations well below 30 μM, may account for some of the variation. Nevertheless, it cannot be completely ruled out that changes occurred within the suboxic layer in the period between Leg 3 and Leg 5. Whether or not these have affected the vertical distributions of Mn at station BS3-6 reported by Lewis and Landing (1991), thereby invalidating a direct comparison with the vertical distributions of the REE at station BS5-2 as performed by Schijf *et al.* (1991), is discussed in Section 6.2.3.

The apparent variation in the oxygen profile complicates an unambiguous definition of the upper boundary of the suboxic layer in terms of σ_T. In this Chapter the isopycnal σ_T = 15.40, coinciding approximately with the 10 μM oxygen level at station BS3-6, will somewhat arbitrarily be taken as the upper boundary of the suboxic layer. Incidently, this isopycnal coincides with the nitrate maximum at station BS3-2 and all of the stations in Figure 6.4c.

6.2.2. Nutrients

Vertical profiles of nitrate (NO_3^-), nitrite (NO_2^-) and ammonium (NH_4^+) are shown in Figure 6.5a. Nitrate concentrations increase below 40 dbar as a result of the oxidation of organic matter by oxygen. Below 70 dbar, where oxygen becomes depleted, nitrate concentrations decrease as oxidation of organic matter continues with nitrate as the oxidant. Ammonium, which is formed during oxidation of organic matter by sulfate (Froelich *et al.*, 1979), first appears at 105 dbar. The minor nitrate maximum at this depth is caused by oxidation of ammonium diffusing upward into the suboxic layer. The minor nitrate maximum is accompanied by a maximum of nitrite, which is an intermediate in the oxidation of ammonium to nitrate. Below 105 dbar ammonium concentrations rapidly increase to nearly 100 μM in the deep water (Fig. 6.5b). Distinct peaks of nitrite just above and below the major nitrate maximum indicate that nitrite plays a role as an intermediate in both nitrification and denitrification (Murray and Izdar, 1989).

The vertical profile of phosphate (PO_4^{3-}) is characterized by two maxima (Fig. 6.6a). These maxima were apparently also present during the U.S. R/V *Atlantis II* cruise in March and April 1969, yet could not always be clearly resolved because of limited sample resolution (Brewer and Murray, 1973; Fonselius, 1974; Shaffer, 1986; Murray *et al.*, 1989). Phosphate concentrations increase below 40 dbar as a result of oxidation of organic matter by oxygen, which also causes nitrate concentrations to increase below that depth. Below 80 dbar phosphate concentrations decrease to essentially zero at about 95 dbar and then increase again to a (possibly multiple) maximum at about 120 dbar. Below this lower maximum, phosphate concentrations continue to increase with depth to 8-9 μM in the deep water.

The phosphate minimum and lower maximum are probably related to the redox chemistry of Mn and Fe. Shaffer (1986) proposed two processes that may account for the observed anomaly dipole, which he called the phosphate shuttle and the phosphate pump. The possible effect of these two processes on the vertical distributions of dissolved Mn and Fe is briefly discussed in Section 6.5.1.

Apart from the minimum and lower maximum, the vertical profile of phosphate resembles vertical profiles of phosphate in the open ocean, with low concentrations near the surface, where phosphate is removed as a result of biological activity, increasing with depth to high concentrations in the deep water, as phosphate is released during decomposition of organic matter (Fig. 6.6b). Similarly, formation of opaline shell material near the surface and dissolution of the opaline shell material at depth gives rise to the vertical profile of silicate (Fig. 6.6c).

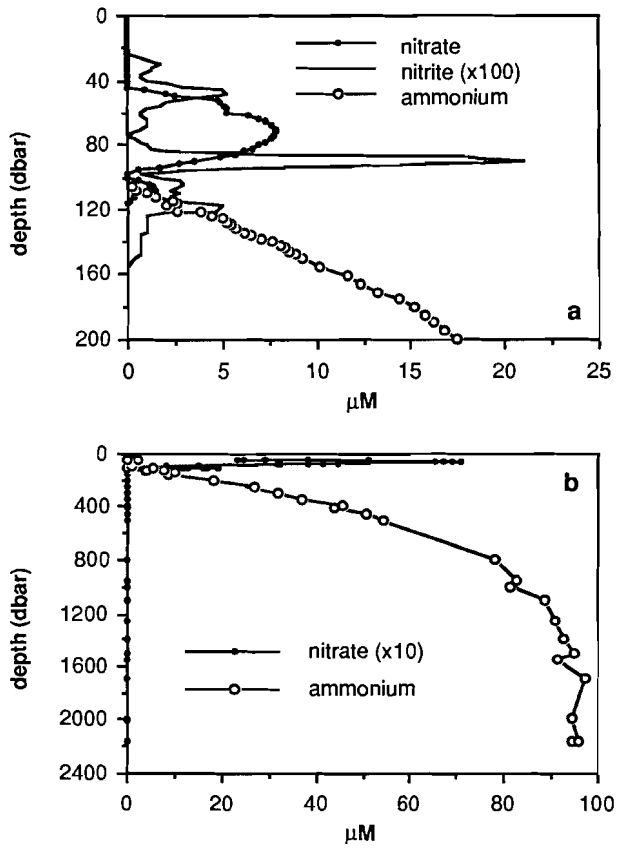

Figure 6.5. Profiles of nitrate, nitrite and ammonium recorded with the pump-profiling system at station BS5-2 on 18 July 1988 (a). Nitrite data were smoothed, using a 3-point moving average. Ammonium data were multiplied by 0.92 as suggested by Friederich *et al.* (1990). Profiles of nitrate and ammonium at station BS5-2 (b). Compilation of ten CTD hydrocasts (Friederich *et al.*,1990).

Opposite page: **Figure 6.6.** Phosphate profile recorded with the pump-profiling system at station BS5-2 on 18 July 1988 (a). Phosphate profile at station BS5-2 (b). Compilation of ten CTD hydrocasts (Friederich *et al.*, 1990). Silicate profile at station BS5-2 (c). Compilation of ten CTD hydrocasts (Friederich *et al.*, 1990).

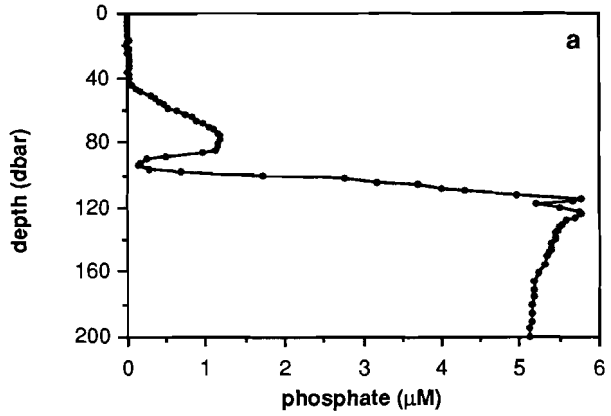
a
depth (dbar)
0
40
80
120
160
200
0
1
2
3
4
5
6
phosphate (μM)

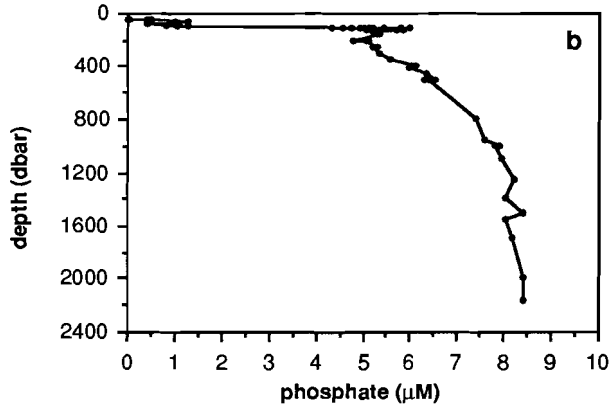
b
depth (dbar)
0
400
800
1200
1600
2000
2400
0
1
2
3
4
5
6
7
8
9
10
phosphate (μM)

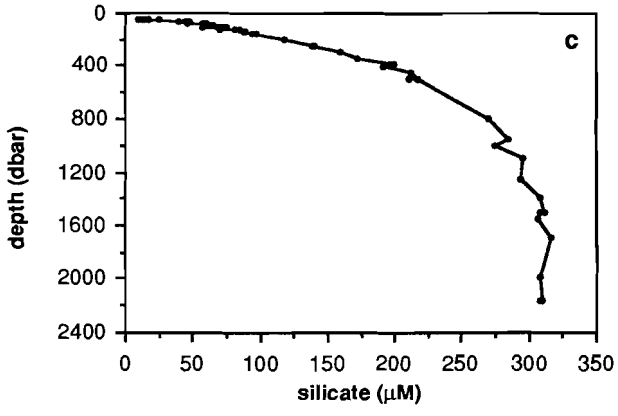
c
depth (dbar)
0
400
800
1200
1600
2000
2400
0
50
100
150
200
250
300
350
silicate (μM)

6.2.3. Mn and Fe

Whereas very little was previously known about the vertical distributions of the REE in the watercolumn of the Black Sea, vertical distributions of some other trace metals, including Mn, Fe, Co, Ni, Cu, Zn, Cd and Pb, were reported in a number of publications (Spencer and Brewer, 1971; Spencer *et al.*, 1972; Brewer and Spencer, 1974; Haraldsson and Westerlund, 1988). The discussion in this Section will be limited to Mn and Fe, since their cycling at oxic-anoxic interfaces is most closely related to that of the REE (Chapter 2).

Spencer and Brewer (1971) fitted a vertical advection-diffusion model curve for a non-radioactive conservative component (Craig, 1974) to vertical profiles of salinity and potential temperature within the linear region of the Θ-S diagram (at that time approximately between 80 and 350 m), in order to obtain an estimate of K/ω, the ratio of the vertical eddy diffusion coefficient (K) and the vertical advection velocity (ω). They found an average K/ω of 0.09 km and from a best estimate of water inflow through the Bosporus (190 km^3/yr) and the assumption that this inflow advects uniformly upward through the halocline, they calculated ω and K to be 0.5 m/yr and 0.014 cm^2/sec respectively. Using these values they subsequently fitted vertical distributions of dissolved Mn to a vertical advection-diffusion model curve for a non-radioactive non-conservative component. For a non-conservative component, the *in situ* production rate or scavenging rate J is some function of depth, whereas J=0 for a conservative component. Dissolved Mn is produced *in situ* from particulate Mn, which settles after precipitating above the oxic-anoxic interface and is reductively dissolved upon entering the anoxic water (Chapter 2). The shape of the vertical distribution of particulate Mn below the particulate Mn maximum led Spencer and Brewer (1971) to assume an exponentially decreasing *in situ* production rate of dissolved Mn

$$J = J_0 e^{-\mu z} \qquad (6.1)$$

where J_0 is the *in situ* production rate of dissolved Mn at z=0 and μ is a parameter which describes the decrease of the *in situ* production rate of dissolved Mn with depth. The vertical distribution of dissolved Mn was fitted within the so called mixing interval, which was taken to be the region between 275 m below and 20 m above the depth where oxygen concentrations decrease to zero, with z=0 at the bottom of the mixing interval and positive upward. From the fit, J_0 and μ were found to be $4.5 \cdot 10^{-4}$ $\mu g\ kg^{-1}\ yr^{-1}$ and $-38\ km^{-1}$ respectively.

With [Mn] representing dissolved Mn concentrations, the upward flux F of dissolved Mn

$$F = K (d[Mn]/dz) + \omega [Mn] \quad (6.2)$$

was calculated to be 675 mg m^{-2} yr^{-1}. In order to sustain the observed vertical distribution of dissolved Mn, the upward flux must completely precipitate and return to the deep water as a downward flux of particulate Mn. The actual downward flux, corresponding to the total *in situ* production of dissolved Mn, was calculated from an integration of (6.1) between the seafloor and the top of the mixing interval to be 875 mg m^{-2} yr^{-1}, indicating a net downward flux of particulate Mn of 200 mg m^{-2} yr^{-1}. Based on an estimate of the total river input of particulate Mn into the Black Sea of 866 mg m^{-2} yr^{-1}, Brewer and Spencer (1974) suggested that the net downward flux of Mn could be balanced, if 22% of the river input stays in suspension and spreads across the basin while 78% is deposited close to the river mouths.

A net downward flux of Mn would imply that the observed vertical distribution of dissolved Mn is only quasi-stationary and that dissolved Mn concentrations in the deep water are increasing. Spencer and Brewer (1971) calculated that it would take the net downward flux approximately 2900 years to accumulate the present standing crop of Mn, agreeing closely with the estimate that present salinity conditions in the Black Sea were established some 3000 years ago (Sorokin, 1983). However, Haraldsson and Westerlund (1988) found that dissolved Mn concentrations in the deep water are probably limited by precipitation of Mn carbonate, something that the model does not take into account.

Also, the calculation of the downward flux of particulate Mn is extremely sensitive to changes in the value of μ. Spencer and Brewer (1971) indicated an uncertainty of 3% in the estimate of μ, leading to a 30% uncertainty in the estimate of the downward flux, which in turn may cause the net downward flux, being the difference of two large numbers, to increase by more than a factor of 2 or even to change into a net upward flux. Precipitation of Mn carbonate below the oxic-anoxic interface could affect the quality of the fit and the value of μ even more seriously. If μ would increase by a factor of 2, the net downward flux would increase by nearly five orders of magnitude. The agreement between the time needed to accumulate the present standing crop of Mn and the time at which the present salinity conditions were established should therefore at least be considered fortuitous, as was already suggested by Spencer and Brewer (1971) themselves.

From equation (6.2) Brewer and Spencer (1974) calculated the upward flux of dissolved Fe to be 43.3 mg m^{-2} yr^{-1}. Unfortunately, the vertical advection-diffusion model could not be used to fit the vertical distribution of dissolved Fe, as it does not take into account the precipitation of Fe sulfide below the oxic-anoxic interface, so that the

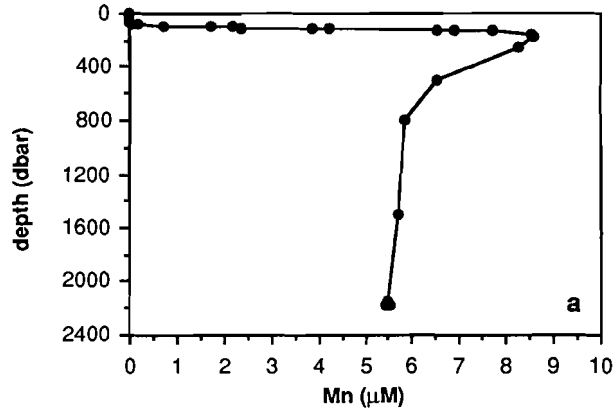
depth (dbar)
0
400
800
1200
1600
2000
2400
0 1 2 3 4 5 6 7 8 9 10
Mn (μM)
a

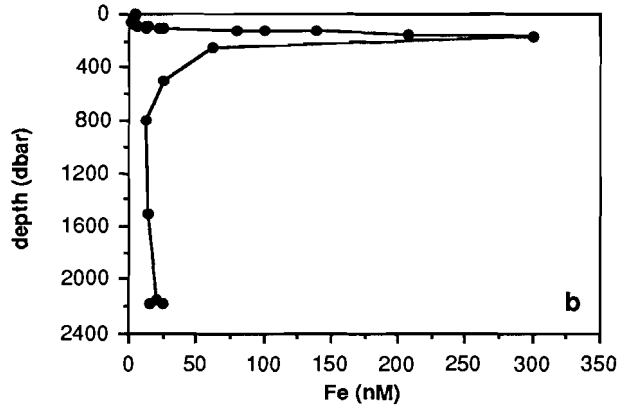
depth (dbar)
0
400
800
1200
1600
2000
2400
0 50 100 150 200 250 300 350
Fe (nM)
b

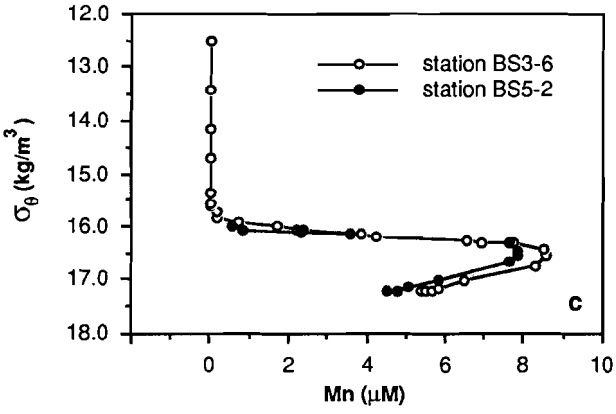
σθ (kg/m3)
12.0
13.0
14.0
15.0
16.0
17.0
18.0
station BS3-6
station BS5-2
0 2 4 6 8 10
Mn (μM)
c

downward flux of particulate Fe could not be determined. Instead, Brewer and Spencer (1974) used the upward flux of dissolved Fe to determine the standing crop of particulate Fe just above the oxic-anoxic interface. A comparison of the upward flux of dissolved Mn with the standing crop of particulate Mn just above the oxic-anoxic interface led to a particulate Mn sinking rate of 11 m/yr. Assuming the same sinking rate for particulate Fe they found a standing crop of particulate Fe of 4 mg/m^3. The observed particulate Fe concentrations just above the oxic-anoxic interface ranged from 4 to 70 mg/m^3 and no maximum could be resolved unambiguously. Brewer and Spencer (1974) suggested that particulate Fe resulting from *in situ* precipitation is masked by particulate Fe associated with detrital silicate, in accordance with the conclusions of Spencer *et al.* (1972).

During Leg 3 of the 1988 Black Sea Expedition samples for analysis of Mn and Fe were collected at station BS3-6 (Lewis and Landing, 1991; Landing and Lewis, 1991). The vertical distribution of dissolved Mn (Fig. 6.7a) is similar to those reported by Spencer and Brewer (1971) and by Haraldsson and Westerlund (1988). It is characterized by a concentration gradient extending over more than three orders of magnitude, which has its onset somewhere between 50 and 70 dbar. The gradient leads to a broad maximum near 200 dbar reaching concentrations of 8.6 μM. Below 200 dbar concentrations decrease again to about 5.5 μM near the bottom.

The possibility that changes had occurred within the suboxic layer in the period between Leg 3 and Leg 5 was discussed in Section 6.2.1. Such changes could affect the vertical distribution of dissolved Mn, thereby invalidating a comparison of the vertical distributions of dissolved Mn at station BS3-6 and dissolved REE at station BS5-2, such as made by Schijf *et al.* (1991). Therefore, some of the samples that had already been analyzed for REE were also analyzed for Mn (Sect. 6.3.). The results are summarized in Table 6.1. Vertical distributions of dissolved Mn *versus* σ_θ at station BS3-6 (Lewis and Landing, 1991) and at station BS5-2 (Table 6.1) are shown in Figure 6.7c. Obviously the two are equal, except for a minor offset in concentration, and the aforementioned comparison (Schijf *et al.*, 1991) is indeed valid. Remarkably, the maximum dissolved Mn concentrations and the dissolved Mn concentrations in the deep water at station BS5-2

Opposite page: **Figure 6.7.** Vertical distributions of dissolved Mn (a) and Fe (b) at station BS3-6 (Lewis and Landing, 1991). Vertical distributions of dissolved Mn *versus* σ_θ at station BS3-6 (Lewis and Landing, 1991) and at station BS5-2 (this work) (c).

BS3-6						BS5-2		
depth (dbar)	σ_θ	Mn diss. (nM)	Mn part. (nM)	Fe diss. (nM)	Fe part. (nM)	depth (dbar)	σ_θ	Mn diss. (nM)
5	12.498	17	0.15	5	9.82	101	16.018	562
15	13.429	12	0.18	4	3.48	106	16.061	849
30	14.161	10	0.12	3	4.15	111	16.103	2324
50	14.715	4	7.00	3	15.57	116	16.140	3584
65	15.378	5	9.36	2	3.18	151	16.307	7628
70	15.558	6	9.61	2	4.63	177	16.490	7887
75	15.622	25	25.85	4	9.99	202	16.568	7887
80	15.738	180	20.56	5	5.01	227	16.653	7628
85	15.862	190	16.00	3	9.72	502	17.026	5820
90	15.932	750	4.48	7	8.24	700	17.130	5047
95	15.994	1750	9.70	12	6.10	1061	17.197	4790
100	16.083	2210	15.59	15	13.49	1365	17.215	4533
105	16.077	2380	11.15	13	12.15	1822	17.223	4533
110	16.138	3880	6.78	26	7.28	2172	17.221	4533
115	16.195	4240	5.06	22	10.28			
120	16.271	6530	1.19	80	7.19			
125	16.306	6920	1.41	100	5.20			
130	16.332	7740	0.59	139	8.20			
150	16.432	8520	0.80	208	7.24			
180	16.546	8590	0.41	300	6.77			
250	16.744	8280	0.61	63	41.50			
500	17.023	6520	0.37	26	24.67			
800	17.157	5830	0.51	13	25.85			
1500	17.219	5700	0.62	14	21.20			
2153	17.221	5480	0.79	21	20.79			
2174	17.221	5420	0.54	16	15.06			
2185	17.221	5520	0.27	25	14.43			

actually agree more closely with those reported by Spencer and Brewer (1971) and by Haraldsson and Westerlund (1988).

The vertical distribution of dissolved Fe (Fig. 6.7b) is rather different from that of Mn. The concentration gradient, extending over nearly two orders of magnitude, leads to a maximum concentration of 300 nM at exactly the same depth as the dissolved Mn maximum, yet the onset of the gradient seems to be situated somewhere between 70 and 90 dbar, somewhat below the onset of the Mn gradient. Below 200 dbar the dissolved Fe concentration rapidly decreases to less than 30 nM, as a result of the precipitation of Fe sulfide. The Fe maximum is consequently much more pronounced than the Mn maximum.

The particulate concentrations of Mn and Fe in Table 6.1 are the sum of three leaches, representing weak acid soluble Mn and Fe, oxidizable and more resistant Mn and Fe solid phases, and refractory particulate matter respectively (Lewis and Landing, 1991). The first two leaches represent >95% of the total amount of Mn. The major part is recovered in the first leach and therefore present as some highly soluble solid phase. For Fe the first two leaches represent 60-70% of the total amount above 200 dbar and >90% below 200 dbar. Below 200 dbar particulate Fe is almost completely recovered in the second leach and therefore probably mainly present as Fe sulfide (Lewis and Landing, 1991), in contrast with the conclusions of Spencer *et al.* (1972), who found that particulate Fe in the Black Sea largely consists of refractory Fe, associated with detrital silicate. Vertical distributions of particulate Fe reported by Spencer *et al.* (1972) were obtained by direct INAA-γ of total particulate matter recovered from 8-10 l of water by pressure-filtration (0.45 μm). They found lowest particulate Fe concentrations in the deep water of about 70 nmol/kg, which is a factor of 2 higher than the maximum concentrations in Table 6.1, indicating that a detailed comparison of the vertical distribution of particulate Fe in Figure 6.8b with those reported by Spencer *et al.* (1972) is not warranted.

The vertical distribution of particulate Mn (Fig. 6.8a) is also very different from those first reported by Spencer *et al.* (1972). Within the attained vertical resolution Spencer *et al.* (1972) could only resolve a single particulate Mn maximum at each station, whereas the maximum in Figure 6.8a is actually a double maximum (Fig. 6.8c). Spencer *et al.* (1972) found large differences between maximum concentrations of particulate Mn at stations far from and near the shelf. In Figure 6.8c the vertical distribution of particulate Mn *versus* σ_θ is compared with

---

Opposite page: **Table 6.1.** Concentrations of dissolved and particulate Mn and Fe at station BS3-6 (Lewis and Landing, 1991) and at station BS5-2 (this work).

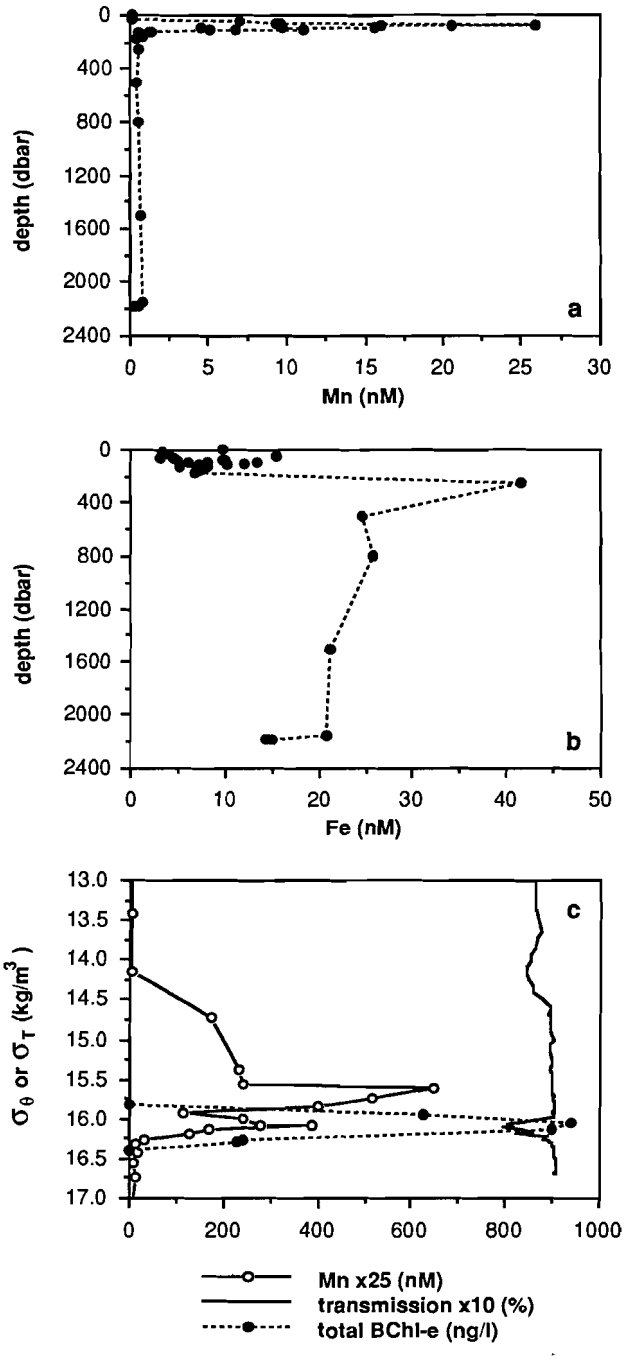
depth (dbar)
0
400
800
1200
1600
2000
2400
a
0
5
10
15
20
25
30
Mn (nM)
depth (dbar)
b
0
10
20
30
40
50
Fe (nM)
σ_θ or σ_T (kg/m^3)
13.0
13.5
14.0
14.5
15.0
15.5
16.0
16.5
17.0
c
0
200
400
600
800
1000
Mn x25 (nM)
transmission x10 (%)
total BChl-e (ng/l)

profiles of total bacteriochlorophyll-e (BChl-e) concentrations (*versus* σ_θ) and light transmission (*versus* σ_T). The profile of light transmission was recorded during a pumpcast on 18 July 1988 at station BS5-2 (Friederich *et al.*, 1990) and the BChl-e analyses were reported for station BS2-2 (42°50'N, 32°00'E) by Repeta *et al.* (1989). It appears that the upper, larger Mn maximum is situated just below what was defined in Section 6.2.1. as the top of the suboxic layer, near the onset of the dissolved Mn gradient and well above the first appearance of sulfide. Below the onset of the particulate Mn gradient (σ_θ = 14.2) particulate Mn concentrations increase gradually with depth down to σ_θ = 15.5, where a distinct change of slope occurs. The upper Mn maximum is not accompanied by any change in light transmission or total BChl-e concentration. The lower, smaller Mn maximum, situated just above the first appearance of sulfide where there is apparently no oxygen to form Mn oxyhydroxides and therefore rather unexpected from a thermodynamic point of view, coincides with a distinct particle maximum and a very pronounced total BChl-e maximum. A second, more modest, broader particle maximum is situated well above the upper Mn maximum. Below the lower Mn maximum particulate Mn concentrations decrease rapidly to low values.

There is ample reason to assume that the lower Mn maximum is the result of bacterial activity. The concomitance of a particle maximum and a BChl-e maximum signifies the presence of a dense sheet of bacteria at the depth of the lower Mn maximum. A similar dense sheet of bacteria was observed in Framvaren Fjord just below the oxic-anoxic interface. The distribution of pigments within the corresponding bacteriochlorophyll maximum indicated that this sheet of bacteria consists of obligate phototrophic bacteria *Chromatium* sp. and *Chlorobium* sp. (Sørensen, 1988). The distribution of pigments within the BChl-e maximum in Figure 6.8c indicates the presence of the obligate phototrophic bacteria *Chlorobium phaeobacteroides* and *Chlorobium phaeovibrioides* (Repeta *et al.*, 1989). Furthermore, the maximum rate of Mn oxidation occurs at the depth of the lower Mn maximum (Tebo, 1991). The absolute rates of Mn oxidation in the Black Sea are 1-4 orders of magnitude higher than observed in any other

---

Opposite page: **Figure 6.8.** Vertical distributions of particulate Mn (a) and of particulate Fe (b) at station BS3-6 (Lewis and Landing, 1991). Vertical distribution of particulate Mn *versus* σ_θ (Lewis and Landing, 1991) and profiles of total bacteriochlorophyll-e (Repeta *et al.*, 1989) *versus* σ_θ and of light transmission *versus* σ_T at stations BS3-6, BS2-2 and BS5-2 respectively (c). Profile of light transmission was recorded with the pump-profiling system on 18 July 1988 (Friederich *et al.*, 1990).

marine environment, also suggesting that Mn oxidation is bacterially mediated. Finally, Mn oxidation was strongly suppressed in the presence of biological inhibitors (Tebo, 1991). Nevertheless, it is difficult to decide, on the basis of these observations, whether the lower Mn maximum is produced *in situ*, or the result of horizontal advection. The matter is discussed in great detail in Tebo (1991).

The vertical distribution of particulate Fe (Fig. 6.8b) is characterized by a concentration gradient below approximately 200 dbar, leading to a maximum particulate Fe concentration of about 40 nM. Due to the limited vertical resolution the exact location of the maximum cannot be accurately determined. Below the maximum the particulate Fe concentration decreases rapidly and is fairly constant at about 20 nM between 500 dbar and the bottom. The sudden increase of particulate Fe concentrations below 200 dbar is the result of Fe sulfide precipitation, as indicated by the distribution of Fe among the three leachates and by the concomitant decrease of dissolved Fe concentrations. Between the surface and 200 dbar the vertical distribution of particulate Fe shows substantial scatter around a concentration of 7-8 nM and no clear structure can be resolved.

6.3. Methods

During the 1988 Black Sea Expedition seawater samples for REE analysis were collected aboard U.S. R/V *Knorr* at station BS5-2 in the centre of the basin and at a station near the exit of the Bosporus (Fig. 6.1). Samples were collected as was described in Chapter 3, using 30 l GoFlo bottles, 0.2 µm polycarbonate membrane filters (Nuclepore, ø142 mm) and storing the filtered seawater samples in clean 5 l low-density PE narrow-mouth bottles. Filters were rinsed with Milli-Q water to remove excess seasalt, folded double three times, packed in PE zip-lip bags and stored in a freezer at -20 °C. During a 'swim call' at station BS5-2 an unfiltered surface seawater sample was collected in a clean 2 l low-density PE narrow-mouth bottle, after swimming away from the R/V as far as possible.

Seawater subsamples of 2 l were spiked and chemically treated as was described in Chapter 3. Concentrations of 10 REE were determined by IDMS (Chapter 3). La was analyzed on a separate double-filament assembly, mostly in the presence of oxygen. Samples from the Bosporus station were not analyzed for La. La analysis failed for nearly 40% of the samples. Although La concentrations are not substantially lower than at Bannock Basin, the Black Sea samples suffered more severely from Ba interference. This may have been caused by the higher dissolved Ba concentrations in the Black Sea: 200-500 nM at station BS3-6 (G.P. Klinkhammer, pers. comm.) *versus* 100-300 nM at Bannock

Basin (De Lange *et al.*, 1990b). Analysis of Gd and Dy was successful for only four and three samples respectively. The method of suppressing isobaric interferences on Gd and Dy by analyzing these elements in the presence of freon was not yet available at that time.

Magnification of the statistical error in the isotopic ratio (1σ), arising from underspiking or overspiking of the samples, was estimated with the computer program REECALC (Chapter 3). Estimated errors were typically <2% for Ce and Nd, <5% for Sm-Dy, <7% for Er-Lu and <10% for La. Duplicate analyses were performed on two samples from station BS5-2, one in the oxic water (40 dbar) and one in the anoxic water (252 dbar). Duplicates are equal within 1-3% of the highest concentration, which is within the errors estimated by REECALC.

Concentrations of dissolved Mn were determined for 14 seawater samples (Table 6.1). The 101 dbar sample was analyzed by GFAAS, using direct injection after sixfold dilution with 3Q 0.1 N nitric acid and standard addition. The 106, 111 and 116 dbar samples were analyzed by GFAAS, using direct injection after twentyfold dilution with 3Q 0.1 N nitric acid without standard addition. The remainder of the samples was analyzed by flame atomic absorption spectrophotometry, using direct injection without dilution. Precision of the Mn analyses was estimated to be better than 5%.

Twelve filters from station BS5-2 were selected for determination of particulate REE concentrations. The filters were thawed on a clean workbench, taken out of the PE zip-lip bags, folded open carefully and transferred to clean 30 ml Teflon PFA vials, handling them with Teflon TFE tweezers only. After adding 20 ml of 3Q 1.75 N hydrochloric acid and 0.2 g of REE1 spike solution, the vials were closed and placed in an ultrasonic bath for two hours. According to De Baar *et al.* (1988) this leach represents >95% of the total REE content of the filters. By adding the spike solution before leaching, any subsequent loss of REE (for instance by incomplete transfer of the leachate) can no longer affect the result of the analysis. The amount of particulate REE on each filter was recovered from 30 l of seawater. De Baar *et al.* (1988) reported particulate REE concentrations for the Cariaco Trench, expressed in moles per litre of seawater, that were 10-20 times lower than the corresponding dissolved REE concentrations. Assuming this to apply to the Black Sea as well, the optimal amount of spike solution for one filter was estimated to equal the optimal amount for a 2 l seawater sample.

The leachates were transferred to clean 30 ml Teflon PFA vials while holding back the filters with the caps and evaporated in the evaporator pots. The dry residues were redissolved in 1 ml of 3Q 0.175 N hydrochloric acid and further treated as was described in Chapter 3 (Sect. 3.5.4.). The resulting REE fractions were analyzed for

depth (dbar)	La	Ce	Nd	Sm	Eu	Gd	Dy	Er	Yb	Lu	Ce/Ce*
0	-	30.77	23.19	5.52	1.51	-	-	-	9.72	1.48	-
30	33.06	16.53	21.82	4.76	1.37	7.37	-	9.01	-	1.28	0.273
40	25.97	18.08	23.17	5.04	1.38	-	-	8.97	-	1.37	0.347
40	-	18.66	23.64	5.03	1.36	-	-	8.96	-	-	-
50	-	12.73	22.70	4.42	1.24	-	-	9.03	7.48	1.30	-
60	-	5.36	16.94	3.56	1.04	-	-	6.17	-	-	-
71	28.41	6.03	16.93	3.69	1.00	-	-	-	7.14	-	0.119
83	19.40	3.54	12.24	2.58	0.76	4.17	6.48	6.69	-	1.11	0.101
95	18.99	(19.60)	(18.21)	(4.11)	(1.16)	(6.68)	-	-	-	-	-
101	-	3.30	7.35	1.55	0.48	-	3.51	5.18	5.78	0.85	-
106	16.77	3.95	7.23	1.44	0.45	-	-	5.29	5.24	0.93	0.142
111	17.27	8.66	10.66	2.31	0.71	-	-	6.15	6.35	1.06	0.278
116	-	19.20	15.68	3.29	0.96	-	-	8.09	8.26	1.20	-
131	-	28.86	17.33	3.48	0.94	5.73	7.43	7.55	-	1.39	-
161	56.43	109.4	44.98	9.16	2.56	-	-	12.71	12.21	1.66	1.002
177	71.03	136.4	54.62	11.14	3.10	-	-	-	14.05	-	1.003
202	89.42	153.8	63.10	12.73	3.51	-	-	-	14.80	-	0.921
227	100.02	180.5	70.85	14.68	4.15	-	-	-	16.08	-	0.965
252	102.51	196.7	77.45	-	4.44	-	-	-	-	2.12	1.008
252	-	198.4	77.47	15.31	-	-	-	17.87	17.15	1.94	-
303	-	(107.2)	(42.73)	(8.73)	(2.50)	-	-	-	(12.71)	-	-
401	89.73	198.2	80.66	16.04	4.50	-	-	16.62	15.53	1.99	1.097
502	93.40	185.3	74.97	15.09	4.00	-	-	15.61	14.89	1.90	1.023
700	-	159.2	67.49	13.70	3.75	-	-	-	14.54	-	-
1061	-	130.1	58.30	12.16	3.23	-	-	-	12.67	-	-
1365	66.40	114.3	51.73	10.24	2.84	-	-	11.87	-	1.48	0.896
1619	61.39	109.6	51.39	10.20	2.77	-	-	11.85	11.19	1.50	0.908
1822	68.95	100.1	48.42	9.86	2.69	-	-	11.11	10.82	1.42	0.779
2172	68.12	101.8	46.96	9.85	2.69	-	-	11.06	11.03	1.36	0.805
shales	295	592	263	49.9	10.6	40.4	33.8	22.4	20.4	3.49	1.000

Ce, Nd, Sm and Yb by IDMS. All particulate REE concentrations were normalized to a sampleweight of 30,000 g, corresponding to the full contents of the 30 l GoFlo bottles. Errors estimated by REECALC were typically <3% for all four elements. Low error magnification suggests that the filters were nearly optimally spiked.

6.4. Results

6.4.1. Dissolved REE

Dissolved REE concentrations and the Ce anomaly (Ce/Ce*) are presented in Table 6.2. Some of the entries in the original datatable (Schijf *et al.*, 1991) have been modified, based on new insights regarding interference corrections. Concentrations in parentheses were not included in the vertical REE distributions (Fig. 6.9 and 6.10). The Ce-Lu fraction of the 95 dbar sample was contaminated during loading of the filament, but the La-Ce fraction was not contaminated. The 303 dbar sample was inadvertently not acidified prior to preconcentration. Comparison with the samples directly above and below demonstrates that about 25% of the HREE and as much as 50% of the LREE was lost by adsorption onto the walls of the sample bottle (Chapter 3). The data points for Ce and Nd at 303 dbar in Figure 6.9 are the average of four determinations of the 300 dbar endmember concentration, which were performed as part of the Black Sea mixing experiments discussed in Chapter 7.

Vertical distributions of dissolved REE at station BS5-2 are shown in Figures 6.9 and 6.10, except for Gd and Dy. Concentrations are elevated at the surface, decreasing with depth to a minimum at about 105 dbar. The vertical distribution of Ce between the surface and 105 dbar is slightly different from that of the strictly trivalent REE. Ce concentrations decrease with depth between the surface and 80 dbar. Between 80 and 105 dbar Ce concentrations remain constant at 3-4 pmol/kg, whereas the trivalent REE continue to decrease at the same rate. Consequently, Ce shows a broad minimum extending between 80 and 105 dbar, whereas the trivalent REE show a sharp minimum near 105 dbar. Between 105 dbar and 300 dbar REE concentrations rapidly increase to a maximum. Below 300 dbar REE concentrations decrease gradually with depth to about half the maximum concentrations at 1400

Opposite page: **Table 6.2.** Dissolved REE concentrations and Ce anomaly (Ce/Ce^*) at station BS5-2. Data in parentheses were not included in any of the Figures (see text). REE abundances in mean shales (μmol/kg) from Piper (1974).

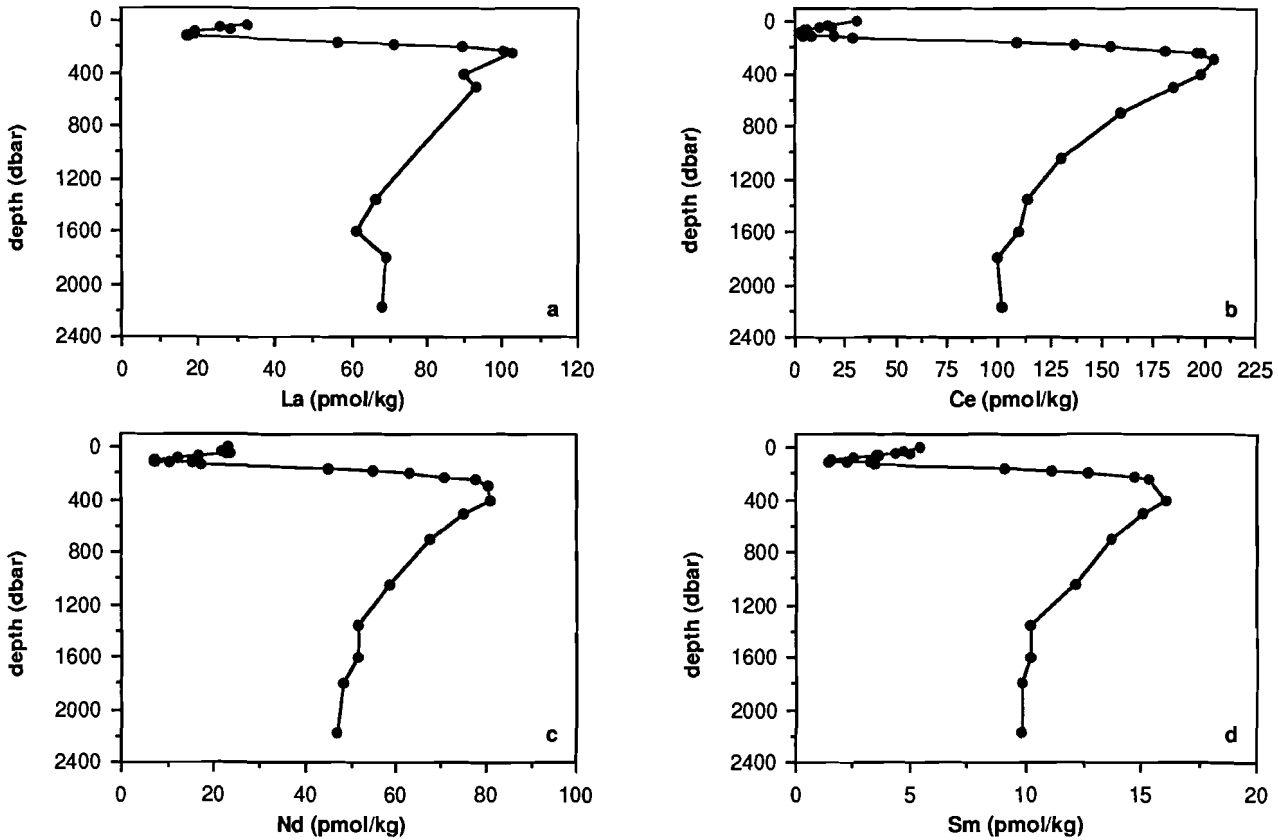
depth (dbar)
0
400
800
1200
1600
2000
2400
a
0
20
40
60
80
100
120
La (pmol/kg)
b
0
25
50
75
100
125
150
175
200
225
Ce (pmol/kg)
c
Nd (pmol/kg)
d
5
10
15
20
Sm (pmol/kg)

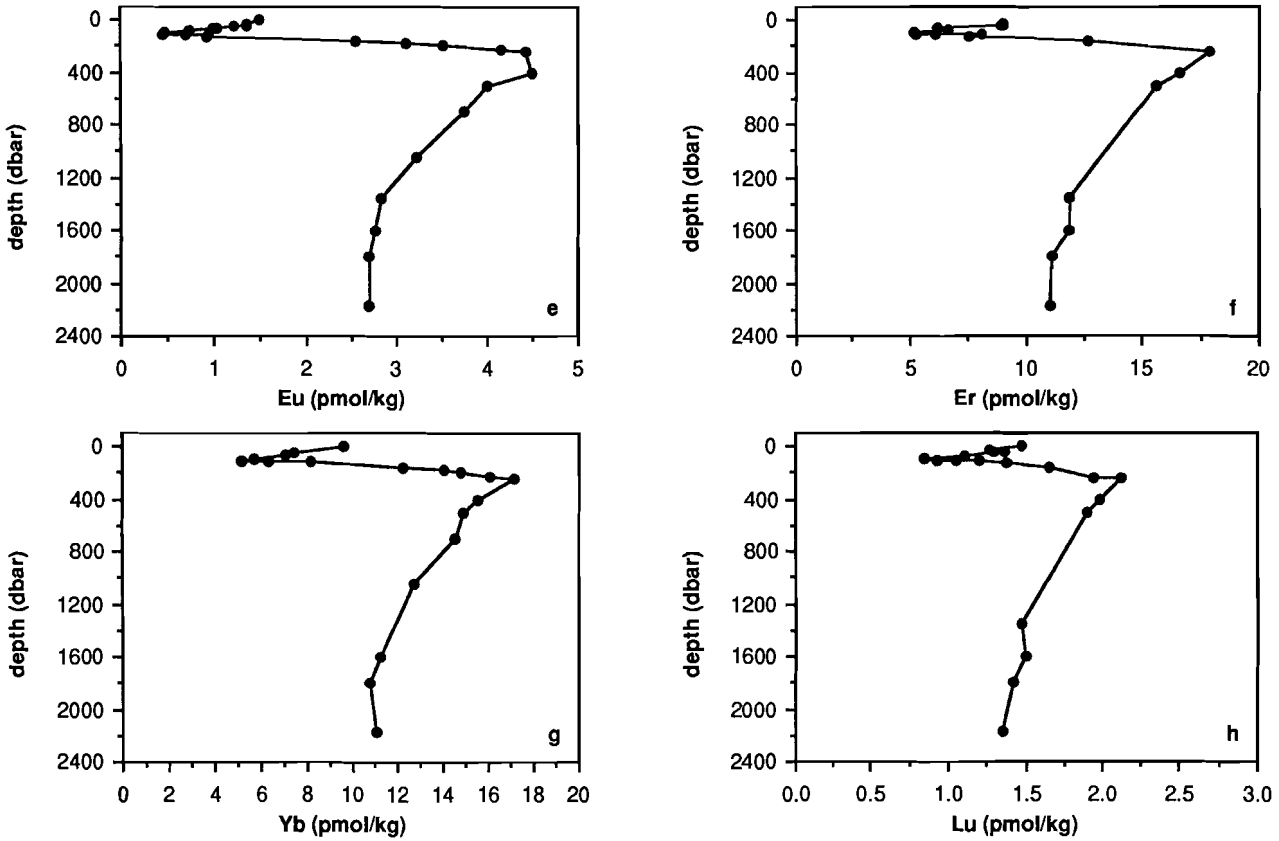

Figure 6.9. Vertical distributions of dissolved REE at station BS5-2. Bottom at approximately 2172 dbar. Insufficient data is available for Gd and Dy to draw reasonable vertical distributions.

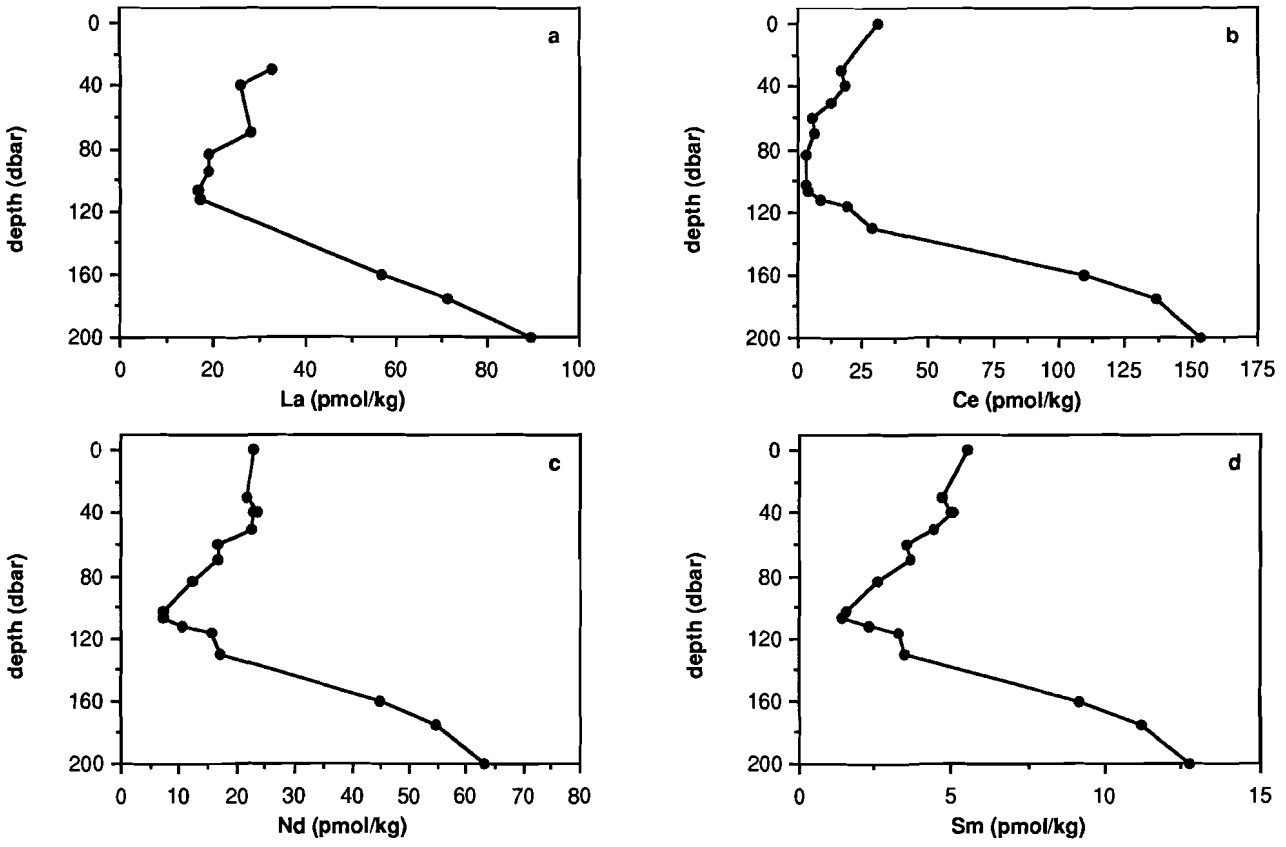
a
depth (dbar)
0
40
80
120
160
200
0
20
40
60
80
100
La (pmol/kg)
b
depth (dbar)
0
40
80
120
160
200
0
25
50
75
100
125
150
175
Ce (pmol/kg)
c
depth (dbar)
0
40
80
120
160
200
0
10
20
30
40
50
60
70
80
Nd (pmol/kg)
d
depth (dbar)
0
40
80
120
160
200
0
5
10
15
Sm (pmol/kg)

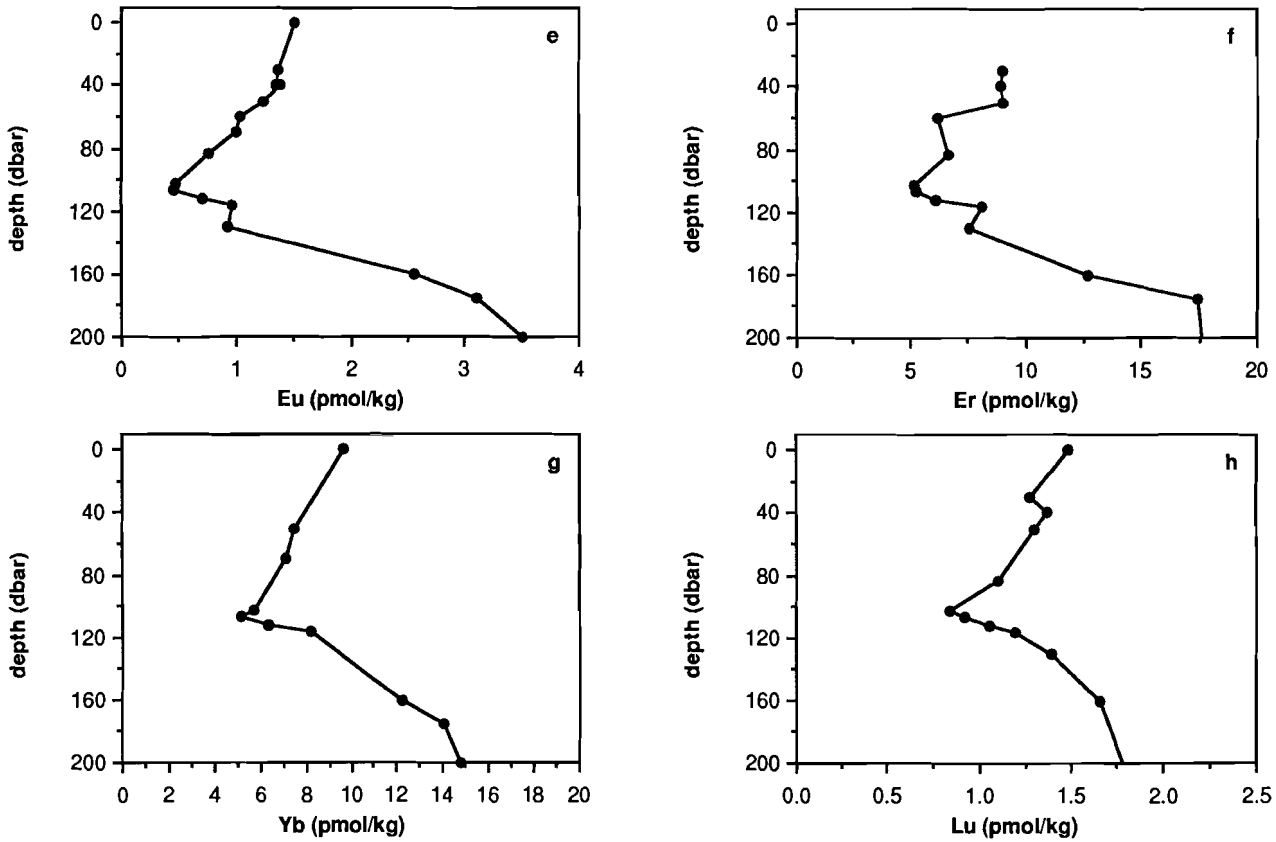

Figure 6.10. Vertical distributions of dissolved REE at station BS5-2. Detail of the top 200 dbar.

dbar. From 1400 dbar down to the bottom at 2172 dbar concentrations do not change markedly.

Ce anomaly data are somewhat scarce, since La analysis failed for a considerable number of samples (Fig. 6.11a). A distinct negative Ce anomaly characteristic of seawater was found between the surface and 80 dbar. Ce depletion increases from about threefold at 30 dbar to about tenfold at 80 dbar as a result of REE scavenging. Below 80 dbar the (negative) Ce anomaly decreases again, in other words Ce becomes less depleted. Between 160 dbar and 500 dbar, the depth range where

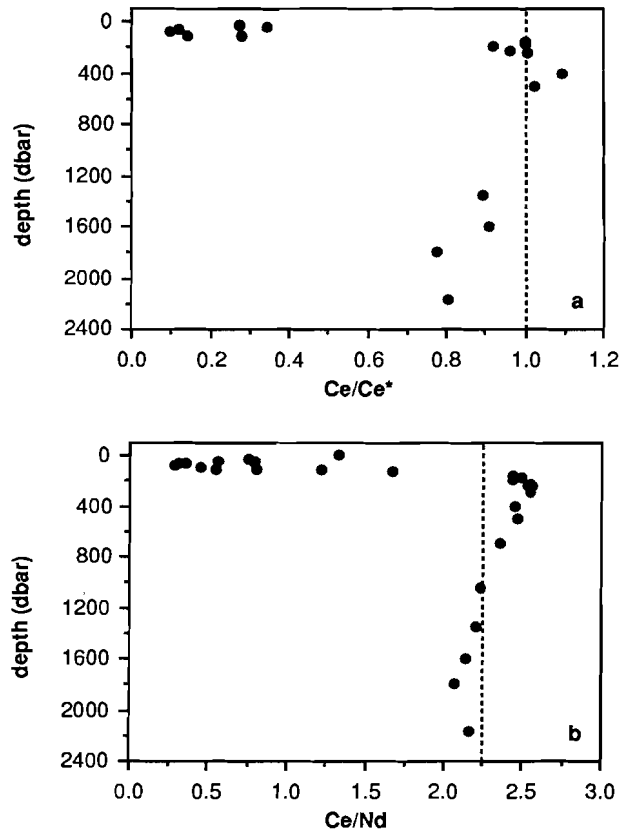

Figure 6.11. Vertical distribution of the dissolved Ce anomaly (Ce/Ce*) at station BS5-2 (a). Dashed line indicates the Ce anomaly in shales, which is 1 by definition. Vertical distribution of the dissolved Ce/Nd ratio at station BS5-2 (b). Dashed line indicates the Ce/Nd ratio in mean shales (~2.25).

the REE reach their maximum concentration, the Ce anomaly disappears, yet, within the uncertainty of the data, no positive Ce anomaly was found at any depth. The limited data below 500 dbar suggest that a negative Ce anomaly developes again with depth. The vertical distribution of the Ce/Nd ratio is shown in Figure 6.11b to emphasize the shape of the vertical distribution of the Ce anomaly in Figure 6.11a. It appears that, whereas no positive Ce anomalies can be distinguished between 160 and 500 dbar, the Ce/Nd ratio is clearly above the value in mean shales between these depths. As was discussed in Chapter 2, this is due to an enrichment of La relative to Nd, which tends to offset the Ce anomaly.

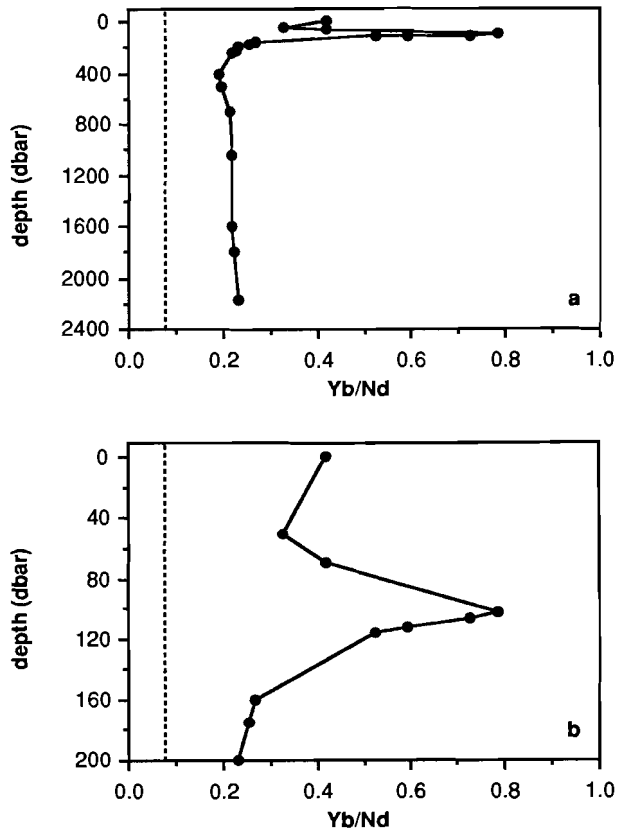

Figure 6.12. Vertical distribution of the dissolved Yb/Nd ratio at station BS5-2 (a) with detail of the top 200 dbar (b). Dashed line indicates the Yb/Nd ratio in mean shales (~0.078).

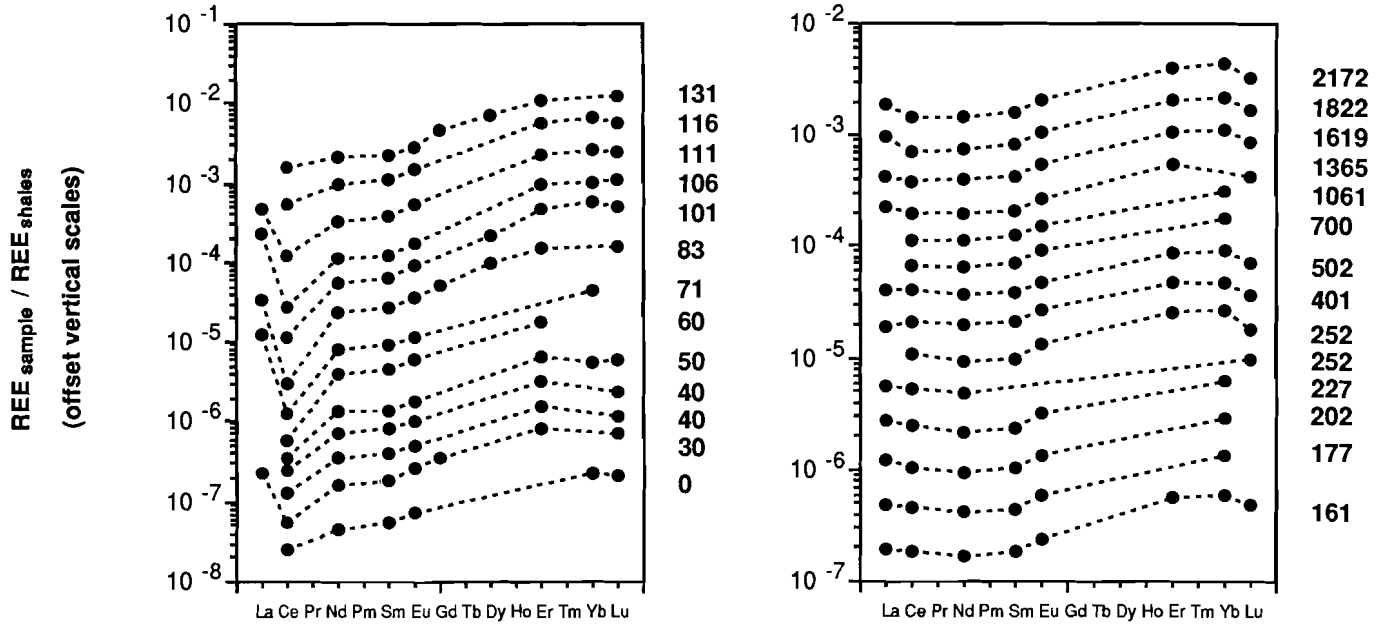

Figure 6.13. REE patterns of dissolved REE at station BS5-2, drawn with offset vertical scales for comparison. Corresponding depths in dbar indicated at the right hand side of each pattern.

The Yb/Nd ratio is above the mean shales value throughout the entire watercolumn (Fig. 6.12). It could only be determined at two depths above 80 dbar. Decreasing REE concentrations and the increasing depletion of Ce below the surface indicate that REE are scavenged between the surface and 80 dbar. The more highly complexed HREE are less effectively scavenged than the LREE and the Yb/Nd ratio should therefore increase with depth as was observed in Bannock Basin (Fig. 5.8). However, the limited data suggest that the Yb/Nd ratio is decreasing below the surface. Although the higher Yb/Nd ratio at the very surface may be an artefact, some other HREE/LREE ratios (*e.g.* Er/Nd, Lu/Nd, Er/Sm) also appear to decrease below the surface. Between 80 and 105 dbar the Yb/Nd ratio increases strongly with depth by about a factor of 4, probably as a result of effective scavenging, as also suggested by the decreasing REE concentrations. Below 105 dbar, where REE concentrations start to increase, the Yb/Nd ratio decreases again to resume the value at 80 dbar. Between 300 dbar, where the REE reach their maximum concentrations, and the bottom the Yb/Nd ratio is constant at a value of approximately 0.24, three times the value in mean shales.

All features discussed above are combined in the REE patterns, shown in Figure 6.13. Although the horizontal elongation of the patterns tends to obscure changes in the Yb/Nd ratio (Fig. 6.12), the successive development and disappearance of the negative Ce anomaly with increasing depth is most conspicuous. At some depths La is evidently enriched relative to Nd.

6.4.2. Particulate REE

Vertical distributions of particulate Ce, Nd, Sm and Yb (Fig. 6.14; Table 6.3) show that particulate REE concentrations are fairly constant throughout the upper 1000 m of the watercolumn, except for a pronounced, sharp maximum at about 115 dbar, 10 m below the onset of the dissolved REE gradients. Concentrations of particulate REE in the deep anoxic water are comparable to concentrations reported by De Baar *et al.* (1988) for particulate REE in deep anoxic waters of the Cariaco Trench, but a factor of 6-7 lower than particulate REE concentrations in the anoxic waters of Saanich Inlet reported by German and Elderfield (1989). Maximum particulate REE concentrations at 115 dbar are a factor of 4-5 higher than maximum particulate REE concentrations in the Cariaco Trench, but a factor of 5-7 lower than maximum particulate REE concentrations in Saanich Inlet.

The particulate Ce/Nd ratio (Fig. 6.15a) is above the value in mean shales throughout the watercolumn, except for a pronounced, sharp minimum approximately between 70 and 115 dbar. Below 70 dbar the

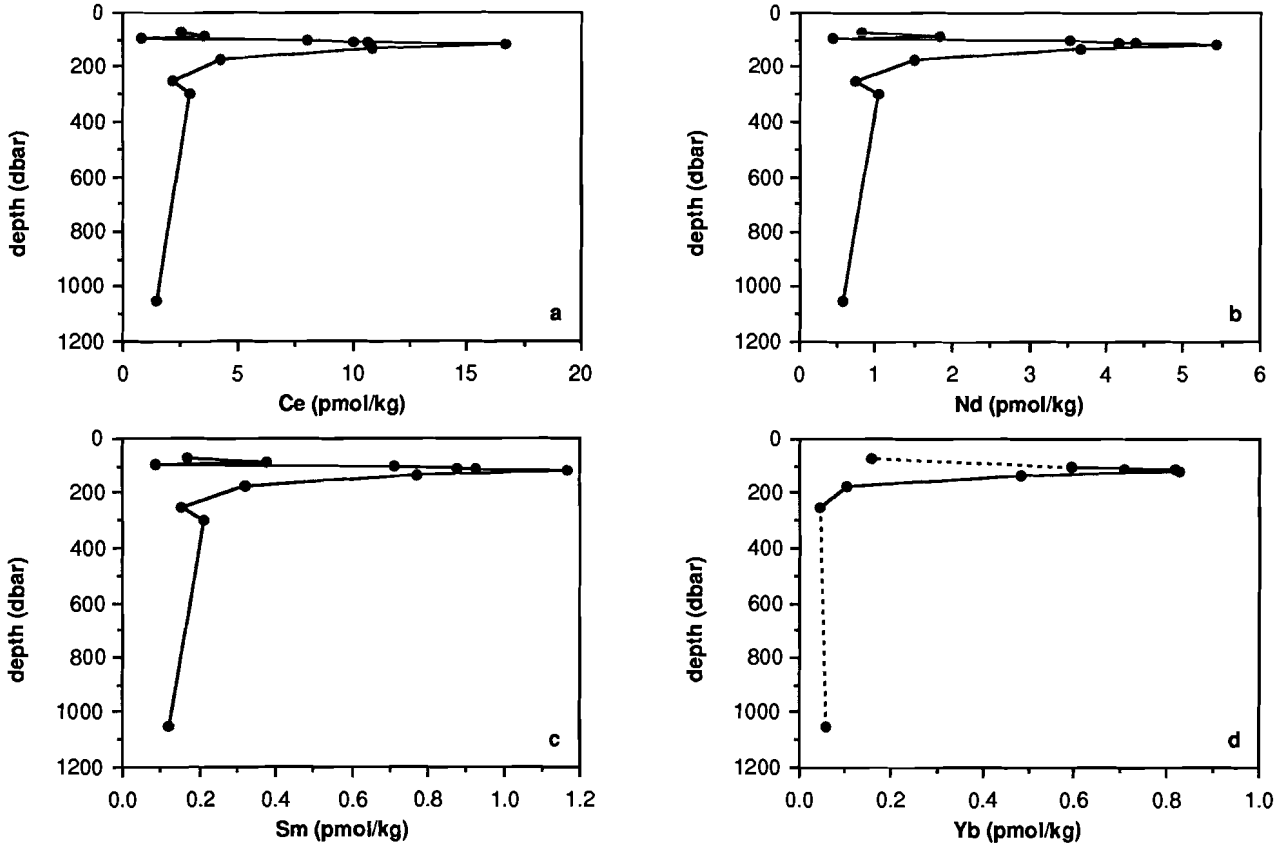

Figure 6.14. Vertical distributions of particulate Ce, Nd, Sm and Yb at station BS5-2.

depth (dbar)	Ce	Nd	Sm	Yb
71	2.56	0.826	0.17	0.16
83	3.58	1.83	0.38	-
95	0.811	0.427	0.088	-
101	8.04	3.54	0.71	0.60
106	10.0	4.38	0.93	0.82
111	10.7	4.17	0.88	0.71
116	16.7	5.42	1.17	0.83
131	10.9	3.68	0.78	0.48
177	4.27	1.52	0.32	0.10
252	2.19	0.731	0.15	0.046
303	2.89	1.05	0.21	-
1061	1.45	0.578	0.12	0.058
shales	592	263	49.9	20.4

Table 6.3. Particulate REE concentrations at station BS5-2. A sampleweight of 30,000 g was assumed for the calculation of all particulate REE concentrations, corresponding to the full contents of the 30 l GoFlo bottles. REE abundances in mean shales (µmol/kg) from Piper (1974).

Ce/Nd ratio abruptly decreases well below the value in mean shales and then increases again between 90 and 115 dbar until it regains the value at 70 dbar. Below 115 dbar the Ce/Nd ratio decreases gradually with depth, but remains above the value in mean shales.

The vertical distribution of the particulate Yb/Nd ratio (Fig. 6.15b) is rather remarkable. Above 130 dbar particulate matter is modestly but significantly HREE enriched as also demonstrated by the particulate REE patterns (Fig. 6.16). The strongest HREE enrichment corresponds to a particulate Yb/Nd ratio of about 0.20 (Fig. 6.15b), which is only as high as the dissolved Yb/Nd ratio of samples in the deep anoxic water (Fig. 6.12a). Below 115 dbar the particulate Yb/Nd ratio rapidly decreases to a minimum near 250 dbar, where particulate matter is actually slightly LREE enriched (Fig. 6.16). LREE enriched particulate matter was also found by De Baar *et al.* (1988) and by German and Elderfield (1989) throughout the oxic watercolumns in the Cariaco Trench and in Saanich Inlet respectively. At 1061 dbar, the only sample below 250 dbar that was analyzed for particulate REE, the Yb/Nd ratio is again slightly above the value in mean shales.

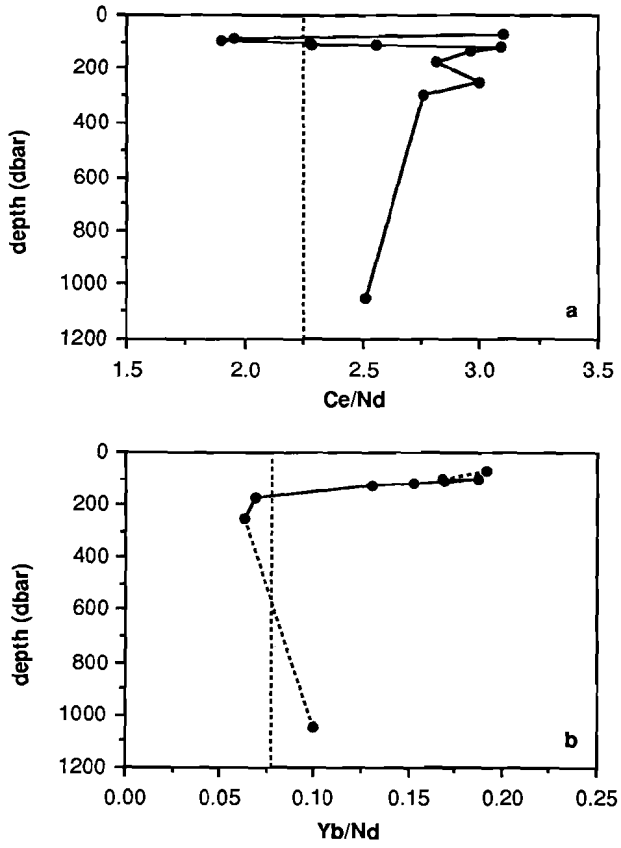

Figure 6.15. Vertical distribution of the particulate Ce/Nd ratio at station BS5-2 (a). Dashed line indicates the Ce/Nd ratio in mean shales (~2.25). Vertical distribution of the particulate Yb/Nd ratio at station BS5-2 (b). Dashed line indicates the Yb/Nd ratio in mean shales (~0.078).

6.4.3. The Bosporus station

Dissolved REE concentrations in three samples from the Bosporus station (Fig. 6.1) are presented in Table 6.4. The watercolumn at this station is characterized by three watermasses of different σ_θ, separated by sharp density gradients (Sect. 6.2.1.; Fig. 6.2b). The three samples were taken from the cores of these three watermasses. Therefore, it should be kept in mind that the vertical REE distributions

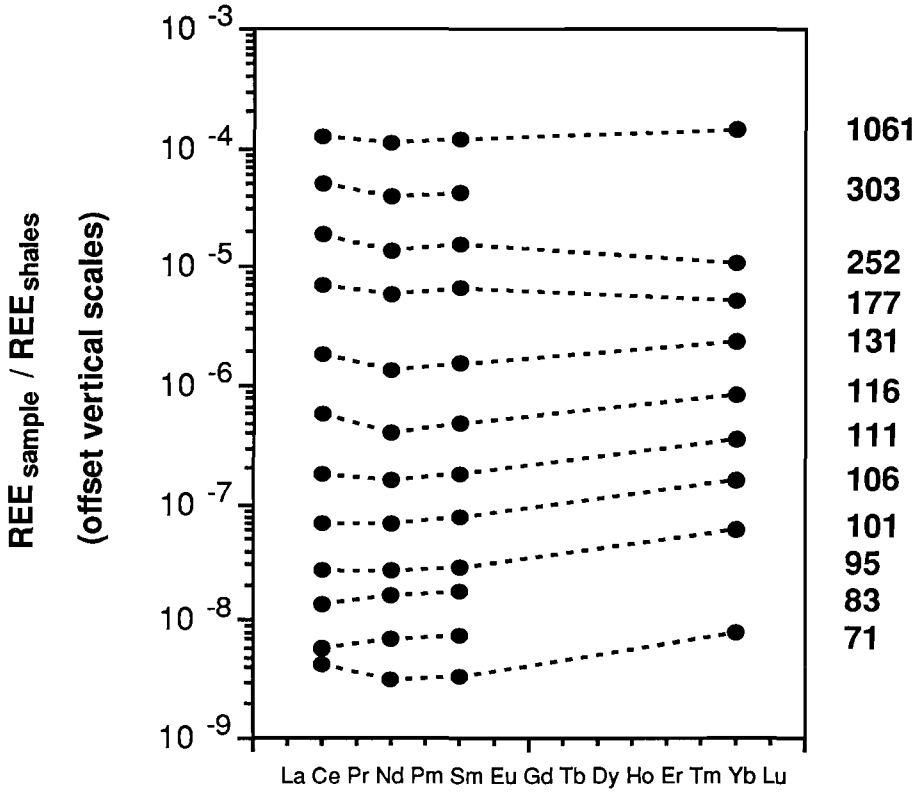

Figure 6.16. REE patterns of particulate REE at station BS5-2, drawn with offset vertical scales for comparison. Corresponding depths in dbar indicated at the right hand side of each pattern.

depth (dbar)	Ce	Nd	Sm	Eu	Gd	Dy	Er	Yb	Lu
8	31.72	24.41	5.61	1.66	-	-	-	10.2	1.57
30	16.87	23.45	5.47	1.56	-	-	10.6	9.37	-
65	13.76	20.22	4.40	1.31	-	-	-	8.13	1.20
shales	592	263	49.9	10.6	40.4	33.8	22.4	20.4	3.49

Table 6.4. Dissolved REE concentrations at the Bosporus station. La was not analyzed for these samples. REE abundances in mean shales (μmol/kg) from Piper (1974).

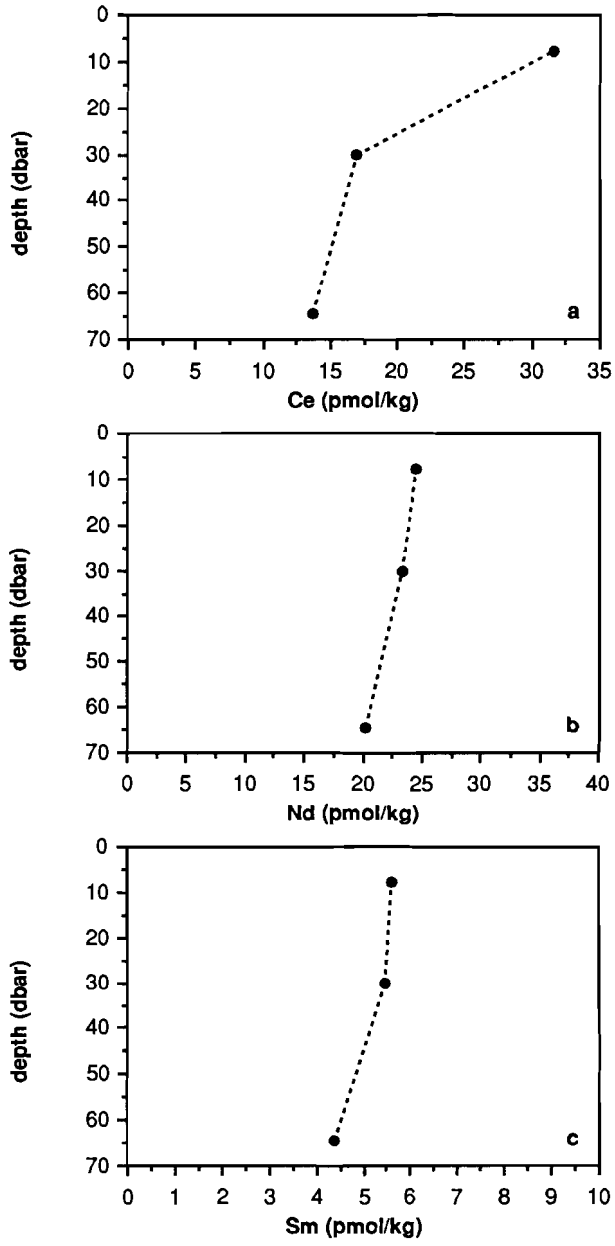

Figure 6.17. (*Continued on page 193*). Vertical distributions of dissolved REE at the Bosporus station. Bottom at approximately 68 dbar. Insufficient data is available for Gd, Dy and Er to draw reasonable vertical distributions. La was not analyzed for these samples.

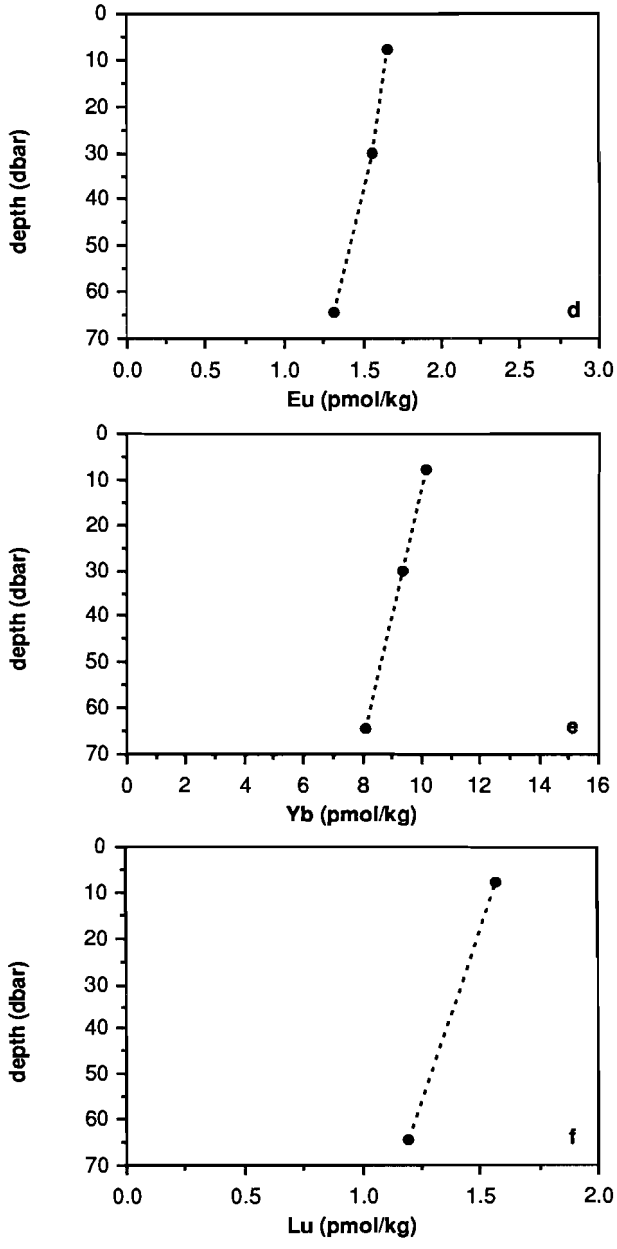

Figure 6.17. (*Continued*).

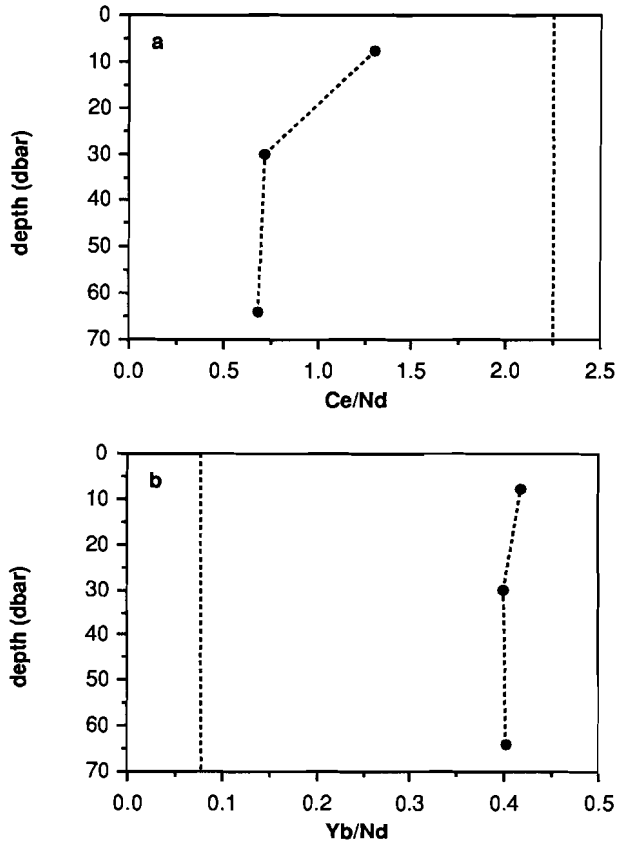

Figure 6.18. Vertical distribution of the dissolved Ce/Nd ratio at the Bosporus station (a). Dashed line indicates the Ce/Nd ratio in mean shales (~2.25). Vertical distribution of the dissolved Yb/Nd ratio at the Bosporus station (b). Dashed line indicates the Yb/Nd ratio in mean shales (~0.078).

in Figure 6.17 are indicative of horizontal rather than vertical processes. Consequently, in the following, REE concentrations will be regarded as a function of watermass and not as a function of depth.

For the strictly trivalent REE there is a minor (but significant) difference in concentration between water originating in the Black Sea (the upper two layers) and water originating in the Mediterranean Sea (the lowermost layer). Concentrations in the upper two layers, while being nearly equal, are a bit higher than corresponding concentrations in the lowermost layer. The difference is relatively larger for the HREE

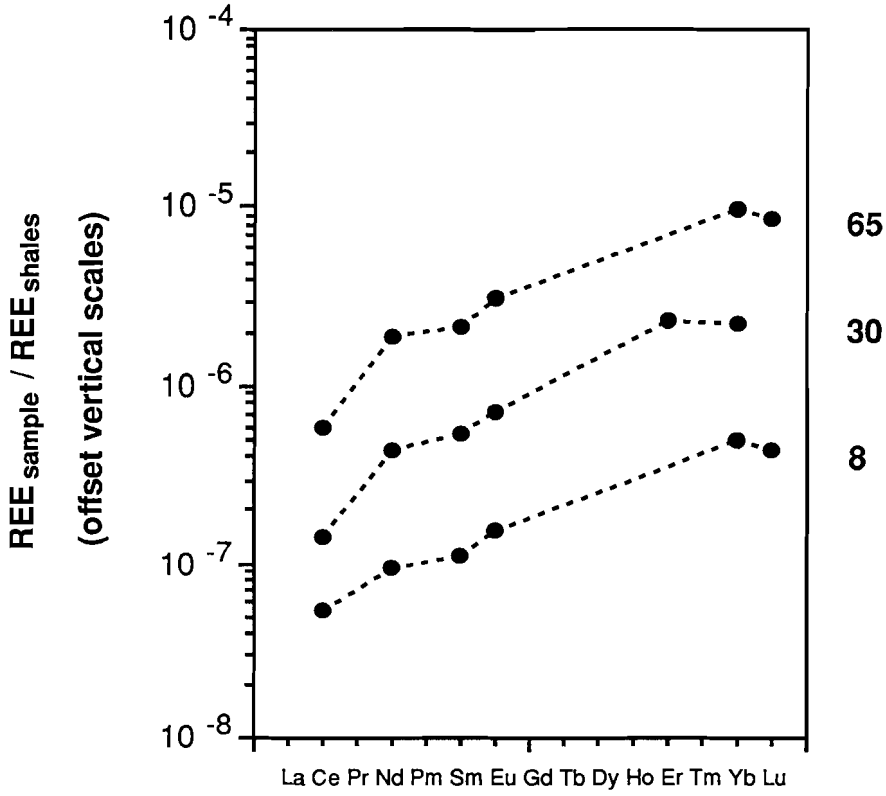

Figure 6.19. REE patterns of dissolved REE at the Bosporus station, drawn with offset vertical scales for comparison. Corresponding depths in dbar indicated at the right hand side of each pattern.

than for the LREE. The vertical distribution of Ce is clearly different from that of the strictly trivalent REE. The Ce concentration in the warm surface layer is almost twice the Ce concentration in the cold intermediate layer (CIL). On the other hand, the relative difference in Ce concentrations between latter layer and the lowermost layer is comparable to the relative difference in concentrations of the strictly trivalent REE.

The anomalous behaviour of Ce in the surface layer is also demonstrated by the Ce/Nd ratio (Fig. 6.18a). The Ce/Nd ratio is used here instead of the Ce anomaly, since La was not analyzed for these samples. Although the Ce/Nd ratio suggests a negative Ce anomaly in all three samples, Ce is clearly less depleted in the surface layer than

in the other two layers, which have almost equal Ce/Nd ratios. The Yb/Nd ratios, which are equal for all three samples within the uncertainty of the measurements (Fig. 6.18b), indicate a distinct HREE enrichment. These characteristics are reproduced in the REE patterns (Fig. 6.19), which are typical of seawater, combining HREE enrichment with a negative Ce anomaly. The Ce anomaly in the surface layer REE pattern is somewhat less pronounced than that in the other two REE patterns.

6.5. Discussion

6.5.1. REE cycling within the suboxic layer

In this Section an attempt is made to shed some light on the complexity of REE cycling within the suboxic layer, by comparing vertical distributions of the REE to vertical distributions of Mn, Fe, oxygen, sulfide and the nutrients. In view of the thickness of the suboxic layer at station BS5-2, it may be possible to resolve the full sequence of oxidation reactions that is initiated by the depletion of oxygen (Chapter 2). Therefore, the sequence of oxidation reactions was chosen as a starting point for the discussion. Reduction of Mn and Fe is probably mediated by bacteria that use Mn and Fe oxides as electron acceptors in the decomposition of organic matter. REE cycling is generally believed to be coupled to the cycling of Mn and Fe. Alternatively, Ce reduction may be mediated by bacteria that use some Ce(IV) solid phase as an electron acceptor in the decomposition of organic matter, possibly leading to decoupling of the cycling of Ce from that of Mn and Fe. In that case, a calculation of the free energy change $\Delta G°$ per mole of carbon oxidized may be used to predict how the Ce(IV) solid phase in question ranks relative to Mn and Fe oxides in the order of electron acceptors.

Since it is not feasible to display the vertical distributions and profiles of all elements and chemical parameters of interest in a single diagram, they are displayed in several groups. All vertical distributions and profiles are plotted as a function of either σ_θ or σ_T, in order to ensure a valid comparison of data from different casts and stations (Sect. 6.2.1.). In Figure 6.20 profiles of oxygen and sulfide are compared with profiles of the nutrients nitrate and phosphate. Initial decomposition of organic matter is signified by the consumption of oxygen and the simultaneous onset of nitrate and phosphate gradients below σ_T = 14.5 (Chapter 2). Oxygen becomes depleted at σ_T = 15.4. Decomposition of organic matter by denitrification is signified by the decrease of nitrate concentrations between σ_T = 15.4 and σ_T = 15.9,

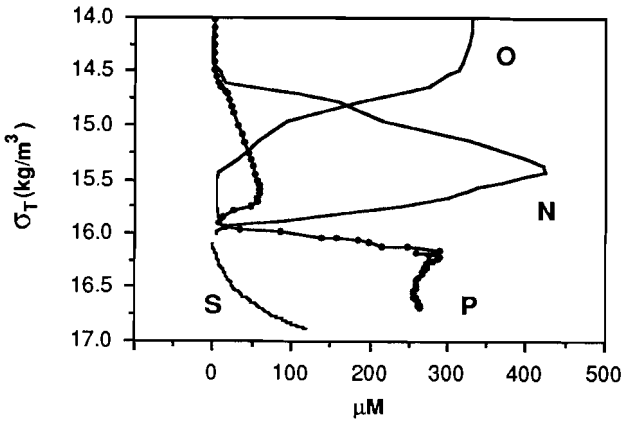

Figure 6.20. Profiles of oxygen (O), nitrate (N), sulfide (S) and phosphate (P) *versus* σ_T recorded with the pump-profiling system. O, N and S were recorded on 13 June 1988 at station BS3-6. P was recorded on 18 July 1988 at station BS5-2. N and P are expanded 50 times for comparison. Data from Friederich *et al.* (1990).

where nitrate becomes depleted, and by the nitrite maximum at σ_T = 15.8 (Fig. 6.5a). The simultaneous appearance of ammonium (Fig. 6.5a) and sulfide indicates that sulfate reduction occurs somewhere below σ_T = 16.22, defined in Section 6.2.1. as the lower boundary of the suboxic layer. The order of electron acceptors is thus oxygen - nitrate - sulfate, in agreement with the predictions of Froelich *et al.* (1979) and Berner (1980).

The vertical distributions of dissolved Mn, Fe and Ce are compared in Figure 6.21a. Reduction of Mn, Fe and Ce is signified by the increase of dissolved Mn, Fe and Ce concentrations respectively. Elderfield and Sholkovitz (1987) proposed that Ce reduction, like reduction of Mn and Fe, may be considered within the framework of the sequence of oxidation reactions associated with the decomposition of organic matter (Chapter 2). They calculated the free energy change per mole of organic carbon oxidized to be $\Delta G°$ = -445 kJ/mol for reduction of CeO_2 and $\Delta G°$ = -427 kJ/mol for reduction of $Ce(OH)_4$. In the order of electron acceptors predicted by Berner (1980), which is oxygen - nitrate - Mn oxide - Fe oxide - sulfate, this ranks both CeO_2 and $Ce(OH)_4$ between nitrate and Mn oxide, yet closer to nitrate (Table 2.2). Detailed inspection of the vertical distributions in Figure 6.21a may contribute to corroboration of these predictions. However, the interpretation of

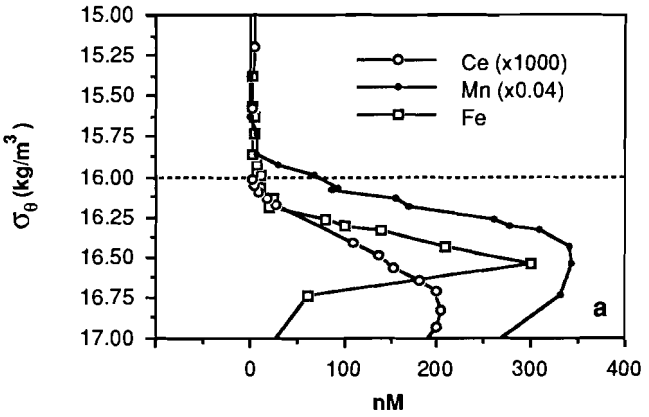
15.00
15.25
15.50
15.75
16.00
16.25
16.50
16.75
17.00
σθ (kg/m3)
Ce (x1000)
Mn (x0.04)
Fe
a
0
100
200
300
400
nM

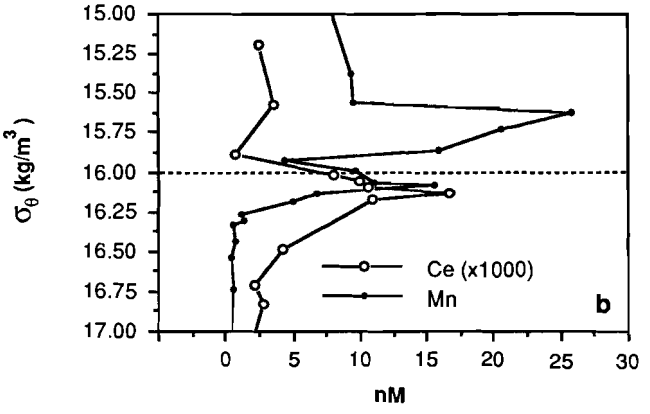
15.00
15.25
15.50
15.75
16.00
16.25
16.50
16.75
17.00
σθ (kg/m3)
Ce (x1000)
Mn
b
0
5
10
15
20
25
30
nM

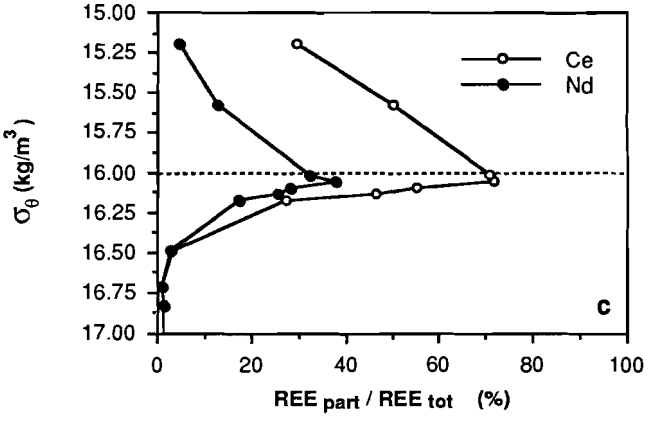
15.00
15.25
15.50
15.75
16.00
16.25
16.50
16.75
17.00
σθ (kg/m3)
Ce
Nd
c
0
20
40
60
80
100
REE part / REE tot (%)

Figure 6.21a in terms of the sequence of oxidation reactions is very complicated for a number of reasons.

First, the concentration gradients in Figure 6.21a lead to upward diffusion of dissolved Mn, Fe and Ce, which are subsequently removed, as a result of oxidation. How far the upward diffusion continues before removal is complete depends upon the rate of oxidation of the element in question. For instance, the Mn gradient may extend much further above the Mn maximum than the Fe gradient above the Fe maximum, since the rate of oxidation of Mn in seawater is generally assumed to be lower than that of Fe (Chapter 4). Very little is known about the rate of Ce oxidation in seawater (Chapter 7), yet experiments by Moffett (1990) indicate that the rate of microbially mediated Ce oxidation is approximately three times lower than the rate of microbially mediated Mn oxidation, over a wide range of absolute rates.

Second, Tebo (1991) found that the lower particulate Mn maximum, which is rather unexpected from a thermodynamical point of view, is probably caused by microbially mediated Mn oxidation. The lower particulate Mn maximum appears to coincide with a light transmission minimum and a maximum of BChl-e concentrations, indicating the presence of a dense sheet of obligate phototrophic brown sulfur bacteria (Sect. 6.2.3.). Due to their photosynthetic activity, the sequence of oxidation reactions may locally be reversed, possibly leading to *in situ* removal of dissolved Mn, thereby affecting its vertical distribution.

Third, several abiotic processes of which the relative importance with respect to microbially mediated processes and with respect to each other is unknown, such as precipitation of Fe sulfide solid phases and possibly of Mn carbonate solid phases (Sect. 6.2.3.), phosphate pumps and shuttles (Shaffer, 1986) and coprecipitation of Ce with or adsorption of Ce onto Mn and Fe solid phases (Chapter 5), may affect the vertical distributions of Mn, Fe and Ce.

Notwithstanding these complications, some general remarks can be made with respect to Figure 6.21a. A comparison of Figures 6.20 and 6.21a shows that the onsets of the gradients of dissolved Mn and Fe are approximately located at the depth where nitrate becomes depleted. This strongly suggests that nitrate preceeds Mn oxide and Fe oxide in

---

Opposite page: **Figure 6.21.** Vertical distributions of dissolved Mn and Fe at station BS3-6 (Lewis and Landing, 1991) and Ce at station BS5-2 (this work) *versus* σ_θ (a). Vertical distributions of particulate Mn at station BS3-6 (Lewis and Landing, 1991) and particulate Ce at station BS5-2 (this work) *versus* σ_θ (b). Particulate Ce and Nd at station BS5-2, expressed as fractions of total Ce and Nd, *versus* σ_θ (c). The dashed lines are for reference.

the order of electron acceptors, in agreement with the predictions of Berner (1980).

It is difficult to determine from a comparison of the vertical distributions of dissolved Mn and Fe in Figure 6.21a, whether Mn reduction preceeds Fe reduction in the sequence of oxidation reactions or *vice versa*. The onset of the dissolved Mn gradient, approximately at σ_θ = 15.8, coincides with the onset of the dissolved Fe gradient and the dissolved Mn maximum at σ_θ = 16.5 coincides with the dissolved Fe maximum. The gradient of dissolved Fe is always below that of dissolved Mn, yet this may be due to their different rates of oxidation. The sharp dissolved Fe maximum and the rapid decrease of dissolved Fe concentrations clearly indicate precipitation of some Fe sulfide solid phase below σ_θ = 16.5. The depth where dissolved Fe reaches its maximum concentration is the depth where the solubility product of this Fe sulfide solid phase is exceeded. If Fe sulfide would not precipitate, the vertical distribution of dissolved Fe would be similar to that of Mn and Ce and the dissolved Fe maximum would probably occur at greater depth. Similarly, precipitation of some Mn carbonate solid phase was inferred by Haraldsson and Westerlund (1988) from a comparison of the Mn carbonate ion activity product and the corresponding solubility product.

The vertical distributions of dissolved Mn and Fe may also be affected by phosphate pumps and shuttles (Shaffer, 1986). Phosphate is a reaction product of the decomposition of organic matter, but does otherwise not take part in the sequence of oxidation reactions. According to the model proposed by Shaffer (1986) 60% of the phosphate anomaly dipole may be accounted for by a phosphate shuttle based on Mn and 40% by a phosphate pump based on Fe. However, whereas the phosphate shuttle operates *in situ*, the phosphate pump operates on the shelf at the sediment-water interface and its contribution to the phosphate dipole anomaly at stations near the centre of the Black Sea therefore critically depends on rates of horizontal advection and diffusion. The calculation by Shaffer (1986) was based on a fit of spline curves to a composition of phosphate profiles recorded at many stations throughout the Black Sea, including both stations near the shelf and stations in open sea. A comparison of Figures 6.20 and 6.21a indicates that phosphate pumps and shuttles are of minor importance relative to other processes affecting the vertical distributions of dissolved Mn and Fe. The concomitance of the phosphate maximum at σ_θ = 16.2 and a distinct change of slope of the dissolved Fe gradient is probably fortuitous.

The onset of the dissolved Ce gradient is located at σ_θ = 16.1 and the dissolved Ce maximum is located at σ_θ = 16.8. Therefore, although the vertical distribution of dissolved Ce is very similar to that of

dissolved Mn, there is a vertical offset of about 0.3 σ_θ units between them, suggesting that the cycling of Ce is decoupled from that of Mn. Possibly, Ce cycling is driven by its own microbially mediated reduction, which may be considered within the framework of the sequence of oxidation reactions associated with the decomposition of organic matter, as proposed by Elderfield and Sholkovitz (1987). However, their conclusion, based on a calculation of the free energy change per mole of carbon oxidized, that Ce reduction preceeds Mn reduction in the sequence of oxidation reactions, appears to be in contrast with the observation that dissolved Ce concentrations begin to increase and reach a maximum at greater depth than dissolved Mn concentrations. Most likely the Ce solid phase involved is not pure CeO_2 or $Ce(OH)_4$, but even if it is, there is a great variety of possible reduction half reactions (De Baar *et al.*, 1988), leading to a broad range of free energy changes per mole of organic carbon oxidized for microbially mediated Ce reduction. Elderfield and Sholkovitz (1987) predicted that CeO_2 and $Ce(OH)_4$ both rank between nitrate and Mn oxide in the order of electron acceptors proposed by Berner (1980). Since the ranges of free energy changes per mole of organic carbon oxidized for denitrification and Mn reduction are widely overlapping (Froelich *et al.*, 1979), Mn reduction may very well preceed Ce reduction in the sequence of oxidation reactions. Alternatively, instead of being driven by microbially mediated reduction, the cycling of Ce might be coupled specifically to that of Fe, which in turn may be decoupled from that of Mn, yet this is hard to prove, since the vertical distribution of dissolved Fe is so strongly affected by precipitation of Fe sulfide.

The vertical distributions of particulate Mn and Ce are compared in Figure 6.21b. The upper particulate Mn maximum is located just above the onset of the dissolved Mn gradient. According to the generally accepted model of Mn cycling at oxic-anoxic interfaces (Chapter 2), the gradient leads to upward diffusion of dissolved Mn, which is subsequently removed, presumably by oxidation and precipitation as Mn oxide solid phases. Upon settling the particulate Mn is reduced, causing dissolution of the precipitate. Oxidation of Mn in the absence of oxygen, which becomes depleted well above the upper particulate maximum (Fig. 6.20), is hard to conceive. Nevertheless, the upper particulate Mn maximum might be the result of oxidation, mediated either by bacteria that use some other electron acceptor than oxygen or by bacteria that are especially adapted to extremely low oxygen concentrations. However, the presence at this depth of a sheet of bacteria is not substantiated by a light transmission minimum (Fig. 6.9c), nor by a maximum of some bacterial pigment (Repeta *et al.*, 1989). The sheet of obligate phototrophic bacteria, containing *Chlorobium* sp. and/or *Chromatium* sp. (Sørensen, 1988; Repeta *et al.*, 1989), that coincides

with the lower particulate Mn maximum (Sect. 6.2.3.) does not extend above $\sigma_\theta = 15.8$ and therefore cannot be related to the upper particulate Mn maximum. Moreover, although the upper particulate Mn maximum is more pronounced than the lower one, the corresponding rate of Mn oxidation is very low (Tebo, 1991).

Indications that oxidation is not the main mechanism for Mn removal at the depth of the upper particulate Mn maximum, were found by Tebo (1991). A negative reaction of particulate Mn from the upper particulate Mn maximum with leucoberbelin blue, a reagent that indicates the presence of Mn(IV), led him to conclude that the upper particulate Mn maximum probably consists of Mn(II) adsorbed onto particulate matter rather than oxidized Mn. Similarly, Moffett (1990) found that under some conditions adsorption of Ce(III) can be a more important mechanism for Ce removal than microbially mediated Ce oxidation. However, in view of the absence of a particle maximum at the depth of the upper particulate Mn maximum, it is not clear onto what particles Mn(II) is adsorbed and why Mn(II) is adsorbed specifically at that depth. The simultaneous presence of a particulate Mn maximum and absence of a particle maximum suggests that the amount of particulate Mn per gram of dry particulate matter is relatively high.

Figure 6.21b shows that the (single) particulate Ce maximum almost exactly coincides with the lower particulate Mn maximum. The particulate Ce maximum is located just above the onset of the dissolved Ce gradient. A model of Ce cycling analogous to the generally accepted model of Mn cycling mentioned above can be envisioned. Apparently, the removal of dissolved Ce, which diffuses upward as a result of the gradient, is related to the presence of the lower particulate Mn maximum. Unfortunately, there is no information on the oxidation state of particulate Ce or on the rate of Ce oxidation at the depth of the particulate Ce maximum. Adsorption of Mn(II) and Ce(III) might be favoured as the most likely mechanism for removal of dissolved Mn and Ce, since *in situ* oxidation of Mn and Ce in the absence of oxygen is hard to conceive. However, if the removal of Ce were completely due to adsorption rather than to oxidation of Ce(III), then Ce would be expected to behave just like the strictly trivalent REE. Moreover, a strongly positive reaction of particulate Mn from the lower particulate Mn maximum with leucoberbelin blue and very high rates of Mn oxidation, along with other evidence (Sect. 6.2.3.), indicate that the lower particulate Mn maximum at least partly consists of oxidized Mn and that Mn oxidation at this depth is probably microbially mediated (Tebo, 1991). Therefore, Ce removal is probably caused by microbially mediated oxidation as well. Moffett (1990), who performed laboratory experiments in order to determine the rate of Ce oxidation in seawater

(Chapter 7), found that abiotic oxidation is not an important mechanism for Ce removal. Evidence that Ce oxidation indeed occurs at the depth of the particulate Ce maximum is provided by the vertical distribution of the dissolved Ce anomaly (see below).

Tebo (1991) argued that microbially mediated Mn oxidation probably occurs in the presence of oxygen near the shelf, where a suboxic layer has not (yet) fully developed (Sect. 6.5.2.) and where coastal upwelling leads to regions of high productivity (Hay *et al.*, 1990). The presence of the lower particulate Mn maximum in the centre of the Black Sea would consequently be the result of horizontal advection. Alternatively, horizontal advection may cause a continuous flux of oxygen toward the centre of the Black Sea, sustaining *in situ* oxidation of Mn within the sheet of bacteria reported by Repeta *et al.* (1989). Tebo (1991) has shown these bacteria to be very active, even at ambient oxygen concentrations, which are extremely low.

Apart from significantly different behaviour within the suboxic layer (Sect. 6.4.1.), the vertical distributions of the trivalent REE, both dissolved and particulate, are very similar to that of Ce (Fig. 6.9b and 6.14). Apparently their cycling is equally decoupled from that of Mn. The vertical distribution of the dissolved Yb/Nd ratio in Figure 6.12 is dominated by a pronounced maximum at about 100 dbar, approximately coinciding with the dissolved REE minima (Fig. 6.9; Table 6.2) and slightly above the particulate REE maxima (Fig. 6.14; Table 6.3). The Yb/Nd ratio increases from a value of 0.3 at 60 dbar to a value of 0.8 at 100 dbar, indicating that the trivalent REE are strongly scavenged just above the onset of their dissolved gradients. Since the strictly trivalent REE cannot actively take part in redox chemistry, their cycling at oxic-anoxic interfaces is generally believed to be passively coupled to the cycling of Mn and/or Fe. According to the model proposed by De Baar *et al.* (1988), the gradients lead to upward diffusion of dissolved trivalent REE, which are subsequently removed by adsorption onto or coprecipitation with Mn and/or Fe oxide solid phases. Upon settling the trivalent REE are released as Mn and Fe are reduced and the precipitate dissolves. The concomitance of the particulate maxima of the trivalent REE and the lower particulate Mn maximum is in support of this model.

Inasmuch as microbially mediated oxidation was found to be an important mechanism for removal of Mn at the depth of the lower particulate Mn maximum, it was assumed above that the same is true for Ce. Strong adsorption of the trivalent REE onto particles, be it particulate organic matter or particulate Mn, as indicated by the dissolved Yb/Nd ratio, suggests that Ce removal at this depth may instead be caused by adsorption of Ce(III). However, the particulate Ce maximum lies at the base of a broad minimum of the dissolved Ce

anomaly (Fig. 6.11a), indicating that Ce is removed much more effectively than the trivalent REE. Within this minimum, which extends throughout the suboxic layer, the Ce anomaly reaches values as low as 0.1. Comparably low dissolved Ce anomalies have been reported only for old water from the deep Indian Ocean (German and Elderfield, 1990) and the deep Pacific Ocean (De Baar *et al.*, 1985a) and for oxic water overlying the anoxic layer in Saanich Inlet, a seasonally anoxic basin in British Columbia (German and Elderfield, 1989). The dissolved Ce anomaly singles out redox chemistry from all other processes affecting the vertical distribution of dissolved Ce (Chapter 2). Therefore, the minimum of the dissolved Ce anomaly clearly demonstrates that Ce is being oxidized at the depth of the particulate Ce maximum. This does not imply that adsorption of Ce(III) is not important. Based on thermodynamic considerations De Baar *et al.* (1985a) demonstrated that oxidation of Ce(III) in solution is extremely unlikely. Since the rate of Ce(III) adsorption is much higher than the rate of Ce(III) oxidation (Moffett, 1990), the distribution of Ce(III) between the dissolved and the particulate phase will probably rapidly reach a pseudo-equilibrium by the same mechanism that is responsible for the removal of trivalent REE (Chapter 5). Subsequent oxidation of the particulate Ce(III) will slowly shift this pseudo-equilibrium to a final equilibrium in favour of the particulate phase.

More effective scavenging of the LREE than of the HREE, as indicated by the vertical distribution of the dissolved Yb/Nd ratio is expected to lead to LREE enrichment of particulate matter at the depth of the particulate REE maxima. However, the vertical distribution of the particulate Yb/Nd ratios clearly shows it to be HREE enriched (Fig. 6.15b). A possible explanation is that the water at the depth of the particulate REE maxima is itself strongly HREE enriched. As was argued in Chapter 2, the HREE may be scavenged more effectively in an absolute sense, simply because there is more of them. Between the onset of the dissolved REE gradients at 100 dbar and the dissolved REE maxima at 300 dbar, the dissolved Yb/Nd ratio decreases approximately from 0.8 to 0.2, indicating that Yb is released more effectively than Nd. This is in apparent contradiction with a simultaneous decrease of the dissolved Yb/Nd ratio (Fig. 6.12), which seems to indicate that Nd is released more effectively than Yb. However, the amount of particulate REE released is minor compared to the standing crop of dissolved REE at the depth of the dissolved REE maxima. Therefore, the change in the dissolved Yb/Nd ratio is probably overwhelmed by a much larger change associated with the increase of dissolved REE concentrations below 100 dbar.

Similar observations with respect to vertical distributions of the dissolved and particulate Er/Nd ratio below the oxic-anoxic interface

in the Cariaco Trench were reported by De Baar *et al.* (1988). Both the particulate and the dissolved Er/Nd ratio are above the mean shales value at the oxic-anoxic interface and decrease toward the mean shales value below (their Figure 8). However, above the oxic-anoxic interface the vertical distribution of the dissolved Er/Nd ratio is very different from the vertical distribution of the dissolved Yb/Nd ratio between the surface and 100 dbar (Fig. 6.12b). Instead of increasing toward a maximum at the oxic-anoxic interface, the dissolved Er/Nd ratio is at a constant high value throughout the oxic layer (De Baar *et al.*, 1988; their Figure 8). Also, particulate REE concentrations are high throughout the oxic layer, without a distinct maximum near the oxic-anoxic interface (their Figure 5). These observations seem to indicate that REE are being scavenged evenly throughout the oxic layer in the Cariaco Trench, whereas in the Black Sea REE scavenging between the surface and 100 dbar is of minor importance compared to REE scavenging at the depth of the lower particulate Mn maximum. On the other hand, both the dissolved Er/Nd ratio in the Cariaco Trench and the dissolved Yb/Nd ratio in the Black Sea decrease from about 0.3 in the oxic water just below the surface to about 0.2 in the deep anoxic water (the Yb/Nd ratio and the Er/Nd ratio in mean shales are nearly equal). Apparently, the difference between the vertical distribution of the dissolved Yb/Nd ratio in the Black Sea and the vertical distribution of the dissolved Er/Nd ratio in the Cariaco Trench is completely due to extreme REE scavenging in the Black Sea at the depth of the lower Mn maximum. Inasmuch as it is the result of bacterial activity, such extreme REE scavenging would not be expected in the Cariaco Trench, because there the oxic-anoxic interface is located at 300 dbar, where there is not enough light for bacteria to survive. Since the particulate Yb/Nd ratio was only determined at one depth between the surface and 100 dbar (Fig. 6.15b), a detailed comparison with the particulate Er/Nd ratio in the oxic layer of the Cariaco Trench is not warranted.

6.5.2. A simple evolutionary model of the suboxic layer

It is very difficult to determine to what extent the formation of the suboxic layer has affected REE cycling at the former oxic-anoxic interface. A detailed interpretation of the vertical distributions of the REE and Mn to that end is impeded by a number of complications. First, there is no previous reliable report on vertical REE distributions in the Black Sea (Sect. 6.1.). Second, there is no previous report on REE distributions within a broad suboxic layer similar to that encountered in the Black Sea. German and Elderfield (1990) reported vertical distributions of dissolved REE within the broad suboxic layer in the Northwest Indian Ocean, yet there anoxic conditions do not occur. Third,

possible changes in the vertical REE distributions may not be caused by the formation of the suboxic layer. Instead, a single underlying mechanism, such as increased horizontal advection, may be causing both the formation of the suboxic layer and the changes in the vertical REE distributions. Fourth, the observed changes in the hydrography indicate that at present the Black Sea is probably not at steady state. Consequently, the observed anomalies in the vertical distributions of the REE and Mn may just be transient features, which portray an intermediate stage in the transition from a sharp oxic-anoxic interface to a broad suboxic layer.

In this Section the most important observations of the 1988 Black Sea Expedition are presented alongside several models that have been put forward to explain hydrographic changes, the formation of the suboxic layer and the observed vertical distributions of dissolved and particulate Mn. These models are combined into a simple evolutionary model of the suboxic layer, which is subsequently used as a tool for interpreting some of the aspects of the observed vertical REE distributions.

Formation of the suboxic layer.

As a logical consequence of the conclusions of Murray *et al.* (1989), it was proposed in several publications that the increased inflow of Mediterranean water through the Bosporus may have led to enhanced horizontal advection in the Black Sea. As a result of this horizontal advection, Mediterranean water containing oxidants such as oxygen or nitrate may have been injected into the top of the anoxic layer resulting in oxidation of the ambient sulfide. Buesseler *et al.* (1991) proposed that oxygen, carried by the advective current, may serve as the primary oxidant. However, Murray and Izdar (1989) argued that neither oxygen nor nitrate can be the primary oxidant since both become depleted well above the first appearance of sulfide. If oxygen or nitrate are oxidizing sulfide, this observation would imply that the flux of sulfide into the suboxic layer resulting from vertical advection and diffusion is exactly cancelled by the flux of oxygen and/or nitrate resulting both from downward diffusion and horizontal advection, which seems very unlikely. Instead, they proposed that oxidation of sulfide is coupled to reduction of metal oxides, specifically oxides of Mn and Fe. Evidence for this is allegedly provided by the fact that 'dissolved Mn and Fe increase rapidly with the sulfide' (Murray and Izdar, 1989).

This idea was expounded in a modified form by Tebo (1991). He suggested that within the suboxic layer Mn is constantly converted back and forth between its oxidized and its reduced form. At the depth

of the lower particulate Mn maximum sulfide may be oxidized by Mn oxides, whereas at the lower boundary of the oxic layer Mn(II) is probably oxidized by oxygen, leading to depletion of both oxygen and sulfide and consequently to formation of a broad suboxic layer. Since the lower particulate Mn maximum was shown by Tebo (1991) to be a direct result of bacterial activity, it seems that these bacteria constitute a key factor in the formation of the suboxic layer. The model of Tebo (1991) raises an important question. If bacteria are oxidizing Mn at the depth of the lower Mn maximum, where do they get the oxygen to do it? Tebo (1991) himself considered several possibilities. Since Mn oxidation cannot occur in the absence of oxygen, he concluded that the lower particulate Mn maximum is probably caused by horizontal advection. Either Mn is oxidized near the shelf where a suboxic layer has not (yet) developed and Mn oxides are subsequently advected to the centre of the Black Sea, or Mn is oxidized *in situ* by bacteria which are sustained by a minor flux of oxygen supplied by horizontal advection. These bacteria should thus be especially adapted to low ambient oxygen concentrations.

The model seems rather elegant, yet it cannot account for some observations. For instance, the particulate Mn maximum near the shelf is both thicker and more intense than in the centre of the Black Sea (Spencer *et al.*, 1972; Kempe *et al.*, 1990; Tebo, 1991). In agreement with this, Tebo (1991) found much higher rates of Mn oxidation at the shelf than in the centre of the Black Sea, probably because at the shelf oxygen is readily available at the depth corresponding to the first appearance of sulfide. However, it is not clear why a suboxic layer has not developed near the shelf, nor why it is much broader in the centre of the Black Sea. Repeta *et al.* (1989) found much higher concentrations of BChl-e in the centre of the Black Sea than at the shelf. They attributed this to the fact that more light is available in the centre of the Black Sea, where the first appearance of sulfide is closer to the surface. The distribution of pigments within the BChl-e maximum is characteristic of obligate phototrophic brown sulfur bacteria. This implies that, if Mn oxidation is microbially mediated, it is most likely mediated by bacteria that are not obligate phototrophic. Moreover, although Tebo (1991) suggested that Mn oxidation may contribute to oxygen consumption, removal of dissolved Mn near the onset of the dissolved Mn gradient is apparently not related to Mn oxidation (Sect. 6.5.1.).

It seems that the lenticular shape of the suboxic layer can only be explained if it is assumed that obligate phototrophic bacteria are responsible for its formation. The following simple model may be envisioned. It is assumed that the bacteria in question need some minimum level of light and sulfide in order to survive (*cf.* Repeta *et al.*,

1989). However, whereas surfaces of equal sulfide concentration coincide with isopycnal surfaces, which are dome-shaped, surfaces of equal light intensity are roughly parallel to the Black Sea surface. Therefore, regardless what caused their upward shift, the 'iso-sulfide' surfaces would first intersect the 'iso-light' surface corresponding to the required minimum level of light at some point in the centre of the Black Sea. As the iso-sulfide surfaces continued to shoale a suboxic layer formed within a circular region expanding concentrically toward the shelf. Since formation of the suboxic layer started in the centre of the Black Sea, this is where it is broadest.

Implications for the cycling of Mn and the REE.

Although this simple model is capable of explaining some aspects of the formation of the suboxic layer, it leaves many problems unsolved. To begin with there is the vertical distributions of dissolved and particulate Mn. How have these changed since the formation of the suboxic layer? The answer is rather surprising. A comparison of the 1988 vertical distributions of dissolved Mn reveal only minor differences with those reported by Spencer and Brewer (1971) and by Haraldsson and Westerlund (1988). Also, Spencer and Brewer (1971) found no differences between vertical distributions of dissolved Mn at stations far from and near the shelf, if plotted *versus* σ_θ. Moreover, the maximum concentrations of particulate Mn reported by Spencer *et al.* (1972) are nearly equal to those found in 1988, both far from the shelf (Table 6.1) and near the shelf (Lewis and Landing, 1991; Tebo, 1991). Apparently, the only new feature is that the particulate Mn maximum actually consists of two separate maxima. However, the vertical resolution attained by Spencer *et al.* (1972) was no better than about 20 m, whereas the two particulate maxima are only 25 m apart (Table 6.1), requiring a vertical resolution of certainly better than 10 m. Therefore, the possibility that the vertical Mn distributions have not changed at all since 1975 cannot be completely ruled out. This does not imply that microbially mediated Mn oxidation and subsequent oxidation of sulfide by Mn oxides does not occur (Luther *et al.*, 1991; Millero, 1991), yet, since this process probably involves bacteria that are not obligate phototrophic, it may already have been active long before the formation of the suboxic layer.

The question whether vertical REE distributions have changed since 1975 cannot be answered, as there is no previous reliable report on vertical REE distributions in the Black Sea for comparison. If the lower particulate Mn maximum is a direct result of the formation of the suboxic layer, then the particulate REE maxima may also not have been there before 1975. Furthermore, according to the model of De Baar

et al. (1988) particulate REE maxima would be expected at the depth of the upper particulate Mn maximum. Close inspection of Figure 6.21b shows that particulate REE concentrations were only determined directly above and directly below the upper particulate Mn maximum. Therefore, any particulate REE maximum at that depth may have been missed. On the other hand, there are reasons not to expect a REE maximum at the depth of the upper particulate Mn maximum. First, there are no dissolved REE available for scavenging. Second, in contradiction with the model of De Baar *et al.* (1988) REE cycling is apparently decoupled from that of Mn (Sect. 6.5.1.). This new observation may be characteristic of any broad suboxic layer within the marine environment. A comparison of vertical distributions of dissolved Mn and REE within the broad suboxic layer in the Northwest Indian Ocean (NWIO) shows no clear evidence of a similar decoupling (Saager *et al.*, 1989; German and Elderfield, 1990). However, a direct comparison of the NWIO with the situation presently encountered in the Black Sea is not appropriate for several reasons. First, anoxic conditions do not occur in the NWIO as inferred from the absence of sulfide. Second, the suboxic layer of the NWIO is highly complex, with strong horizontal advection at various depth horizons leading to multiple maxima of dissolved Mn (Saager *et al.*, 1989). Third, vertical distributions of particulate Mn and REE were not reported for the NWIO.

Another problem yet to be solved is the chemical mechanism underlying the formation of the suboxic layer. In Framvaren Fjord conditions also seem to be in favour of formation of a broad suboxic layer (Sørensen, 1988), yet a broad suboxic layer is not observed. Apparently, the mere presence of light, sulfide and bacteria is not sufficient to initiate the process. Black Sea hydrographic data as presented by Tebo (1991) show that the first appearance of sulfide coincides with the same isopycnal ($\sigma_T \approx 16.1$) at stations far from and near the shelf. On the other hand, oxygen becomes depleted at $\sigma_T \approx 16.1$ at the station near the shelf yet at $\sigma_T \approx 15.4$ at the station far from the shelf. This seems to indicate that formation of the suboxic layer is primarily due to consumption of oxygen rather than sulfide. This is in disagreement with the assertion that sulfur bacteria are responsible for formation of the suboxic layer. Some other species of obligate phototrophic bacteria may be responsible instead, yet then it remains to be determined what it is that they oxidize. It is not likely to be Mn(II), because this would have substantially affected the vertical distribution of dissolved Mn since 1975.

Clearly, much more data is needed in order to settle all these questions. Such data should include highly detailed vertical distributions of both particulate and dissolved Mn, Fe and REE at potentially interesting locations, for instance Framvaren Fjord and the

Northwest Indian Ocean. Also, information is needed on vertical distributions of particulate REE in the open ocean. Frequent monitoring of the Black Sea may help to determine whether possible near-future changes in the suboxic layer are followed by changes in the vertical distributions of Mn and the REE.

6.5.3. Dissolved REE fluxes through the Bosporus

Considerations contributing to a simple REE mass balance for the Black Sea, presented in this Section, are focussed on the Bosporus inflow/outflow system, first because it is the main cause of present hydrographic conditions in the Black Sea and second because presently there is no data available on other sources or sinks of REE to the Black Sea.

The hydrography of the Bosporus is described in great detail in a large number of publications (*e.g.* Bogdanova, 1961; Gunnerson and Özturgut, 1974; Sorokin, 1983; Tolmazin, 1985). The magnitudes of the inflow of Mediterranean water and the outflow of Black Sea water through the Bosporus are well known. Part of the Black Sea water flowing out through the Bosporus is entrained in the Mediterranean water flowing in opposite direction and returned to the Black Sea (Bogdanova, 1961; Boudreau and Leblond, 1989). In the present discussion the values 176 km^3/yr and 340 km^3/yr (Sorokin, 1983; Tolmazin, 1985) are adopted for the inflow and outflow respectively, not including the entrainment flow. The magnitude of the entrainment flow may be calculated from a balance of salinity or temperature. In the terminology of Buesseler *et al.* (1991):

$$P_{ss} = F_o P_o + (1 - F_o) P_i \qquad (6.3)$$

where P_o is some conservative property in the outflow (Black Sea endmember), P_i in the inflow (Mediterranean endmember) and P_{ss} in the inflow after entraining a fraction F_o of Black Sea endmember. F_o may be calculated from the salinity profile in Figure 6.2a. As was already suggested by Buesseler *et al.* (1991) on the basis of a Θ-S diagram, it is assumed here that the entrained water originates in the CIL, since it directly overlies the inflow (Sect. 6.2.1.). From Figure 6.2a, P_o = 18.1 ppt and P_{ss} = 35.8 ppt. For the Mediterranean endmember P_i = 38.5 ppt is adopted and consequently F_o = 13%. A calculation based on temperature (Fig. 6.2a) leads to a similar result (F_o = 11%). Boudreau and Leblond (1989) used a physical approach to calculate the magnitude of the entrainment flow and found F_o = 20%. Buesseler *et al.* (1991) calculated F_o from a balance of salinity and arrived at F_o = 88-92%, in sharp contrast with these results. They used P_{ss} = 20.8 ppt, obtained from a

salinity profile recorded at their station 24, near the exit of the Bosporus, yet further offshore than the Bosporus station (Fig. 6.1). It is unlikely that salinity decreases from 35.8 ppt to 20.8 ppt merely by dilution within the short distance between the Bosporus station and station 24. Instead, Figure 6.2b demonstrates that the potential density of water in the lowermost layer, consisting of Mediterranean endmember mixed with the entrainment flow, is very high (σ_θ = 26.9). It is therefore expected to spread out across the Black Sea basin close to the bottom (Bogdanova, 1961). Since the salinity profile at station 24, where the water depth is 500 m, does not extend below 200 m, it is possible that Buesseler *et al.* (1991) have missed this layer altogether.

Removal of dissolved REE upon mixing of relatively fresh Black Sea water with highly saline Mediterranean water is unlikely, since such removal is already largely completed at salinities below 5 ppt (Elderfield *et al.*, 1990). It is therefore assumed that the REE behave conservatively within the Bosporus inflow/outflow system and that the concentrations of dissolved REE in the Mediterranean endmember may be calculated from (6.3). Ce and Nd are taken as an example. Values for P_{ss} (Ce - 13.8 pmol/kg, Nd - 20.2 pmol/kg) and P_o (Ce - 16.9 pmol/kg, Nd - 23.5 pmol/kg) are obtained from Table 6.4 and with F_o = 0.13, P_i is calculated to be 13.3 pmol/kg and 19.7 pmol/kg for Ce and Nd respectively. The calculated Ce concentration is within the range of Ce concentrations reported for the overlying seawater at Bannock Basin (Chapter 5), yet the calculated Nd concentration is slightly lower. A detailed comparison of REE concentrations in the Mediterranean endmember and REE concentrations at Bannock Basin is not appropriate. Although the inflow is referred to in this Chapter as the Mediterranean endmember, it actually originates in the Sea of Marmara, which is connected to the Mediterranean Sea by the Dardanelles (Sect. 6.2.1.). REE concentrations in the Sea of Marmara may well be different from REE concentrations in the Mediterranean Sea. Moreover, Bannock Basin is located in the Ionian Sea, whereas the entrance to the Dardanelles is located in the Aegean Sea. In view of the complex hydrography of the eastern Mediterranean (Chapter 4) the vertical REE distributions in the overlying seawater at Bannock Basin must certainly not be considered representative of vertical REE distributions in the Aegean Sea.

For the concentrations of dissolved Ce and Nd in the Black Sea endmember, a weighted average of the concentrations in the surface layer and in the CIL is taken (Table 6.4), weighing each concentration with the thickness of the corresponding layer (Fig. 6.2b). The weighted averages are Ce = 20.9 pmol/kg and Nd = 23.7 pmol/kg.

Net dissolved Ce and Nd fluxes through the Bosporus can now be calculated from the Ce and Nd endmember concentrations and the magnitudes of inflow and outflow. Net particulate Ce and Nd fluxes

cannot be calculated, since particulate REE concentrations were not determined at the Bosporus station. A comparison of Table 6.4 and Table 6.2 shows that dissolved REE concentrations at the Bosporus station and at station BS5-2 are nearly equal for depths corresponding to the same isopycnal, in the upper 30 m of the watercolumn. Assuming this to be true also for particulate REE concentrations, it is inferred that particulate REE comprise a negligible fraction of total REE in the outflow (Fig. 6.21c). In the inflow the fraction of particulate REE may be higher, due to sediment resuspension. Expressing concentrations as mol/km^3, which is nearly equivalent to pmol/kg, the net dissolved Ce and Nd fluxes out of the Black Sea through the Bosporus, F_{Ce} and F_{Nd}, are

$$F_{Ce} = 20.9 \times 340 - 13.3 \times 176 = 4765 \text{ mol/yr} \qquad (6.4a)$$

$$F_{Nd} = 23.7 \times 340 - 19.7 \times 176 = 4591 \text{ mol/yr} \qquad (6.4b)$$

The Bosporus inflow/outflow system is thus a net sink of dissolved Ce and Nd to the Black Sea. Vertical REE distributions at the shallow inshore Bosporus station may be dominated by local REE inputs. Local REE inputs, not originating in the Black Sea itself, do not contribute to REE exchange between the Black Sea and the Mediterranean Sea and should therefore not be included in the calculation. Upon replacing the Ce concentration in the Black Sea endmember (20.9 pmol/kg) by the Ce concentration in the CIL (16.9 pmol/kg), in order to correct for possible atmospheric input, as suggested by the high Ce concentration in the surface layer, the first term in (6.4a) is reduced by 20%, yet the result is still a net dissolved Ce flux out of the Black Sea. A similar correction for Nd hardly changes the outcome of the calculation, since the Nd concentrations in the surface layer and in the CIL are nearly equal. Consequently, the proposition of a net dissolved Ce and Nd flux out of the Black Sea can be maintained, even in case of substantial local REE inputs at the Bosporus station.

At this stage it is not possible to determine the magnitude of all fluxes that constitute a complete REE mass balance for the Black Sea. REE concentrations in rain water, contributing 129 km^3/yr to the Black Sea water balance (Sorokin, 1983), were determined by Kolesov *et al.* (1975), but, as stated before (Sect. 6.1.), these are not reliable. The inflow and outflow through the Kerch Strait, connecting the Black Sea and the Sea of Azov, is only a minor component in the Black Sea water balance and the Sea of Azov is therefore not expected to be a major source (or sink) of REE to the Black Sea. Also unknown are REE concentrations in the major rivers Danube, Dniepr and Dniestr. Frost *et al.* (1986) used a Nd concentration of about 280 pmol/kg in 'southern European rivers', in their Nd mass balance for the Mediterranean Sea.

Multiplied by the annual river discharge to the Black Sea (Sorokin, 1983), this would amount to a dissolved Nd flux of nearly 10^5 mol/yr. However, this flux may be reduced by as much as 30-100% as a result of REE removal during estuarine mixing (Elderfield *et al.*, 1990).

Even less is known about the magnitude of particulate REE fluxes. Frost *et al.* (1986) calculated a particulate Nd flux of about 10^7 mol/yr for 'southern European rivers' with about the same total annual discharge as given by Sorokin (1983) for rivers draining into the Black Sea, far exceeding the corresponding dissolved Nd flux. Inasmuch as rivers are probably the most important source of REE to the Black Sea, artificial reduction of the annual river discharge to the Black Sea, as a result of water withdrawal for hydroenergy production and agricultural purposes (Tolmazin, 1985), may have had a profound effect on the Black Sea REE mass balance. Annual discharge of the Don, Kuban, Dniepr and Dniestr rivers and hence probably their dissolved and particulate REE input had been reduced by as much as 30-50% in 1985 (Tolmazin, 1985). Accumulation of water in large storage reservoirs along the rivers, causing untimely sedimentation, may have led to further reduction of the river particulate REE input. In several publications (Murray *et al.*, 1989; Murray and Izdar, 1989; Buesseler *et al.*, 1991) it is suggested that artificial reduction of annual river discharge is responsible for recent (Sect. 6.2.1.) and possibly near-future changes in the hydrography of the Black Sea, which in turn affect REE cycling within the suboxic layer and consequently REE exchange between the surface layer and the deep water (Sect. 6.5.2.).

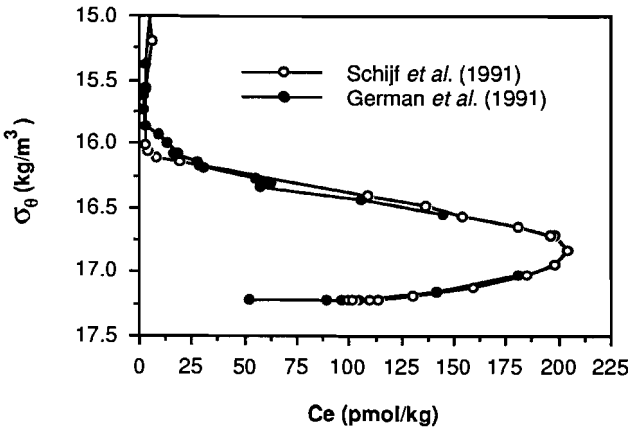

Figure 6.22. Vertical distributions of dissolved Ce at station BS3-6 (German *et al.*, 1991b) and at station BS5-2 (this work) *versus* σ_θ.

For a more detailed description of the role of vertical REE fluxes in the Black Sea REE mass balance it is imperative to subdivide the watercolumn into two or more boxes, portraying the restricted vertical mixing between the oxic surface layer and the anoxic deep water (Fonselius, 1974; Top and Clarke, 1983; Boudreau and Leblond, 1989). For instance, such a subdivision would make it possible to allow for the fact that the Bosporus is at the same time a sink of REE to the surface layer and a source of REE to the deep water. The entrainment flow causes direct transfer of REE from the surface layer to the deep water, yet the major cause of REE exchange between the surface layer and the deep water are vertical REE fluxes associated with REE cycling within the suboxic layer. Until the underlying mechanisms are thoroughly understood, reliable calculations of the magnitude of latter vertical REE fluxes cannot be made. In the mean time, some preliminary estimates of REE exchange between oxic and anoxic water are presented in the next Section.

6.5.4. The use of the vertical advection-diffusion model

It was described in Section 6.2.3. how Spencer and Brewer (1971) used a vertical advection-diffusion model to estimate the vertical fluxes of dissolved and particulate Mn in the watercolumn of the Black Sea. The striking similarity of the vertical distributions of dissolved Mn (Fig. 6.7a) and dissolved REE (Fig. 6.9) at station BS5-2 suggests that the vertical advection-diffusion model may also be used to calculate vertical fluxes of the REE. Moreover, vertical distributions of the dissolved Ce anomaly (Fig. 6.11a) and the dissolved Yb/Nd ratio (Fig. 6.12) indicate that REE removal by scavenging or precipitation of solid phases is probably insignificant below the dissolved REE maxima at 300 dbar (Sect. 6.5.1.). However, there are some restrictions to the use of the vertical advection-diffusion model, that may apply to the Black Sea. The most important is, that the vertical advection-diffusion model should not be used if there is a chance of horizontal advection (Craig, 1974), since it is strictly one-dimensional and does not allow for features in the vertical distribution of the element under consideration that can be explained in terms of horizontal processes.

The possibility of substantial horizontal advection within the upper Black Sea watercolumn is mentioned in many publications (Top and Clarke, 1983; Hay *et al.*, 1990; Kempe *et al.*, 1990; Buesseler *et al.*, 1991; Tebo, 1991). Horizontal advection is caused primarily by the inflow of Mediterranean water through the Bosporus, in combination with the general circulation pattern. Within the Bosporus, the Mediterranean water, with its relatively high temperature and salinity, entrains water from either the CIL or the warmer surface layer. Upon

reaching the Black Sea the mixture can sink to any depth and spread out across the basin, depending on the resulting density (Bogdanova, 1961). The inflow may have increased as a result of artificial reduction of the annual river discharge (Sect. 6.5.2.). Such an increase could be responsible for the formation of the suboxic layer (Murray *et al.*, 1989; Murray and Izdar, 1989; Buesseler *et al.*, 1991) as well as for the observed vertical distribution of particulate Mn (Tebo, 1991). Another potential source of horizontal advection is the Northwestern Shelf, where the coldest temperatures and low river discharge in winter result in the formation of the CIL, which spreads across the entire Black Sea basin on a timescale of about one year.

Cores of horizontally advected water may be identified from a diagram of potential temperature *versus* salinity (Θ-S diagram). The vertical advection-diffusion model curve should be fitted to the vertical distribution of the element under consideration in a region where potential temperature and salinity are linearly related (Craig, 1974). Spencer and Brewer (1971) found a linear correlation of salinity and potential temperature between salinities of 20.0 ppt and 21.9 ppt and accordingly fitted the vertical advection-diffusion curve to profiles of salinity and potential temperature in the depth interval 80-350 m. A detailed inspection of the Θ-S diagram corresponding to Figure 6.3a (not shown) reveals that a linear correlation is presently found between salinities of 20.0 ppt and 21.5 ppt equivalent to the depth interval 80-200 dbar. The lower boundary of the mixing interval has thus shifted up by about 150 m. The new mixing interval does not include the CIL, which is found at station BS5-2 between 35 and 75 dbar (Sect. 6.2.1.). Spencer and Brewer (1971) found evidence in the Θ-S diagram of a core of horizontally advected Mediterranean water at a depth of about 700 m. Although it is possible that this core has also shifted up, it probably spreads across the Black Sea at depths below 200 dbar (Sect. 6.5.3.).

Whereas the new mixing interval still, albeit barely, includes the suboxic layer and the dissolved Mn maximum, it does no longer include the dissolved REE maxima. Consequently, fitting a vertical advection-diffusion model curve to the vertical distributions of dissolved REE, in order to determine μ and J_0 in equation (6.1), is not feasible. Spencer and Brewer (1971) used equation (6.1) to calculate the downward flux of particulate Mn. However, as was discussed in Section 6.2.3., the outcome of this calculation is extremely sensitive to the value of μ, in other words even if μ and J_0 could be determined for the REE the calculation of the downward particulate REE fluxes would not be very meaningful.

On the other hand, it is possible to calculate the upward flux of dissolved REE from equation (6.2). Spencer and Brewer (1971)

estimated the values of K and ω from K/ω by assuming that the inflow of Mediterranean water through the Bosporus advects upward uniformly throughout the Black Sea (Sect. 6.2.3.). An increase of this inflow since the 1969 *Atlantis II* Cruise as a result of artificial reduction of the annual river discharge (Sect. 6.5.2.), may have led to a higher value of ω. Goyet *et al.* (1988) recently reported K/ω = 0.055 km, lower than the value of 0.09 reported by Spencer and Brewer (1971), which they surprisingly ascribed to a lower value of K. Assuming instead that the value reported by Goyet *et al.* (1988) is due to an increase of ω, an ω of 0.8 m/yr is obtained.

Upward dissolved REE fluxes will be compared with the corresponding maximum particulate REE concentrations and are therefore calculated only for those REE for which particulate concentrations were determined (Table 6.3). Average dissolved gradients between 101 dbar and 252 dbar are calculated from Table 6.2. They are 1.3 pmol kg^{-1} m^{-1}, 0.46 pmol kg^{-1} m^{-1}, 0.091 pmol kg^{-1} m^{-1} and 0.075 pmol kg^{-1} m^{-1} for Ce, Nd, Sm and Yb respectively. Maximum dissolved concentrations of Ce and Nd, occurring near 300 dbar (Fig. 6.10), were determined as part of the Black Sea mixing experiments (Chapter 7). The average of four analyses of the 300 dbar endmember is 205 pmol/kg for Ce and 80.4 pmol/kg for Nd. The 300 dbar endmember was not analyzed for Sm and Yb, yet their maximum dissolved concentrations are estimated from Figure 6.9 to be 16 pmol/kg and 17 pmol/kg respectively. Replacing d[Mn]/dz by d[REE]/dz and [Mn] by [REE] in equation (6.2), taking K = 0.014 cm^2/sec = 44 m^2/yr and ω = 0.8 m/yr and using $nmol/m^3$ rather than pmol/kg the fluxes are

$$J_{Ce} = 44 \times 1.3 + 0.8 \times 205 = 221.2 \text{ nmol } m^{-2} yr^{-1} \quad (6.5a)$$

$$J_{Nd} = 44 \times 0.46 + 0.8 \times 80 = 84.2 \text{ nmol } m^{-2} yr^{-1} \quad (6.5b)$$

$$J_{Sm} = 44 \times 0.091 + 0.8 \times 16 = 16.8 \text{ nmol } m^{-2} yr^{-1} \quad (6.5c)$$

$$J_{Yb} = 44 \times 0.075 + 0.8 \times 17 = 16.9 \text{ nmol } m^{-2} yr^{-1} \quad (6.5d)$$

Assuming that the surface area of the Black Sea at the depth of the particulate REE maxima is about 400.000 km^2, the exchange of Nd through this surface as a result of REE cycling within the suboxic layer is about $34 \cdot 10^3$ mol/yr. This may be compared to the amount of Nd transported to the deep water by the Bosporus entrainment flow. This flow was calculated in Section 6.5.3. to be 26.3 km^3/yr, carrying a dissolved Nd concentration of 23.5 mol/km^3, which amounts to a downward Nd transport of about 600 mol/yr. REE transport to the deep

water as a result of the entrainment flow is thus only 1.8% of the REE exchange between the surface layer and the deep water associated with REE cycling within the suboxic layer.

The upward dissolved REE fluxes maintain the observed standing crop of particulate REE by removal of dissolved REE at the depth of the particulate REE maxima. It is assumed here that the dissolved REE are removed completely and instantaneously. Settling of the precipitate gives rise to downward fluxes of particulate REE. The particulate REE are released at depth upon dissolution of the precipitate and maintain the observed standing crop of dissolved REE. In order to maintain stationary vertical distributions of dissolved and particulate REE, the upward dissolved REE fluxes and the downward particulate REE fluxes must be equal. Assuming this to be true and following the approach of Brewer and Spencer (1974) 'average particulate sinking rates' may be calculated, by dividing each dissolved REE flux by the corresponding maximum particulate REE concentration (Table 6.3). The resulting average particulate sinking rates are 13.2 m/yr, 15.5 m/yr, 14.4 m/yr and 20.4 m/yr for Ce, Nd, Sm and Yb respectively. Whereas the upward dissolved fluxes of Ce, Nd and Sm span more than an order of magnitude, their average particulate sinking rates are remarkably close. The average particulate sinking rate of Yb is somewhat higher, yet the assumption of complete and instantaneous removal may not be completely valid for Yb, in view of its higher degree of complexation. The average particulate sinking rates for the REE are nearly identical to the average sinking rate of particulate Mn, calculated by Brewer and Spencer (1974) to be 11 m/yr. Brewer and Spencer (1974) calculated this average particulate sinking rate by dividing the upward flux of dissolved Mn, calculated from equation (6.2), by a particulate Mn standing crop of about 1 μmol/kg. However, such high concentrations were observed only for stations close to the shelf, where the rate of Mn oxidation is probably much higher (Tebo, 1991). Except for one sample, all particulate Mn concentrations at stations near the centre of the Black Sea were below about 65 nmol/kg (Spencer *et al.*, 1972), which is much closer to the maximum concentrations presented in Table 6.1. Dividing the downward flux of dissolved Mn by this maximum particulate Mn concentration, an average particulate sinking rate of about 190 m/yr is obtained, more than an order of magnitude higher than the average sinking rate for particulate REE. On the other hand, it is still an order of magnitude lower than the value of $6 \cdot 10^{-5}$ m/s = 1900 m/yr, which was found by Sherrell (1989) for the sinking rate of freshly precipitated Mn solid phases in the open ocean (Chapter 4).

Although the calculation of average particulate sinking rates has some illustrative value, it is mechanistically meaningless. For instance, the downward particulate REE flux could be carried either by

fast-sinking particles containing a low concentration of REE or by slow-sinking particles containing a high concentration of REE. In fact, the situation is even more complicated. The particulate REE are distributed between a fine-grained precipitate, which settles extremely slowly or not at all, and large fecal pellets, which settle very fast. Buesseler *et al.* (1990) showed that ^{144}Ce, originating from the 1986 Chernobyl nuclear power station accident, was rapidly transported to great depth by scavenging onto sinking biogenic particles in the highly productive southwestern part of the Black Sea. From sediment trap experiments (Buesseler *et al.*, 1987, 1990; Hay *et al.*, 1990) it was found that these particles can attain sinking rates of up to 200 m/day. Moreover, small particles constantly aggregate to form larger particles, whereas large particles constantly disaggregate to form smaller particles (Clegg and Whitfield, 1991). Nevertheless, the fact that the average sinking rates for these four REE are nearly equal, whereas the corresponding fluxes range over more than an order of magnitude, suggests that the particulate REE maxima may be accounted for by complete removal of the upward diffusive flux of dissolved REE, resulting from the dissolved REE gradients.

Since the actual downward fluxes of particulate REE cannot be determined from the available data, a comparison with the fluxes calculated above is not possible. Spencer and Brewer (1971) found the downward flux of particulate Mn calculated from equation (6.1) to be higher than the flux calculated from equation (6.2). Brewer and Spencer (1974) explained this difference in terms of an external input of particulate REE supplied by rivers. The major part of the annual river discharge is supplied to the northwestern part of the Black Sea and the general (cyclonic) circulation pattern in the western Black Sea basin would tend to move the particulate load associated with this discharge away from station BS5-2. On the other hand, water transported toward station BS5-2 by the same circulation pattern originates in the highly productive southwestern shelf and may thus carry substantial amounts of Mn and REE, converted to the particulate form by bacterial activity (Tebo, 1991). From sediment trap experiments, the particle flux in the Black Sea was found to be highly variable, both in space and in time (Hay *et al.*, 1990). The apparent discrepancy between this high spatial and temporal variability and the excellent basinwide correlation of the lamination in recent sediments is still a subject of discussion.

6.6. Conclusions

Conclusion 1. Vertical profiles of oxygen, nitrate and sulfide are in general accordance with the sequence of oxidation reactions

associated with the decomposition of organic matter as predicted by Froelich *et al.* (1979) and Berner (1980). Mn, Fe and Ce appear to rank between nitrate and sulfate in the order of electron acceptors, yet it could not be unambiguously determined how they rank among each other. The vertical distribution of dissolved Ce seems to contradict the stoichiometries for oxidation of organic matter by CeO_2 or $Ce(OH)_4$ proposed by Elderfield and Sholkovitz (1987). The vertical distribution of particulate Mn is characterized by two maxima. The upper maximum coincides with the onset of the dissolved Mn gradient and is apparently associated with the normal cycling of Mn at oxic-anoxic interfaces. The lower maximum coincides both with the onsets of the dissolved REE gradients and with the (single) particulate REE maxima. Various lines of evidence show that Mn oxidation and REE cycling at that depth is bacterially mediated. It is uncertain whether the lower particulate Mn maximum and related phenomena are produced *in situ* or horizontally advected upon being produced near the shelf.

Conclusion 2. Various evolutionary models of the Black Sea suboxic layer are at some points inconsistent with available data. Although the model of Tebo (1991) seems at present the most promising, it cannot account for the lenticular shape of the suboxic layer. This shape can be explained with a simple evolutionary model, assuming that the suboxic layer was formed by obligate phototrophic bacteria that consume oxygen. It cannot be unambiguously demonstrated that the vertical distributions of Mn and the REE have changed since 1975, indicating that Mn cycling may not be the key factor in the formation of the suboxic layer. The apparent decoupling of REE cycling from that of Mn may be characteristic of any suboxic layer forming a transition between fully oxic and fully anoxic conditions and may not have been observed before due to the limited vertical extent of such layers in most marine anoxic basins.

Conclusion 3. REE fluxes estimated from a hydrographic model of the Bosporus and a vertical distribution of dissolved REE near the exit of the Bosporus suggest that the Bosporus is a net sink of dissolved REE to the Black Sea. At this stage it is not possible to make reliable estimates of all fluxes that constitute a complete REE mass balance for the Black Sea. Particulate and dissolved REE concentrations in rivers and rain water are as yet unknown, but preliminary estimates based on the annual river discharge and on dissolved and particulate REE concentrations in 'southern European rivers' (Frost *et al.*, 1986) suggest that rivers are a major source of REE to the Black Sea. Recent artificial changes in the magnitude and distribution of the annual discharge of some major rivers may therefore have had a profound effect on the Black Sea REE mass balance.

Conclusion 4. A complete REE mass balance for the Black Sea

should include a subdivision of the watercolumn into two or more boxes, portraying the restricted vertical mixing between the oxic, fresh, surface layer and the anoxic, more saline, deep water. Exchange of REE between 'surface box' and a 'deep water box' is caused by the Bosporus entrainment flow and by the vertical REE fluxes associated with REE cycling within the suboxic layer. Although fitting a vertical advection-diffusion curve to the vertical distribution of dissolved REE is not feasible, since the present mixing interval no longer includes the dissolved REE maxima, the upward REE flux can be estimated from (6.2). Whereas these fluxes range over more than an order of magnitude throughout the REE series, the average particulate REE sinking rates, calculated from a balance of fluxes, are nearly equal, indicating that the particulate REE maxima may be accounted for by complete removal of the upward diffusive flux of dissolved REE, resulting from the dissolved REE gradients.

Concluding remark: Very recently German *et al.* (1991b) reported vertical distributions of dissolved REE at station BS3-6, the same station for which Lewis and Landing (1991) reported the vertical distributions of dissolved Mn and Fe. A direct comparison of these vertical REE distributions with the vertical Mn distribution of Lewis and Landing (1991), who took samples from exactly the same GoFlo bottles, led German *et al.* (1991) to conclude that REE cycling takes place at the oxic-suboxic interface and is therefore not decoupled from the cycling of Mn, in agreement with the model of De Baar *et al.* (1988). They further stated that a comparison of the vertical distributions of dissolved REE at station BS5-2 with the vertical distribution of dissolved Mn at station BS3-6, as was performed by Schijf *et al.* (1991), is not appropriate, because of the different times of sampling. However, a comparison of samples collected at different stations or of samples collected at the same station at different times by plotting concentrations *versus* σ_θ is a generally accepted and oceanographically sound practice, as has convincingly been demonstrated in this Chapter (see for instance Figures 6.4a,c and 6.7c). In fact, when so compared, the vertical distribution of dissolved Ce at station BS5-2 (Fig. 6.9a) and that of German *et al.* (1991b) are remarkably similar (see Fig. 6.22 on page 213). A minor discrepancy near the top of the dissolved Ce gradient warrants further discussion, yet can at the present time only be ascribed to the dynamic nature both of the suboxic layer and of the watercolumn as a whole, especially at stations BS3-6 and BS5-2, since they were located at the boundary between the two major Black Sea gyres. This will be the subject of a future publication (Schijf *et al.*, in prep.)

CHAPTER 7 The Black Sea mixing experiments

7.1. Introduction

Over the past two decades major improvements in analytical and clean sampling techniques have led to a renewed interest in trace metal marine geochemistry. The wealth of data that has been the result of this renewed interest has greatly advanced our understanding of many aspects of trace metal marine geochemistry. In particular, an ever more detailed understanding of trace metal scavenging has encouraged marine geochemists to develop models that can reproduce and eventually even predict the effects of trace metal scavenging on the distribution and abundance of trace metals in the oceans.

REE scavenging is especially suited for modeling, since the unique properties of the REE (Chapter 2) enable its effects to be described in terms of relative abundances rather than absolute concentrations. The REE scavenging model of Byrne and Kim (1990) that was discussed in Chapter 5 has been quite successful in reproducing some prominent features of REE marine geochemistry, such as HREE enrichment and La and Gd anomalies. Nevertheless, it should be regarded only as a first step, inasmuch as it is founded exclusively on REE complexation and disregards other processes that are known to contribute to REE scavenging, notably Ce redox chemistry. The model of Byrne and Kim (1990) is an equilibrium model *i.e.* all reactions involved are implicitly assumed to occur instantaneously or at least on a timescale that is negligible with respect to the residence time of particulate matter. Although the oceanic redox chemistry of Ce is still poorly understood, studies of the oceanic redox chemistry of Mn, which has a marine chemistry very similar to that of Ce, indicate that a realistic description of Ce scavenging almost certainly calls for a kinetic model.

Many of the kinetic scavenging models that have been developed to date deal with Th scavenging (Nozaki *et al.*, 1987; Honeyman *et al.*, 1988; Clegg and Whitfield, 1991), which seems to be governed by adsorption-desorption. Jannasch *et al.* (1988) have shown the kinetics of Th adsorption to be complex, yet Clegg and Whitfield (1991) were able to construct a relatively simple kinetic scavenging model that satisfactorily reproduced the vertical distributions of dissolved and particulate concentrations of all four radioactive Th isotopes that occur in seawater, notwithstanding the fact that these isotopes derive from different sources and have half lifes ranging from tens of days to billions of years. A sensitivity study led Clegg and Whitfield (1991) to suggest that carefully planned measurements of particulate and dissolved concentrations of the same four isotopes, focussing especially on their distribution between large and small particles, may

be used to determine key kinetic parameters such as particle aggregation-disaggregation and pseudo first order Th adsorption-desorption rate constants.

For Ce, the development of a kinetic scavenging model and the determination of the necessary kinetic parameters may appear to be less straightforward than for Th. The mechanisms and kinetics of the oceanic redox chemistry of Ce are largely unknown and what little is known has mainly been inferred indirectly from studies of manganese nodules, pore waters of reducing sediments and marine anoxic basins (*e.g.* Elderfield *et al.*, 1981a,b; Elderfield and Greaves, 1981; Elderfield and Sholkovitz, 1987; De Baar *et al.*, 1988; Elderfield, 1988). More accurate estimates of Ce oxidation and reduction rates and a better understanding of the processes that set these rates can only be obtained when Ce redox chemistry is studied in the laboratory under controlled and reproducible conditions. Whereas the oceanic redox chemistry of Mn and Fe has been studied extensively in the laboratory (*e.g.* Sung and Morgan, 1981; Sunda *et al.*, 1983; Millero *et al.*, 1987b,c; Sunda and Huntsman, 1988; Tebo, 1991), a search of the literature for laboratory studies of the oceanic redox chemistry of Ce yielded only two publications, which are now briefly reviewed.

Carpenter and Grant (1967) studied the removal of radioactive ^{141}Ce, added to unfiltered and filtered coastal seawater, as a function of time, particle size and total ^{141}Ce concentration, which ranged from $7 \cdot 10^{-11}$ mol/kg to as high as $4 \cdot 10^{-7}$ mol/kg. Depending on the origin and pretreatment of the seawater, a certain fraction of the added ^{141}Ce rapidly became associated with the particulate phase. The newly formed particulate ^{141}Ce could be separated from the dissolved phase by filtration to an extent that strongly increased with decreasing poresize of the filter. Carpenter and Grant (1967) concluded the removal of Ce to be caused by adsorption rather than by the precipitation from solution of some Ce solid phase. A difference in fluorescence between Ce(III) and Ce(IV) was used to determine the effect of pH on the oxidation state of Ce added to coastal seawater. With pH increasing from 7 to 8.5 an increasing amount of the Ce, which was added as Ce(III), was oxidized and became associated with the particulate phase. Ce oxidation appeared to be inhibited by high concentrations of phosphate, which Carpenter and Grant (1967), based on the experiments of Mayer and Schwartz (1950), attributed to the formation of a strong Ce(III) phosphate complex. The experiments of Mayer and Schwartz (1950) and their interpretation in terms of an equilibrium association constant for the Ce(III) phosphate complex were discussed in Chapter 5.

Moffett (1990) reported Ce oxidation rates that were determined

by studying the removal of radioactive ^{139}Ce and ^{152}Eu (which was used as non-redox control), added to seawater from the Sargasso Sea and to coastal seawater (Vineyard Sound, MA) in amounts small enough to keep their concentrations below the natural total Ce and Eu concentrations respectively. In the Sargasso Sea seawater as well as in the coastal seawater Ce oxidation rates were found to be approximately three times lower than the corresponding Mn oxidation rates, which were determined during the same experiments, even though individual Ce oxidation rates differed by up to two orders of magnitude. In the coastal seawater Ce removal appeared to be caused more by adsorption of Ce(III) onto Mn oxides than by Ce oxidation. Moffett (1990) found the rate of Ce(III) adsorption to be much higher than that of Ce oxidation and therefore suggested that the relative contribution of latter process to Ce scavenging is probably largest in areas of low particle flux. In all experiments Ce oxidation could be eliminated by addition of sodium azide poison and was thus entirely microbially mediated. A vertical profile of Ce oxidation rates in the Sargasso Sea showed a distinct surface minimum, presumably caused by photoinhibition of Ce oxidation and possibly also by photoreduction of Ce(IV), in analogy with Mn (Sunda *et al.*, 1983; Sunda and Huntsman, 1988), which, as stated before, has a marine geochemistry very similar to that of Ce. This result suggests an alternative explanation for the large dissolved Ce maxima and positive Ce anomalies in surface waters of the Sargasso Sea reported by De Baar *et al.* (1983), which were originally explained in terms of enhanced emission of Ce(III) from nearby reducing sediments and lateral spreading of this signal over considerable distances as a result of slow Ce oxidation. On the other hand, as was already discussed in Chapter 2, vertical distributions of dissolved REE concentrations in the Sargasso Sea recently reported by Sholkovitz and Schneider (1991) and confirmed by new analyses of library samples from the original U.S. R/V *Oceanus* #86/1 cruise (Chapter 2) make the observations of De Baar *et al.* (1983) somewhat questionable.

In this final short Chapter four mixing experiments are described that were performed aboard U.S. R/V *Knorr* during the 1988 Black Sea Expedition in order to study Ce scavenging and redox chemistry in the Black Sea suboxic layer. The idea for the mixing experiments was formed only aboard the R/V and was largely inspired by the unique hydrographical and chemical conditions that were encountered in the Black Sea, in particular the presence of a broad suboxic layer (Chapter 6). Since there was no time to carefully design and prepare the mixing experiments, they have been performed in a rather improvised manner. Consequently, some possibly critical parameters such as pH and oxygen concentration may have been poorly constrained. Nevertheless, the

results lead to several valuable conclusions and are certainly interesting enough to merit discussion in a separate Chapter.

7.2. Methods

7.2.1. Sampling

The mixing experiments were performed on four consecutive days (23-26 July 1988) at station BS5-2 (Fig. 6.1). Each morning the same two seawater samples, which will hereafter be referred to as 'endmembers', were freshly collected in 30 l GoFlo bottles mounted on a CTD Rosette frame, as described in Chapter 6. One was collected at about 300 dbar, well into the anoxic water, where elevated dissolved REE concentrations were expected. In fact, this later appeared to be the depth of the dissolved REE maxima (Chapter 6). The other was collected at the depth of the particle maximum, as indicated by a distinct minimum in the light transmission profile. At that time the particle maximum was assumed to coincide with the particulate Mn maximum. However, the vertical distribution of particulate Mn concentrations reported by Lewis and Landing (1991) later revealed the presence of a larger, shallower particulate Mn maximum that is not matched by any feature in the light transmission profile. On the other hand, the particulate REE maxima do coincide with the light transmission minimum and not with the upper particulate Mn maximum (Fig. 6.8c). The depth of the particle maximum seems to have varied considerably during the period 23-26 July 1988 (see the discussion in Sect. 7.3.), yet in this Chapter it is consistently listed as ~120 dbar, while the corresponding endmember is referred to as 'the 120 dbar endmember'.

As soon as the Rosette frame was on deck, both endmembers were filtered through 0.2 μm polycarbonate membrane filters (Nuclepore, ø142 mm). Filtered 300 dbar endmember and filtered and unfiltered 120 dbar endmember were collected for REE analysis in clean 60 ml low-density PE narrow-mouth bottles and acidified to pH 2 with 100-200 μl of 3Q 6.5 N hydrochloric acid. In addition, either filtered or unfiltered 300 dbar endmember was collected in a clean 5 l low-density PE narrow-mouth bottle. The mixing experiments were performed in the reaction vessel (Fig. 7.1) described by Millero *et al.* (1987a). The reaction vessel was first rinsed and then filled with either filtered or unfiltered 120 dbar endmember, which was subsequently left to equilibrate with the atmosphere at a temperature of 25 °C for 1-1.5 hours. The 5 l low-density PE narrow-mouth bottle with the 300 dbar endmember was closed and placed in a waterbath at 25 °C for the same period of time. At t = 0 the 300 dbar endmember was mixed with the 120 dbar endmember in a ratio of about 1:3 and the reaction vessel was

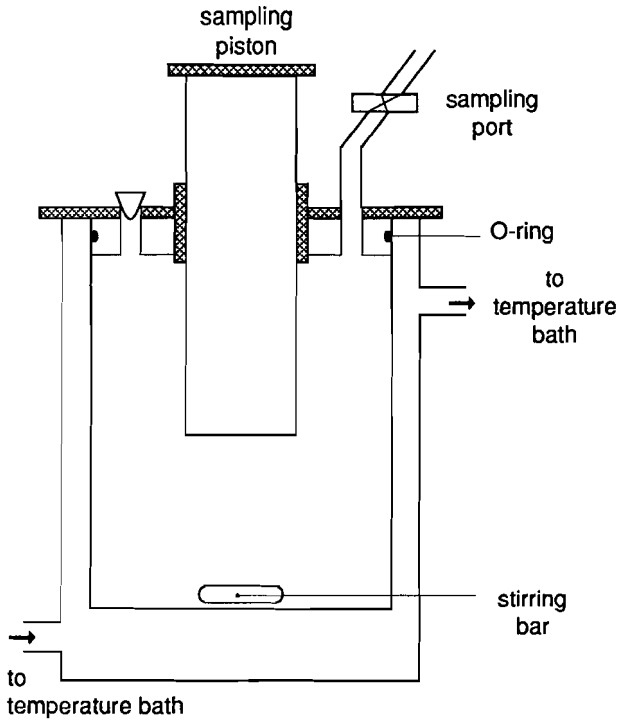

Figure 7.1. Schematic drawing of the reaction vessel, kindly provided by F.J. Millero. See Millero *et al.* (1987a) for description.

closed. Throughout each mixing experiment a constant temperature of 25 °C was maintained inside the reaction vessel and the mixture was continuously stirred with the magnetic stirring bar. Subsamples were collected through 0.2 µm polycarbonate membrane filters (Millipore Swinnex-25 disc filter holder, ø20 mm) into clean 60 ml low-density PE narrow-mouth bottles and acidified to pH 2 with 100-200 µl of 3Q 6.5 N hydrochloric acid. Roughly, subsamples were taken every 15-30 minutes for a period of 1-2 hours, then every hour for a period of 2-3 hours and finally every 2-3 hours until the end of the day. One final subsample was taken the next morning.

7.2.2. Analyses

In a clean 30 ml Teflon vial 1 ml of sample was diluted gravimetrically with 10 ml of Milli-Q water by means of an adjustable pipette, using a clean pipette tip for each sample. After dilution Mn

]concentrations were determined by GFAAS, using standard calibration curves in 3Q 0.1 N nitric acid (Chapter 4). The filtered 120 dbar endmember that was collected on 23 July 1988 was injected without dilution and the resulting Mn concentration was not corrected for matrix effects. Within the precision of the analyses (~5%) no changes in the Mn concentration with time could be resolved for any of the mixing experiments. Therefore, only endmember Mn concentrations, which are used for comparison with endmember REE concentrations (Sect. 7.3.), are presented in this Chapter; they are listed in Table 7.1.

After removing 1 ml of sample for Mn analysis each sample was weighed on an analytical balance (Sartorius 1608 MP6) and subsequently spiked with 0.03-0.05 g of REE1 spike solution. Since the samples were about 40 times smaller than the 2 l seawater samples that are normally used for REE analysis, they should have been spiked with only 0.2/40 = 0.005 g of REE1 spike solution. However, it was assumed that the weighing error for so small an amount of spike solution would probably exceed the error that results from overspiking the samples ten times (Chapter 3). After spiking, the samples were left to equilibrate for one week.

The Chelex preconcentration described in Chapter 3 was slightly modified in view of the smaller samplesize. The Chelex columns were preconditioned as described in Section 3.5.3. The samples were neutralized with 1 N ammonia solution and their pH was checked by putting a small drop of sample on a piece of non-bleeding pH-indicator paper with an adjustable pipette (Labsystems Finnpipette 4007020, 5-50 µl), using a clean pipette tip for each sample. The samples were then buffered at pH 5.7 with 400 µl of 6 N ammonium acetate buffer and their pH was checked once more. Rather than attaching the columns to the separatory funnels they were left in the rack and the samples were poured onto the resin bed in small batches directly from the sample bottles. The empty sample bottles were dried in the evaporator pots (Chapter 3) and weighed, in order to determine the exact sampleweights.

Major seasalt cations were eluted with 30 ml of 1 N ammonium acetate buffer, in six batches of 5 ml. The effluent pH was checked and if it was found to be higher than 5.5, extra 5 ml batches of 1 N ammonium acetate buffer were pipetted onto the resin bed until a pH of 5.5 or less was attained. Excess buffer was removed with 24 ml of Milli-Q water, in six batches of 4 ml. The final effluent pH was checked and usually found to be about 4.7. The REE were eluted into clean 30 ml Teflon vials with 22 ml of 3.5 N nitric acid. All further chemistry was performed exactly as described in Chapter 3. After the AG 50W-X8 separation (Sect. 3.5.4.) only the Ce-Lu fraction was kept for analysis; the La-Ce fraction was discarded.

Experiment 1:

endmember	Mn (µmol/kg)	Ce (pmol/kg)	Nd (pmol/kg)
120 dbar f	3.03	25.52	21.77
120 dbar u *	3.81	33.28	20.57
300 dbar f	8.04	202.33	79.88

Experiment 2:

endmember	Mn (µmol/kg)	Ce (pmol/kg)	Nd (pmol/kg)
120 dbar f	6.36	45.25	23.99
120 dbar u *	6.37	51.00	25.75
300 dbar f *	6.86	207.37	81.15

Experiment 3:

endmember	Mn (µmol/kg)	Ce (pmol/kg)	Nd (pmol/kg)
120 dbar f	2.39	17.23	14.17
120 dbar u *	2.87	22.28	15.87
300 dbar f *	7.07	205.02	80.53

Experiment 4:

endmember	Mn (µmol/kg)	Ce (pmol/kg)	Nd (pmol/kg)
120 dbar f *	0.025	5.03	7.60
300 dbar f *	6.82	203.74	80.15

Table 7.1. Concentrations of Mn, Ce and Nd in filtered (f) and unfiltered (u) endmembers, which were freshly collected shortly before each mixing experiment. Endmembers actually used in the mixing experiments are indicated with an asterisk (*). The unfiltered 300 dbar endmember that was used in experiment 1 was not analyzed separately.

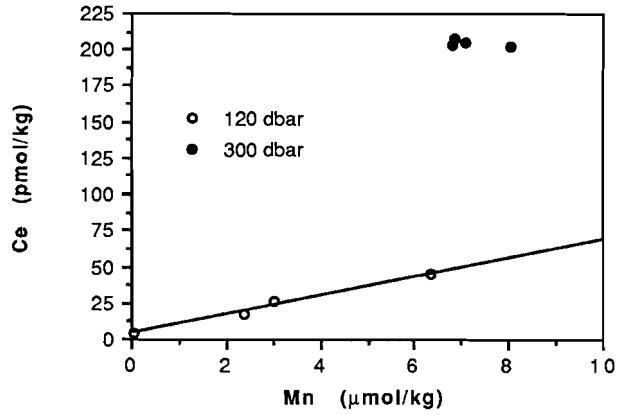

Figure 7.2. Ce concentrations *versus* Mn concentrations for filtered seawater from 120 dbar and from 300 dbar. Concentrations show a linear relation for the 120 dbar endmember, portraying the simultaneous linear variation of dissolved Ce and Mn concentrations with depth in that depth range. Below about 180 dbar, where dissolved Mn reaches its maximum concentration, the linear relation breaks down.

REE concentrations were determined by IDMS (Chapter 3). Initially it was tried to determine the concentrations of all REE (except La). It appeared that Ce and Nd concentrations could be determined for most samples, yet Sm analysis was successful for less than half of the samples while for all other REE the signals were always either too low or not stable enough to determine concentrations with acceptable accuracy and precision. The few successful Sm analyses that came out of these first attempts suggest a behaviour very similar to that of Nd (Sect. 7.3.), yet their number is not enough to justify a detailed discussion. After the first series of twelve samples no further attempts were made to analyze any REE other than Ce and Nd.

Errors in the concentrations as estimated from the statistical errors in the isotopic ratios (1σ) with the computer program REECALC (Chapter 3) are generally < 2% for Ce and < 5% for Nd. These errors are somewhat larger than normal, which is probably due to poor stability of the signals as a result of the smaller samplesize or to the overspiking of the samples. The smaller samplesize also made the blank problem, which is usually negligible when normal 2 l seawater samples are analyzed (Chapter 3), a matter of some concern. Therefore, two procedural blanks were determined as follows. Approximately 10 ml of

Milli-Q water was spiked in a clean 30 ml Teflon vial with about 0.04 g of REE1 spike solution and buffered to pH 5.7 with 400 µl of 6 N ammonium acetate buffer. The REE were extracted exactly as described above for the samples from the mixing experiments. Blank concentrations could be determined only for a few REE for reasons given above. Results were already presented in Table 3.4 as absolute amounts (in pmol). For a 50 ml sample these values amount to 6.2 pmol/kg for Ce and 1.4 pmol/kg for Nd, which is about 9% and 4% of the lowest Ce and Nd concentrations respectively. Although these blanks are not to be considered negligible they are highly irreproducible and may not be representative of the average procedural blank. Moreover, the discussion of the results of the mixing experiments (Sect. 7.3.) will focus more on reaction rates than on absolute concentrations. Since it was found that the observed reaction rates are hardly affected by the subtraction of a constant blank, the blanks were not corrected for.

7.3. Results and discussion

Ce and Nd endmember concentrations are presented in Table 7.1. Ce and Nd concentrations of the filtered 300 dbar endmember each show a total variation of only 2%, which is within the precision of the analyses. Ce and Nd concentrations of the filtered 120 dbar endmember show much larger variations, yet the Ce and Nd concentrations of the corresponding unfiltered 120 dbar endmember are always higher by about 6 pmol/kg and 1.7 pmol/kg respectively, except for experiment 1 where the Nd concentration of the unfiltered is somewhat lower than that of the filtered 120 dbar endmember. These calculated particulate Ce and Nd concentrations, which are the difference of two large numbers, are in fair agreement with the measured particulate Ce and Nd concentrations at 116 dbar presented in Table 6.3.

In Figure 7.2 it is shown that the Ce and Mn concentrations of the filtered 120 dbar endmember (Table 7.1) are positively correlated. In the 120 dbar depth range both dissolved Ce and dissolved Mn concentrations increase approximately linearly with depth (Chapter 6). From these gradients a linear relation between dissolved Ce and Mn concentrations was derived, which nearly matched the line in Figure 7.2 (not shown). The same was found for Nd. With increasing depth below 180 dbar dissolved Ce concentrations continue to increase whereas dissolved Mn concentrations remain constant or decrease slightly and the linear relation breaks down, which is why the Ce and Mn concentrations of the filtered 300 dbar endmember form a separate field in Figure 7.2.

Apparently, the four 120 dbar endmembers were collected at four

Experiment 1:

Station BS5-2, 25 July 1988
120 dbar unfiltered + 300 dbar unfiltered

t (min)	Ce (pmol/kg)	Nd (pmol/kg)
10	139.10	59.58
25	135.77	55.25
42	102.12	45.69
60	91.63	42.50
92	93.06	44.50
120	83.38	37.44
182	89.60	40.79
299	79.02	38.18
449	-	-
612	79.05	37.74
1294	106.42	49.92

Experiment 2:

Station BS5-2, 24 July 1988
120 dbar unfiltered + 300 dbar filtered

t (min)	Ce (pmol/kg)	Nd (pmol/kg)
5	(682.17)	(283.59)
18	139.06	68.35
35	115.53	53.37
51	117.91	52.58
72	86.49	41.36
96	92.23	45.73
130	70.67	35.71
191	-	-
248	85.01	40.60
307	-	-
429	93.72	44.17
552	102.31	44.52
1193	144.70	62.37

Table 7.2. Concentrations of dissolved Ce and Nd as a function of time. Each sample was collected the indicated number of minutes after the mixing of the two endmembers. Concentrations in parentheses exceed those of the 300 dbar endmember (Table 7.1),

Experiment 3:

Station BS5-2, 26 July 1988
120 dbar unfiltered + 300 dbar filtered + 20 ml formaldehyde

t (min)	Ce (pmol/kg)	Nd (pmol/kg)
18	(462.57)	(181.81)
55	119.85	53.77
84	102.26	48.14
115	87.26	36.61
143	82.92	39.87
205	75.97	-
319	86.51	41.69
503	68.83	38.02
630	95.32	47.46
1191	83.60	45.52

Experiment 4:

Station BS5-2, 23 July 1988
120 dbar filtered + 300 dbar filtered

t (min)	Ce (pmol/kg)	Nd (pmol/kg)
17	93.00	41.22
78	87.10	44.08
136	110.44	64.15
196	126.34	60.85
373	(214.10)	(86.66)
560	86.46	46.97
740	(224.85)	(89.70)
1280	116.15	43.50

probably as a result of contamination. The corresponding samples were not included in the Figures.

different depths. However, the 120 dbar endmember was always collected at the depth of the light transmission minimum (Sect. 7.2.1.) and the particulate Ce and Nd concentrations show very little variation, which together would imply that the particle maximum has shifted relative to the vertical distributions of dissolved Ce and Nd concentrations. While occupying station BS5-2 for more than one week, significant variability in the depth and intensity of the light transmission minimum was noted, most likely due to the fact that station BS5-2 was located at the boundary between the two major Black Sea gyres.

Ce and Nd concentrations of the subsamples are presented in Table 7.2 as a function of time, expressed as the number of minutes after mixing of the endmembers (t = 0). Concentrations in parentheses exceed those of the filtered 300 dbar endmember. The corresponding subsamples were regarded as contaminated and therefore not included in any of the Figures. In Figures 7.3 and 7.4 the natural logarithm of dissolved Ce and Nd concentrations is shown as a function of time.

In experiment 1 (Fig. 7.3a and 7.4a) neither of the endmembers was filtered prior to mixing. Ce and Nd concentrations decrease rapidly until a minimum is reached after about 150 minutes. Concentrations subsequently increase again at a much lower rate, a trend that still seems to continue at the end of the experiment ($t \approx 1300$). In experiment 2 (Fig. 7.3b and 7.4b) only the 300 dbar endmember was filtered prior to mixing. Ce and Nd concentrations decrease rapidly during the first 150 minutes and then slowly increase again throughout the rest of the experiment, very similar to what is observed for experiment 1. It may be assumed that the 300 dbar endmember contained much less particulate matter than the 120 dbar endmember and hence that its filtration had little effect on the concentration of particulate matter at t = 0, since the latter was collected at the depth of the particle maximum (Sect. 7.2.1.).

The initial removal and subsequent release of Ce and Nd, which will hereafter be referred to as 'reaction 1' and 'reaction 2', both

---

Opposite page: **Figure 7.3.** The natural logarithm of Ce concentrations as a function of time expressed as the number of minutes after the mixing of the two endmembers (t = 0). Dashed lines indicate endmember concentrations. Solid lines are fits to the data, except for horizontal lines which represent the mean of all data within some interval of time. Data in the intervals $0 < t < 150$ and $t > 150$ were fitted separately. a) experiment 1. b) experiment 2. c) experiment 3. d) experiment 4.

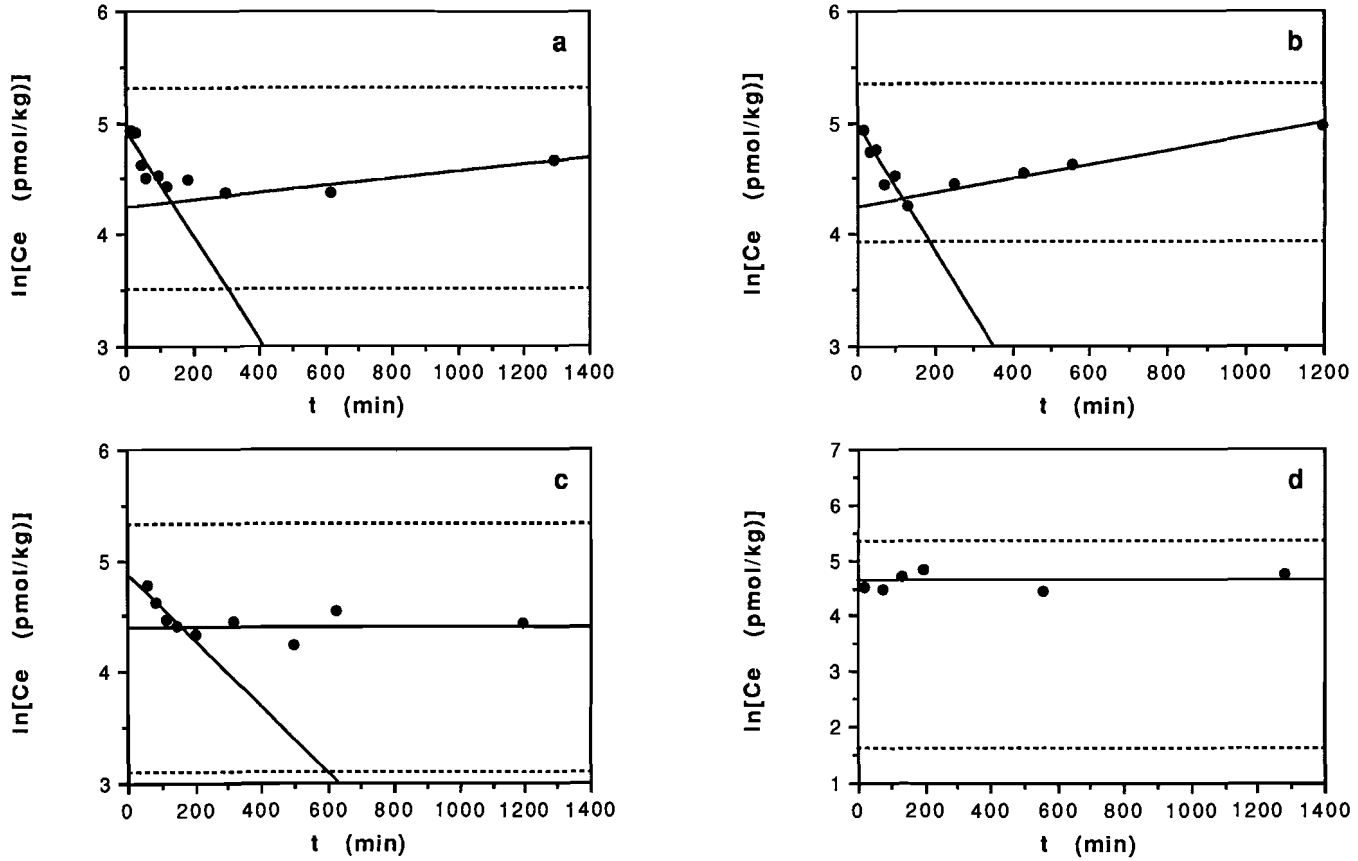
a
b
c
d
ln[Ce (pmol/kg)]
t (min)

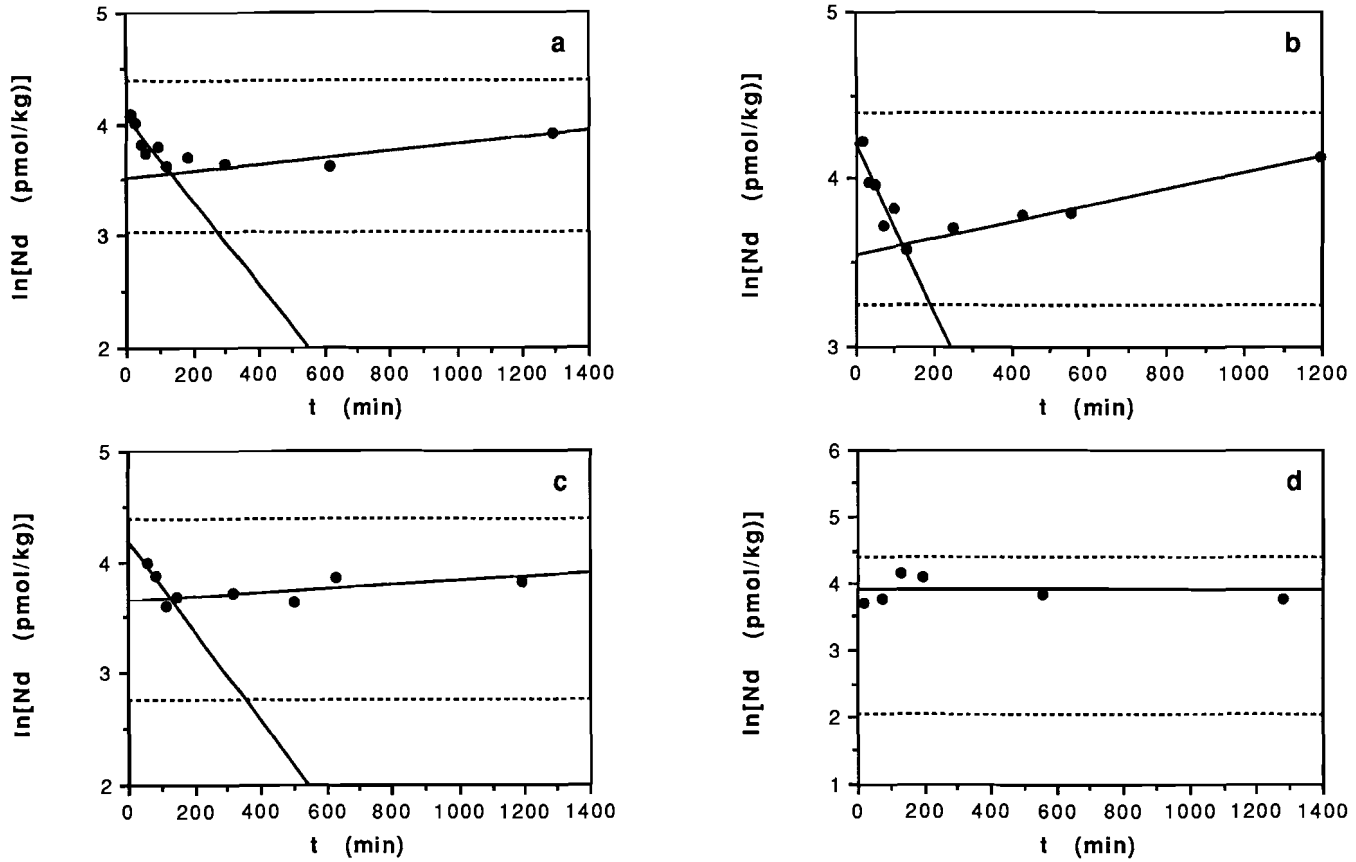

Figure 7.4. The natural logarithm of Nd concentrations as a function of time. See further Figure 7.3.

appear to be first order in concentration *i.e.* they can be described by differential equations

$$d[M]/dt = -k'_1 \times [M] \qquad (7.1a)$$

and

$$d[M]/dt = k'_2 \times [M] \qquad (7.1b)$$

respectively, where [M] are dissolved Ce or Nd concentrations and k'_1 and k'_2 are pseudo first order rate constants. The solution to such equations are functions of the form

$$[M] = [M]_0 \exp(kt) \qquad (7.2)$$

where $[M]_0$ is the dissolved Ce or Nd concentration at t = 0 and k is $-k'_1$ or k'_2. The pseudo first order rate constants k were determined from linear fits to the data in plots of ln[M] *versus* t, as shown in Figures 7.3 and 7.4. Data in the intervals $0 < t < 150$ and $t > 150$ were fitted separately to determine k'_1 and k'_2 respectively. The results are listed in Table 7.3.

Since Nd is not a redox element, its removal during reaction 1 is most likely caused by adsorption onto particulate matter. In Tables 6.1 and 7.1 it is shown that the 120 dbar endmember contained large amounts of dissolved (reduced) Mn and Fe. During equilibration of the 120 dbar endmember with the atmosphere (Sect. 7.2.1.) oxygen probably oxidized the dissolved Mn and Fe so that Mn and Fe oxides, which are known to be excellent scavengers of the REE (Wang *et al.*, 1983; Olivarez and Owen, 1989), were present at t = 0. It must be noted at this point that Mn oxidation is generally assumed to be much slower than Fe oxidation. The pseudo first order rate constants k'_1 for Ce in experiments 1 and 2 are $4.65 \cdot 10^{-3}$ min^{-1} and $5.68 \cdot 10^{-3}$ min^{-1}, or 28%/h and 34%/h, respectively (Table 7.3), almost two orders of magnitude higher than even the highest oxidation rates found by Moffett (1990). Moffett (1990) did not explicitly report Ce adsorption rates, yet he did state that "Ce(III) uptake occurs on a shorter timescale than Ce(III) oxidation." Jannasch *et al.* (1988) studied the adsorption of Th onto natural particulate matter. Using the two-reaction model of Nyffeler *et al.* (1984) they found an overall pseudo first order rate constant ($k_1 + k_{-1}$) for reversible adsorption of 6.4 day^{-1} or 27%/h, very similar to the pseudo first order rate constants k'_1 for Ce in experiments 1 and 2. The removal of both Ce and Nd during reaction 1 is probably largely caused by adsorption onto Mn or Fe oxides. The pseudo first order rate constant k'_1 is 24% and 12% higher for Ce than for Nd in experiments 1 and 2

	Ce	Nd
Experiment 1:		
k'_1 (min^{-1})	$4.65 \cdot 10^{-3}$	$3.75 \cdot 10^{-3}$
k'_2 (min^{-1})	$3.21 \cdot 10^{-4}$	$2.92 \cdot 10^{-4}$
Experiment 2:		
k'_1 (min^{-1})	$5.68 \cdot 10^{-3}$	$5.04 \cdot 10^{-3}$
k'_2 (min^{-1})	$6.30 \cdot 10^{-4}$	$4.93 \cdot 10^{-4}$
Experiment 3:		
k'_1 (min^{-1})	$2.96 \cdot 10^{-3}$	$4.01 \cdot 10^{-3}$
k'_2 (min^{-1})	0	$1.78 \cdot 10^{-4}$
Experiment 4:		
k'_1 (min^{-1})	0	0
k'_2 (min^{-1})	0	0
Experiments 1 and 2 combined:		
k'_{Ce} (min^{-1})	$5.26 \cdot 10^{-3}$	
k'_{Nd} (min^{-1})		$4.51 \cdot 10^{-3}$

Table 7.3. Pseudo first order rate constants for the initial removal (k'_1) and subsequent release (k'_2) of Ce and Nd. k'_1 and k'_2 were determined from linear fits to the data for $0 < t < 150$ and $t > 150$ respectively, as shown in Figures 7.3 and 7.4. Constants equal to zero correspond to the horizontal lines in latter Figures, which are not fits to the data. k'_{Ce} and k'_{Nd} were determined as described in the text.

respectively (Table 7.3), which may be due to their different degree of complexation, causing Ce to be scavenged more effectively than Nd (Chapter 2), or to Ce oxidation. Moreover, the pseudo first order rate constant k'_1 is 22% and 34% higher in experiment 2 than in experiment 1 for Ce and Nd respectively. The latter may be due to the high concentration of Mn (and probably also of Fe) in the 120 dbar endmember of experiment 2, leading to a larger amount of Mn and Fe

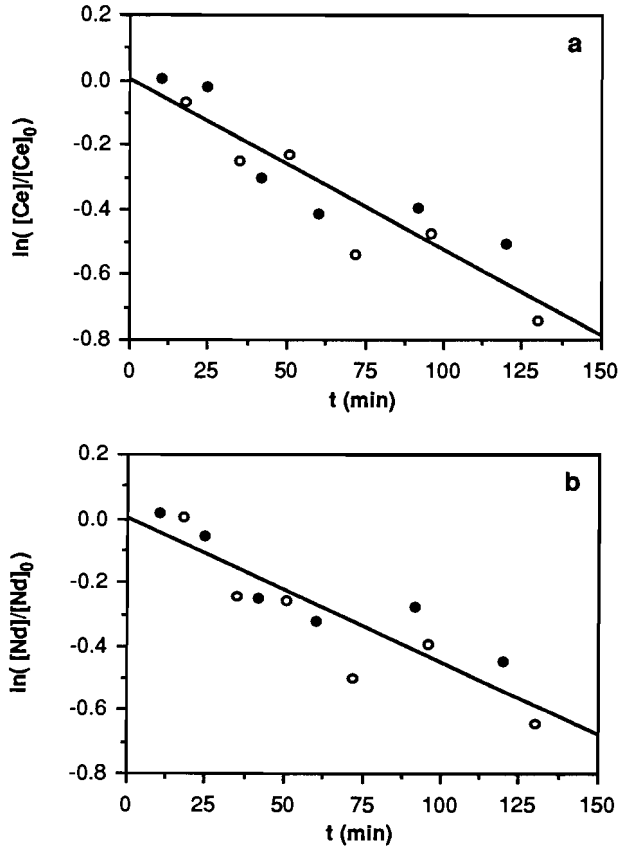

Figure 7.5. The natural logarithm of Ce (a) and Nd (b) concentrations, normalized to Ce and Nd concentrations at t = 0, as a function of time in the interval 0 < t < 150. Data from experiments 1 (solid symbols) and 2 (open symbols) combined. Solid lines are fits to the data.

oxides at t = 0, although this cannot be verified with the available data.

On the other hand, standard deviations of all pseudo first order rate constants k'_1 in experiments 1 and 2 are about 20% (1σ), which means that the aforementioned differences are less significant than they may seem at first. Therefore, in Figure 7.5 the natural logarithm of Ce and Nd concentrations is shown again as a function of time in the interval 0 < t < 150, combining data from both experiments. In order to make a valid comparison, Ce and Nd concentrations were normalized to

$[Ce]_0$ and $[Nd]_0$, the Ce and Nd concentrations at t = 0, which were determined from the linear fits in Figures 7.3a,b and 7.4a,b. The data in Figures 7.5a and b can be described by differential equations of the form

$$d[M]_n/dt = -k \times [M]_n \qquad (7.3)$$

where $[M]_n = [M]/[M]_0$ are normalized Ce or Nd concentrations and k is k'_{Ce} or k'_{Nd} respectively. Latter constants were determined as before and are listed in Table 7.3. The pseudo first order rate constant k'_{Ce} is now 16% higher than k'_{Nd}, yet standard deviations are about 15% (1σ), so the difference is still not very significant. The similarity of k'_{Ce} and k'_{Nd} suggests that Ce removal during reaction 1 is largely caused by adsorption onto particulate matter and that Ce oxidation plays only a minor role, in agreement with what was found by Moffett (1990) in coastal seawater from Vineyard Sound, MA (Sect. 7.1.). This result may be compared with the relative turnover rates that were derived by De Baar *et al.* (1988) from dissolved Ce and Nd gradients at the oxic-anoxic interface of the Cariaco Trench. They found the ratio of Ce and Nd turnover rates to be 6.4 : 2.4 = 2.7 : 1, clearly higher than the ratio 1.2 : 1 of k'_{Ce} and k'_{Nd}, and attributed the relatively high Ce turnover rate to Ce redox chemistry.

The apparently sudden release of Ce and Nd after 2.5 hours (reaction 2) is most intriguing. It is about an order of magnitude slower than the initial removal of Ce and Nd (Table 7.3). Like the k'_1, the pseudo first order rate constants k'_2 are larger for Ce than for Nd and larger in experiment 2 than in experiment 1. Although the standard deviations of the k'_2 in experiment 1 are large because of the limited number of datapoints for t > 150 (n = 3, t = 182 was rejected), the differences seem to be more significant than for k'_1.

Release after initial removal was also reported for Mn by Tebo (1991), who performed experiments to determine Mn oxidation rates during Leg 3 of the 1988 Black Sea Expedition. At depths of 72 and 76 m (σ_θ = 15.52 and 15.65 respectively) at station BS3-6, the same location as station BS5-2 (Chapter 6), and in the absence of oxygen, he found initial rapid removal of the ^{54}Mn tracer, followed after 2.5 hours by slower release back into solution. Tebo (1991) attributed the initial removal to exchange of $^{54}Mn(II)$ with Mn(II) bound to surfaces and the subsequent release to dissolution of Mn solid phases, possibly manganate(III,IV) minerals. However, it is not likely that either of the endmembers in experiments 1 and 2 contained any soluble REE minerals, nor that such minerals were formed before or during the experiments, so the explanation of Tebo (1991) does not apply to Ce and Nd. Since Nd is not a redox element its release during reaction 2 can only be caused

by dissolution of the Mn or Fe oxides onto which it was initially adsorbed. Luther *et al.* (1991) and Millero (1991) independently suggested that Mn and Fe oxides are important oxidants of sulfide in the Black Sea. At t = 0 sulfide is introduced together with the 300 dbar endmember, which contains about 100 μM, to a final concentration of about 25 μM. Alternatively, throughout the suboxic layer Nealson *et al.* (1991) found several species of bacteria capable of reducing both Mn and Fe oxides. Especially abundant at the depth of the particle maximum was the species *Shewanella putrefaciens*, which displays a remarkable respiratory versatility *i.e.* it can use a variety of electron acceptors for the oxidation of organic matter, including oxygen, nitrate, nitrite, Mn oxides and Fe oxides. These bacteria may well have been present in the (unfiltered) 120 dbar endmember.

Whether sulfide or bacteria were the cause, reduction of Mn and Fe may have commenced directly upon mixing and in case of the bacteria even before mixing. Apparently this did not initially interfere with the adsorption of Ce and Nd. Presumably the rate of Ce and Nd adsorption is so much higher than that of Mn and Fe reduction, that any Ce or Nd released by the dissolution of Mn or Fe oxides was immediately readsorbed, until 2.5 hours after mixing the amount of Mn or Fe oxides became too small for the adsorption of Ce and Nd to continue. Consequently, further dissolution of Mn or Fe oxides caused Ce and Nd to be released at a rate that was controlled by the rate of Mn or Fe reduction. If the reduction of Mn and Fe was microbially mediated some alternative explanations come to mind. Possibly, before starting on the Mn or Fe oxides the bacteria preferred some other oxidant that became exhausted 2.5 hours after mixing, or they suffered a thermal shock from which they needed until 2.5 hours after mixing to recover, or again their activity was triggered 2.5 hours after mixing by a certain combination of conditions that was brought about by reaction 1. To determine whether the reduction of Mn and Fe was microbially mediated or abiotical, experiment 2 was repeated with addition at t = 0 of 20 ml formaldehyde (final concentration 0.7%), which is an inhibitor of microbial activity.

Although experiment 3 is a repetition of experiment 2, it is best to be compared with experiment 1, in view of the possibility that the rates of Ce and Nd removal during reaction 1 are related to the concentrations of dissolved Mn or Fe in the 120 dbar endmember (Table 7.1). Formaldehyde was not added until t = 0 and therefore cannot have affected the formation of Mn or Fe oxides during equilibration of the 120 dbar endmember with the atmosphere. The pseudo first order rate constants k'_1 in experiment 3 (Table 7.3) show that the rate of Ce removal is inhibited by about 35% in the presence of formaldehyde, whereas the removal of Nd is not affected at all. If the reduction of Mn

and Fe was microbially mediated then it must have been inhibited by formaldehyde. However, formaldehyde may also have interfered directly with the solution chemistry of Mn. Rosson *et al.* (1984) found that 2% formaldehyde causes 44% desorption of ^{54}Mn tracer from Mn oxide (δMnO_2) after 1 hour and that 3.7% formaldehyde causes 7% dissolution of the same Mn oxide after 30 minutes. Moreover, as was argued before, the rate of Ce and Nd removal during reaction 1 is controlled by the rate of Ce and Nd adsorption rather than by the rate of Mn or Fe reduction. Therefore, the fact that the removal of Nd was not inhibited by formaldehyde does not necessarily indicate that Mn and Fe reduction, microbially mediated or otherwise, did not occur during reaction 1. On the other hand, the removal of Ce does seem to have been inhibited by formaldehyde. There is no reason why the removal of Ce should be inhibited more strongly than that of Nd, unless it is caused for a considerable part by microbially mediated Ce oxidation. Since the results of experiments 1 and 2 show that Ce oxidation hardly contributed to Ce removal at all and certainly did not account for 35%, it must be assumed that the difference is not statistically significant, or that the k'_1 of Ce in experiment 3 is an analytical artefact.

The pseudo first order rate constants k'_2 (Table 7.3) show that the rate of Nd release is inhibited by about 40% in the presence of formaldehyde, while that of Ce is completely eliminated ($k'_2 = 0$), as indicated by the horizontal line in Figure 7.3c. Since the rate of Ce and Nd release during reaction 2 is controlled by the rate of Mn or Fe reduction, the inhibition of Ce and Nd release indicates that Mn and Fe reduction are inhibited and therefore, at least for a major part, microbially mediated. Again, it is not clear why the release of Ce is more strongly inhibited than that of Nd.

The purpose of experiment 4, where both endmembers were filtered prior to mixing, was to test the importance of particulate matter. However, the interpretation of the results is complicated by the low concentrations of dissolved Mn and Fe in the 120 dbar endmember (Table 7.1). Neither reaction 1 nor reaction 2 seems to occur ($k'_1 = k'_2 = 0$), as signified by the horizontal lines in Figures 7.3d and 7.4d. The concentrations of dissolved Mn and Fe in the filtered 120 dbar endmember are 25 nM (Table 7.1) and about 5 nM (Table 6.1) respectively, which is more than two orders of magnitude lower than in any of the other experiments. Even if all this Mn and Fe was oxidized during equilibration with the atmosphere, the amount of Mn and Fe oxides at t = 0 may have been too low for adsorption of Ce and Nd to occur at any rate. It was suggested above that the microbial activity causing reaction 2 may have been triggered by certain solution conditions that were brought about by reaction 1. In that case, reaction

2 simply did not occur because these solution conditions failed to be created.

On the other hand, the concentrations of dissolved Mn and Fe in the filtered 120 dbar endmember are about three orders of magnitude higher than the concentrations of dissolved Ce and Nd at t = 0. It could therefore be argued that reactions 1 and 2 would still have occurred as in experiments 1 and 2, had not both endmembers been filtered. Filtration of the 120 dbar endmember may have removed the Mn and Fe reducing bacteria that were presumably present in the other three experiments. This would strongly inhibit, if not eliminate, reaction 2, yet it would not affect reaction 1, which after all is merely abiotical adsorption of Ce and Nd onto Mn and Fe oxides. In that case, the fact that reaction 1 does not occur indicates that the oxidation of Mn or Fe during equilibration with the atmosphere is also microbially mediated or otherwise requires the presence of particulate matter.

Unfortunately, a fair comparison between experiment 4 and the other three experiments cannot really be made and it is difficult to decide whether the absence at t = 0 of Mn and Fe oxides, or of particulate matter and bacteria causes reaction 1 and 2 not to occur.

7.4. Conclusions

Conclusion 1. The results presented in this Chapter show that the IDMS method is sensitive enough to determine Ce and Nd concentrations, comparable to those found in the anoxic water of the Cariaco Trench (De Baar *et al.*, 1988), in seawater samples as small as 60 ml, with acceptable accuracy and precision. Consequently, laboratory experiments that study REE scavenging or the oceanic redox chemistry of Ce (using Nd as non-redox control) can be performed within the natural range of REE concentrations without the need for radiotracers or very large samples.

The remaining conclusions strictly pertain to the results of the mixing experiment described in this Chapter.

Conclusion 2. Ce oxidation hardly contributed to the removal of Ce, in agreement with the results of Moffett (1990) for coastal seawater from Vineyard Sound, MA. Ce removal rates are almost two orders of magnitude higher than the highest Ce oxidation rates reported by Moffett (1990) and very similar to Nd removal rates, which strongly points towards adsorption onto particulate matter as the major mechanism for Ce removal.

Conclusion 3. The initial removal of Ce and Nd seems to have been governed by adsorption onto Mn or Fe oxides, which were probably

formed during equilibration of the 120 dbar endmember with the atmosphere before mixing. Differences in the Ce and Nd removal rates between the various experiments seem to be related to the concentrations of dissolved Mn and Fe in the 120 dbar endmember (the experiment with the lowest initial concentrations showed no removal whatsoever). Apparently, the rate of Ce and Nd adsorption is determined by the amount of Mn or Fe oxides present at t = 0. Unfortunately, the differences are not always statistically significant.

Conclusion 4. The release of Ce and Nd is most likely the result of reductive dissolution of the Mn or Fe oxides onto which they were initially adsorbed. The reduction of Mn and Fe may have been caused by oxidation of sulfide, which is introduced together with the 300 dbar endmember, or it may be mediated by Mn and Fe reducing bacteria, which may have been present in the (unfiltered) 120 dbar endmember. The fact that the release of Ce and Nd is inhibited in the presence of formaldehyde strongly suggests that reduction of Mn and Fe is largely microbially mediated. Sulfide and probably also Mn and Fe reducing bacteria are present at t = 0, so that reduction of Mn and Fe may commence directly upon and possibly even before mixing. Presumably the rate of Ce and Nd adsorption is so much higher than that of Mn and Fe reduction, that any Ce or Nd released by the dissolution of Mn or Fe oxides was immediately readsorbed, until 2.5 hours after mixing the amount of Mn or Fe oxides became too small for the adsorption of Ce and Nd to continue.

References

Addy S.K., and E.W. Behrens. (1980). Time of accumulation of hypersaline anoxic brine in Orca Basin (Gulf of Mexico), Marine Geology, 37, 241-252.

Anonymus. (1986). A gas bleed system for thermal ionisation mass spectrometers, VG Isotopes Technical Information, pjw7 02.685.

Bacon M.P. (1988). Tracers of chemical scavenging in the oceans: boundary effects and large-scale chemical fractionation, Philopsophical Transactions of the Royal Society of London, A325, 147-160.

Baes Jr. C.F. and R.E. Mesmer. (1981). The thermodynamics of cation hydrolysis, American Journal of Science, 281, 935-962.

Balistrieri L.S. and J.W. Murray. (1984). Marine scavenging: trace metal adsorption by interfacial sediment from MANOP Site H, Geochimica et Cosmochimica Acta, 48, 921-929.

Balistrieri L.S., P.G. Brewer and J.W. Murray. (1981). Scavenging residence times of trace metals and surface chemistry of sinking particles in the deep ocean, Deep-Sea Research, 28A, 101-121.

Banner J.L., G.N. Hanson and W.J. Meyers. (1988). Rare earth element and Nd isotopic variations in regionally extensive dolomites from the Burlington-Keokuk Formation (Mississippian): implications for REE mobility during carbonate diagenesis, Journal of Sedimentary Petrology, 58, 415-432.

Berner R.A. (1980). Early diagenesis - A theoretical approach. In H.D. Holland (Ed.), Princeton Series in Geochemistry, 241 pp, Princeton University Press, Princeton, New Jersey.

Béthoux J.-P. (1980). Mean water fluxes across sections in the Mediterranean Sea, evaluated on the basis of water and salt budgets and of observed salinities, Oceanologica Acta, 3, 79-88.

Béthoux J.-P., P. Courau, E. Nicolas and D. Ruiz-Pino. (1990). Trace metal pollution in the Mediterranean Sea, Oceanologica Acta, 13 (4), 481-488.

Bogdanova A.K. (1961). The distribution of Mediterranean waters in the Black Sea, Deep-Sea Research, 10, 665-672.

Boldrin A. and S. Rabitti. (1990). Hydrography of the brines in the Bannock and Tyro anoxic basins (eastern Mediterranean), Marine Chemistry, 31, 21-33.

Boudreau B.P. and P.H. Leblond. (1989). A simple evolutionary model for water and salt in the Black Sea, Paleoceanography, 4 (2), 157-166.

Boyle E.A., S.D. Chapnick, X.X. Bai and A. Spivack. (1985). Trace metal enrichments in the Mediterranean Sea, Earth and Planetary Science Letters, 74, 405-419.

Bregant D., G. Catalano, G. Civitarese and A. Luchetta. (1990). Some chemical characteristics of the brine in Bannock and Tyro Basins: salinity, sulphur compounds, Ca^{2+}, F^-, pH, A_t, PO_4^{3-}, SiO_2, NH_3, Marine Chemistry, 31, 35-62.

Brewer P.G. and D.W. Spencer. (1974). Distribution of some trace elements in Black Sea and their flux between dissolved and particulate phases. In E.T. Degens and D.A. Ross (Ed.), The Black Sea - Geology, Chemistry, and Biology, 137-143, American Association of Petroleum Geologists, Tulsa, Oklahoma.

Brewer P.G. and J.W. Murray. (1973). Carbon, nitrogen and phosphorus in the Black Sea, Deep-Sea Research, 20, 803-818.

Broenkow W.W. and J.D. Cline. (1969). Colorimetric determination of dissolved oxygen at low concentrations, Limnology and Oceanography, 14, 450-454.

Brookins D.G. (1989). Aqueous geochemistry of rare earth elements. In B.R. Lipin and G.A. McKay (Ed.), Geochemistry and mineralogy of rare earth elements. Reviews in Mineralogy, 21, 201-225, The Mineralogical Society of America, Washington, D.C.

Brooks J.M., D.A. Wiesenburg, H. Roberts, R.S. Carney, I.R. MacDonald, C.R. Fisher, N.L. Guinasso Jr., W.W. Sager, S.J. MacDonald, R.A. Burke Jr., P. Aharon and T.J. Bright. (1990). Salt, seeps and symbiosis in the Gulf of Mexico - A preliminary report of

deepwater discoveries using DSV *Alvin*, EOS Transactions of the American Geophysical Union, 71 (45), 1772-1773.
Bruland K.W. (1989). Complexation of zinc by natural organic ligands in the central North Pacific, Limnology and Oceanography, 34 (2), 269-285.
Bruland K.W. (1983). Trace elements in sea-water. In J.P. Riley and R. Chester (Ed.), Chemical Oceanography, 2nd ed., Vol. 8, 157-220, Academic Press, London.
Bruland K.W., R.P. Franks, G.A. Knauer and J.H. Martin. (1979). Sampling and analytical methods for the determination of copper, cadmium, zinc, and nickel at the nanogram per liter level in sea water, Analytica Chimica Acta, 105, 233-245.
Buat-Ménard P., J. Davies, E. Remoudaki, J.C. Miquel, G. Bergametti, C.E. Lambert, U. Ezat, C. Quetel, J. la Rosa and S.W. Fowler. (1989). Non-steady-state biological removal of atmospheric particles from Mediterranean waters, Nature, 340, 131-134.
Buesseler K.O., H.D. Livingston and S.A. Casso. (1991). Mixing between oxic and anoxic waters of the Black Sea as traced by Chernobyl cesium isotopes. In J.W. Murray (Ed.), Black Sea Oceanography - Results from the 1988 Black Sea Expedition. Deep-Sea Research, 38 (2A), S725-S745.
Buesseler K.O., H.D. Livingston, S. Honjo, B.J. Hay, T. Konuk and S. Kempe. (1990). Scavenging and particle deposition in the southwestern Black Sea - evidence from Chernobyl radiotracers, Deep-Sea Research, 37 (3), 413-430.
Buesseler K.O., H.D. Livingston, S. Honjo, B.J. Hay, S.J. Manganini, E. Degens, V. Ittekkot, E. Izdar and T. Konuk. (1987). Chernobyl radionuclides in a Black Sea sediment trap, Nature, 329, 825-828.
Burrell D.C. (1965). The determination of nickel and cobalt in natural waters by atomic absorption spectrophotometry: a preliminary study, Atomic Absorption Newsletter, 4, 309-311.
Byrne R.H., J.H. Lee and L.S. Bingler. (1991). Rare earth element complexation by PO_4^{3-} ions in aqueous solution, Geochimica et Cosmochimica Acta, 55, 2729-2735.
Byrne R.H. and K.-H. Kim. (1990). Rare earth element scavenging in seawater, Geochimica et Cosmochimica Acta, 54, 2645-2656.
Byrne R.H. and L.S. Bingler. (1989). Comment on "Cerium: a chemical tracer for paleo oceanic redox conditions" by Y.-G. Liu, M.R.U. Miah and R.A. Schmitt, Geochimica et Cosmochimica Acta, 53, 1475-1476.
Byrne R.H., L.R. Kump and K.J. Cantrell. (1988). The influence of temperature and pH on trace metal speciation in seawater, Marine Chemistry, 25, 163-181.
Camerlenghi A. (1990). Anoxic basins of the eastern Mediterranean: geological framework, Marine Chemistry, 31, 1-19.
Cantrell K.J. and R.H. Byrne. (1987a). Rare earth element complexation by carbonate and oxalate ions, Geochimica et Cosmochimica Acta, 51, 597-605.
Cantrell K.J. and R.H. Byrne. (1987b). Temperature dependence of europium carbonate complexation, Journal of Solution Chemistry, 16 (7), 555-566.
Carpenter J.H. (1965). The Chesapeake Bay Institute technique for the Winkler dissolved oxygen method, Limnology and Oceanography, 10, 141-143.
Carpenter J.H. and V.E. Grant. (1967). Concentration and state of cerium in coastal waters, Journal of Marine Research, 25, 228-238.
Christell R., S. Forberg and T. Westermark. (1961). Some experiments on the use of the chelating ion exchanger Dowex A-1 in nuclear chemistry, Journal of Inorganic & Nuclear Chemistry, 19, 187-189.
Clegg S.L. and M. Whitfield. (1991). A generalized model for the scavenging of trace metals in the open ocean - II. Thorium scavenging, Deep-Sea Research, 38 (1), 91-120.
Coale K.H. and K.W. Bruland. (1988). Copper complexation in the Northeast Pacific, Limnology and Oceanography, 33 (5), 1084-1101.
Condie K.E. (1991). Another look at rare earth elements in shales, Geochimica et Cosmochimica Acta, 55, 2527-2531.
Copin-Montegut G., P. Courau and E. Nicolas. (1986). Distribution and transfer of trace elements in the western Mediterranean, Marine Chemistry, 18, 189-195.

Corselli C. and F.S. Agib. (1987). Brine formation and gypsum precipitation in the Bannock Basin, eastern Mediterranean, Marine Geology, 75, 185-199.
Craig H. (1974). A scavenging model for trace elements in the deep sea, Earth and Planetary Science Letters, 23, 149-159.
Crookes W. (1887). Genesis of the elements, The Chemical News and Journal of Physical Science, 55, 83-99.
David F. (1991). Recent advances in the thermodynamics of trivalent actinides, in press.
De Baar H.J.W. (1991). On cerium anomalies in the Sargasso Sea, Geochimica et Cosmochimica Acta, 55, 2981-2983.
De Baar H.J.W. (1983). The marine geochemistry of the rare earth elements, Ph.D. Thesis, 278 pp, Woods Hole Oceanographic Institution.
De Baar H.J.W., J. Schijf and R.H. Byrne. (1991). Solution chemistry of the rare earth elements in seawater, European Journal of Solid State and Inorganic Chemistry, 28, 357-373.
De Baar H.J.W., C.R. German, H. Elderfield and P. van Gaans. (1988). Rare earth element distributions in anoxic waters of the Cariaco Trench, Geochimica et Cosmochimica Acta, 52, 1203-1219.
De Baar H.J.W., P.M. Saager and J.T.M. de Jong. (1987). Dissolved Mn in the east Mediterranean and its hypersaline anoxic basins, EOS Transactions of the American Geophysical Union, 68, 199-200.
De Baar H.J.W., M.P. Bacon, P.G. Brewer and K.W. Bruland. (1985a). Rare earth elements in the Pacific and Atlantic Oceans, Geochimica et Cosmochimica Acta, 49, 1943-1959.
De Baar H.J.W., P.G. Brewer and M.P. Bacon. (1985b). Anomalies in rare earth distributions in seawater: Gd and Tb, Geochimica et Cosmochimica Acta, 49, 1961-1969.
De Baar H.J.W., M.P. Bacon and P.G. Brewer. (1983). Rare-earth distributions with a positive Ce anomaly in the western North Atlantic Ocean, Nature, 301, 324-327.
De Domenico M. and E. De Domenico. (1989). Bannock Basin: first approach to water microbiology. In M.B. Cita, A. Camerlenghi and C. Corselli (Ed.), Anoxic basins of the eastern Mediterranean. Results of the third conference. Bergamo (Italy) December 14-16 1988. Ricerca scientifica ed educazione permanente, 72, 100-101, Università degli studi di Milano. Dipartimento di scienze della terra.
Degens E.T. and D.A. Ross (Ed.). (1969). Hot brines and recent heavy metal deposits in the Red Sea, 600 pp, Springer-Verlag, Berlin.
De Lange G.J., J.J. Middelburg, C.H. van der Weijden, G. Catalano, G.W. Luther III, D.J. Hydes, J.R.W. Woittiez and G.P. Klinkhammer. (1990a). Composition of anoxic hypersaline brines in the Tyro and Bannock Basins, eastern Mediterranean, Marine Chemistry, 31, 63-88.
De Lange G.J., N.A.I.M. Boelrijk, G. Catalano, C. Corselli, G.P. Klinkhammer, J.J. Middelburg, D.W. Müller, W.J. Ullman, P. van Gaans and J.R.W. Woittiez. (1990b). Sulphate-related equilibria in the hypersaline brines of the Tyro and Bannock Basins, eastern Mediterranean, Marine Chemistry, 31, 89-112.
De Lange G.J., G. Catalano, G.P. Klinkhammer and G.W. Luther III. (1990c). The interface between oxic seawater and the anoxic Bannock brine; its sharpness and the consequences for the redox-related cycling of Mn and Ba, Marine Chemistry, 31, 205-217.
De Lange G.J. and H.L. ten Haven. (1983). Recent sapropel formation in the eastern Mediterranean, Nature, 305, 797-798.
Derry L.A. and S.B. Jacobsen. (1990). The chemical evolution of Precambrian seawater: evidence from REEs in banded iron formations, Geochimica et Cosmochimica Acta, 54, 2965-2977.
Deuser W.G. (1975). Reducing environments. In J.P. Riley and G. Skirrow (Ed.), Chemical Oceanography, 2nd ed., Vol. 3, 1-37, Academic Press, London.
Deuser W.G. (1970). Carbon-13 in Black Sea waters and implications for the origin of hydrogen sulfide, Science, 168, 1575-1577.

Dittmar W. (1884), Report on the scientific results of the exploring voyage of H.M.S. Challenger, Vol. 1, H.M. Stationery Office, London.
Elderfield H. (1988). The oceanic chemistry of the rare-earth elements, Philosophical Transactions of the Royal Society of London, A325, 105-126.
Elderfield H., R. Upstill-Goddard and E.R. Sholkovitz. (1990). The rare earth elements in rivers, estuaries, and coastal seas and their significance to the composition of ocean waters, Geochimica et Cosmochimica Acta, 54, 971-991.
Elderfield H. and E.R. Sholkovitz. (1987). Rare earth elements in the pore waters of reducing nearshore sediments, Earth and Planetary Science Letters, 82, 280-288.
Elderfield H. and M.J. Greaves. (1983). Determination of the rare earth elements in sea water. In C.S. Wong, E. Boyle, K.W. Bruland, J.D. Burton and E.D. Goldberg (Ed.), Trace Metals in Sea Water, 427-445, Plenum Press, New York.
Elderfield H. and M.J. Greaves. (1982). The rare earth elements in seawater, Nature, 296, 214-219.
Elderfield H. and M.J. Greaves. (1981). Negative cerium anomalies in the rare earth element patterns of oceanic ferromanganese nodules, Earth and Planetary Science Letters, 55, 163-170.
Elderfield H., C.J. Hawkesworth, M.J. Greaves and S.E. Calvert. (1981a). Rare earth element geochemistry of oceanic ferromanganese nodules and associated sediments, Geochimica et Cosmochimica Acta, 45, 513-528.
Elderfield H., C.J. Hawkesworth, M.J. Greaves and S.E. Calvert. (1981b). Rare earth element zonation in Pacific ferromanganese nodules, Geochimica et Cosmochimica Acta, 45, 1231-1234.
Emerson S., R.E. Cranston and P.S. Liss. (1979). Redox species in a reducing fjord: equilibrium and kinetic considerations, Deep-Sea Research, 26A, 859-878.
Erba E. (1989). New findings of gelatinous pellicles from the anoxic Bannock and Tyro Basins. In M.B. Cita, A. Camerlenghi and C. Corselli (Ed.), Anoxic basins of the eastern Mediterranean. Results of the third conference. Bergamo (Italy) December 14-16 1988. Ricerca scientifica ed educazione permanente, 72, 45-46, Università degli studi di Milano. Dipartimento di scienze della terra.
Erba E., E. Parisi, H.L. ten Haven, M. Nip and J.W. de Leeuw. (1987). Gelatinous pellicles in deep anoxic hypersaline basins from the eastern Mediterranean, Marine Geology, 75, 165-183.
Faktor M.M. and R. Hanks. (1969). Calculation of the third ionisation potentials of the lanthanons, Journal of Inorganic & Nuclear Chemistry, 31, 1649-1659.
Fashchuk D.Ya. and T.A. Ayzatullin. (1986). A possible transformation of the anaerobic zone of the Black Sea, Oceanology, 26, 171-178.
Florence T.M. and G.E. Batley. (1976). Trace metals species in sea-water - I, removal of trace metals from sea-water by a chelating resin, Talanta, 23, 179-186.
Florence T.M. and G.E. Batley. (1975). Removal of trace metals from seawater by a chelating resin, Talanta, 22, 201-204.
Fonselius S.H. (1974). Phosphorus in Black Sea. In E.T. Degens and D.A. Ross (Ed.), The Black Sea - Geology, Chemistry, and Biology, 144-150, American Association of Petroleum Geologists, Tulsa, Oklahoma.
Forchhammer G. (1865). On the composition of sea-water in the different parts of the ocean, Philosophical Transactions of the Royal Society of London, 155, 203-262.
Friederich G.E., L.A. Codispoti and C.M. Sakamoto. (1990). Bottle and pumpcast data from the 1988 Black Sea expedition, Monterey Bay Aquarium Research Institute Technical Report No. 90-3.
Froelich P.N., G.P. Klinkhammer, M.L. Bender, N.A. Luedtke, G.R. Heath, D. Cullen, P. Dauphin, D. Hammond, B. Hartman and V. Maynard. (1979). Early oxidation of organic matter in pelagic sediments of the eastern equatorial Atlantic: suboxic diagenesis, Geochimica et Cosmochimica Acta, 43, 1075-1090.
Frost C.D., R.K. O'Nions and S.L. Goldstein. (1986). Mass balance for Nd in the Mediterranean Sea, Chemical Geology, 55, 45-50.

Ganor E. and Y. Mamane. (1982). Transport of Saharan dust across the eastern Mediterranean, Atmospheric Environment, 16 (3), 581-587.
German C.R., A.P. Fleer, M.P. Bacon and J.M. Edmond. (1991a). Hydrothermal scavenging at the Mid-Atlantic Ridge: radionuclide distributions, Earth and Planetary Science Letters, 105, 170-181.
German C.R., B.P. Holliday and H. Elderfield. (1991b). Redox cycling of rare earth elements in the suboxic zone of the Black Sea, Geochimica et Cosmochimica Acta, 55, 3553-3558.
German C.R. and H. Elderfield. (1990). Rare earth elements in the NW Indian Ocean, Geochimica et Cosmochimica Acta, 54, 1929-1940.
German C.R., G.P. Klinkhammer, J.M. Edmond, A. Mitra and H. Elderfield. (1990). Hydrothermal scavenging of rare-earth elements in the ocean, Nature, 345, 516-518.
German C.R. and H. Elderfield. (1989). Rare earth elements in Saanich Inlet, British Columbia, a seasonally anoxic basin, Geochimica et Cosmochimica Acta, 53, 2561-2571.
Goldberg E.D. (1965). Minor elements in seawater. In J.P. Riley and G. Skirrow (Ed.), Chemical Oceanography, 1st ed., Vol. 1, 163-196, Academic Press, London.
Goldberg E.D., M. Koide, R.A. Schmitt and R.H. Smith. (1963). Rare-earth distributions in the marine environment, Journal of Geophysical Research, 68 (14), 4209-4217.
Goldstein S.J. and S.B. Jacobsen. (1988). Rare earth elements in river waters, Earth and Planetary Science Letters, 89, 35-47.
Goyet C., A. Bradshaw and P.G. Brewer. (1988). Measurements of the CO_2/carbonate system in the Black Sea, EOS Transactions of the American Geophysical Union, 69 (44), 1240.
Greaves M.J., M. Rudnicki and H. Elderfield. (1991). Rare earth elements in the Mediterranean Sea and mixing in the Mediterranean outflow, Earth and Planetary Science Letters, 103, 169-181.
Greaves M.J., H. Elderfield and G.P. Klinkhammer. (1989). Determination of the rare earth elements in natural waters by isotope-dilution mass spectrometry, Analytica Chimica Acta, 218, 265-280.
Greenberg R.R. and H.M. Kingston. (1983). Trace element analysis of natural water samples by neutron activation analysis with chelating resin, Analytical Chemistry, 55 (7), 1160-1165.
Greenberg R.R. and H.M. Kingston. (1982). Simultaneous determination of twelve trace elements in estuarine and sea water using pre-irradiation chromatography, Journal of Radioanalytical Chemistry, 71 (1-2), 147-167.
Gromet L.P., R.F. Dymek, L.A. Haskin and R.L. Korotev. (1984). The "North American shale composite": its compilation, major and trace element characteristics, Geochimica et Cosmochimica Acta, 48, 2469-2482.
Gunnerson C.G. and E. Özturgut. (1974). The Bosporus. In E.T. Degens and D.A. Ross (Ed.), The Black Sea - Geology, Chemistry, and Biology, 99-114, American Association of Petroleum Geologists, Tulsa, Oklahoma.
Hanson G.N. (1976). Rare earth element analysis by isotope dilution, National Bureau of Standards Special Publication, 422, 937-949.
Haraldsson C. and S. Westerlund. (1988). Trace metals in the water columns of the Black Sea and Framvaren Fjord, Marine Chemistry, 23, 417-424.
Haskin M.A. and L.A. Haskin. (1966). Rare earths in European shales: a redetermination, Science, 154, 507-509.
Hay B.J., S. Honjo, S. Kempe, V.A. Ittekkot, E.T. Degens, T. Konuk and E. Izdar. (1990). Interannual variability in particle flux in the southwestern Black Sea, Deep-Sea Research, 37 (6), 911-928.
Hebeda E.H. and J. Schijf. (1991). Bleeding CCl_2F_2 as a tool to enhance the emission of metalions and to suppress isobaric interferences by oxide-ions during a multi

element-analysis of rare earth elements on a thermal ionization mass spectrometer, International Journal of Mass Spectrometry and Ion Processes, 104, 227-234.
Helm L. and A.E. Merbach. (1991). Structure and dynamics of lanthanide (III) ions in solution: a neutron scattering contribution, European Journal of Solid State and Inorganic Chemistry, 28, 245-250.
Henderson P. (Ed.). (1984). Rare earth element geochemistry, Developments in Geochemistry, 2, 510 pp, Elsevier Science Publishers, Amsterdam.
Henneke E. and G.J. de Lange. (1990). The distribution of DOC and POC in the water column and brines of the Tyro and Bannock Basins, Marine Chemistry, 31, 113-122.
Hering J.G. and F.M.M. Morel. (1989). Slow coordination reactions in seawater, Geochimica et Cosmochimica Acta, 53, 611-618.
Høgdahl O.T., S. Melsom and V.T. Bowen. (1968). Neutron activation analysis of lanthanide elements in sea water. In R.F. Gould (Ed.), Trace inorganics in water, 73, 308-325, American Chemical Society, Washington, D.C.
Honeyman B.D., L.R. Balistrieri and J.W. Murray. (1988). Oceanic trace metal scavenging: the importance of particle concentration, Deep-Sea Research, 35 (2), 227-246.
Hooker P.J., R.K. O'Nions and R.J. Pankhurst. (1975). Determination of rare-earth elements in USGS standard rocks by mixed-solvent ion exchange and mass spectrometric isotope dilution, Chemical Geology, 16, 189-196.
Huynh Ngoc L. and N.E. Whitehead. (1986). Nickel and cobalt determination in the North West Mediterranean by differential pulse cathodic stripping voltammetry, Oceanologica Acta, 9 (4), 433-438.
Hydes D.J., G.J. de Lange and H.J.W. de Baar. (1988). Dissolved aluminium in the Mediterranean, Geochimica et Cosmochimica Acta, 52, 2107-2114.
Jacobs L., S. Emerson and S.S. Huested. (1987). Trace metal geochemistry in the Cariaco Trench, Deep-Sea Research, 34 (5/6), 965-981.
Jacobs L., S. Emerson and J. Skei. (1985). Partitioning and transport of metals across the O_2/H_2S interface in a permanently anoxic basin: Framvaren Fjord, Norway, Geochimica et Cosmochimica Acta, 49, 1433-1444.
Jacobs L. and S. Emerson. (1982). Trace metal solubility in an anoxic fjord, Earth and Planetary Science Letters, 60, 237-252.
Jannasch H.W., B.D. Honeyman, L.S. Balistrieri and J.W. Murray. (1988). Kinetics of trace element uptake by marine particles, Geochimica et Cosmochimica Acta, 52, 567-577.
Job A. (1903). Activité de quelques sels de terres rares, comme excitateurs d'oxydation, Comptes rendus hebdomadaires des scéances de l'Académie des Sciences, 136, 45-47 (in French).
Job A. (1902). Glucose et carbonates de cérium. Sur un nouveau mécanisme d'oxydation provoquée, Comptes rendus hebdomadaires des scéances de l'Académie des Sciences, 134, 1052-1054 (in French).
Jongsma D., A.R. Fortuin, W. Huson, S.R. Troelstra, G.T. Klaver, J.M. Peters, D. van Harten, G.J. de Lange and L. ten Haven. (1983). Discovery of an anoxic basin within the Strabo Trench, eastern Mediterranean, Nature, 305, 795-797.
Kempe S., G. Liebezett, A.-R. Diercks and V. Asper. (1990). Water balance in the Black Sea, Nature, 346, p. 419.
Kim K.-H., R.H. Byrne and J.H. Lee. (1991). Gadolinium behavior in seawater: a molecular basis for Gd anomalies, in press.
Kingston H.M., I.L. Barnes, T.J. Brady, T.C. Rains and M.A. Champ. (1978). Separation of eight transition elements from alkali and alkaline earth elements in estuarine and seawater with chelating resin and their determination by graphite furnace atomic absorption spectrometry, Analytical Chemistry, 50 (14), 2064-2070.
Klinkhammer G. H. Elderfield and A. Hudson. (1983). Rare earth elements in seawater near hydrothermal vents, Nature, 305, 185-188.

Knauss K.G., T.J. Wolery and K.J. Jackson. (1991). Reply to comments by R.E. Mesmer on "A new approach to measuring pH in brines and other concentrated electrolytes", Geochimica et Cosmochimica Acta, 55, 1177-1179.

Knauss K.G., T.J. Wolery and K.J. Jackson. (1990). A new approach to measuring pH in brines and other concentrated electrolytes, Geochimica et Cosmochimica Acta, 54, 1519-1523.

Kolesov G.M., V.V. Anikiyev and V.S. Savenko. (1975). On the geochemistry of rare earth elements in the waters of the Black Sea, Geochemistry International, 12 (1), 82-88.

Krauskopf K.B. (1956). Factors controlling the concentrations of thirteen rare metals in sea-water, Geochimica et Cosmochimica Acta, 9, 1-32B.

Kremling K. and H. Petersen. (1981). The distribution of zinc, cadmium, copper, manganese and iron in waters of the open Mediterranean Sea, "Meteor" Forschungs Ergebnisse, A/B (23), 5-14.

Kuehner E.C., R. Alvarez, P.J. Paulsen and T.J. Murphy. (1972). Production and analysis of special high-purity acids purified by sub-boiling distillation, Analytical Chemistry, 44 (12), 2050-2056.

Landing W.M. and B.L. Lewis. (1991). Thermodynamic modeling of trace metal speciation in the Black Sea. In E. Izdar and J.W. Murray (Ed.), Black Sea Oceanography. NATO ASI Series C: Mathematical and Physical Sciences, 351, 125-160, Kluwer Academic Publishers, Dordrecht, The Netherlands.

Laumond F., G. Copin-Montegut, P. Courau and E. Nicolas. (1984). Cadmium, copper and lead in the western Mediterranean Sea, Marine Chemistry, 15, 251-261.

Lee C., N.B. Kim, I.C. Lee and K.S. Chung. (1977). The use of a chelating resin column for preconcentration of trace elements from sea-water in their determination by neutron-activation analysis, Talanta, 24, 241-245.

Lewis B.L. and W.M. Landing. (1991). The biogeochemistry of manganese and iron in the Black Sea. In J.W. Murray (Ed.), Black Sea Oceanography - Results from the 1988 Black Sea Expedition. Deep-Sea Research, 38 (2A), S773-S803.

Li Y.-H. and S. Gregory. (1974). Diffusion of ions in sea water and in deep-sea sediments, Geochimica et Cosmochimica Acta, 38, 703-714.

Liu Y.-G., M.R.U. Miah and R.A. Schmitt. (1988). Cerium: a chemical tracer for paleo oceanic redox conditions, Geochimica et Cosmochimica Acta, 52, 1361-1371.

Loÿe-Pilot M.D., J.M. Martin and J. Morelli. (1986). Influence of Saharan dust on the rain acidity and atmospheric input to the Mediterranean, Nature, 321, 427-428.

Luther III G.W., T.M. Church and D. Powell. (1991). Sulfur speciation and sulfide oxidation in the water column of the Black Sea. In J.W. Murray (Ed.), Black Sea Oceanography - Results from the 1988 Black Sea Expedition. Deep-Sea Research, 38 (2A), S1121-S1137.

Luther III G.W., G. Catalano, G.J. de Lange and J.R.W. Woittiez. (1990). Reduced sulfur in the hypersaline anoxic basins of the Mediterranean Sea, Marine Chemistry, 31, 137-152.

Luttrell Jr. G.H., C. More and C.T. Kenner. (1971). Effect of pH and ionic strength on ion exchange and chelating properties of an iminodiacetate ion exchange resin with alkaline earth ions, Analytical Chemistry, 43 (11), 1370-1375.

MacKenzie F.T., M. Stoffyn and R. Wollast. (1978). Aluminium in seawater: control by biological activity, Science, 199, 680-682.

Mackin J.E. and R.C. Aller. (1984). Dissolved Al in sediments and waters of the East China Sea: implications for authigenic mineral formation, Geochimica et Cosmochimica Acta, 48, 281-297.

Malanotte-Rizzoli P. and A. Hecht. (1988). Large-scale properties of the Eastern Mediterranean: a review, Oceanologica Acta, 11 (4), 323-335.

Marinsky J.A., L.E. Glendenin and C.D. Coryell. (1947). The chemical identification of radioisotopes of neodymium and of element 61, The Journal of the American Chemical Society, 69, 2781-2785.

Martell A.E. and R.M. Smith. (1977), Critical stability constants. Volume 3: other organic ligands, 495 pp, Plenum Press, New York.
Masuda A. and Y. Ikeuchi. (1979). Lanthanide tetrad effect observed in marine environment, Geochemical Journal, 13, 19-22.
Mayer S.W. and S.D. Schwartz. (1950). The association of cerous ion with sulfite, phosphate and pyrophosphate ions, Journal of the American Chemical Society, 72, 5106-5110.
Mesmer R.E. (1991). Comments on "A new approach to measuring pH in brines and other concentrated electrolytes" by K.G. Knauss, T.J. Wolery and K.J. Jackson, Geochimica et Cosmochimica Acta, 55, 1175-1176.
Michard A. (1989). Rare earth element systematics in hydrothermal fluids, Geochimica et Cosmochimica Acta, 53, 745-750.
Michard A. and F. Albarède. (1986). The REE content of some hydrothermal fluids, Chemical Geology, 55, 51-60.
Michard A., F. Albarède, G. Michard, J.F. Minster and J.L. Charlou. (1983). Rare-earth elements and uranium in high-temperature solutions from East Pacific Rise hydrothermal vent field (13°N), Nature, 303, 795-797.
Middelburg J.J., G.J. de Lange and C.H. van der Weijden. (1987). Manganese solubility in marine pore waters, Geochimica et Cosmochimica Acta, 51, 759-763.
Millero F.J. (1992). Stability constants for the formation of rare earth inorganic complexes as a function of ionic strength, Geochimica et Cosmochimica Acta, in press.
Millero F.J. (1991). The oxidation of H_2S in Black Sea waters. In J.W. Murray (Ed.), Black Sea Oceanography - Results from the 1988 Black Sea Expedition. Deep-Sea Research, 38 (2A), S1139-S1150.
Millero F.J. (1977). Thermodynamic models for the state of metal ions in seawater. In E.D. Goldberg (Ed.), The Sea, Vol. 7, 653-693, John Wiley & Sons, New York.
Millero F.J., S. Hubinger, M. Fernandez and S. Garnett. (1987a). Oxidation of H_2S in seawater as a function of temperature, pH, and ionic strength, Environmental Science & Technology, 21 (5), 439-443.
Millero F.J., S. Sotolongo and M. Izaguirre. (1987b). The kinetics of oxidation of Fe(II) in seawater, Geochimica et Cosmochimica Acta, 51, 793-801.
Millero F.J., M. Izaguirre and V.K. Sharma. (1987c). The effect of ionic interactions on the rates of oxidation in natural waters, Marine Chemistry, 22, 179-191.
Millero F.J. and D.R. Schreiber. (1982). Use of the ion pairing model to estimate activity coefficients of the ionic components of natural waters, American Journal of Science, 282, 1508-1540.
Moffett J.W. (1990). Microbially mediated cerium oxidation in sea water, Nature, 345, 421-423.
Morel F. and J. Morgan. (1972). A numerical method for computing equilibria in aqueous chemical systems, Environmetal Science & Technology, 6, 58-67.
Morley N.H., J.D. Burton and P.J. Statham. (1991). Observations on dissolved trace metals in the Golfe du Lion, in press.
Murphy K. and J. Dymond. (1984). Rare earth element fluxes and geochemical budget in the eastern equatorial Pacific, Nature, 307, 444-447.
Murray R.W., M.R. Buchholtz ten Brink, D.C. Gerlach, G. P. Russ III and D.L. Jones. (1991a). Rare earth, major, and trace elements in chert from the Franciscan Complex and Monterey Group, California: Assessing REE sources to fine-grained marine sediments, Geochimica et Cosmochimica Acta, 55, 1875-1895.
Murray R.W., M.R. Buchholtz ten Brink, H.J. Brumsack, D.C. Gerlach and G. P. Russ III. (1991b). Rare earth elements in Japan Sea sediments and diagenetic behavior of Ce/Ce^*: Results from ODP Leg 127, Geochimica et Cosmochimica Acta, 55, 2453-2466.
Murray J.W. and E. Izdar. (1989). The 1988 Black Sea oceanographic expedition: overview and new discoveries, Oceanography Magazine, 2, 15-21.

Murray J.W., H.W. Jannasch, S. Honjo, R.F. Anderson, W.S. Reeburgh, Z. Top, G.E. Friederich, L.A. Codispoti and E. Izdar. (1989). Unexpected changes in the oxic/anoxic interface in the Black Sea, Nature, 338, 411-413.

Murray J.W., B. Spell and B. Paul. (1983). The contrasting geochemistry of manganese and chromium in the eastern tropical Pacific. In C.S. Wong, E. Boyle, K.W. Bruland, J.D. Burton and E.D. Goldberg (Ed.), Trace metals in sea water, 643-669, Plenum Press, New York.

Nealson K.H., C.R. Myers and B.B. Wimpee. (1991). Isolation and identification of manganese-reducing bacteria and estimates of microbial Mn(IV)-reducing potential in the Black Sea. In J.W. Murray (Ed.), Black Sea Oceanography - Results from the 1988 Black Sea Expedition. Deep-Sea Research, 38 (2A), S907-S920.

Nozaki Y., H.-S. Yang and M. Yamada. (1987). Scavenging of thorium in the ocean, Journal of Geophysical Research, 92 (C1), 772-778.

Nugent L.J. (1970). Theory of the tetrad effect in the lanthanide(III) and actinide(III) series, Journal of Inorganic & Nuclear Chemistry, 32, 3485-3491.

Nyffeler U.P., Y.-H. Li and P.H. Santschi. (1984). A kinetic approach to describe trace element distribution between particles and solution in natural aquatic systems, Geochimica et Cosmochimica Acta, 48, 1513-1522.

Olivarez A.M. and R.M. Owen. (1989). REE/Fe variations in hydrothermal sediments: implications for the REE content of seawater, Geochimica et Cosmochimica Acta, 53, 757-762.

Orians K.J. and K.W. Bruland. (1986). The biogeochemistry of aluminium in the Pacific Ocean, Earth and Planetary Science Letters, 78, 397-410.

Ovchinnikov I.M. and Ye.A. Plakhin. (1984). Formation of the intermediate waters of the Mediterranean Sea in the Rhodes cyclonic gyre, Oceanology, 24 (3), 317-319.

Paulson A.J. (1986). Effects of flow rate and pretreatment on the extraction of trace metals from estuarine and coastal seawater by Chelex-100, Analytical Chemistry, 58, 183-187.

Pektas H. (1956). The influence of the Mediterranean water on the hydrography of the Black Sea, 4th Technical Papers Meeting, Fisheries Center of Istanbul, Mediterranean General Fisheries Council.

Piper D.Z. (1974). Rare earth elements in the sedimentary cycle: a summary, Chemical Geology, 14, 285-304.

Pitzer K.S. (1973). Thermodynamics of electrolytes. I. Theoretical basis and general equations, The Journal of Physical Chemistry, 77 (2), 268-277.

Pitzer K.S. and G. Mayorga. (1973). Thermodynamics of electrolytes. II. Activity and osmotic coefficients for strong electrolytes with one or both ions univalent, The Journal of Physical Chemistry, 77 (19), 2300-2308.

Plakhin Ye.A. (1972). Vertical winter circulation in the Mediterranean, Oceanology, 12, 344-350.

Plakhin Ye.A. (1971). Formation of distinct deep-water in the Mediterranean by convective mixing, Oceanology, 11, 524-529.

Rabitti S. and A. Boldrin. (1989). Vertical structure of temperature, conductivity, and transmittance in eastern Mediterranean anoxic basins. In M.B. Cita, A. Camerlenghi and C. Corselli (Ed.), Anoxic basins of the eastern Mediterranean. Results of the third conference. Bergamo (Italy) December 14-16 1988. Ricerca scientifica ed educazione permanente, 72, 67-69, Università degli studi di Milano. Dipartimento di scienze della terra.

Rahn K.A. (1976). The chemical composition of the atmospheric aerosol, Technical Report, 265 pp, University of Rhode Island, Graduate School of Oceanography.

Redfield A.C., B.H. Ketchum and F.A. Richards. (1963). The influence of organisms on the composition of sea water. In M.N. Hill (Ed.), The Sea, Vol. 2, 26-77, John Wiley & Sons, New York.

Repeta D.J., D.J. Simpson, B.B. Jorgensen and H.W. Jannasch. (1989). Evidence for anoxygenic photosynthesis from the distribution of bacteriochlorophylls in the Black Sea, Nature, 342, 69-72.
Riley J.P. and D. Taylor. (1968). Chelating resins for the concentration of trace elements from sea water and their analytical use in conjunction with atomic absorption spectrophotometry, Analytica Chimica Acta, 40, 479-485.
Rosson R.A., B.M. Tebo and K.H. Nealson. (1984). Use of poisons in determination of microbial manganese binding rates in seawater, Applied and Environmental Microbiology, 47 (4), 740-745.
Saager P.M. (1987). Trace metals in the North West Indian Ocean, M.Sc. Thesis, 89 pp, State University of Utrecht, The Netherlands.
Saager P.M., J. Schijf and H.J.W. de Baar. (1991). Trace metal distributions in seawater and anoxic brines of the eastern Mediterranean, Geochimica et Cosmochimica Acta, in press.
Saager P.M., H.J.W. de Baar and P.H. Burkill. (1989). Manganese and iron in Indian Ocean waters, Geochimica et Cosmochimica Acta, 53, 2259-2267.
Schijf J., H.J.W. de Baar, J.R. Wijbrans and W.M. Landing. (1991). Dissolved rare earth elements in the Black Sea. In J.W. Murray (Ed.), Black Sea Oceanography - Results from the 1988 Black Sea Expedition. Deep-Sea Research, 38 (2A), S805-S823.
Schindler P.W. (1975). Removal of trace metals from the oceans: a zero order model, Thalassia Jugoslavica, 11 (1/2), 101-111.
Schnetzler C.C., H.H. Thomas and J.A. Philpotts. (1967). Determination of rare earth elements in rocks and minerals by mass spectrometric, stable isotope dilution technique, Analytical Chemistry, 39 (14), 1888-1890.
Schuhmann S. and J.A. Philpotts. (1979). Mass-spectrometric stable-isotope-dilution analysis for lanthanides in geochemical materials. In K.A. Gschneidner Jr. and L. Eyring (Ed.), Handbook on the physics and chemistry of rare earths, Vol. 4, 471-481, North-Holland Publishing Company, Amsterdam.
Scientific staff of Cruise *Bannock* 1984-12. (1985). Gypsum precipitation from cold brines in an anoxic basin in the eastern Mediterranean, Nature, 314, 152-154.
Shaffer G. (1986). Phosphate pumps and shuttles in the Black Sea, Nature, 321, 515-517.
Sherrell R.M. (1989). The trace metal geochemistry of suspended oceanic particulate matter, Ph.D. Thesis, 211 pp, Woods Hole Oceanographic Institution.
Sherrell R.M. and E.A. Boyle. (1988). Zinc, chromium, vanadium and iron in the Mediterranean Sea, Deep-Sea Research, 35 (8), 1319-1334.
Shokes R.F., P.K. Trabant, B.J. Presley and D.F. Reid. (1977). Anoxic, hypersaline basin in the northern Gulf of Mexico, Science, 196, 1443-1446.
Sholkovitz E.R. (1990). Rare-earth elements in marine sediments and geochemical standards, Chemical Geology, 88, 333-347.
Sholkovitz E.R. (1988). Rare earth elements in the sediments of the North Atlantic Ocean, Amazon delta, and East China Sea: reinterpretation of terrigenous input patterns to the oceans, American Journal of Science, 288, 236-281.
Sholkovitz E.R. and D.L. Schneider. (1991). Cerium redox cycles and rare earth elements in the Sargasso Sea, Geochimica et Cosmochimica Acta, 55, 2737-2743.
Sholkovitz E.R., D.J. Piepgras and S.B. Jacobsen. (1989). The pore water chemistry of rare earth elements in Buzzards Bay sediments, Geochimica et Cosmochimica Acta, 53, 2847-2856.
Sholkovitz E.R. and H. Elderfield. (1988). Cycling of dissolved rare earth elements in Chesapeake Bay, Global Biogeochemical Cycles, 2 (2), 157-176.
Skei J. (1983). Geochemical and sedimentological considerations of a permanently anoxic fjord - Framvaren, South Norway, Sedimentary Geology, 36, 131-145.
Sørensen K. (1988). The distribution and biomass of phytoplankton and phototrophic bacteria in Framvaren, a permanently anoxic fjord in Norway, Marine Chemistry, 23, 229-241.

Sorokin Yu.I. (1983). The Black Sea. In B.H. Ketchum (Ed.), Estuaries and enclosed seas. Ecosystems of the world, 26, 253-292, Elsevier Scientific Publishing Company, Amsterdam.

Spencer D.W., P.G. Brewer and P.L. Sachs. (1972). Aspects of the distribution and trace element composition of suspended matter in the Black Sea, Geochimica et Cosmochimica Acta, 36, 71-86.

Spencer D.W. and P.G. Brewer. (1971). Vertical advection diffusion and redox potentials as controls on the distribution of manganese and other trace metals dissolved in waters of the Black Sea, Journal of Geophysical Research, 76 (24), 5877-5892.

Spivack A.J. and G.J. Wasserburg. (1988). Neodymium isotopic composition of the Mediterranean outflow and the eastern North Atlantic, Geochimica et Cosmochimica Acta, 52, 2767-2773.

Spivack A.J., S.S. Huested and E.A. Boyle. (1983). Copper, nickel and cadmium in the surface waters of the Mediterranean. In C.S. Wong, E. Boyle, K.W. Bruland, J.D. Burton and E.D. Goldberg (Ed.), Trace metals in sea water, 505-512, Plenum Press, New York.

Stanley Jr. J.K. and R.H. Byrne. (1990). The influence of solution chemistry on REE uptake by *Ulva lactuca* L. in seawater, Geochimica et Cosmochimica Acta, 54, 1587-1595.

Statham P.J., J.D. Burton and D.J. Hydes. (1985). Cd and Mn in the Alborean Sea and adjacent North Atlantic: geochemical implications for the Mediterranean, Nature, 313, 565-567.

Stenni B. and A. Longinelli. (1990). Stable isotope study of water, gypsum and carbonate samples from the Bannock and Tyro Basins, eastern Mediterranean, Marine Chemistry, 31, 123-135.

Strelow F.W.E. (1980). Quantitative separation of lanthanides and scandium from barium, strontium and other elements by cation-exchange chromatography in nitric acid, Analytica Chimica Acta, 120, 249-254.

Strelow F.W.E. (1966). Separation of trivalent rare earths plus Sc(III) from Al, Ga, In, Tl, Fe, Ti, U and other elements by cation-exchange chromatography, Analytica Chimica Acta, 34, 387-393.

Strelow F.W.E. (1960). An ion exchange selectivity scale of cations based on equilibrium distribution coefficients, Analytical Chemistry, 32 (9), 1185-1188.

Strelow F.W.E. and P.F.S. Jackson. (1974). Determination of trace and ultra-trace quantities of rare-earth elements by ion exchange chromatography-mass spectrography, Analytical Chemistry, 46 (11), 1481-1486.

Strelow F.W.E., R. Rethemeyer and C.J.C. Bothma. (1965). Ion exchange selectivity scales for cations in nitric acid and sulfuric acid media with a sulfonated polystyrene resin, Analytical Chemistry, 37 (1), 106-111.

Sunda W.G. and S.A. Huntsman. (1988). Effect of sunlight on redox cycles of manganese in the southwestern Sargasso Sea, Deep-Sea Research, 35 (8), 1297-1317.

Sunda W.G., S.A. Huntsman and G.R. Harvey. (1983). Photoreduction of manganese oxides in seawater and its geochemical and biological implications, Nature, 301, 234-236.

Sung W. and J.J. Morgan. (1981). Oxidative removal of Mn(II) from solution catalysed by the γ-FeOOH (lepidocrocite) surface, Geochimica et Cosmochimica Acta, 45, 2377-2383.

Sverjensky D.A. (1984). Europium redox equilibria in aqueous solution, Earth and Planetary Science Letters, 67, 70-78.

Tebo B.M. (1991). Manganese(II) oxidation in the suboxic zone of the Black Sea. In J.W. Murray (Ed.), Black Sea Oceanography - Results from the 1988 Black Sea Expedition. Deep-Sea Research, 38 (2A), S883-S905.

Ten Haven H.L., G.J. de Lange and G.Th. Klaver. (1985). The chemical composition and origin of the Tyro brine, eastern Mediterranean, a tentative model, Marine Geology, 64, 337-342.

Thirlwall M.F. (1982). A triple-filament method for rapid and precise analysis of rare earth elements by isotope dilution, Chemical Geology, 35, 155-166.
Tolmazin D. (1985). Changing coastal oceanography of the Black Sea. I: northwestern shelf, Progress in Oceanography, 15, 217-276.
Tomadin L., R. Lenaz, V. Landuzzi, A. Mazzucotelli and R. Vannucci. (1984). Wind-blown dusts over the Central Mediterranean, Oceanologica Acta, 7 (1), 13-22.
Top Z. and W.B. Clarke. (1983). Helium, neon and tritium in the Black Sea, Journal of Marine Research, 41 (1), 1-17.
Topp N.E. (1965), The chemistry of the rare-earth elements, 164 pp, Elsevier Publishing Company, Amsterdam.
Trefry J.H., B.J. Presley, W.L. Keeney-Kennicutt and R.P. Trocine. (1984). Distribution and chemistry of manganese, iron, and suspended particulates in Orca Basin, Geo Marine Letters, 4, 125-130.
Turekian K.K. (1977). The fate of metals in the oceans, Geochimica et Cosmochimica Acta, 41, 1139-1144.
Turner D.R., M. Whitfield and A.G. Dickson. (1981). The equilibrium speciation of dissolved components in freshwater and seawater at 25 °C and 1 atm pressure, Geochimica et Cosmochimica Acta, 45, 855-881.
Ullman W.J., G.W. Luther III, G.J. de Lange and J.R.W. Woittiez. (1990). Iodine chemistry in deep anoxic basins and overlying waters of the Mediterranean Sea, Marine Chemistry, 31, 153-170.
Ullyott P. and O. Ilgaz. (1946). The hydrography of the Bosphorus: an introduction, Geographical Review, 36 (1), 44-66.
Van der Sloot H.A., D. Hoede, G. Hamburg, J.R.W. Woittiez and C.H. van der Weijden. (1990). Trace elements in suspended matter from the anoxic hypersaline Tyro and Bannock Basins (eastern Mediterranean), Marine Chemistry, 31, 187-203.
Van der Weijden C.H., J.J. Middelburg, G.J. de Lange, H.A. van der Sloot, D. Hoede and J.R.W. Woittiez. (1990). Profiles of the redox-sensitive trace elements As, Sb, V, Mo and U in the Tyro and Bannock Basins (eastern Mediterranean), Marine Chemistry, 31, 171-186.
Van Gaans, P.F.M. (1989). WATEQX - a restructured, generalized, and extended FORTRAN 77 computer code and database format for the WATEQ aqueous chemical model for element speciation and mineral saturation, for use on personal computers or mainframes, Computers & Geosciences, 15 (6), 843-887.
Van Geen A., P. Rosener and E. Boyle. (1988). Entrainment of trace-metal-enriched Atlantic-shelf water in the inflow to the Mediterranean Sea, Nature, 331, 423-426.
Wang J.M., R. Ballad, P. Grimaldi and W. Lei. (1983). Extraction of thorium, uranium and cerium from fresh water using manganese dioxide coprecipitation, Journal of Radioanalytical Chemistry, 76 (1), 105-108.
Weast R.C. and M.J. Astle (Ed.). (1982), CRC Handbook of Chemistry and Physics, 63rd edition 1982-1983, CRC Press, Inc., Boca Raton, Florida.
Webster R.K. (1960). Mass spectrometric isotope dilution analysis. In A.A. Smales and L.R. Wager (Ed.), Methods in geochemistry, 202-246, Interscience Publishers Inc., New York.
White G., M. Relander, J. Postal and J.W. Murray. (1989). Hydrographic data from the 1988 Black Sea Oceanographic Expedition, University of Washington School of Oceanography Special Report No. 109.
Wiesenburg D.A., J.M. Brooks and B.B. Bernard. (1985). Biogenic hydrocarbon gases and sulfate reduction in the Orca Basin brine, Geochimica et Cosmochimica Acta, 49, 2069-2080.
Wüst G. (1961). On the vertical circulation of the Mediterranean Sea, Journal of Geophysical Research, 66 (10), 3261-3271.
Zhorov V.A., S.G. Boguslavskiy, A.G. Kobylyanskaya, V.P. Ronkova and R.I. Ivanov. (1982). Trends in the spatial distribution of oxygen in the Black Sea during the summer, Geochemistry International, 18 (5), 65-73.

Curriculum vitae

Johan Schijf werd geboren op 9 september 1965 te De Zilk (gemeente Noordwijkerhout). In 1983 behaalde hij het diploma ongedeeld VWO, alsmede een certificaat voor het vak Latijn, aan de openbare scholengemeenschap Huygenwaard te Heerhugowaard. In datzelfde jaar begon hij met de studie Natuurkunde aan de Rijksuniversiteit te Groningen. Na de richting Experimentele Natuurkunde te hebben gekozen studeerde hij in 1987 cum laude af bij Prof. Dr. R.H. Siemssen op het doctoraalverslag "Angular momentum transfer studies for the ^{20}Ne + ^{209}Bi,^{232}Th reactions at 204.4 MeV". Van september 1987 tot september 1991 was hij als assistent in opleiding (a.i.o.) in dienst van de Rijksuniversiteit te Utrecht. In die periode was hij gedetacheerd bij het voormalig NWO Laboratorium voor Isotopen-Geologie (IGO) te Amsterdam, thans onderdeel van de Faculteit der Aardwetenschappen van de Vrije Universiteit.

Lijst van publicaties:

- Hebeda E.H. and J. Schijf (1991). Bleeding CCl_2F_2 as a tool to enhance the emission of metal ions and to suppress isobaric interferences by oxide ions during a multi-element analysis of rare earth elements on a thermal ionization mass spectrometer. International Journal of Mass Spectrometry and Ion Processes, 104, 227-234.
- De Baar H.J.W., J. Schijf and R.H. Byrne (1991). Solution chemistry of the rare earth elements in seawater. European Journal of Solid State and Inorganic Chemistry, 28, 357-373.
- Schijf J., H.J.W. de Baar, J.R. Wijbrans and W.M. Landing (1991). Dissolved rare earth elements in the Black Sea. In J.W. Murray (Ed.), Black Sea Oceanography - Results from the 1988 Black Sea Expedition. Deep-Sea Research, 38(2A), S805-S823.
- Saager P.M., J. Schijf and H.J.W. de Baar (1991). Trace metal distributions in seawater and anoxic brines of the eastern Mediterranean. Submitted for publication in Geochimica et Cosmochimica Acta.
- De Baar H.J.W., C. Brussaard, J. Hegeman, J. Schijf and M.H.C. Stoll (1992). Sea-trials of three different methods for non-volatile dissolved organic carbon in seawater during the JGOFS North Atlantic Pilot Study. Marine Chemistry, in press.